AIRCRAFT FUSELAGE DESIGN STUDY

PARAMETRIC MODELING, STRUCTURAL ANALYSIS, MATERIAL EVALUATION AND OPTIMIZATION FOR AIRCRAFT FUSELAGE

Master of Science Thesis

ILHAN ŞEN

December 10, 2010

TU Delft Delft University of Technology

TATA STEEL

Delft University of Technology

Faculty of Aerospace Engineering

in cooperation with

Tata Steel RD&T

AIRCRAFT FUSELAGE DESIGN STUDY

PARAMETRIC MODELING, STRUCTURAL ANALYSIS, MATERIAL EVALUATION AND OPTIMIZATION FOR AIRCRAFT FUSELAGE

Master of Science Thesis

For obtaining the degree of Master of Science in Aerospace Engineering at Delft University of Technology

by

ILHAN ŞEN

under the supervision of

PROF. DR. IR. R. BENEDICTUS

DR. IR. R. C. ALDERLIESTEN

DR. IR. C. D. RANS

IR. B. M. NEELIS

Final Version

December 10, 2010

Abstract

The strong search for lightweight materials has become a trend in the aerospace industry. Aircraft manufacturers are responding to this trend and new aerospace materials are introduced to build lighter aircrafts. However material manufacturers, like Tata Steel, are unfamiliar with the determination of running loads and the behavior of materials in fuselage structures. Therefore an evaluation tool is needed for determining the running loads and evaluating the performance of new materials. This will give material manufacturers better insight in what properties and performance are specifically needed for materials in aircraft structures.

The goal of this project is to develop an analytic design, analysis and evaluation tool for both metal and composite fuselage configurations in Visual Basic Application in order to gain insight into the structural performance of these material classes and to estimate the weight and required structural dimensions for both aluminum and composite fuselages.

The fuselage geometry is setup parametrical and modeled as a simplified tube with variable cross-section without cut-outs and wing box, and it is divided in bays and skin panels. By modeling the aerodynamic-, gravity-, ground reaction forces and internal pressure a free body diagram and force/moment distribution is created for several flight and ground load cases, like 1G flight, lateral gust or landing load cases. The critical load cases are used for analysis.

The running loads, like bending stress, longitudinal stress, circumferential stress and shear stress are calculated for the entire aircraft fuselage. A clear load pattern is created in order to evaluate the materials. The materials are evaluated for strength, stability and several other failure modes, like fatigue and crack growth. The skin panels are optimized for these evaluation methodologies and after doing so a minimum fuselage weight is obtained for conventional aircraft configurations.

The Airbus A320 is taken as reference aircraft and the running loads and optimization results of the model are validated with this aircraft. The model proved to be valid and is therefore considered suitable to be used as an analysis and evaluation tool.

The final stage of the project involved an initial assessment of aluminum and composite as structural material.

Acknowledgement

This report is the final thesis report of my study Aerospace Engineering at Delft University of Technology. The research on this thesis is conducted in cooperation with Tata Steel (formerly Corus). The developed tool will be part of a large analysis tool, which will be used by Tata Steel to evaluate new materials for a complete aircraft structure.

It could not have been realized without help of many people. I would like to take the opportunity to thank all the persons that contributed to the result of this thesis. First and foremost, I would like to thank my supervisors at the university: Prof. Dr. Ir. Rinze Benedictus, Dr. Ir. René C. Alderliesten and Dr. Ir. Calvin D. Rans.

Further, I would like to thank Tata Steel for providing me a good environment and facilities to complete this project. Also, I would like to thank my supervisor at Tata Steel Dr. Ir. Reinier de Rijck for offering this subject and guidance during my project. I am indebted to many of my colleagues to support me during my project, especially Ir. Bas M. Neelis, who gave me guidance during my project and had always time to discuss my work.

Lastly, I would like to thank my family for giving me the support through all these years and I offer my regards and blessings to all of those who supported me in any respect during the completion of the project.

Ilhan Şen

December 10, 2010

Contents

List of Figures

List of Tables

List of Symbols

Latin symbols

a	Horizontal distance between nose landing gear and center of gravity
	Acceleration of aircraft
	Temperature gradient
a_0	Initial crack length
a_c	Crack length
$a_{c_{crit}}$	Critical crack length
a_f	Final/critical crack length
A	Cross sectional area
A_b	Area subtended by skin panels at the center of cross-section
A_h	Aspect ratio horizontal tail
A_v	Aspect ratio vertical tail
b	Width, stringer spacing or stiffener pitch
	Horizontal distance between main landing gear and center of gravity
b_e	Effective width
b_f, b_{f_1}, b_{f_2}	Fuselage width
b_{wing}	Wing length
c	End fixity coefficient
$\bar{c}$	Mean aerodynamic chord (MAC)
$\bar{c}_v$	Mean aerodynamic chord vertical tail
C	Paris's coefficient
C_1, C_2, C_3, C_4	S-N curve constant
C_L	Lift coefficient
C_{L_α}	Lift curve slope
C_{L_h}	Horizontal tail lift coefficient
$C_{L_{h_{\delta_e}}}$	Elevator lift coefficient

$C_{L_{v_\beta}}$	Side lift coefficient
C_m	Pitching moment coefficient
$C_{m_{ac}}$	Pitching moment coefficient around aerodynamic center
d_1, d_2	Cross-section parameter
D	Force
	Stiffness matrix of laminate of the skin only
D_{fbh_d}	Diameter front bulkhead
D_{rbh_d}	Diameter rear bulkhead
e_M	Height distance between main landing gear and center of gravity
e_N	Height distance between nose landing gear and center of gravity
E	Elastic modulus
E_{mean}	Mean elastic modulus
f	Dynamic factor
F	Force or load
	Variable parameter
F_c	Critical load or compressive load
F_{cs}	Crippling stress load
F_{fs}	Reaction force front wing spar
F_{rs}	Reaction force rear wing spar
F_{tail}	Vertical tail load
g	Gravity acceleration
G	Shear modulus
h_{cg}	Height of center of gravity to ground
h_f	Fuselage height
h_{st}	Stiffener height
H_M	Horizontal component of reaction force of main landing gear
H_N	Horizontal component of reaction force of nose landing gear
I	Moment of inertia
I_{yy}	Moment of inertia around y-axis
I_{yz}	Moment of inertia around y-axis and z-axis
I_{zz}	Moment of inertia around z-axis
I_Z	Yaw moment of inertia
j	Safety factor

k_c	Buckling coefficient
k_{DT}	Diagonal tension factor
k_{dt_0}	Average diagonal tension factor
k_g	Gust alleviation factor
k_r	Aircraft response factor for abrupt elevator maneuvers
k_s	Shear buckling coefficient
K_{ir}	Main end fixity coefficient
K_{Ic}	Fracture toughness
K_{pcs}	Passenger cabin supplies factor
K_{pwt}	Portable water and closets factor
K_s	Shear buckling coefficient
K_{se}	Safety equipment factor
K_{wing}	Wing proportionality factor
$l_1, l_2, l_3, l_4, l_5, l_6$	Length of fuselage section
l_f	Length of fuselage
l_c	Cabin length
l_v	Distance between aircraft center of gravity and vertical tail lift center
L	Length or frame pitch
	Lift
L'	Effective length
L_h	Horizontal tail lift
L_s	Length of skin panel
L_v	Vertical tail lift
L_w	Wing lift
m	Paris's exponent
M	Bending moment or pitching moment
	Aircraft mass
	Mach number
M_A	Bending moment at point A
M_{ac}	Pitching moment around aerodynamic center
M_B	Bending moment at point B
M_{cr}	Critical Mach number
M_y	Bending moment around y-axis
M_z	Bending moment around z-axis

MS	Margin of safety
MTOW	Maximum take-off weight
MZFW	Maximum zero fuel weight
n	Load factor, Ramberg and Osgood parameter
n_L	Landing load factor
N	Number of cycles
$N_{cabcrew}$	Number of cabin crew
N_cr	Critical load for foam-filled stiffener/panel face wrinkling
N_{ii}	Inspection interval
N_{th}	Inspection threshold
N_f	Number of frames
$N_{flightcrew}$	Number of flight crew
N_{nlg}	Nose landing gear reaction force
N_{pax}	Number of passengers
N_s	Number of stringers
$N_{x_{cr}}$	Critical skin buckling load or critical buckling load for compression
$N_{xy_{cr}}$	Critical buckling load for shear
OEW	Operating empty weight
p	Pressure
p_0	Pressure at ground level
p_{cab}	Cabin pressure
p_{op}	Pressure at maximum operating altitude
P	Load
P_{crit_0}	Critical compressive load at $\tau = 0$
P_{el}	Total electric generator power
P_p	Pocket folding load
P_{pocket}	Pocket folding load at $\tau = 0$
q	Distributed load
	Dynamic pressure ($^1/_2\rho V^2$)
$q_1, q_2, q_3, q_4, q_5, q_6$	Distributed load per section
q_b	Open section shear flow
q_s	Shear flow distribution
q_{s_0}	Shear flow in panel with cut
Q	Shear load

r_M	Main landing gear rolling radius
r_N	Nose landing gear rolling radius
R	Radius
	Constant for ideal gas
	SN-curve parameter
R_1, R_2, R_3	Radius parametrical cross-section
R_A, R_B	Radius elliptical cross-section
S	Surface area or wing area
	Material maximum shear stress
S_e	Elevator area
S_{fl}	Floor surface area
S_{cg_f}	Front cargo surface area
S_{cg_r}	Rear cargo surface area
S_h	Horizontal tail area
S_G	Fuselage gross weight
S_v	Vertical tail area
S_{wing}	Wing area
t	Thickness
t_0	Initial thickness
t_{fi}	Thickness of stiffener integral flange
t_{min}	Minimum thickness
t_p	Skin pad thickness (includes t_{sk})
t_{root}	Wing root thickness
t_{sk}	Skin thickness
T	Torsion moment
	Engine thrust
T_{cr}	Critical torsion moment for buckling
T_{tot}	Total engine thrust
TH	Tsai-Hill criterion
U_E	Equivalent gust velocity
vol_{bulk}	Bulk volume
vol_{fus}	Fuselage volume
V	Flight speed
V_B	Design speed for maximum gust intensity

V_C	Cruise speed
V_D	Dive speed
V_E	Equivalent airspeed
V_M	Main landing gear vertical reaction force
V_N	Nose landing gear vertical reaction force
w	Stringer spacing, width of panel
W	Weight of aircraft
W_1, W_2, W_3, W_4, W_5, W_6	Aircraft section weight
W_{ac}	Weight of air-conditioning system
W_{APU}	Weight of APU systems
W_{APUG}	Weight of APU group
W_{bcc}	Weight of baggage and cargo containers
W_{crew}	Weight of crew members
W_{el}	Weight of electrical system
W_{eng}	Engine weight
W_{eq}	Equipment and services weight
W_{fbh}	Front bulkhead weight
W_{fl}	Floor weight
$W_{fl_{cg_f}}$	Front cargo floor weight
$W_{fl_{cg_r}}$	Rear cargo floor weight
$W_{fl_{grid}}$	Weight of floor grid
$W_{fl_{grid_{cg}}}$	Weight of cargo floor grid
W_{fuel}	Fuel weight
W_{fur}	Weight of furnishing and equipment
W_{fus}	Fuselage structural weight
W_h	Horizontal tail weight
W_{hypn}	Weight of hydraulic and pneumatic system
W_{ieg}	Weight of instruments, navigational and electronic equipment
W_{mis}	Miscellaneous equipment weight
W_{mlg}	Main landing gear weight
W_n	Nacelle weight
W_{nlg}	Nose landing gear weight
W_{pay}	Payload weight

W_{pc}	Weight for passenger comfort related items
W_{prop}	Propulsion group weight
W_{pt}	Paint weight
W_{pwr}	Power plant weight
W_{rbh}	Rear bulkhead weight
W_{res_f}	Residual fuel weight
$W_{seatrail}$	Weight of seat rail
W_{sc}	Surface control weight
W_{tail}	Tail weight
$W_{tail_{str}}$	Tail structure penalty weight
W_v	Vertical tail weight
W_{wing}	Wing weight
$W_{wing_{str}}$	Wing structure penalty weight
x_{ac}	Distance from aircraft nose to aerodynamic center
x_{ac_h}	Distance from aircraft nose to aerodynamic center of horizontal tail
x_{cg}	Distance from aircraft nose to center of gravity
x_{fs}	Distance from aircraft nose to front wing spar
x_{rs}	Distance from aircraft nose to rear wing spar
x_{fbh}	Distance from aircraft nose to front bulkhead
x_{mlg}	Distance from aircraft nose to main landing gear
x_{nlg}	Distance from aircraft nose to nose landing gear
x_{rbh}	Distance from aircraft nose to rear bulkhead
X	Material maximum normal stress in x-direction
y	Coordinate of y-axis
y_1, y_2	Cross-section parameter
y_{eng}	Distance from aircraft symmetry line to aircraft engine
Y	Material maximum normal stress in y-direction
z	Coordinate of z-axis
z_{cab}	Cabin altitude
z_{op}	Maximum operating altitude

Greek symbols

α	Diagonal tension angle
β	Side slip angle
	Geometry constant
δ	Deflection
δ_e	Elevator deflection
$\delta_{e_{MAX}}$	Maximum elevator deflection
ΔC_L	Increment lift coefficient
Δp	Pressure difference
ΔS	Stress on panel
Δt	Thickness step
ε	Strain
η	Plasticity reduction factor
η_h	Tail configuration efficiency
θ	Cross-sectional angle
λ	Wave length
$\lambda_{\frac{1}{4}}$	Wing sweep angle at $^1/_4$ chord
λ_h	Horizontal tail sweep angle
λ_v	Vertical tail sweep angle
μ	Aircraft mass ratio
	Friction factor between main landing gear and ground
μ_v	Lateral mass ratio
ν	Poisson's ratio
ρ	Radius of inertia
	Density or air density at altitude
ρ_0	Air density at ground level
σ	Stress in material
σ_a	Stress amplitude
$\sigma_{0.2}$	Yield stress
σ_{circ}	Circumferential stress
σ_{crack}	Critical stress for crack growth
σ_{crip}	Forced crippling stress
σ_{cs}	Crippling stress

$\sigma_{fatigue}$	Fatigue stress
σ_{hoop}	Hoop stress
σ_{long}	Longitudinal stress
σ_x	Longitudinal stress, bending stress
σ_y	Circumferential stress
τ	Shear stress
τ_{bp_0}	Pocket shear buckling at $P = 0$
τ_{bp_i}	Pocket i shear buckling at $P = 0$, $i = 1, 2$
τ_{crit_0}	Critical shear stress at $P = 0$
τ_{xy}	Shear stress
ϕ_1, ϕ_2	Cross-sectional angle
ψ	Cross-sectional angle

Indices

adm	Admissible
all	Allowable
applied	-
b	Buckling
b/2	Midway between stiffeners
c	Compression, core material
comp	Compression
cr, crit	Critical
crip	Crippling
DT	Diagonal Tension
e	Elastic, effective
est	Estimation
f	Facing
flat	-
fr	Frame
FR	(Super) Frame
ir	Inter rivet
L	At frame
L/2	Midway between frames
L0	Zero slenderness

lateral	-
left	-
max	Maximum
n	Number of stringer $n = 1, 2, 3$
p	Plastic or skin pad
right	-
s	Secant
shear	-
sk	Skin
skin	-
st, str	Stringer/stiffener
ST	(Super) Stiffener
sti	Stiffener inner flange
stiffener	-
stsk	Stiffener skin side flange
t	Tangent or tension
tens	Tension
ult	Ultimate
yld	Yield

List of Acronyms

APU Auxiliary Power Unit

BC Boundary Conditions

C Clamped

CFRP Carbon Fibre Reinforced Plastics

CO_2 Carbon-dioxide

ESDU Engineering Sciences Data Unit

F Free

FEM Finite Element Method

HSB Handbuck Struktur Bereichnung

LL Limit Load

MAC Mean Aerodynamic Chord

MTOW Maximum Take Off Weight

MS Margin of Safety

MZFW Maximum Zero Fuel Weight

OEW Operating Empty Weight

PFatLL Percentage of pocket folding at limit load

RF Reserve Factor

SS Simply Supports

TH Tsai-Hill

UL Ultimate Load

Chapter 1

Introduction

In the aviation industry there is a drive towards more sustainable and low-emission aircraft due to market constraints and customer needs. The airline operators are demanding for reduction in operating cost, since there are concerns about the rising cost of fuel. Consequently, aircraft manufacturers are trying to build lighter aircraft in order to save fuel and reduce the CO_2 emissions. New and advanced materials are in an increasing degree adopted in aircraft structures to achieve this. The improvements of aircraft structures are mainly achieved by improving the material and configuration properties under the skin.

Therefore aircraft manufacturers have been gradually increasing its reliance on composite materials and Fiber Metal Laminates. For example, the Boeing 777 featured an all-composite empennage and composite floor beams. The Boeing 787 fuselage is built in five main sections consisting of composite materials that account for 50% of the aircraft's total structural weight. Another example is the introduction of Fiber Metal Laminates in the Airbus A380. Also new composite materials and production methods will be applied to the fuselage of the new Airbus A350.

In the past valuable data is successfully gathered for applications of these new materials, which has led to improvements on fabrication process and material quality. These improvements are now offering the technical and economical possibility to extend the application of new materials to the wing and fuselage structures.

However at this time a problem arises for material manufacturers, like Tata Steel. It becomes harder and opaque to decide what kind of materials should be developed and what the influences of these new materials would impose on the aircraft structure. The aircraft manufacturers have their highly developed analysis programs to predict the performance of materials, unfortunately material manufacturers are missing this luxury and are unfamiliar with the determination of running loads on a fuselage structure. An analysis tool for determining the running loads and evaluating the performance of new materials will give material manufacturers better insight in requirements for new materials for aircraft structure.

Within the scope of the above-described developments and the needs of material manufacturers, the potential of new materials and structural configurations in aircraft fuselages is investigated using a parametric analysis tool. This analysis tool is applied on both aluminum and composite material concepts.

1.1 Research objectives

The objective of this graduation project is to develop a parametric design, analysis and evaluation tool for both metal and composite fuselage configurations in order to gain insight in the structural performance of different material designs and obtain the required panel thickness of the analyzed configuration. This tool is validated with a fuselage of an Airbus A320 transport aircraft. The model objective is split in three parts:

- *Develop a parametric model for an aircraft fuselage to determine the running loads for various load cases.*
- *Extend the model in order to evaluate metal and composite fuselage configurations on the basis of specific design criteria for input panel thickness.*
- *Extend the model by adding an optimization process in order to obtain the required panel thickness with minimized weight.*

1.2 Model choice

In order to create the model several options are evaluated. For example, a decision has been made between creating an analytical model and a FEM model. For this project it is chosen to create an analytical model for several reasons. The easiest way to create a parametric geometry is changing the aircraft parameters, which is much easier on an input file than changing dimensions in a FEM model. Thus the input for an analytical model is also very easy and the model gives a fast global idea of the analyzed material. Further the analytical model explicitly formulates the behavior of the equations; therefore the documentation of the knowledge is clear. While the FEM model implicitly formulates the behavior of the equations, which is an implicit commitment of knowledge. Therefore a FEM model is not easy transmissible or easily extendable and adaptable, like the analytical model.

1.3 Methodology

For the evaluation of the fuselage structure, an extended analysis approach is used, including aircraft specifications, the identification of fuselage loads and evaluation of material and structural concepts. A parametric model is programmed in Visual Basic Application with the following set up, which fulfills the objective requirements of this thesis:

- The creation of the geometry and cross-section of the fuselage and determination of the moment of inertia of the structure.
- The analysis of the moments and forces on the fuselage for each load cases by creating a suitable sets of load distributions on the fuselage.
- The calculation of the running loads and stresses and evaluation of material and fuselage configurations.
- The optimization of the skin structure for metal structures.
- The extension of the evaluation and optimization process for composite materials.
- The calculation of structural weight of fuselage.

1.4 Structure of report

The report is setup as follows. First, the model assumptions are discussed in chapter 2. Secondly, a detailed overview about the theory used in the tool is given in chapter 3 for the geometry, chapter 4 for the applied forces on the fuselage, chapter 5 over the selected load cases, chapter 6 for determining the running loads and chapter 7 and 8 for the evaluation methodologies and optimization for the fuselage structure. The complete model procedure is explained in chapter 9. Further the validation results of the model are presented and discussed in chapter 10 and the composite discussion is given in chapter 11. Finally the conclusion and recommendation are given in chapter 12 and 13.

Chapter 2

Model Approach

In this chapter the assumptions made for the configuration are discussed and the data of the reference aircraft is given. The assumptions made are used to simplify the fuselage geometry in order to make it suitable for the tool. The data of the reference aircraft are needed to model the geometry and aircraft weight distribution.

2.1 Assumptions

The assumptions that have been made with regard to the configuration are:

- The method is designed for commercial transport aircraft.
- The aircraft has 2 or 4 engines attached to the wing.
- The main landing gear is attached to the wing.
- The wing loads are transferred into fuselage through the wing spars.
- The airframe equipment and services weight is modeled to be distributed across the fuselage length as are the fuselage structural weight and the payload.
- The tail weight, the tail lift force, the nose landing gear weight and the front and rear bulkhead weights are modeled as concentrated forces.
- When on the ground the normal force due to the nose gear is also modeled as a concentrated force.
- When on the ground the lift forces are zero.
- The fuselage cross-section can have a cylindrical, a double bubble or a triple bubble shape.
- The horizontal tail is attached to the fuselage.
- The fuselage is modeled without cut-outs (no windows, (cargo or service)doors, etc.)
- The fuselage is modeled without center wing box.
- The nose landing gear is located after front bulkhead.
- The aerodynamic center of horizontal tail is located before center of gravity of tail.
- The front and rear section cross-section radius is linearly changing.

2.2 Reference aircraft for validation

In this model an Airbus A320 is taken as reference aircraft to run and validate the model. General information about this aircraft is given below [1], which are needed for the input file, which is given in appendix C. The aircraft dimensions and basic operating data are given in table 2.1 and 2.2. In appendix A, detailed pictures of this aircraft are given. These dimensions are used as reference for the model geometry. The design weights of the Airbus A320 are given in table 2.3. These weights will be used to define the internal load distribution of the aircraft.

Overall length	37.57 m
Tail height	11.76 m
Fuselage diameter	3.95 m
Maximum cabin width	3.70 m
Cabin length	27.51 m
Wingspan (geometric)	34.10 m
Wing area (reference)	122 m^2
Wing sweep (25% chord)	25°
Wheel base	12.64 m
Wheel track	7.59 m
Cargo capacity	37.41 m^3

Table 2.1: Aircraft dimensions

Cockpit crew	Two
Seating capacity	180 (1-class, maximum), 164 (1-class, typical), 124 (2-class, typical)
Service ceiling	12,000 m
Range (w/max. passengers)	4,800 (6,100) km
Max. operating Mach number	0.82
Bulk hold volume	37.41 m^3
Engines	two V2500 or CFM56-5B
Engine thrust range	98-120 kN

Table 2.2: Basic operating data

Maximum ramp weight	73,900 (78,400) kg
Maximum takeoff weight	73,500 (78,000) kg
Maximum landing weight	64,500 (66,000) kg
Maximum zero fuel weight	61,000 (62,500) kg
Maximum fuel capacity	24,210 (30,190) L
Typical volumetric payload	16,600 kg

Table 2.3: Design weights

Chapter 3

Geometry

In this chapter a detailed overview of the geometry creation is given. The model is able to generate various fuselage geometries, since it is set up to be parametric. The fuselage length and shape as well as the fuselage cross-section are changeable. By changing the input parameters other aircraft fuselages can be generated. The fuselage consists of frames and bays. Each bay consists of stringers and skin panels. The stringers have fixed area and properties along the fuselage to be defined in the input file. For the skin panel an uniform initial thickness is chosen, however these initial thicknesses are changing for each panel depending on the evaluation criteria. There is also the possibility to enter the skin panel thicknesses manually.

3.1 Fuselage layout

The simplest modeling shape of a fuselage is assuming to be a cylinder. The length of the cylinder is equal to the length of the fuselage. However the nose and the tail sections of a fuselage are smaller compared to the center section of the fuselage. Therefore the fuselage model is split into three sections: the nose, center and tail section. The nose section has a starting radius of 20% of the original input radius; this radius linearly increases till the input radius. The whole center section is equal to the input radius. The tail section starts with a radius equal to the radius of the center section and decreases to 20% of this radius. The nose section starts at the nose of the fuselage and ends at the position of the nose landing gear, the center section goes from this point till the rear bulkhead and the tail section starts at the rear bulkhead till the tail end of the fuselage. The following layout for the fuselage is created.

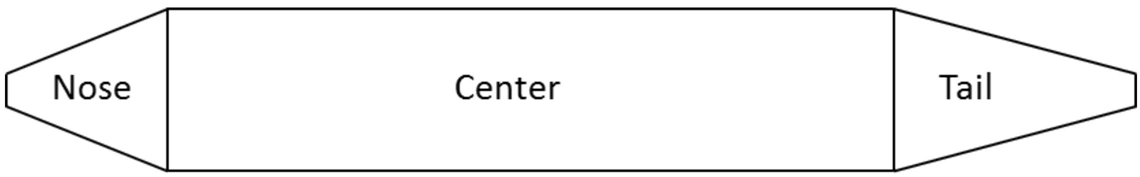

Figure 3.1: Fuselage lay-out

3.2 Frames and bays

The fuselage bending moment and shear forces change in longitudinal direction. Therefore it makes sense to divide the fuselage into multiple parts in lengthwise direction, by creating frames and bays. The fuselage frames are the circumferential reinforcements of the fuselage outer surface. The number of frames is variable by a minimum of seven and is an input for the model.

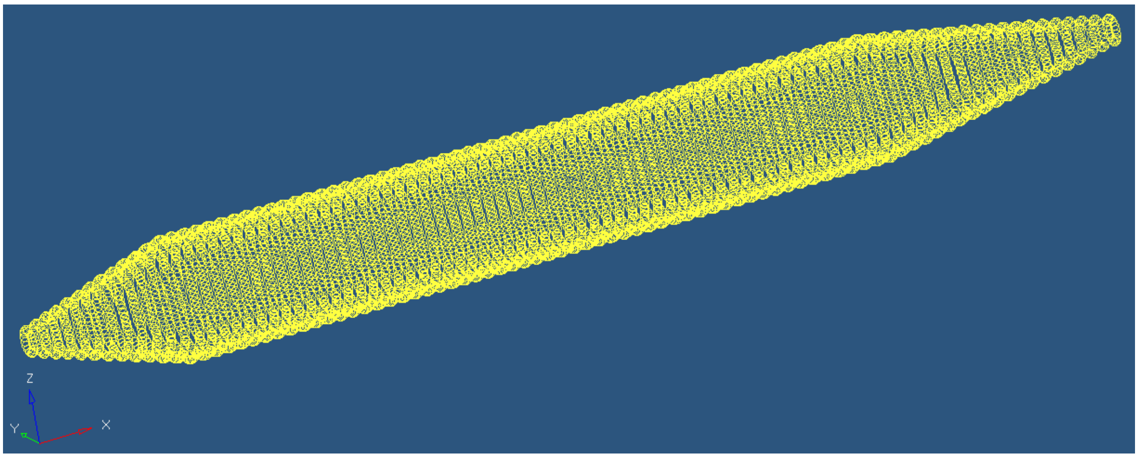

Figure 3.2: Fuselage lay-out generated in Hypermesh

In the fuselage there are seven fixed frames defined. The first frame is assumed at the nose and the last frame assumed at the tail end. Between these frames the other five frames are at the front and rear bulkhead, front and rear spar and nose landing gear location. The positions of these frames are dependent on the aircrafts specification; therefore it is an input for the model.

The positions of the remaining frames are divided by ratio depending on the distances between the fixed frames and are equally distributed between these fixed frames. The fuselage bay is the space between two frames and therefore dependent on the number of frames. The number of bays is equal to the number of frames minus one. The division of the fuselage in bays will allow dimensioning the different panels of the fuselage to the bending moment and shear force that apply to that specific location on the fuselage.

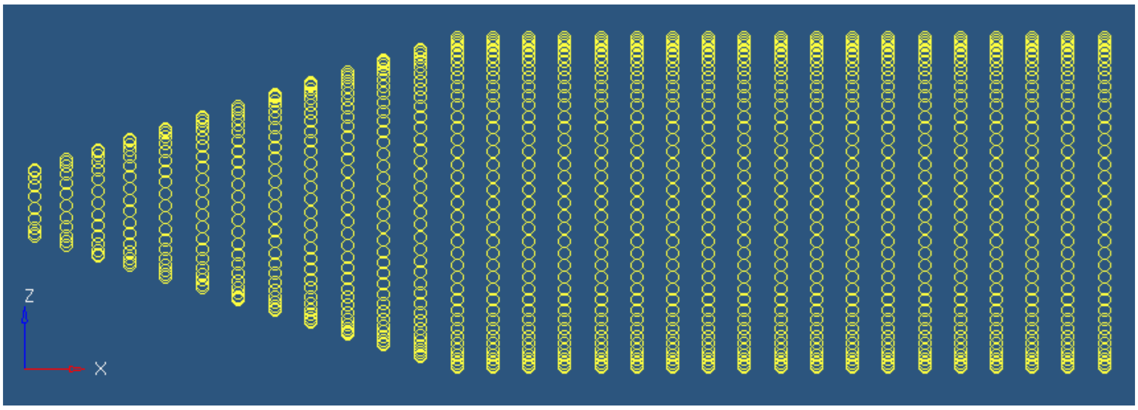

Figure 3.3: Fuselage frame distribution zoomed in front

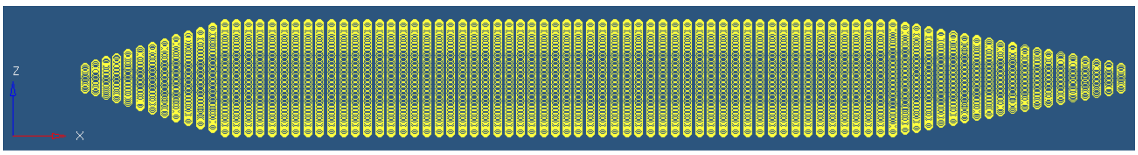

Figure 3.4: Fuselage frame distribution

3.3 Cross-section

In circumferential direction the loads have a different effect on the fuselage. A moment on the fuselage will cause bending of the fuselage. The top part will experience tension due to positive bending, the bottom part will experience compression and the sides will experience shear stresses. Therefore it is chosen to divide the cross-section in multiple skin parts, which depends on the number of stringers and hereby creates fuselage panels. This allows every fuselage panel to be dimensioned not only to the right moment or shear force, but also to the specific type of stress the fuselage panel is subjected to. This division allows every individual panel to be optimized for different materials. Therefore a mix of material in the fuselage design is an option. For this model

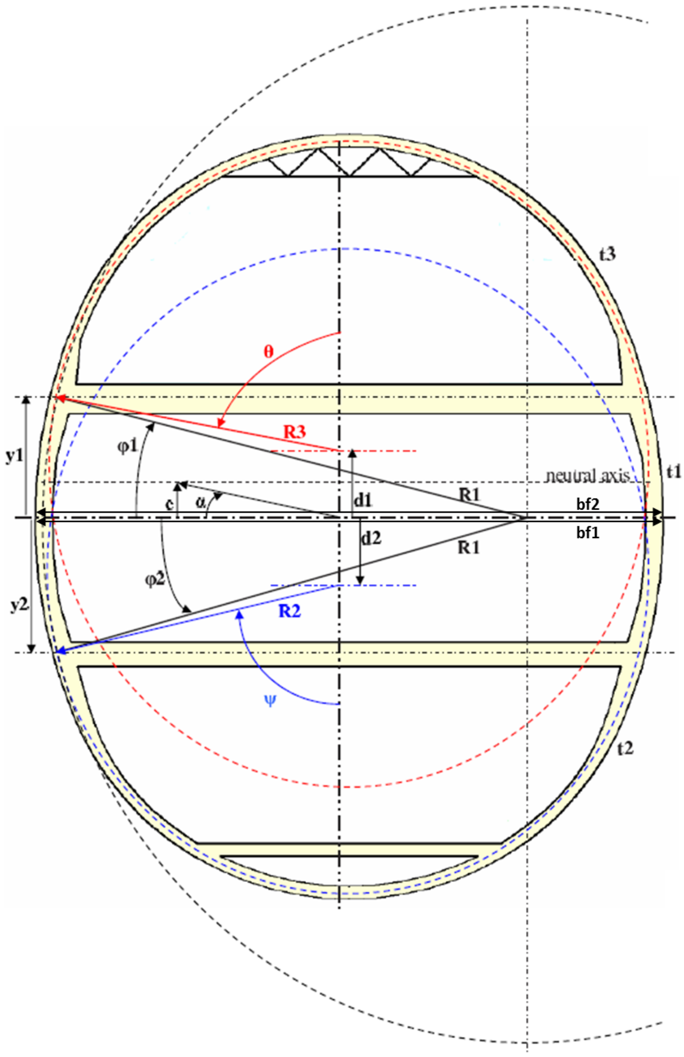

Figure 3.5: Definitions in fuselage cross-section

various cross-section types are definable using figure 3.5 [2]. The following relations (distances and angles) are needed to create the cross-section.

$$y_1 = 0.5\sqrt{2}\frac{b_{f_1}}{2} \qquad y_2 = 0.5\sqrt{2}\frac{b_{f_2}}{2} \tag{3.1}$$

$$\phi_1 = \arcsin\frac{y_1}{R_1} \qquad \phi_2 = \arcsin\frac{y_2}{R_1} \tag{3.2}$$

$$\theta = \frac{90 \cdot \pi}{180} - \arcsin\frac{y_1 - d_1}{R_3} \qquad \psi = \frac{90 \cdot \pi}{180} - \arcsin\frac{y_2 - d_2}{R_2} \tag{3.3}$$

For a cylindrical fuselage d_1 and d_2 will be zero, for a double bubble fuselage cross-section only d_1 or d_2 will be zero. The distances y_1 and y_2 determine the angles ϕ_1, ϕ_2, ψ and θ. These angles determine where the borders of the cross-sectional panel are. For a cylindrical fuselage each angle should be $45°$.

The stringers are evenly distributed on the cross-section. Using the cross-section relations the y and z coordinates of the stringers and mid-point of the skin panels are determined. The fuselage cross-section as results of the parametrical cross-section generation is generated in Hypermesh with plotting the y and z coordinates of stringers for the reference aircraft, which is given in figure 3.6.

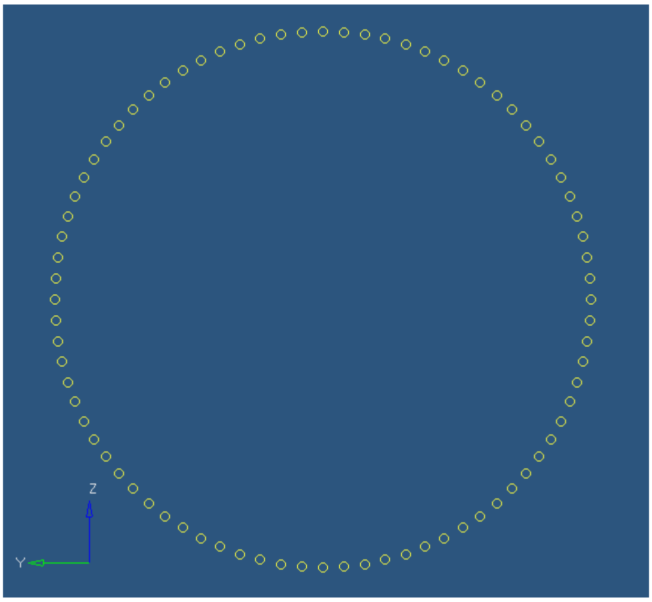

Figure 3.6: Cross-section of model generated in Hypermesh

3.3.1 Floor support beam

When considering a triple or double bubble fuselage cross-section a change in fuselage radius should coincide with the location of a floor and the panel border. This is necessary because a change in fuselage radius will cause a sideward force due to the unequal hoop stress. The floor members will carry this sideward force [3]. The equilibrium of this situation is as follows:

$$\sigma_1 = \frac{pR_1}{t_1} \qquad \sigma_2 = \frac{pR_2}{t_2} \tag{3.4}$$

$$\cos\alpha_2 = \frac{w}{R_1} \qquad \cos\alpha_2 = \frac{w}{R_2} \tag{3.5}$$

Vertical equilibrium:

$$pR_1\frac{w}{R_1} - pR_2\frac{w}{R_2} = 0 \tag{3.6}$$

Horizontal equilibrium:

$$pR_1 \sin\alpha_1 + pR_2 \sin\alpha_2 = T \tag{3.7}$$

The parameters are defined in figure 3.7.

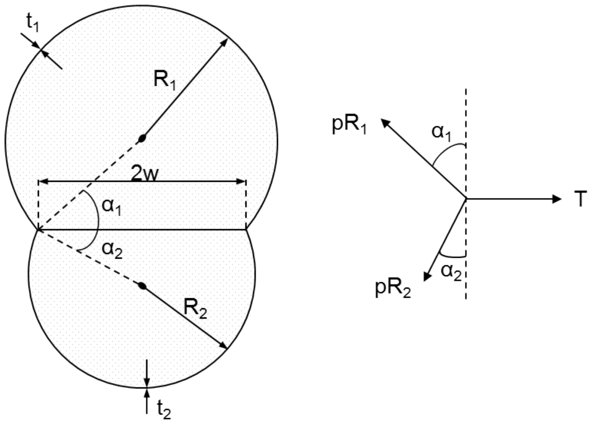

Figure 3.7: Floor beam allows cabin pressure to be carried by membrane stresses

3.3.2 Reference radius

Further for calculation of the hoop stress a reference radius is taken for double bubble or cylindrical, because a double bubble or cylindrical cross-section have various radii [4]. The determination of reference radius is seen in figure 3.8.

$$R_{ref} = R_A \qquad \text{or} \qquad R_{ref} = \frac{R_1 + R_1 + d_1 + d_2}{2} \tag{3.8}$$

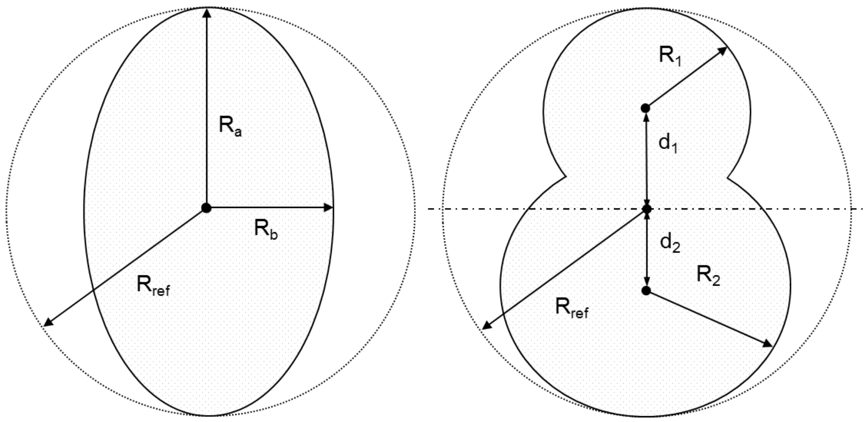

Figure 3.8: Reference ratio for cylindrical cross-section

3.4 Idealization of structure

The cross-section of the fuselage is idealized in order to simplify the calculation for the moment of inertia. The stringers are simplified to booms with area A_{str}, and location y_{str} and z_{str}. The (bended) skin panels are assumed to be flat with thickness t_{sk}, width b_{sk} and location y_{sk} and z_{sk}. A sketch of the idealization with the defined parameters is given in figure 3.9.

3.4.1 Neutral Axis

The neutral axis always passes through the centroid of area of a cross-section but its position of the neutral axis compared to the reference axis depends on the form of the applied loading and

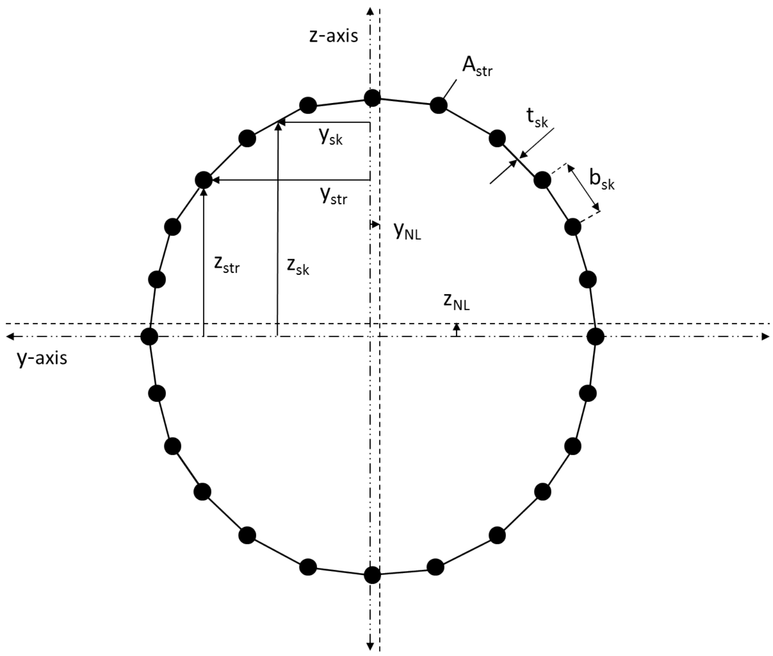

Figure 3.9: Idealization of the cross-section

the geometrical properties of the cross-section. The shift of the neutral line is determined by [5]:

$$y_{NL} = \sum_{n=1}^{N_s} \left[\frac{t_{sk_n} b_{sk_n} y_{sk_n} + \frac{E_{str}}{E_{sk}} A_{str_n} y_{sk_n}}{t_{sk_n} b_{sk_n} + \frac{E_{str}}{E_{sk}} A_{str_n}} \right] \tag{3.9}$$

$$z_{NL} = \sum_{n=1}^{N_s} \left[\frac{t_{sk_n} b_{sk_n} z_{sk_n} + \frac{E_{str}}{E_{sk}} A_{str_n} z_{sk_n}}{t_{sk_n} b_{sk_n} + \frac{E_{str}}{E_{sk}} A_{str_n}} \right] \tag{3.10}$$

Where N_s is the number of stringers and n is $1, 2, 3, \ldots, N_s$. The y and z axis are then $y = y_{ref} - y_{NL}$ and $z = z_{ref} - z_{NL}$, if the cross-section is not symmetric. Otherwise there is no difference between the reference axis and neutral axis.

3.4.2 Moment of Inertia

The moment of inertia of the cross-section is needed to calculated the stress distribution on the fuselage due to the bending moment, which will be discussed in chapter 6.

The moment of inertia around the y and z axis is given by [5]:

$$I_{yy} = \sum_{n=1}^{N_s} \left[t_{sk_n} b_{sk_n} z_{sk_n}^2 + \frac{E_{str}}{E_{sk}} A_{str_n} z_{sk_n}^2 \right] \tag{3.11}$$

$$I_{zz} = \sum_{n=1}^{N_s} \left[t_{sk_n} b_{sk_n} y_{sk_n}^2 + \frac{E_{str}}{E_{sk}} A_{str_n} y_{sk_n}^2 \right] \tag{3.12}$$

$$I_{yz} = \sum_{n=1}^{N_s} \left[t_{sk_n} b_{sk_n} y_{sk_n} z_{sk_n} + \frac{E_{str}}{E_{sk}} A_{str_n} y_{sk_n} z_{sk_n} \right] \tag{3.13}$$

3.5 Description of elements

3.5.1 Skin panel

The skin panels are assumed to be between two stringers with a thickness t_{sk} and spacing b_{sk}. The number of skin panels is equal to the number of stringers.

3.5.2 Stringer properties

The number of stringers is constant along the mid-section of the fuselage. In the front and rear section the number of stringers is determined by ratio depending on the size of the cross-section. This is done to prevent small stringer spacing at the front and rear section, since the cross-section is smaller.

In the first instance the stringer is idealized to a boom with a fixed area. This is done to determine the moment of inertia of the cross-section. In a later stadium a detailed property for the stringer is given to evaluate the stringer material as well as the stringer configuration. The detailed stringer can be created by defining the dimensions given in figure 3.10. During the material evaluation this property is also evaluated by determining the moment of inertia for the specific stringer.

3.5.3 Frame properties

The frame has the same mechanical properties as the stringer. The dimensions are defined similarly using the dimensions in figure 3.10.

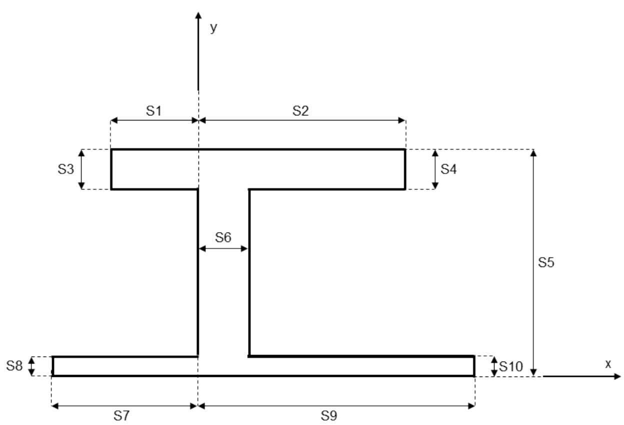

Figure 3.10: Stringer and frame properties

3.5.4 Padding properties

The padding is assumed to be integrated into the skin at the stringer side. Figure 3.11 shows an illustration of padding.

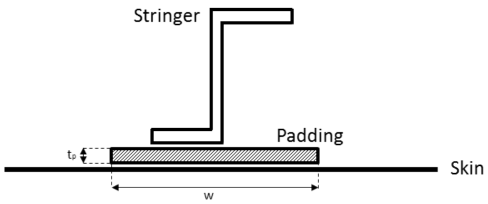

Figure 3.11: Padding properties

Chapter 4

Forces

In this chapter the weights and forces acting on the fuselage are explained. The Free Body Diagram for an aircraft fuselage is derived and the calculation of force and moment distribution on the fuselage is given.

4.1 Forces acting on fuselage

The forces that act on the aircraft's fuselage can be categorized in four different types:

- Aerodynamic forces
- Gravity forces
- Ground reaction forces
- Internal pressure

4.1.1 Aerodynamic forces

The aerodynamic forces are the lift and drag forces. The tail lift force is modeled as a concentrated force on the fuselage acting at the location of the horizontal stabilizer aerodynamic center. The wing lift force is transferred to the fuselage through the front and rear wing spar. The contribution of the drag to the bending moment is assumed to be negligible. The magnitude of the two lift components can be calculated as follows [6].

The lift forces equal the aircraft weight times the load factor, both when in horizontal equilibrium ($n = 1$) and when accelerating upward due to maneuvers or gust ($n \neq 1$). The value for the load factor is calculated using the load cases.

$$L = L_w + L_h = nW \tag{4.1}$$

The pitching moment around an axis through the aerodynamic center is:

$$M = M_{ac} + nW(x_{cg} - x_{ac}) - L_h(x_{ac_h} - x_{ac}) \tag{4.2}$$

The definition of the x locations are given in figure 4.1. The lift and pitching moment are defined as:

$$L = C_L \frac{1}{2} \rho V^2 S \tag{4.3}$$

$$M = C_m \frac{1}{2} \rho V^2 S \bar{c} \tag{4.4}$$

In non-dimensional form this can be written as:

$$C_m = C_{m_{ac}} + \frac{nW\frac{x_{cg}-x_{ac}}{\bar{c}}}{qS} - C_{L_h}\frac{(x_{ac_h}-x_{ac})}{\bar{c}}\eta_h\frac{S_h}{S} \tag{4.5}$$

The tail configuration efficiency is $\eta_h = \frac{q_h}{q} = 0.85$, $\bar{c}$ can be determined graphically in method by Torenbeek [7] and $C_{m_{ac}} = 0$ during flight. The horizontal tail lift coefficient:

$$C_{L_h} = \frac{C_{m_{ac}}\bar{c}qS + nW(x_{cg}-x_{ac})}{\eta_h qS_h(x_{ac}-x_{ac_h})} \tag{4.6}$$

The aerodynamic force found in this section is only to balance the aircraft during a steady flight with various load factors or for landing. Other aerodynamic forces will be introduced in chapter 5 for horizontal and vertical tail. These aerodynamic forces are included separately and are added above the steady aerodynamic forces depending on the used load cases.

4.1.2 Gravity forces

The gravity forces are the forces exerted on the fuselage by the weight of the aircraft components, such as wing, tail and bulkheads. The total aircraft weight is the weight of payload, fuel and operational empty weight (OEW):

$$\mathrm{MTOW} = \mathrm{OEW} + W_{fuel} + W_{pay} \tag{4.7}$$

The fuel weight and the payload are inputs for the model. The fuel is stored in the wing and sometimes partly in the wing-fuselage center section. The payload consist of passengers and cargo together. The payload is evenly distributed between the front and rear bulkhead.

The OEW is divided into three groups that can each be divided into smaller groups:

- Airframe structure

  This group consists of wing, fuselage, tail, landing gear and surface controls.

- Propulsion group

  The propulsion group consists of the engines; items associated with engine installation and operation, the fuel system and thrust reversing provisions.

- Airframe equipment and services

  This group includes the APU, instruments, hydraulic, electric and electronic systems, furnishing and equipment, air conditioning, anti-icing equipment and some other miscellaneous equipment.

The calculation of all weight components will be treated in appendix B. Table 4.1 and figure 4.1 show the distribution of all weight components. The weights of both bulkheads are modeled as concentrated forces acting on the fuselage. The same holds for the weight of the nose landing gear, the tail weight, the tail plane lift force and the nose wheel reaction force. The last is of course only taken into account when the aircraft is on the ground. When the aircraft is on the ground the lift forces are assumed to be zero. There are two other discrete forces acting on the fuselage. These are the forces exerted by the front and rear wing spar. The sum of these forces are calculated by solving the horizontal equilibrium of the fuselage:

$$F_{fs}+F_{rs} = n\cdot(q_1l_1+q_2l_2+q_3l_3+q_4l_4+q_5l_5+q_6l_6+W_{fbh}+W_{rbh}+W_{nlg}+W_{tail})-N_{nlg}-L_h \tag{4.8}$$

By taking the moment around the rear wing spar the front spar force is calculated as follows:

$$\begin{aligned} F_{fs} = \frac{1}{(x_{rs}-x_{fs})}\cdot\Big(&\frac{1}{2}nq_1l_1^2 + nq_2l_2(\frac{1}{2}l_2+l_4) + \frac{1}{2}nq_4l_4^2 + nq_6l_6(l_2+l_4+\frac{1}{2}l_6) \\ &+nW_{fbh}(l_2+l_4) + nW_{nlg}(x_{rs}-x_{nlg}) - \frac{1}{2}n(q_1+q_3)l_3^2 - nq_5l_5(l_3+\frac{1}{2}l_5) \\ &-nW_{tail}(x_{cg_h}-x_{rs}) - nW_{rbh}(x_{rbh}-x_{rs}) + L_h(x_{ac_h}-x_{rs})\Big) \end{aligned} \tag{4.9}$$

Load	Weight components	Range
q_1	Fuselage, passenger floor, air conditioning system, electrical system, furnishing and equipment, hydraulic and pneumatic system, instruments, navigational and electronic system, surface control group, automatic pilot system, cockpit controls, payload, miscellaneous	front bulkhead - rear bulkhead (l_1)
q_2	Front cargo floor	front bulkhead - front spar (l_2)
q_3	Rear cargo floor	rear spar - rear bulkhead (l_3)
q_4	Wing-fuselage support structure, center section fuel	front spar - rear spar (l_4)
q_5	APU, tail plane support structure	rear spar - end of fuselage (l_5)
q_6	none	nose - front bulkhead (l_6)

Table 4.1: Distribution of aircraft weight components

Using equation 4.8 and 4.9 the rear spar force can be calculated. Since all the forces and weights acting on the fuselage are known the load (force and moment) distribution can be created. This will be treated in section 4.2.

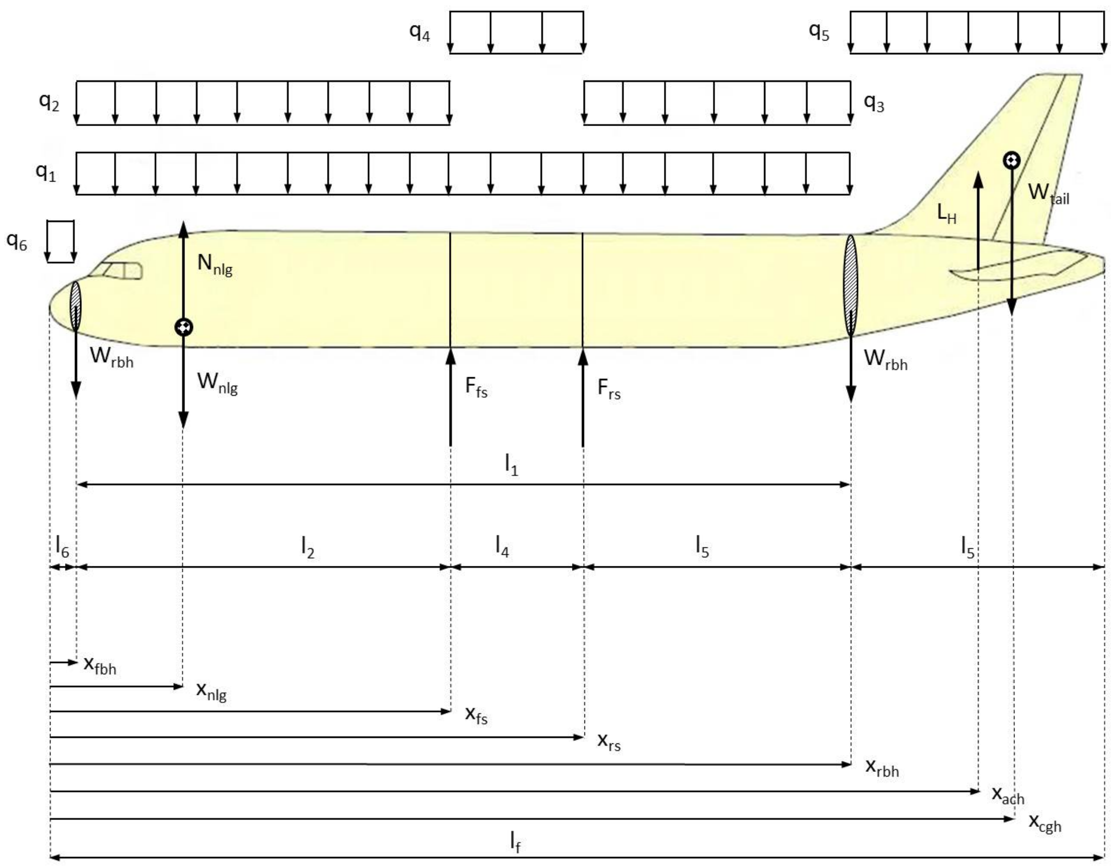

Figure 4.1: Forces acting on the aircraft

4.1.3 Ground reaction forces

Ground reaction forces are forces resulting from ground maneuvering and are transferred into the fuselage through the front landing gear and the front and rear spar (which transfer the loads from the main landing gear). Ground reaction forces include forces resulting from landing and braking. In case of a landing the fuselage is bent in the same way as during in-flight maneuvering. Niu [8] states that the load factor resulting from landing is smaller than the maximum load factor. The larger the aircraft the lower the landing load factor. The landing load case will be discussed in section 5.7. A braked roll as stated by the FAR regulations §25.493 will be treated in section 5.9.

4.1.4 Internal Pressure

During flight an artificial pressure level is maintained in the fuselage which is essential for transporting people. The resulting pressure difference results in a hoop stress in the fuselage skin. In circumferential direction hoop stress is largest [4]:

$$\sigma_{hoop_{circ}} = \frac{\Delta p R}{t} \tag{4.10}$$

In longitudinal direction the hoop stress is:

$$\sigma_{hoop_{long}} = \frac{\Delta p R}{2t} \tag{4.11}$$

The pressure difference Δp is the internal pressure minus the pressure at maximum cruise altitude. The internal pressure level is equal to a pressure altitude of 2400 m. Recent designs like the Airbus A350 and Boeing 787 use a higher internal pressure that is more comfortable to the passengers. This pressure is equal to a pressure altitude of 1800 m. As a consequence the pressure difference increases from about 49500 N/m^2 to about 61500 N/m^2. This will increase the minimum skin thickness needed to withstand the pressure difference. In section 5.11 the pressurization will be treated.

4.2 Load distribution

The forces described in section 4.1 produce a bending moment and a shear force in the fuselage structure. The loads vary in lengthwise direction. To obtain the right bending moment and shear force on each fuselage bay the load distribution is calculated using a method by Timoshenko [9]. This method considers the fuselage as a beam loaded by forces and moments. These forces produce internal forces at the cross-section of the beam. The illustration in figure 4.2 shows how these internal forces and moments are calculated for one fuselage cross-section considering it as a cantilever beam [2].

The beam is loaded by a force F at location corresponding to the current frame location. The beam is cut at location x, which corresponds to the location of the next frame. The left part is isolated as a free body. To keep the body in equilibrium a force D and a moment M_B at the cross-section counteract the force F and moment M_A at the other end. Actually D and M_B represent the action of the right hand part of the beam on the left hand part. The vertical equilibrium of forces and the moments around the cross-section give:

$$\sum F = 0 \rightarrow D = F \qquad \sum M = 0 \rightarrow M_B = Fx + M_A \tag{4.12}$$

The force D and bending moment M_B for fuselage frame B have now been determined. The internal forces for the next frame are calculated in the same way. The force F is then force D and moment M_A is M_B.

This method is applied to the entire fuselage. The acting forces and moments are calculated for each fuselage cross-section. A force and moment line across the entire fuselage is obtained. These resulting force and moment lines are used to determine the running loads. For running load determination the acting forces and moments on a bay are used. Therefore forces and moments on the current bay are obtained by interpolation between the two neighboring frames.

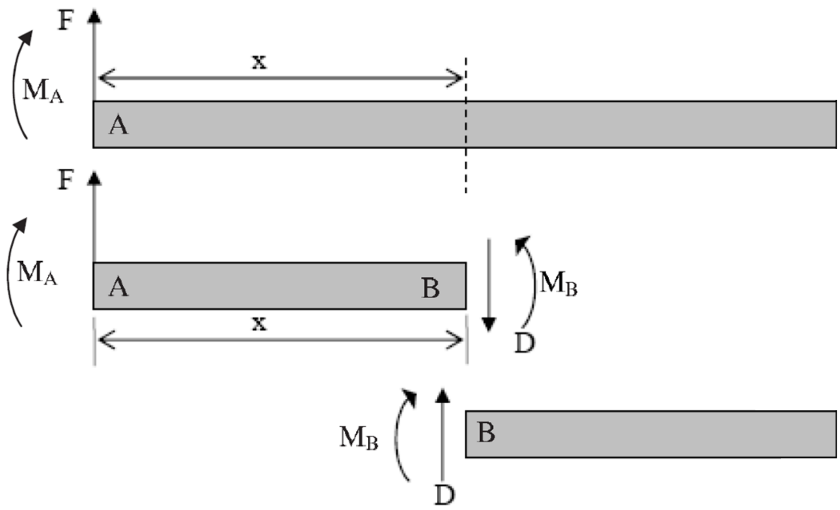

Figure 4.2: Calculation of load distribution

Chapter 5

Load cases

In this chapter the load cases are discussed, which are used in the model to generate a load distribution among the fuselage structure. Each load case can happen once a lifetime or even every flight. The aircraft structure should be designed to withstand the forces for each load cases and even for a combination of load cases.

5.1 Aviation regulations

The aviation regulations for large airplanes are clustered in the JAR-25 [10]. These are technical requirements, which define how aircraft manufacturers should prove that structural integrity of their aircraft is guaranteed to ensure the safety of persons, either direct or indirect, with an acceptable small possibility of fatal accidents.

As far as fuselage structures are concerned, the requirements address four different load categories, i.e. flight loads, flight loads combined with internal pressure, ground loads and internal overpressure alone. The aircraft structure must be able to withstand the described conditions in combination with the aircraft operational configuration at the time of these conditions. A thorough analysis of these load cases is hence required.

5.2 Limit load cases

Several load cases are considered as the dominant conditions for the fuselage analysis and therefore considered in this analysis. These limit load cases are:

Flight cases (with and without cabin pressurization)

- Symmetric maneuver and gust loads
- Lateral gust
- Horizontal tail elevator deflection
- Side slipping flight

Ground cases

- Three-point landing
- Two-point landing
- Abrupt ground braking

Internal pressurization

- Cabin pressurization (1.33 times normal pressurization)

Using the available aircraft data, the fuselage loads are estimated by implementing theoretical approaches. The fuselage load estimations are bases on both theory and practice provided by Lomax [11] and Torenbeek [7] bundled in Astori [12]. The implemented methods are described in the next section. All loads mentioned are limit loads. Unless stated otherwise a safety factor of 1.5 has been applied to obtain the ultimate loads, FAR §25.303.

5.3 Unit and combined load cases

	Unit Load Cases (ULC)	**Load**
ULC1	Cabin Pressurization	Pressurization (no aerodynamic loads, no weights)
ULC2	1G	Weight (no aerodynamic loads, no pressurization)
ULC3	Lateral Gust	Vertical tail side gust (no weight, no pressurization)
ULC4	Symmetrical Horizontal Tail Deflection	100-100% distribution downward (-) and upward (+) (no pressurization, no weight)
ULC5	Side Slipping Flight	Vertical tail reaction (no pressurization, no weight)
ULC6	Three-point Level Landing	Weight, nose landing gear reaction (no pressurization, no aerodynamic loads)
ULC7	Abrupt Ground Breaking	Weight, nose landing gear reaction and horizontal distributed acceleration (no pressurization, no aerodynamic loads)

Table 5.1: Unit load cases

	Combined Load Cases (CLC)	**ULC**
CLC8	-1G Maneuver	-ULC2
CLC9	-1G Maneuver + Cabin Pressurization	-ULC2 + ULC1
CLC10	2.5G Maneuvre	2.5·ULC2
CLC11	2.5G Maneuver + Cabin Pressurization	2.5 · ULC2 + ULC1
CLC12	Lateral Gust + Cabin Pressurization	ULC3 + ULC1
CLC13	-Lateral Gust + Cabin Pressurization	-ULC3 + ULC1
CLC14	Horizontal Deflection Upward + Cabin Pressurization	ULC4 + ULC1
CLC15	1G Maneuver + Horizontal Deflection Upward	ULC2 + ULC4
CLC16	1G Maneuver + Horizontal Deflection Downward	ULC2 - ULC4
CLC17	1G Maneuver + Cabin Pressurization + Horizontal Deflection Downward	ULC1 + ULC2 - ULC4
CLC18	1.33 times Cabin Pressurization ($1.33 \cdot \Delta p$)	1.33 · ULC1

Table 5.2: Combined load cases

5.4 Maneuver loads

In-flight maneuvering causes a maneuver load factor. This factor represents the ratio of the aerodynamic force to the weight of the airplane. The maneuvering envelope (V-n diagram) describes the variation of the load factor with airspeed for maneuvers [6], see figure 5.1. At lower speeds the maximum load factor is constrained by the maximum lift coefficient; at higher speeds it may be restricted as specified by JAR §25.337, for civil transport category aircraft.

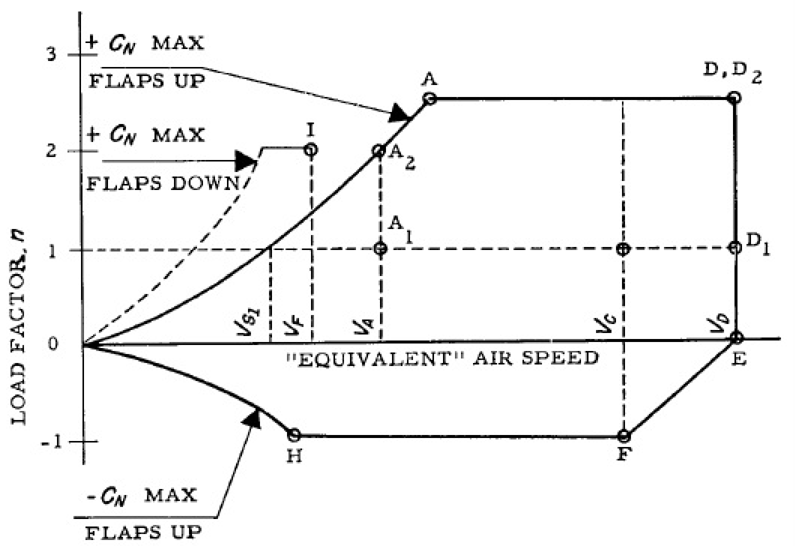

Figure 5.1: Maneuvering loads

The formula that links the velocity with load factor, when no additional constraints are defined, comes from the definition of lift and load factor as follows:

$$V_E = \sqrt{\frac{nW}{\frac{1}{2}\rho C_L S}}\sqrt{\frac{\rho}{\rho_0}} \tag{5.1}$$

Where, n is the load factor, W is the aircraft weight, ρ and ρ_0 the air density at altitude and ground level, C_L is the maximum lift coefficient, and S is the wing reference area.

The maximum lift coefficient can be estimated with simplified formulas based on Howe [13]:

$$C_L = 1.5\cos\lambda_{\frac{1}{4}}, \quad \text{flaps up} \qquad C_L = (1.5 + \Delta C_L)\cos\lambda_{\frac{1}{4}}, \quad \text{flaps down} \tag{5.2}$$

Where, $\lambda_{\frac{1}{4}}$ is the sweep angle at 25% chord and ΔC_L is the lift coefficient maximum increment due to loading and trailing edge flaps extraction. The latter factor ΔC_L depend on the type of high lifting devices installed.

The positive and negative maneuver load factors can be fixed to 2.5 and -1.0. The maximum bending moment on the fuselage will be obtained for this maximum load factor in combination with maximum airplane weight. In calculation it is assumed this weight is the MTOW. In the free body diagram method described in section 4.1.2 all weight components will be multiplied with this load factor.

Due to the weight distribution and the load factor the fuselage will experience downward bending moment for positive load factor, which will cause tension at top panels, compression at bottom panels and shear at side panels with the maximum forces at the center section of the aircraft, where the bending moment and forces are the largest. If the load factor is negative, top panels will experience compression, the bottom panels will experience tension and side panels shear. These load case will have large impact in dimensioning of the mid-section of the aircraft.

5.4.1 Gust load factor

Besides maneuver loads the flight loads include gust loads. When an aircraft in flight counters an upwards gust it experiences a very rapid change in direction of relative wing. The aircraft will experience an angle of attack increase. Assuming no change in forward velocity this larger angle of attack will lead to a larger lifting force. This in turn means an increase in load factor. The link between airspeed and load factor is linear and defined by [6]:

$$n = 1 \pm \frac{k_g C_{L_\alpha} \frac{1}{2} \rho_0 V_E U_E}{\frac{W}{S}} \tag{5.3}$$

Where n is the load factor, W is the aircraft weight, C_L is the lift coefficient, α is the angle of attack, S is the wing reference area, k_g is the gust alleviation factor, U_E is the equivalent gust velocity, V_E is the equivalent airspeed and ρ_0 is the air density at ground level.

The gust alleviation factor, which accounts for the fact that a gust is not sharp-edged, is defined as follows:

$$k_g = \frac{0.88\mu}{5.3 + \mu} \tag{5.4}$$

Where the aircraft mass ratio μ is defined by:

$$\mu = 2\frac{W/S}{\rho g C_{L_\alpha}} \tag{5.5}$$

Where W/S is the wing loading, g is the gravity acceleration and ρ is the air density.

The inertia factor of the aircraft is represented by C_{L_α}, the lift curve slope. The lift curve slope is a function of Mach number and is described by Howe [13]:

$$C_{L_\alpha} = \frac{2\pi}{\frac{2}{A} + \sqrt{(\frac{2}{A})^2 + \frac{1}{\cos^2 \lambda} - M_{cr}^2}} \tag{5.6}$$

Where A is the wing aspect ratio, λ is the wing sweep angle and M_{cr} is the critical Mach number.

The gust velocity and the aircraft forward velocity influence the load factor as well. When at very high speeds a high speed gust is encountered it will lead to a very high load factor. Therefore boundaries have been set for aircraft speed-gust combinations that are not to be exceeded by the pilot. This is depicted in the gust load diagram in figure 5.2. The dotted lines indicate the gust speeds, the continuous lines form the operating boundary.

The gust velocity U_E is by regulations [10] defined as a function of the flight airspeed and altitude, as indicated in table 5.3. V_B is the design speed for maximum gust intensity, V_C is the cruise speed and V_D is the dive speed. At altitudes higher than 20000 ft the gust velocity must be interpolated with the value at 50000 ft.

Gust velocities U_E [ft/s]		
Airspeed	0 to 20000 ft	50000 ft
V_B	66	38
V_C	50	25
V_D	25	12.5

Table 5.3: Gust velocities

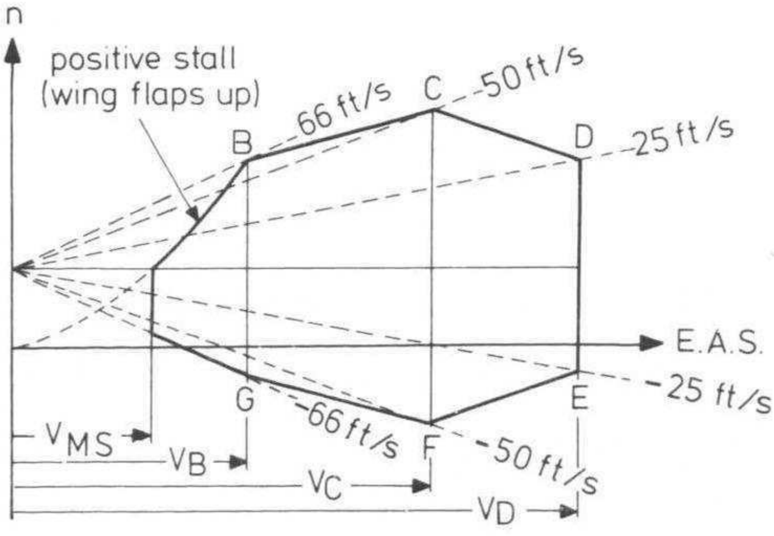

Figure 5.2: Gust envelope

The parameter influencing the gust load factor is the wing loading W/S. The higher the wing loading the lower the gust load factor will be. Large aircraft generally have a higher wing loading than smaller aircraft and will be less sensitive to gust. For a specific aircraft the highest gust load factor on the fuselage is obtained for the configuration in which the aircraft has the smallest wing loading, i.e. when flying empty. This makes a straightforward comparison of the gust and maneuver load case based on the load factor difficult. In case the gust load factor is higher, the gust load case does not necessarily result in a higher fuselage bending moment or shear force since the mass in this case smaller.

The positive and negative gust load factors can also be fixed to 2.5 and -1.0. The maximum bending moment on the fuselage will be obtained for this maximum load factor in combination with maximum airplane weight (MTOW). The loads experienced during gust is assumed to be equal to critical maneuver load; therefore the model will be run for the load factor 2.5 and -1.0.

5.5 Lateral gust

The lateral gust loads on the vertical tail seem to be more important than the loads due to abrupt maneuvers, over swing, abrupt check backs and engine out conditions, according to Lomax [11]. The lateral gust formula according to JAR-25 [10] is hereafter reported:

$$L_v = k_g \cdot \frac{1}{2}\rho_0 \cdot U_E \cdot V_E \cdot S_v \cdot C_{L_{v_\beta}} \tag{5.7}$$

Where L_V is the side load on vertical tail, C_{L_V} is the side lift coefficient, β is the side slip angle, S_V is the vertical tail reference area, k_g is the gust alleviation factor, U_E is the equivalent gust velocity, V_E is the equivalent airspeed and ρ_0 is the air density at ground level.

The gust alleviation factor is defined by:

$$k_g = 0.88\frac{\mu_v}{5.3 + \mu_v} \tag{5.8}$$

Where μ_v is the lateral mass ration, defined by:

$$\mu_v = 2\frac{I_Z}{\rho \bar{c}_v C_{L_{v_\beta}} S_v l_v^2} \tag{5.9}$$

Where finally I_Z is the aircraft yaw moment of inertia, c_v is the mean geometric chord of the vertical tail, l_v is the distance between aircraft center of gravity and vertical tail lift center and ρ is the air density at altitude. I_Z is approximately determined by considering the fuselage and wings to be a couple of prismatic bodies, with mass uniformly distributed.

Since the vertical tail is typically a low aspect ratio wing with high fuselage interference, the side lift coefficient derivative with respect to side slip angle β cannot be computed with the usual wing method, but better with the following formula, provided by Torenbeek [7]:

$$C_{L_{v_\beta}} = \frac{2\pi}{1 + \frac{3}{A_v \cos \lambda_v}} \tag{5.10}$$

Where A_v is the vertical tail aspect ratio and λ_v is the vertical tail sweep angle. The considered gust velocities are given in table 5.3. The used gust velocity is 50 ft/s. The load is concentrated in the vertical tail aerodynamic center, as shown in figure 5.3.

The lateral gust causes compression and tension on the side panels. The variation of compression or tension depends on the direction of the lateral force. The top and bottom panels are subjected to shear. The focus of the load lies on the mid and rear section, since the lateral force is kept in equilibrium by the lateral spar forces. This load case will be critical for dimensioning of the panels in the mid and rear section of the fuselage.

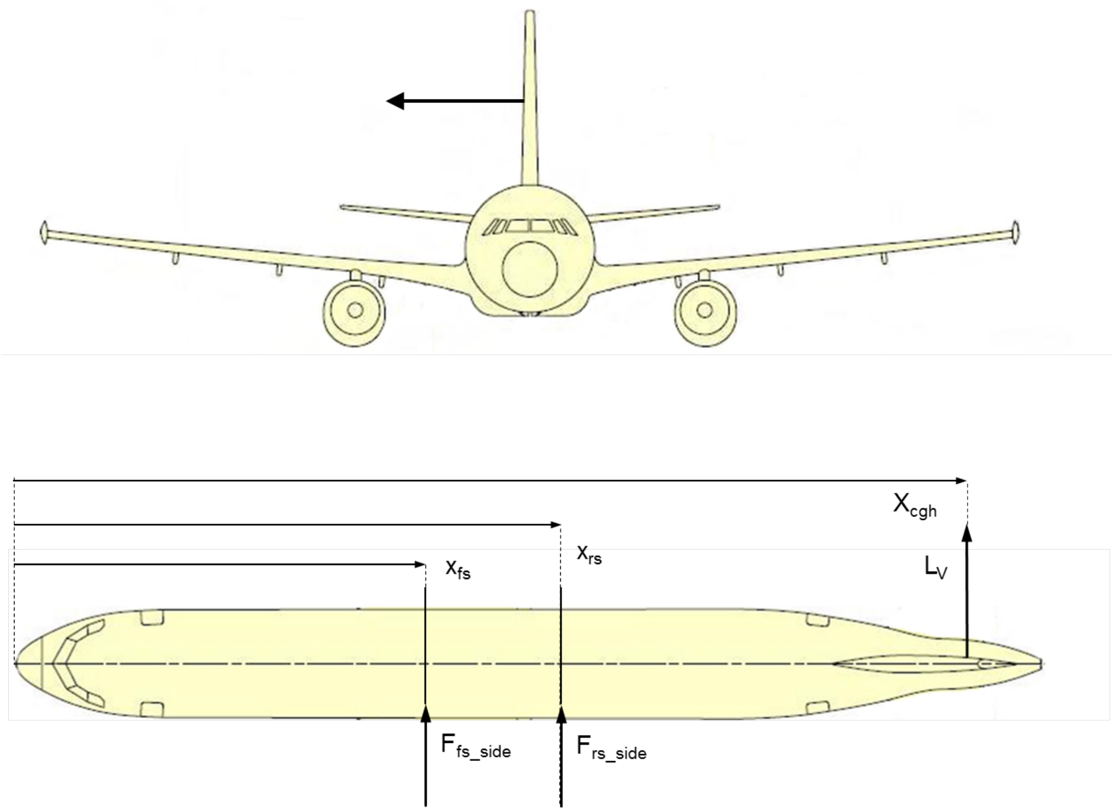

Figure 5.3: Vertical tail load

5.6 Horizontal tail elevator deflection

The elevator deflection condition concerns an asymmetrical and symmetrical horizontal tail load as indicated in JAR-25 [10]. In the symmetrical case 100% of the maximum loading are acting on both semi-tails, however in the asymmetrical case 100% of the maximum loading act on one semi-tail and 80% on the other. In this model only the symmetrical case is used, with possibility to change to the asymmetrical case when desired. Further the horizontal tail load can work downwards and upwards, both conditions are taken into account.

A simplified approach derived from [11], considers the maximum tail load L_H consequent to an abrupt elevator maneuver, described by 5.11.

$$L_h = k_r \cdot \frac{1}{2}\rho V^2 \cdot S_h \cdot \ C_{L_{h_{\delta_e}}} \cdot \delta_{e_{MAX}} \tag{5.11}$$

Where C_{L_h} is the tail coefficient, S_h is the horizontal tail reference surface, δ_e is the elevator deflection, k_r is the aircraft response factor for abrupt elevator maneuvers and ρ is the air density at altitude.

This formula neglects the balanced 1G tail lifting condition that normally is negligible with respect to maximum tail load. It is advised by Lomax [11] to set $k_r = 0.9$, that is actually a worst condition since it ranges from 0.7 to 0.9. The computation of L_H requires the evaluation of the derivative $C_{L_{h_{\delta_e}}}$, which is given by [7]:

$$\frac{C_{L_{h_{\delta_e}}}}{C_{L_{h_\alpha}}} = \sqrt{\frac{S_e}{S_h}} \tag{5.12}$$

Where α is the angle of attack, S_e is the elevator surface and S_h is the horizontal tail surface.

The lift coefficient slope can be estimated with the following equation already mentioned in the vertical tail calculations:

$$C_{L_{h_\alpha}} = \frac{2\pi}{1 + \frac{3}{A_h \cos \lambda_h}} \tag{5.13}$$

Where A_h is the horizontal tail aspect ratio and λ_h is the horizontal tail sweep angle. The illustration of the symmetrical loading on the horizontal semi-tails, with loads applied to the aerodynamic centers, is given in figure 5.3.

The horizontal deflection causes tension at top panels and compression at bottom panels if it works downward. Compression at top panels and tension at bottom panels are caused if the horizontal force works upward. In both cases the side panels experience shear. The horizontal force is critical for the mid and rear section, since the force is kept in equilibrium by the two wing spar forces.

5.7 Three-point level landing

For the three-point level landing condition, the nose landing gear vertical reaction is relevant for structural analysis. The computation includes the horizontal component due to wheel spin-up. The nose landing gear vertical reaction V_N is given by Lomax [11]:

$$V_N = (n_L - 1)W\frac{F}{1+F} \tag{5.14}$$

Where n_L is the landing load factor and W is the weight of the aircraft. Variable F is defined by:

$$F = \frac{b + 0.25e_M}{a + b - 0.25e_N} \tag{5.15}$$

Where, a is the horizontal distance between nose landing gear and center of gravity, b is the horizontal distance between main landing gear and center of gravity and h_{cg} is the height of center

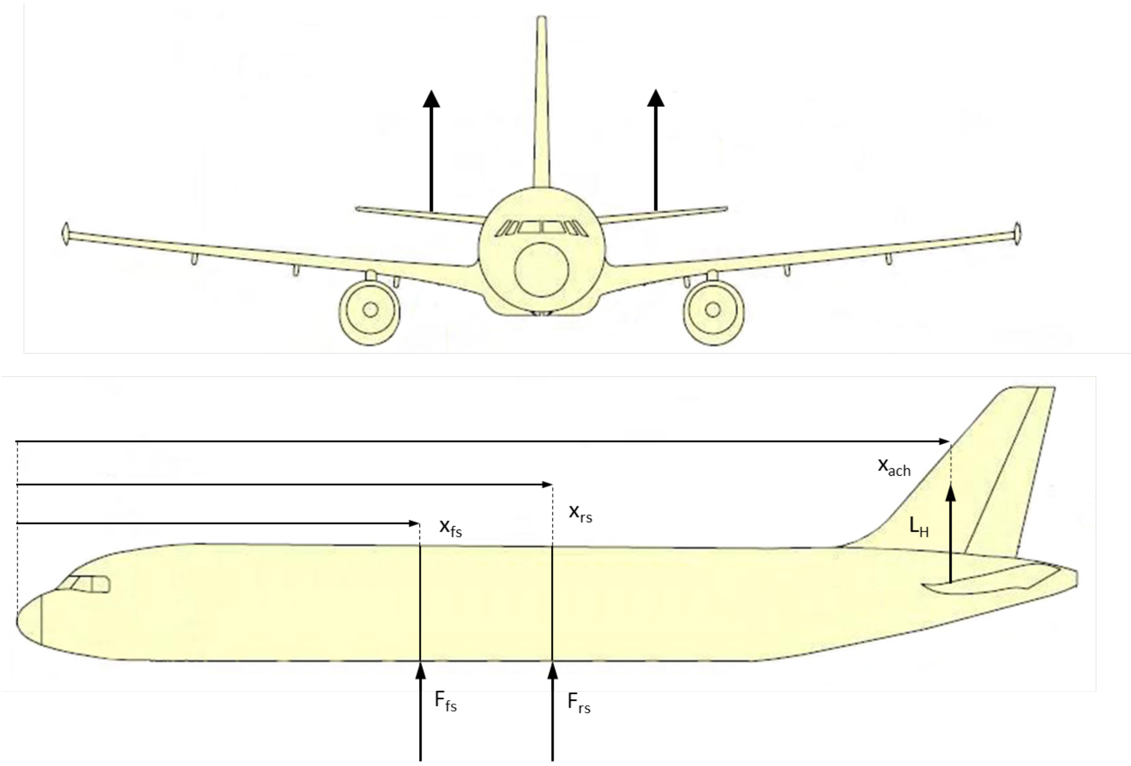

Figure 5.4: Symmetrical horizontal tail loads

of gravity to ground. Further, $e_M = h_{cg} - r_M$ and $e_N = h_{cg} - r_N$ with r_M is the main gear wheel rolling radius and r_N is the nose gear wheel rolling radius. The illustration of situation is given in figure 5.5

The horizontal component on the gears due to spin up can be estimated as follows:

$$H_M = 0.7 \cdot V_M \tag{5.16}$$

$$H_N = 0.7 \cdot V_N \tag{5.17}$$

The horizontal landing gear components are relevant for landing gear strut sizing and not in the fuselage stress distributions; therefore it is neglected in this case.

Normally the landing load factor n_L is set to values lower than 2.5 for the transport category aircraft. In this case a landing load factor of 2 is assumed in order to find the load distribution due to the landing.

The landing will have a compared load distribution with the maneuver and gust load distributions, since the aircraft is still flying on the ground, only a normal force is expected in the nose.

5.8 Two-point level landing

This load condition is eliminated, because available references indicate that typical load factors for the transport category aircraft are lower than 2.5; then this load condition is reasonably included in the symmetrical maneuver/gust loads.

![h]

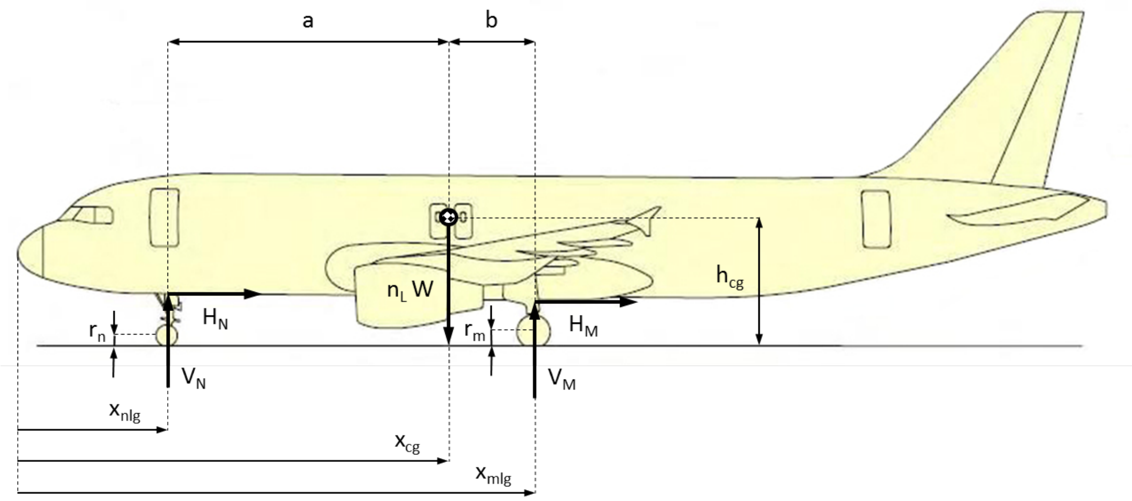

Figure 5.5: Forces during three-point level

5.9 Abrupt ground breaking

The worst condition is the start of full braking, which induces a pitch nose down angular acceleration and consequent overload on the nose landing gear. The breaking is considered to be at its limit level given by the maximum friction factor between the ground and the tire. The main landing gear wheels are considered to brake only, since the nose wheels are free.

According to JAR §25.493 [10], the nose landing gear vertical reaction V_N due to a sudden breaking is given by the following equation:

$$V_N = \frac{W}{a+b} \cdot \frac{f \cdot \mu \cdot a \cdot h_{cg}}{a+b+\mu \cdot h_{cg}} \tag{5.18}$$

Where, W is the weight, a is the horizontal distance between nose landing gear and center of gravity, b is the horizontal distance between main landing gear and center of gravity and h_{cg} is the height of center of gravity to ground, μ is the friction factor between the main landing gear and ground, which is normally 0.8, and f is the dynamic factor, which is normally 2.0. The illustration of situation is given in figure 5.6.

Since this condition the aircraft is breaking, a longitudinal component of acceleration should be considered. The acceleration is approximated as followed. The vertical load on main landing gear, in steady conditions, is given by:

$$V_M = W - V_N \tag{5.19}$$

This is a rather hazardous hypothesis, because the nose landing gear load is computed with a dynamic factor, meaning that the aircraft is experiencing a pitch rotational acceleration.

If the braking is done close to the maximum friction coefficient μ, the longitudinal force is described by:

$$H_M = \mu \cdot V_M \tag{5.20}$$

This means an acceleration of the aircraft given by:

$$a = \frac{H_M}{M} \tag{5.21}$$

Where M represents the aircraft mass.

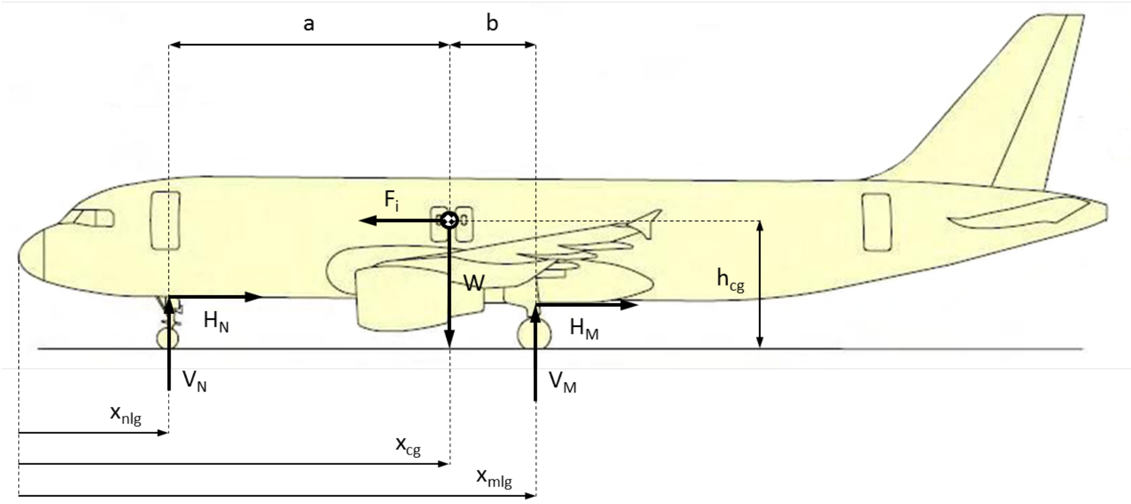

Figure 5.6: Forces during braking

5.10 Side slipping flight

Flying with side slip causes sideways bending of the fuselage. The highest side slip angles are obtained during an in-flight engine failure case. The asymmetrical thrust causes a moment around the center of gravity. The pilot has to neutralize that moment with a rudder deflection. Eventually a steady flight will be established. Maximum side slip angles are 8°, but an over swing factor of 1.6 should be applied [14]. Figure 5.7 shows the side slip situation. The tail force that will cause the fuselage sideways bending moment is calculated as followed:

$$\sum M_{cg} = 0 \qquad \rightarrow \qquad 0 = Ty_{eng} F_{tail} \cos\beta(x_{ac_h} - x_{cg}) \tag{5.22}$$

$$F_{tail} = \frac{Ty_{eng}}{\cos\beta x_{ac_h} - x_{cg})} \tag{5.23}$$

5.11 Pressurization

The differential pressure is a function of the maximum operating altitude and is given by the following equation:

$$\Delta p = p_{cab} - p_{op} = p_0 \cdot \left[\left(1 - \frac{a z_{cab}}{T_0}\right)^{\frac{gR}{a}} - \left(1 - \frac{a z_{op}}{T_0}\right)^{\frac{gR}{a}} \right] \tag{5.24}$$

Where, p_{cab} is the cabin pressure, $p_{op_{alt}}$ is the pressure at maximum operational altitude, p_0 is the ground pressure equal to 101.325 kPa, a is the absolute vertical temperature gradient equal to 0.0065 K/m, z_{cab} is the cabin altitude, which is in this case 2400 m, T_0 is the ground temperature equal to 288.15 K, z_{op} is the maximum operational altitude, g is the gravity constant of 9.81 m/s^2, and R is the constant for ideal gas of 287.05 J/kg·K.

The pressurization causes internal pressure forces in the aircraft. These forces cause tension all over the fuselage, during the flight due to pressurization the compression caused at bottom is relatively decreased due to counteraction of the stresses. The pressurization is applied between the front bulkhead and the rear bulkhead, in the section fore and after there is no pressure difference between outside and inside pressure, therefore no pressure forces are exerted in these sections.

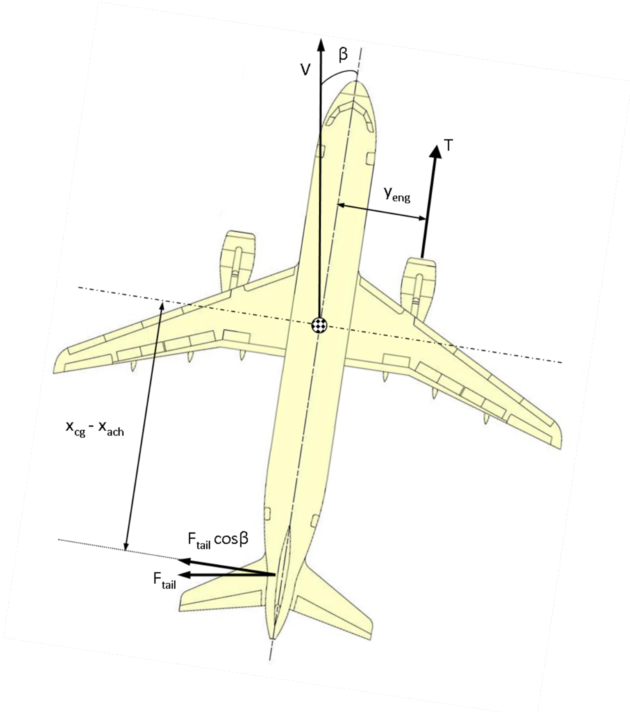

Figure 5.7: Forces during side slipping flight

Chapter 6

Running loads

In this chapter the running load and stress distribution derivation from the loads for the fuselage are explained. In the first instance the fuselage cross-section is idealized and from the idealized situation the bending stress on the stringer and skin panel combination is calculated. The shear flow caused by shear force and torsion is also calculated for the skin panels.

6.1 Bending

The bending moments M_y and M_z cause the fuselage to bend. A part of fuselage is subject to tensile stresses, while the other part is in compression. The line separating these two regions is called the neutral axis. It is a straight line and it always goes through the center of gravity of the cross-section. The stresses applied on the fuselage can be derived from the general equation [5]:

$$\sigma_x = (\frac{M_z I_{yy} - M_y I_{yz}}{I_{yy} I_{zz} - I_{yz}^2})y + (\frac{M_y I_{zz} - M_z I_{yz}}{I_{yy} I_{zz} - I_{yz}^2})z \tag{6.1}$$

The fuselage cross-section can have theoretically non symmetric shapes; therefore this general equation is programmed into the model for the calculation of the bending stress.
If the cross-section of the fuselage is symmetric about the y-axis or about the z-axis (or both), then $I_{xy} = 0$. This simplifies the above equation to:

$$\sigma_x = \frac{M_y}{I_{yy}} z + \frac{M_z}{I_{zz}} y \tag{6.2}$$

The direct stress is calculated for each stringer and neighboring skin panels. In other words the calculated stress on a location of stringer is the total stress working on the stringer and the half of the two neighboring skin panels. Since the equation of the bending stress does not specify the specific bending stress in the stringer and skin panel, the bending stress is converted to a force which applies to this specific part, see figure 6.1, whereas later the specific stress in the stringer and skin panel are calculated separately according to the applied force and material for the stringer and skin panel. The applied force distribution on the fuselage can be calculated by:

$$F = \sigma_x \cdot \left(\frac{E_{str}}{E_{sk_{mean}}} A_{str} + \frac{E_{sk_{left}}}{E_{sk_{mean}}} \frac{1}{2} A_{sk_{left}} + \frac{E_{sk_{right}}}{E_{sk_{mean}}} \frac{1}{2} A_{sk_{right}} \right) \tag{6.3}$$

In this equation it is assumed that each skin panel as well as stringer can have different materials, therefore the E-modulus is taken into account by normalizing the E-modulus by defining the weighted cross-sectional area.

$$E_{mean} = \frac{A_{str} E_{str} + A_{sk_{right}} E_{sk_{right}} + A_{sk_{left}} E_{sk_{left}}}{A_{str} + A_{sk_{right}} + A_{sk_{left}}} \tag{6.4}$$

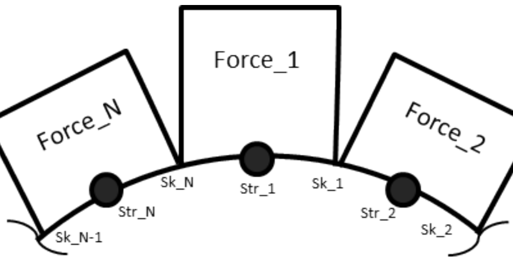

Figure 6.1: Calculated force on each stringer and skin

The top part of the cross-section will experience tension force and the bottom part compression force, or vice versa, depending on the applied bending moment. The maximum absolute value for the forces is always at the real top and bottom of the cross-section, because it has the largest arm to the neutral line of the cross-section. The bending stress close to the neutral line is smaller and obviously zero at the neutral line. The schematic distribution of the load on the fuselage cross-section is given by figure 6.2. The separate stringer and skin stress is needed for the evaluation

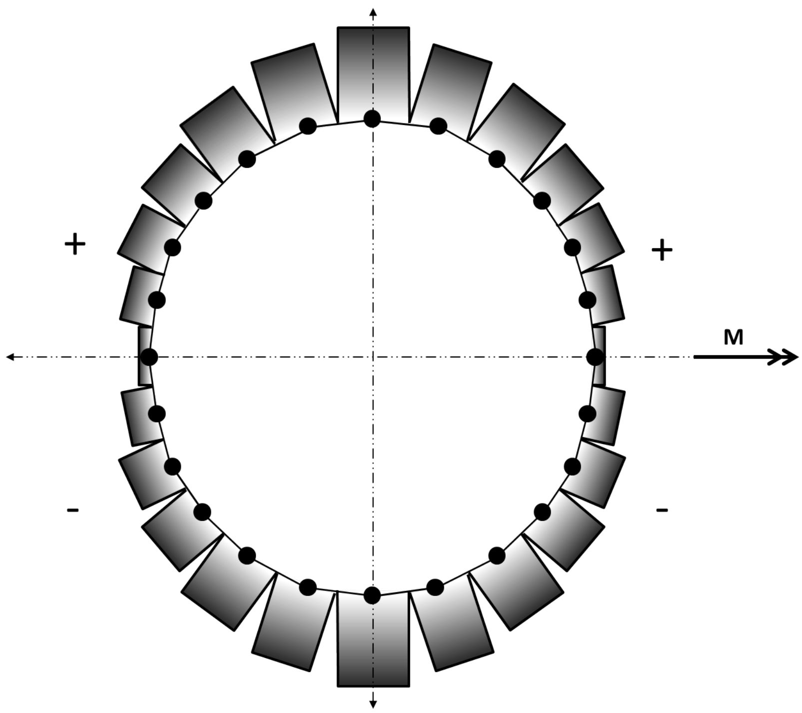

Figure 6.2: Force distribution on the fuselage cross-section

of materials. The stress in a material is described by strain times E-modulus or force divided by area [5]:

$$\sigma = \varepsilon E = \frac{F}{A} \tag{6.5}$$

The stringer and skin combination can experience different stresses, but the strain will always be equal. The strain for the stringer and skin combination is given by the following equation:

$$\varepsilon = \frac{F}{A_{str}E_{str} + \frac{1}{2}A_{sk_{left}}E_{sk_{left}} + \frac{1}{2}A_{sk_{right}}E_{sk_{right}}} \tag{6.6}$$

Since the strain ε is known, the corresponding stresses can be calculated in the specific parts.

$$\sigma_{str} = \varepsilon E_{str} \qquad \sigma_{sk_{left}} = \varepsilon E_{sk_{left}} \qquad \sigma_{sk_{right}} = \varepsilon E_{sk_{right}} \tag{6.7}$$

On each skin panel applies two different forces and therefore two different stresses are derived for each panel. The overall stress on a skin panel is assumed to be the average of the found stresses.

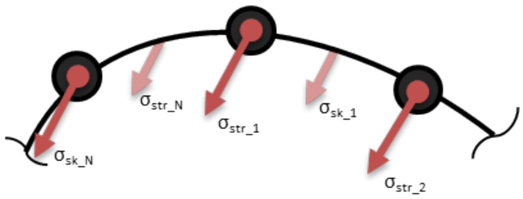

Figure 6.3: Calculated stress on each stringer and skin

6.2 Shear

The shear forces F_y and F_z cause shear stress on the fuselage. The shear flow is the gradient of a shear stress force through the body. For a fuselage cross-section, the determination of the shear flow distribution in the skin produced by shear is basically the analysis of an idealized single cell closed section beam. The shear flow distribution is therefore given by the following equation [5]:

$$q_{s_n} = q_{b_n} + q_{s_0} \tag{6.8}$$

Equation 6.8 is applicable to loading cases in which the shear loads are not applied through the section shear center so that the effects of shear and torsion are included simultaneously. The first term on the right-hand side of equation 6.8 is the 'open section' shear flow q_{b_n}. Therefore a 'cut' in one of the skin panels are needed to calculate q_{b_n} for each panel, which is given equation 6.9. The shear flow in the panel with a cut is assumed to be zero $q_{b_1} = 0$.

$$\begin{aligned} q_{b_n} = &-\left(\frac{F_y I_{zz} - F_z I_{yz}}{I_{yy} I_{zz} - I_{yz}^2}\right)\left(t_{sk_n} b_{sk_n} z_{sk_n} + \frac{E_{str}}{E_{sk}} A_{str_n} z_{str_n}\right) \\ &-\left(\frac{F_z I_{yy} - F_y I_{yz}}{I_{yy} I_{zz} - I_{yz}^2}\right)\left(t_{sk_n} b_{sk_n} y_{sk_n} + \frac{E_{str}}{E_{sk}} A_{str_n} y_{str_n}\right) + q_{b_{n-1}} \end{aligned} \tag{6.9}$$

The shear flow q_{s_0} in the panel with a cut is found by taking moments about a convenient moment center of the cross section. Since the q_{b_n} are constant between booms, the shear flow q_{s_0} is given by:

$$q_{s_0} = \sum_{n=1}^{N} \frac{2A_{b_n} q_{b_n}}{2A_{b_n}} \tag{6.10}$$

In which A_{b_n} is the individual areas subtended by the skin panels at the center of the cross section. The complete shear flow distribution follows by adding the value of q_{s_0} to the q_{b_n} shear flow distribution, which gives the final distribution, see figure 6.4.

6.3 Torsion

A fuselage is basically a single closed section beam. The shear flow distribution produced by a pure torque is therefore given by the following equation [5]:

$$q = \frac{T}{2A} \tag{6.11}$$

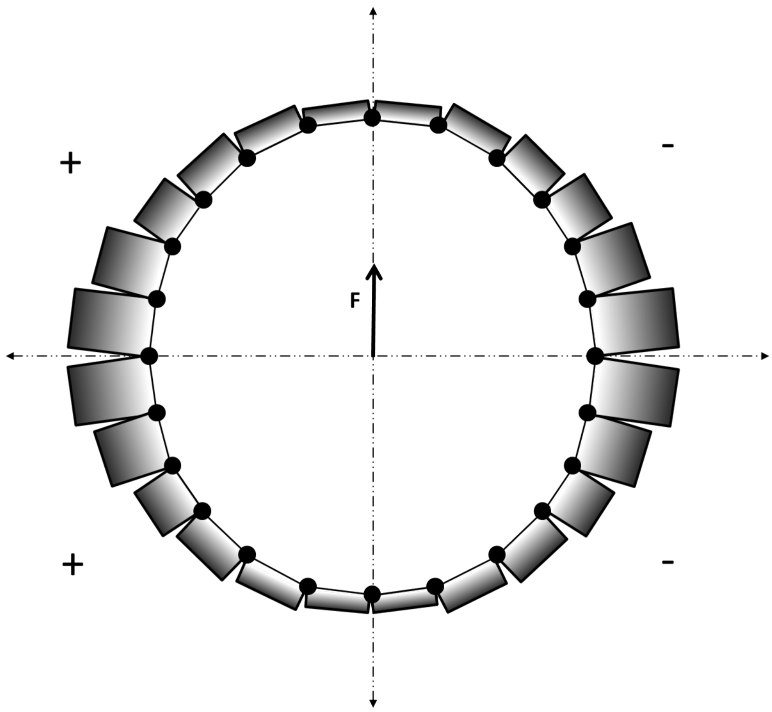

Figure 6.4: Shear flow distribution on the fuselage cross-section

It makes no difference whether or not the section has been idealized since, in both cases, the stringers are assumed not the carry the shear stress. The shear flow due to torsion is added to the shear flow generated by the shear force depending on the load cases.

6.4 Pressure

When a thin-walled tube or cylinder is subjected to internal and external pressure a hoop (circumferential) and longitudinal stress are produced in the wall as explained earlier in section 4.1.4. The stress in circumferential direction at a point in the tube or cylinder wall can be expressed as:

$$\sigma_{circ} = \frac{\Delta p R}{t} \tag{6.12}$$

The stress in longitudinal direction at a point in the tube or cylinder wall can be expressed as:

$$\sigma_{long} = \frac{\Delta p R}{2t} \tag{6.13}$$

A schematic view of both stresses are given in figure 6.5 and 6.6.

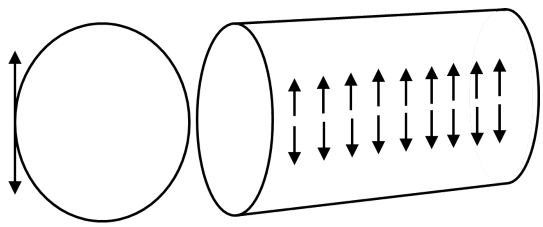

Figure 6.5: Circumferential stress

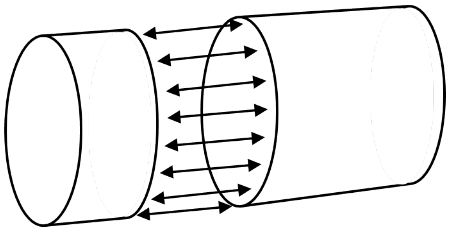

Figure 6.6: Longitudinal stress

6.5 Stress type

6.5.1 Tension

The tension caused by the bending moment is calculated. For the pressurized parts of the fuselage the hoop stress working in longitudinal direction must be added to the tension level, because the longitudinal stress due pressure generates tension all over the fuselage. Tension is reacted by the skin and stringer together. The material yield stress is set as the limiting factor for the allowable stress.

6.5.2 Compression

The compression caused by the bending moment is also calculated. The compressed areas are critical, because of the buckling. Compression is reacted by the skin and stringer together. Besides the material yield stress, the material buckling is also a limiting factor for the allowable stress. In the most cases the material buckling is the critical factor.

6.5.3 Shear

The shear caused by the shear forces and torsion is calculated. Shear is reacted only by the skin. The limiting factors in shear areas are the buckling criteria as well as the material shear yield stress.

6.5.4 Combined loading

For metal buckling analysis besides compression and shear also combined loading will be applied. In the case of combined loading buckling is caused by compression and shear.

6.5.5 Pressure

The circumferential stress caused by the pressure is calculated. This stress is considerably the same all over the fuselage and is depending on the radius of the cross-section. Pressure is reacted by skin only in circumferential direction and both skin and stringer in longitudinal direction. The limiting factors for the circumferential and longitudinal stresses are to meet the inspection threshold (fatigue), inspection interval (crack growth) and two-bay-crack.

Chapter 7

Evaluation methodology

In this chapter the design criteria with corresponding evaluation methodology is discussed for aluminum and composite. For aluminum crack and buckling analysis is performed. For composite strength and buckling analysis is performed to determine whether the input panel thicknesses are able to withstand the forces acting on the fuselage.

7.1 Structural aspects

There are five major structural aspects that have to be considered during the design phase of an aircraft:

- Static ultimate strength of undamaged structure
- Yield strength of undamaged structure
- Fatigue life of the airframe (crack initiation)
- Static residual strength of damaged structure
- Residual life of damaged structure (crack growth)

Designing for these aspects will provide a structure which will meet the static strength and damage tolerance requirements of the aircraft. The three latter aspects are very important for the airworthiness and the economics of the present and future aircraft generation. The failure modes with its corresponding design criteria and allowable data is given in table 7.1.

7.2 Fatigue

Fatigue is a phenomenon caused by repetitive loads on a structure. It depends on the magnitude and frequency of these loads in combination with the applied materials and structural shape. Fatigue-critical areas are at the fuselage upper part and at the joints of the fuselage frames to the wing spars [8].

The FAA requirements with respect to damage tolerance state that cracks present in the structure should not grow beyond a critical length that leads to catastrophic failure between inspection intervals. This imposes crack initiation limitations on the structure. To make sure these requirements are met, a fatigue design stress is used for fatigue sensitive areas of the fuselage. This design stress may not be exceeded.

In circumferential direction the fatigue sensitive loading is the hoop stress. The hoop stress is the result of the inflation of the fuselage to maintain an artificial pressure level inside the fuselage.

Mode of Failure	Design Criteria	Allowable Data
Static strength	Undamaged structure must sustain ultimate loads	Static properties
Deformation	Deformation of undamaged structure at limit loads may not interfere with safe operation	Static properties and creep properties
Fatigue crack initiation	• Damage tolerant structure must meet service life requirements • Safe life components must remain crack free in service	Fatigue properties
Residual static strength	Damaged structure must support limit loads without catastrophic failure	• Static properties • Fracture toughness properties
Crack growth life	For damage tolerant structure inspection techniques and frequency must be specified	• Crack growth • Fracture toughness properties

Table 7.1: Design criteria for sizing aircraft structures

The hoop stress is cyclic and occurs once a flight. The hoop stress should not exceed the fatigue stress, which sets a lower boundary for the skin thickness:

$$t_{min} = \frac{\Delta pR}{\sigma_{fatigue}} \tag{7.1}$$

In longitudinal direction only the fuselage top panels are sensitive to fatigue as they are relatively heavily loaded in tension due to the downward bending moment and the fuselage internal pressure together. The fatigue loads in longitudinal direction are not that easy to predict as there is no straight forward standard load pattern that is repeated every flight. The method used here is to find a load factor that is typically encountered every flight.

The load factor has been determined in the following way. The NLR have done research on a standardized load sequence on transport aircraft wing structures [15]. They conclude that all calculated load spectra for different aircraft are in a relatively small band and hence the establishment of a standardized spectrum is justified. From this load spectrum it is deduced that the load encountered once every flight is 50% higher than the average 1G flight load. This is translated to a load factor of 1.5 experienced once a flight on the fuselage. The 2.5G flight load case will include this effect, since the load factor is larger than the needed load factor of 1.5.

7.3 Two-bay-crack criterion

The damage tolerance criteria as specified in the FAR 25 considered longitudinal cracks in the skin between two frames. Since tension hoop stresses in fuselage skins due to internal pressure are highest midway between frames fatigue cracking is likely to occur mid bay. Items like cracks stoppers arrest the cracks and confine them between two frames.

Swift [16] argues that this crack initiation scenario is not the most critical, but the high bearing stresses at the first fastener adjacent to the shear clip cut-out combined with skin stresses due to internal pressure and the frame bending stress create another critical location in the fuselage skin. This location occurs more than 15,000 times in a typical wide body aircraft, making this location very important. Skin cracking at that location will automatically propagate into two bays, see figure 7.1 for illustration.

The two-bay-crack criterion states that a crack through a frame (and thus crack in two bays) should not result in catastrophic failure. Airbus has designed its latest aircraft A380 and A350 using this criterion. It is expected in the future to appear in FAR 25. Designing for two-bay-crack

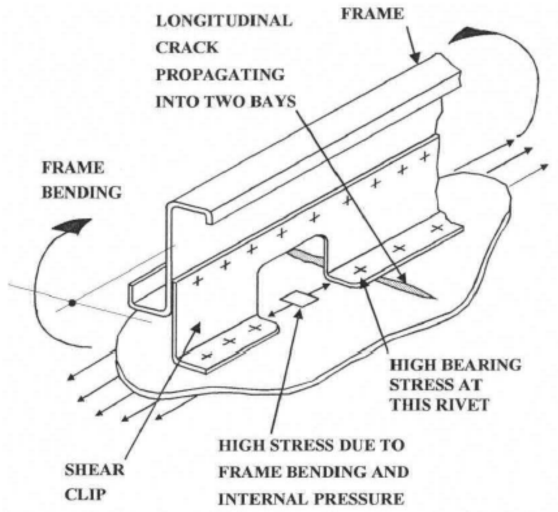

Figure 7.1: Two-bay longitudinal crack initiation

means placing an extra requirement on the skin thickness. Like designing for fatigue this is done through defining a design stress that is not to be exceeded. The skin thickness should be such that this value is not exceeded for 1.15 times the normal operation pressure [3]. The value for this stress σ_{crack} is calculated using the crack growth predictions method.

$$t_{min} = \frac{1.15\Delta pR}{\sigma_{crack}} \tag{7.2}$$

7.4 Mode of Failure

7.4.1 Fatigue crack initiation

The design fatigue stress $\sigma_{fatigue}$ is calculated using the available SN-curves for specific materials. For aluminum 2024-T4 the SN- curve for $K = 2.5$ is taken from Handbuck Struktur Berechnung 6311-01 D86 [17]. The SN-curve is described by the following function:

$$\sigma_a = C_1 + \frac{C_2 - C_1}{\exp\left(\frac{\log N}{C_3}\right)^{C_4}} \quad \text{and} \quad \log N = C_3 \left[\ln \frac{C_2 - C_1}{\sigma_a - C_1}\right]^{\frac{1}{C_4}} \tag{7.3}$$

Where σ_a is the stress amplitude, N is the number of cycles and C are constants related to the specific material.

The fuselage is fully pressurized during flight and on the ground there are no pressure loads. Therefore the minimum stress is equal to the zero $\sigma_{min} = 0$ and the maximum stress is equal to

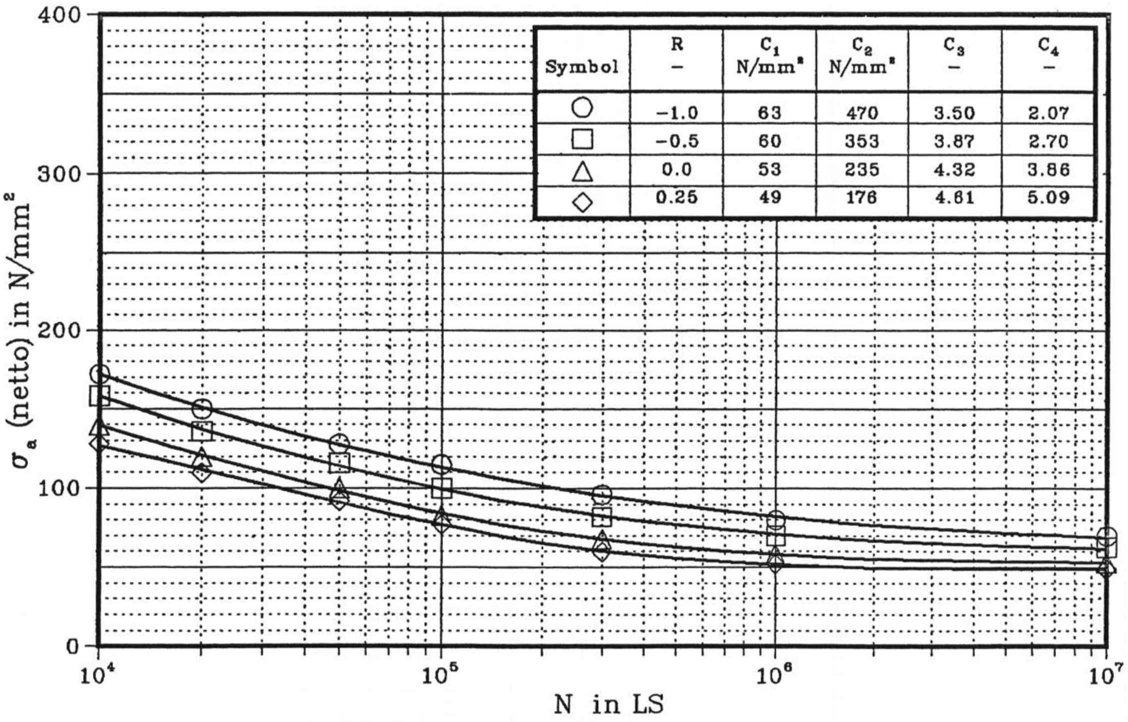

Figure 7.2: SN-curve of Aluminum 2024-T4 for $K = 2.5$

the hoop stress or in limit case equal to the design fatigue stress $\sigma_{max} = \sigma_{fatigue}$. Further the following relations are known:

$$\sigma_a = \frac{\sigma_{max} - \sigma_{min}}{2} \tag{7.4}$$

$$R = \frac{\sigma_{min}}{\sigma_{max}} \tag{7.5}$$

Since $R = 0$ in the situation of a fuselage, the maximum stress is two times the stress amplitude, which also equals the design fatigue stress $\sigma_{fatigue} = \sigma_{max} = 2\sigma_a$. For the corresponding $R = 0$, the constants for SN-curve are $C_1 = 53$ N/mm^2, $C_2 = 235$ N/mm^2, $C_3 = 4.32$, $C_4 = 3.66$, which will be used in equation 7.3.

An inspection threshold time N_{th} is linked to the design fatigue stress. The number of cycles N for the current hoop stress level on the panel is found by calculating σ_a and reading out N from figure 7.2 or calculating it from equation 7.3. Once N is found the safety margin for the current number of cycles is determined, which should be equal or lower than N_{th} in order to meet the requirement.

$$MS = \frac{N_{th}}{N} \leq 1 \tag{7.6}$$

The inspection threshold is the number of cycles when the aircraft should be inspected for cracks. For metals the inspection threshold is set to the half-life of an aircraft, because of the possibility for plastic deformation of the material. For composite the inspection threshold is set to the life of an aircraft, because composites materials are not capable to deform plastically, thus an initiated crack will be critical at the first. The used method is valid for loaded panels. Using the criteria for complete aircraft a safety factor should be used above the critical inspection threshold in order to guarantee the safety of the aircraft during flight, since the fatigue behavior of an aircraft is still not predictable. The maximum life time of an Airbus A320 is approximately 65,000 hours. Assuming an average flight of 1.5 hours means 40,000 cycles in lifetime. The critical inspection threshold it set to $N_{th} = 4 \cdot 20,000$, which is the half-life on an aircraft with a safety factor of 4 in order to validate it for the whole structure. This analysis can be done for other materials if the SN-curve is known, unfortunately no SN-curve for composite is found to do the same analysis for composite structure.

7.4.2 Crack growth

The crack growth rate is described by the Paris-Erdogan Law [18]. The inspection interval is defined as the number of load cycles needed for fracture is given by the following equation:

$$N = \frac{1}{C\Delta S^m} \int_{a_0}^{a_f} \frac{\partial a}{(\beta\sqrt{\pi a})^m} \tag{7.7}$$

Where a is the crack length, ΔS is the stress on the panel, this is taken as 1.15 times the circumferential stress, β depends on the geometry and should probably change for a full scale model, however it is assumed that $\beta = 1$. The starting crack length is set to $a_0 = 1$ mm and the critical crack length is set to $a_f = 75$ mm. m and C are material constant, called the Paris's exponent and Paris's coefficient, respectively, for aluminum 2024 is taken $m = 3$ and $C = 2.5389 \cdot 10^{-11}$.

Further an inspection interval is defined, for the Airbus A320 the inspection interval is approximately 10,000 hours. Assuming an average flight of 1.5 hours means 7,000 cycles till inspection. Therefore the critical inspection interval is set to $N_{ii} = 4 \cdot 7,000$, where 4 is the safety factor used, since the effect of crack growth is only for stiffened panels and not for complete structures. The safety margin is given by:

$$MS = \frac{N_{ii}}{N} \leq 1 \tag{7.8}$$

7.4.3 Fracture toughness

Fracture toughness is a property which describes the ability of a material containing a crack to resist fracture, and is an important property of a material for design. It is denoted as K_{Ic} and the crack length a_c depends on fracture toughness [19].

$$K_{Ic} = \beta\sigma_c\sqrt{\pi a_c} \rightarrow a_c = \frac{1}{\pi}\left(\frac{K_{Ic}}{\beta\sigma_c}\right)^2 \tag{7.9}$$

Where σ_c is the critical stress and β is the geometry constant. Further it is assumed that $\sigma_c = 1/2 \cdot \sigma_{hoop}$ and $\beta = 1$. The fracture toughness property of aluminium 2024 is $K_{Ic} = 40$ MPa$\sqrt{\text{m}}$. The critical crack length is set to $a_{c_{crit}} = 600$ mm, which is equal to the length of two-bays divided by a safety factor of 1.15 in order to meet to the two-bay-crack criteria. The safety margin is calculated by:

$$MS = \frac{a_c}{a_{c_{crit}}} \leq 1 \tag{7.10}$$

7.4.4 Static strength and deformation

In order to comply with the static strength the structure must sustain ultimate loads and no deformation of structure should happen at limit loads. Therefore the limit loads should be lower than the yield strength of material, and the ultimate loads, which are 1.5 times the limit loads, should be lower than the ultimate strength. For aluminum this criteria is included in the upcoming buckling analysis, however for composite it is not. The margins for static strength are given by:

$$MS_{yld} = \frac{\sigma_x}{R_{0.2_{tens}}} \qquad MS_{yld} = \frac{\sigma_x}{R_{0.2_{comp}}} \tag{7.11}$$

$$MS_{yld} = \frac{\sigma_y}{R_{0.2_{tens}}} \qquad MS_{yld} = \frac{\tau_{xy}}{R_{0.2_{shear}}} \tag{7.12}$$

$$MS_{ult} = 1.5\frac{\sigma_x}{R_{m_{tens}}} \qquad MS_{ult} = 1.5\frac{\sigma_x}{R_{m_{comp}}} \tag{7.13}$$

7.5 Composite analysis

The buckling and strength for composite are checked for each panel, from ply level (material failure) to the skin and stiffener buckling, and further to the global buckling of a panel. Further the buckling due to the torsion load is also evaluated.

7.5.1 Stiffness matrix

A composite material consists of several layers and is in this study assumed to be quasi-isotropic. Therefore the stiffness can change depending on the direction. In order to do a composite analysis it is required to setup a stiffness matrix for the composite panel. It is assumed that the E-modulus and the Poisson's ratio is the same in all directions. The stiffness matrix is valid for the composite panel and it includes the thickness t and width of the panel b [20], which is needed for the composite analysis.

$$D = \begin{bmatrix} D(1,1) & D(1,2) & \cdots & 0 \\ D(2,1) & D(2,2) & \cdots & 0 \\ \vdots & \vdots & \ddots & \vdots \\ 0 & 0 & \cdots & D(6,6) \end{bmatrix} \tag{7.14}$$

With,

$$D(1,1) = D(2,2) = \frac{E}{12(1-\nu^2)}bt^3 \tag{7.15}$$

$$D(1,2) = D(2,1) = \frac{E\nu}{12(1-\nu^2)}bt^3 \tag{7.16}$$

$$D(6,6) = \frac{E(1-\nu)}{24(1-\nu^2)}bt^3 \tag{7.17}$$

7.5.2 Material failure

Material failure is evaluated with the Tsai-Hill criterion. The Tsai-Hill criterion considers the interaction between different stress components. The Tsai-Hill criterion is used to predict how a long fiber composite (ply) will fail under a combined set of (in - plane) stresses. Unlike the simple maximum stress criterion, it accounts for mixed mode failure, in which operation of the mechanism (e.g. transverse failure) is assisted by stresses tending primarily to cause another type (e.g. shear stresses) [21] [22]. The criterion can be expressed:

$$TH = \frac{\sigma_x^2}{X^2} - \frac{\sigma_x\sigma_y}{XY} + \frac{\sigma_y^2}{Y^2} + \frac{\tau_{xy}^2}{S^2} \tag{7.18}$$

Where σ, τ, X, Y, and S are applied normal stress, applied normal shear stress, material maximum normal stress in x direction, material maximum normal stress in y direction, and material maximum shear stress, respectively.

There is no distinction made between tensile and compression strengths. Further the Tsai-Hill failure criterion cannot predict different failure modes including fiber failure, matrix failure, and fiber-matrix interface failure.

7.5.3 Skin buckling

The stability of the skin or panel facing is mainly activated for a foam-filled stiffened panel optimization problem and evaluated by assuming that the long edges of length L_S of a long plate (skin) are built-in, where the compressive loads should not exceed the critical buckling loads N_{xcr} [23]:

$$N_{x_{cr}} = \frac{\pi^2}{w^2}[4.53\sqrt{D_{(1,1)}D_{(2,2)}} + 2.62(D_{(1,2)} + 2D_{(6,6)})] \tag{7.19}$$

Where D is the stiffness matrix of the laminate of the skin only, and w is the stiffener spacing. The safety margin is given by:

$$MS_{x_{cr}} = \frac{F}{N_{x_{cr}}} \leq 1 \tag{7.20}$$

7.5.4 Foam-filled stiffener/Panel face wrinkling

The face wrinkling of foam filled panel or stiffener is a local phenomenon. For an isotropic core material with an isotropic facing, the critical load against wrinkling is defined as [23]:

$$N_{cr} = 1.5\sqrt[3]{\frac{2D_{(1,1)}a^2}{\pi^2}} \qquad \text{where} \qquad a = \frac{2\pi E_c}{(3-v_c)(1+v_c)} \tag{7.21}$$

Where D, E_c, and v_c are the stiffness matrix of the facing, Young modulus and Poisson's ratio of the core material, respectively. The safety margin is given by:

$$MS_{cr} = \frac{F}{N_{cr}} \leq 1 \tag{7.22}$$

7.5.5 Panel (global) buckling

Critical buckling load for a four sided simply supported panel in compression is expressed as [23]:

$$N_{x_{cr}} = \frac{\pi^2}{L_s^2}[D_{(1,1)}\frac{L_s^2}{w^2} + D_{(2,2)}\frac{w^2}{L_s^2} + 2(D_{(1,1)} + 2D_{(6,6)})] \tag{7.23}$$

Where w is the total width of the panel. The safety margin is given by:

$$MS_{x_{cr}} = \frac{F}{N_{x_{cr}}} \leq 1 \tag{7.24}$$

The buckling load due to shear loads is expresses as [23]:

$$N_{xy_{cr}} = \frac{4}{L_s^2}\sqrt[4]{D_{(1,1)}D_{(2,2)}^3}(15.07 + 7.08K) \qquad \text{when} \qquad K \leq 1 \tag{7.25}$$

$$N_{xy_{cr}} = \frac{4}{L_s^2}\sqrt[4]{D_{(2,2)}(D_{(1,2)} + 2D_{(6,6)})}\left(18.59 + \frac{3.56}{K}\right) \qquad \text{when} \qquad K > 1 \tag{7.26}$$

Where,

$$K = \frac{2D_{(6,6)} + D_{(1,2)}}{\sqrt{D_{(1,1)}D_{(2,2)}}} \tag{7.27}$$

The safety margin is given by:

$$MS_{xy_{cr}} = \frac{F}{N_{xy_{cr}}} \leq 1 \tag{7.28}$$

7.5.6 Torsion buckling

The value of torsion load at which buckling can occur is expressed as [24]:

$$T_{cr} = 4\pi R^2 t_1 \tau_{cr}[0.8K_s E_f \frac{h+t_1-t_2}{R}] \tag{7.29}$$

Where E_f is the Young modulus of the facing. The buckling coefficient K_s is a function of section length L_s and analytical expressed in Sullins (Eq. 98) [25]. The safety margin is given by:

$$MS_{cr} = \frac{T}{T_{cr}} \leq 1 \tag{7.30}$$

7.6 Metal analysis

The methodology for static analysis of a stiffened panel, combining local buckling of both skin and stiffener elements and global buckling of the panel as a whole (post-buckled design) is discussed in this section for metals. Loading may consist of shear loading or compressive loading separately or both loads combined. These standard engineering equations were bundled in [26].

7.6.1 Compression of stiffened panel

7.6.1.1 Column buckling

Elastic and inelastic column buckling, called Euler buckling is given by:

$$F_c = \frac{c\pi^2 E}{(L/\rho)^2} \tag{7.31}$$

$$F_c = \frac{c\pi^2 E_t}{(L/\rho)^2} \tag{7.32}$$

Where c is the end fixity coefficient (boundary condition) and $\rho = \sqrt{I/A}$ the radius of inertia. Let L' is the effective length of the column which equals the length between inflection points of the deflected column under load. Then $L' = {}^{L}/_{\sqrt{c}}$, with $c = 1$ for pinned end, zero and restraint against rotation or $c = 4$ for clamped ends, full restraint against rotation.

7.6.1.2 Buckling strength of flat sheet in compression, shear, bending and under combined stress systems

Elastic buckling strength of flat sheet in compression is given by:

$$\sigma_{cr} = \frac{\pi^2 k_c E}{12(1-v_e^2}\left(\frac{t}{b}\right)^2 \tag{7.33}$$

Where k_c is the buckling coefficient which depends on edge boundary conditions and sheet aspect ratio (a/b). In generally for simply supported panels the k_c is equal to 4.

7.6.1.3 Inelastic buckling strength of flat sheet in compression

Plasticity correction is required when:

$$\sigma_{cr} > 0.5\sigma_{0.2} \tag{7.34}$$

The inelastic buckling strength is then reduced to:

$$\sigma_{cr} = \frac{\eta\pi^2 k_c E}{12(1-v_e^2)}\left(\frac{t}{b}\right)^2 \tag{7.35}$$

Or:

$$\sigma_{cr} = \eta \sigma_{cr_e} \tag{7.36}$$

Where the plasticity reduction factor, η, depends on the problem type is given in table 7.2. The plasticity reduction factor should be determined iteratively.

Loading	Boundary condition	Equation
Compression and bending	Flange with one unloaded hinged edge	$\eta_1 = \left(\frac{1-v^2}{1-v^2}\right)\frac{E_s}{E}$
	Flange with one unloaded fixed edge	$\eta_2 = \eta_1\left(0.33 + 0.335\sqrt{1+3\frac{E_t}{E_s}}\right)$
	Plate with unloaded hinged edges	$\eta_3 = \eta_1\left(0.5 + 0.25\sqrt{1+3\frac{E_t}{E_s}}\right)$
	Plate with unloaded fixed edges	$\eta_4 = \eta_1\left(0.352 + 0.324\sqrt{1+3\frac{E_t}{E_s}}\right)$
Compression	Column	$\eta_5 = {}^{E_t}/_{E}$
Shear	All conditions	$\eta_6 = {}^{G_s}/_{G}$

Table 7.2: Plasticity reduction factor depending on problem type

7.6.1.4 Material description by Ramberg and Osgood

The Ramberg and Osgood model is used for the stress strain relation:

$$\varepsilon = \frac{\sigma}{E} + 0.002\left(\frac{\sigma}{\sigma_{0.2}}\right)^n \tag{7.37}$$

$$E_s = \frac{\sigma}{\varepsilon} \tag{7.38}$$

$$\frac{1}{E_t} = \frac{n}{E_s} + \frac{1-n}{E} \tag{7.39}$$

$$v = \frac{E_s}{E}v_e + \left(1 - \frac{E_s}{E}\right)v_p \tag{7.40}$$

The Poisson's ratio is an interpolation of the ideal elastic Poisson's ratio v_e and the fully plastic Poisson's ratio, which is $v_p = 0.5$ for incompressible media. The stress level must be solved iteratively for strain.

7.6.1.5 Buckling breakdown

Skin buckling or pocket folding

- Skin side flange not considered for local buckling (connected to skin by rivets etc.)
- Web buckling
- Cap buckling
- Cap flange buckling (if not just flanged edge)

Inter rivet buckling

- Skin inter rivet buckling
- Stiffener inter rivet buckling

7.6.1.6 Local buckling

Skin

The boundary condition for the skin is that it is simply supported by both frames and stiffeners and the limits are defined by the aspect ratio of frame pitch to stiffener pitch $a/b > 1$. The value for k_c is 4 and η_4 is used for plasticity reduced factor.

Web and cap (flanged)

The boundary condition for web and cap is that it is simply supported by skin side slide flange and inner flange. The value for k_c is 4 and η_4 is used for plasticity reduced factor.

Blade stiffener and cap (not-flanged)

The boundary condition for the blade stiffened and cap is that it is simply supported by the flange and the other side is free. The value for k_c is 0.43 and η_1 is used for plasticity reduced factor.

Local buckling coefficient	Boundary condition	Plasticity correction factor
$k_c = 0.43$	F-SS	η_1
$k_c = 0.80$	F-C	η_2
$k_c = 4.0$	SS-SS	η_3
$k_c = 5.x$	SS-C	
$k_c = 6.98$	C-C	η_4

Table 7.3: Local buckling coefficients, boundary condition and plasticity correction factors (F = free, C = clamped, SS = simply supports)

7.6.1.7 Inter-rivet buckling

The column buckling equivalent is given by equation 7.41 with $L = p = \mathrm{RivetPitch}$, $\rho = \sqrt{\frac{I}{A}} = \sqrt{\frac{1/12wt^3}{wt}}$.

$$\sigma_{ir} = \frac{c\pi^2 E_t}{\left(\frac{L}{\rho}\right)^2} = c\pi^2 \frac{E_t}{12}\left(\frac{t}{p}\right)^2 = c\pi^2 \eta_5 \frac{E}{12}\left(\frac{t}{p}\right)^2 \tag{7.41}$$

For the plasticity correction of column buckling η_5 is used. Several riveting possibilities are given, which are listed in table 7.4 together with its end fixity coefficient c, ($K_{ir} = 1/c^{0.5}$). The commonly used rivet type is countersunk.

	Bruhn C7.14	ESDU 020108	Rothwell TH 02.01.28
Flathead rivet	4	4	3.29
Spotweld	3.5	3.5	2.88
Brazier rivet	3.0	3.0	
Countersunk rivet	1.0	1.5	1.23
Snap head rivet		3.0	
Round head rivet			2.46

Table 7.4: Rivets types with corresponding end fixity coefficient c

7.6.1.8 Stiffener crippling

The stiffener crippling is given by:

$$\sigma_{cs} = \frac{\sum A_i \sigma_{cr}}{\sum A_i} \tag{7.42}$$

Where A_i is the area of the section item i and σ_{cr} is the buckling stress of item i.

7.6.1.9 Lateral instability stress

Lateral instability is general buckling of the entire stiffener under a compression load, which buckles the inner flange in its plane. The web provides an elastic support (spring support) over its entire length (length from frame to frame). This is represented by column buckling, where the column is the inner flange of the stiffener.

Elastic support of the flange by the web is defined by cantilever beam bending, where the web is encastered at the skin and bends along its height. The deflection of the web at the flange becomes:

$$\delta = \frac{PL^3}{3EI} \tag{7.43}$$

Where $P = q \cdot w$, $L = h$, $I = \frac{1}{12} \cdot w \cdot t^3$ and q is the distributed load from the flange, w is the width and h is the web height. The stiffness per unit width is then:

$$\frac{dq}{dw} = \frac{3E\frac{1}{12}t^3}{h^3} = \frac{E}{4}\left(\frac{t}{h}\right)^3 = \beta \tag{7.44}$$

Column buckling is then defined by:

$$F_c = \frac{c\pi^2 E_t}{\left(\frac{L}{\rho}\right)^2} = \frac{\pi^2 E_t l}{AL^2} c \tag{7.45}$$

Where, the inner flange inertia in its plane is:

$$I = \frac{1}{12} t h^3 \tag{7.46}$$

The length is the distance between the frames and the coefficient c is dependent on the wavelength, elastic web support and flange stiffness and inertia:

$$c = m^2 + \frac{\beta L^4}{m^2 \pi^4 EI} \tag{7.47}$$

The number of half wave lengths m can be found from minimization:

$$\frac{dF_c}{dm} = 0 \tag{7.48}$$

Then,

$$m_0 = \frac{L}{\pi} \sqrt[4]{\frac{\beta}{EI}} \tag{7.49}$$

The buckling stress can be found by substituting both bounding integers. A plasticity correction must be made by the correction factor η_5 for column buckling. Further there is no lateral instability for blade stiffeners and closed stiffeners, e.g. head stiffeners.

7.6.1.10 Allowable stress at zero slenderness

The slenderness ratio is given by L'/ρ, where L' is the effective column length. According to Bruhn C7.25 [27], F_{cs} is the column crippling load, assumed to occur at $L'/\rho = 0$. Skin zero slenderness stress equals the skin yield stress, stiffener zero slenderness stress is the minimum of the yield, the crippling and the lateral stability stress:

$$\sigma_{L0_{skin}} = \sigma_{0.2} \tag{7.50}$$

$$\sigma_{L0_{stiffener}} = \min\left(\sigma_{0.2}; \sigma_{crip}; \sigma_{lateral}\right) \tag{7.51}$$

These stresses give the strains by means of the Ramberg Osgood equation, for both stiffener and skin. Finally the minimum stain (ε_{L0}) is taken from both skin and stiffener, which gives the section minimum strain and thus stiffener and skin stress (σ_{L0}). The minimum stiffener stress at zero slenderness includes the lateral instability stress, which is controversial as this stress is a global buckling stress, where L'/ρ is not zero!

7.6.1.11 Load carrying width

Von Karman supposed that only the effective parts of the plate are able to carry the load after buckling. The middle of the plate simply carries no load after buckling. This gives the effective width:

$$b_e = b\sqrt{\frac{\sigma_{cr}}{\sigma_{max}}} \tag{7.52}$$

The simple equation represents the behavior in real structures surprisingly well and gives in nearly all cases conservative estimates.
Bruhn (C7.11) [27] uses the von Karman method as well and states that the sheet effective width is the theoretical width of the sheet that carries the same stress as the stiffener when the skin is buckled. For standard size stiffeners the von Karman relation is reduces to:

$$b_e = 1.90t\sqrt{\frac{E}{\sigma_{max}}} \tag{7.53}$$

With local skin coefficient $k_c = 4.0$. In case of light stiffeners the factor 1.90 becomes 1.70, which follows from $k_c = 3.20$. When fixed or clamped edge condition between stiffener and skin then the factor becomes 2.52, which follows from $k_c = 6.98$, in general this is only the case for closed section stiffeners.

For two skins side flanges with each one rivet row, two times the effective width is used for calculations, see figure 7.3. When the skin side flange has two rivet rows only one effective width is used for calculations, as the overlap is too big to take two effective widths into account. However the crippling stress of the stiffener is calculated based on a skin side flange with a thickness of $3/4$ the sum of the flange thickness plus the sheet thickness.

For integral stiffeners two cases exist:

1. $t_{sk} < t_{fi} < 2t_{sk}$ (relative thin skin side flange) and
2. $t_{fi} > 2t_{sk}$ (thick skin side flange).

For the local skin buckling stress $t = (t_{sk} + t_{fi})/2$ and the effective stiffener area is the area of the stiffener upper section plus the area of the sheet of width b_e, which has both thickness t_{fi} and $t_s k$.

The effective width is calculated as standard, where crippling stress is calculated for the stiffener section including the integral skin part. Half the effective width is situated on both sides of the integral section. The effective width for varying stiffeners is given in figure 7.3.
Rothwell [3] gives as generalized rule: load carrying width is approximately one half of the stiffener pitch. ESDU data sheet 02.01.24 [28] shows the stiffness ratio after buckling to be approximately one half for a simply supported flat rectangular plate, where the wave length is equal to the plate width.

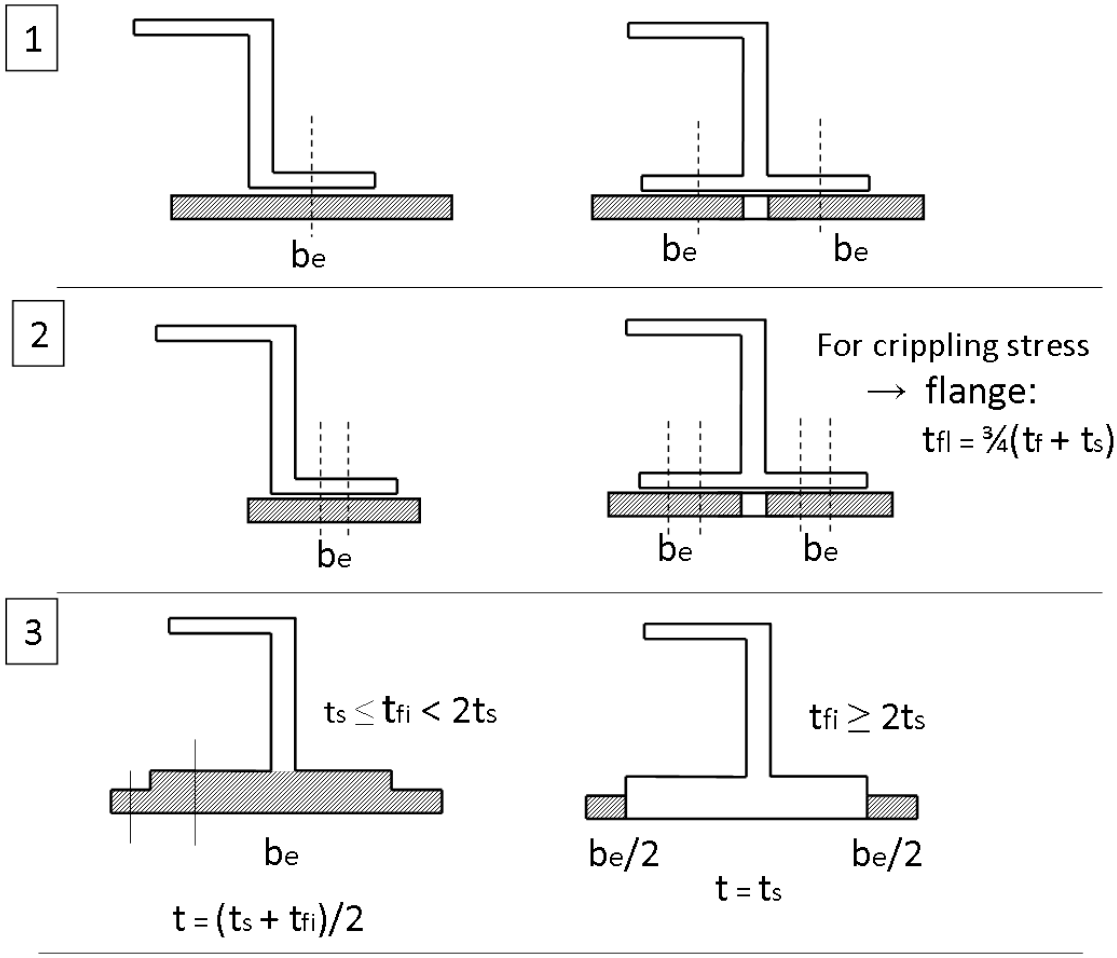

Figure 7.3: Effective width for varying stiffeners

7.6.1.12 Average stress in the super-stiffener at zero slenderness

From the load carrying width an average stress in the super-stiffener can be determined, or the load capacity for zero slenderness.

$$\sigma_{L0} = \frac{S_{stiffener}}{S}\sigma_{L0_{stiffener}} + \frac{S_{skin_e}}{S}\sigma_{L0_{skin}} \tag{7.54}$$

Where S_{skin_e} is the effective skin cross-section area and $S_{stiffener}$ the string cross-section area.

7.6.1.13 Super stiffener

Super stiffener can be visualized as one stiffener section with two half skin pockets. The super stiffener fails by either one of the following modes:

- local buckling of skin
- local buckling of stiffener
- column buckling

7.6.1.14 Engesser modified law

For the column stiffness and column load use is made of modified material properties called Engesser modified law: Replace $\sigma_{0.2}$ by σ_{L0} in the Ramberg Osgood relation for both skin and stiffener, only when superstiffener is evaluated. Then the equivalent homogeneous material secant modulus and tangent modulus of the column are:

$$E_s = \left(\frac{S_{sk}}{S}\right) E_{s_{sk}} + \left(\frac{S_r}{S}\right) E_{s_{st}} \tag{7.55}$$

$$E_t = \left(\frac{S_{sk}}{S}\right) E_{t_{sk}} + \left(\frac{S_r}{S}\right) E_{t_{st}} \tag{7.56}$$

The corresponding column load is:

$$P = S_{sk}\sigma_{sk} + S_{st}\sigma_{st} \tag{7.57}$$

7.6.1.15 Local buckling

Stiffener local buckling

Local buckling of stiffener (cap/web/flange buckling and inter-rivet buckling of flange) gives a maximum strain, which determines the skin stress, which gives a load carrying width and subsequently a load-carrying capacity.

Skin local buckling

Local buckling of skin (inter rivet buckling) gives a maximum strain, which gives the load carrying width and determines the stiffener stress, which gives the load-carrying capacity. Each time the load carrying width has to be determined as it is a function of the stress in the load carrying part of the skin.

Calculation procedure

The calculation procedure is given as follows:

- Determine uniform strain in column
  - local buckling of stiffener
  - local buckling of skin
  - any given/picked strain
- Stress in skin
- Stress in stiffener
- Effective width
- Load carrying capacity by: $P = S_{sk}\sigma_{sk} + S_{st} + \sigma_{st}$

7.6.1.16 Column buckling of super stiffener

The column buckling load is defined by Euler:

$$\sigma_{crit} = \frac{\pi^2 E_t}{\lambda^2} \tag{7.58}$$

$$P_{crit} = \frac{\pi^2 E_t I}{L^2} \tag{7.59}$$

Where the inertia of the super stiffener column I depends on the load carrying width (dependent on stress ratio) and the Secant modulus from the Engesser Modified Law. The buckling column buckling length L is equal to:

$$L = K \cdot L_p \tag{7.60}$$

Where K is the Main end fixity coefficient and L_p is the frame pitch. For very stiff frames the frames act as rigid nodes for the column and thus $K = 0.5$. For flexible frames the frames prevent out of plane movement, but don't restrict rotation thus $K = 1.0$.

The load carrying capacity of the column is reached when the applied load $P(\varepsilon)$ converges to the critical load P_{crit}, see figure 7.4.

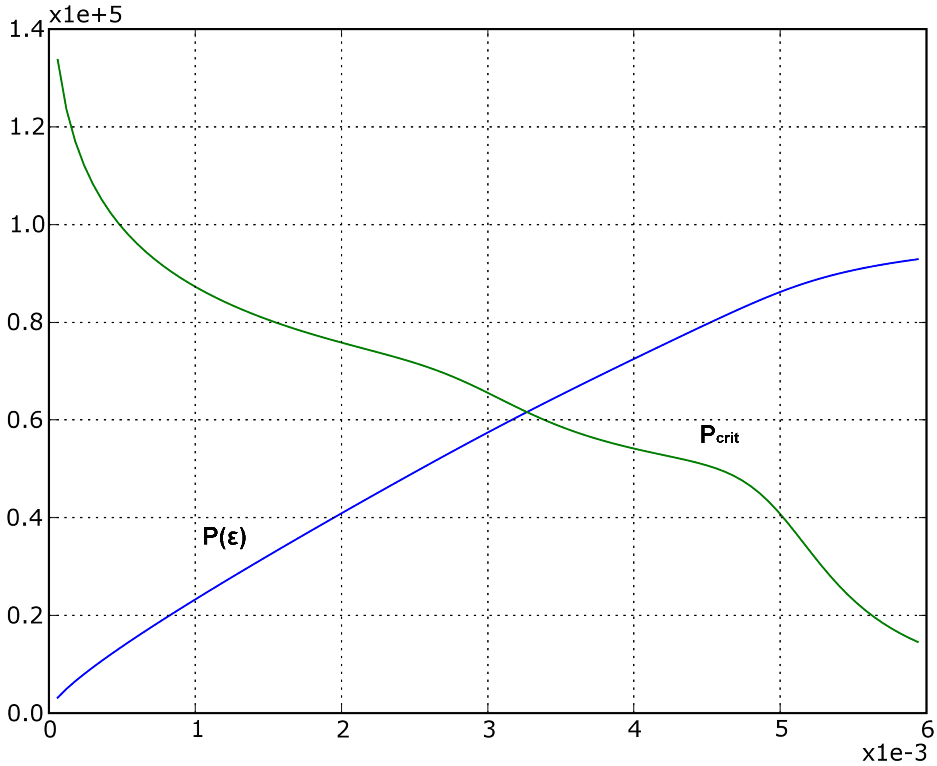

Figure 7.4: Applied load $P(\varepsilon)$ and Euler buckling load P_{crit}

7.6.1.17 Load carrying capacity

The reserve factor is:

$$RF = \frac{P_{adm}}{P_{applied}} \tag{7.61}$$

$$MS = \frac{P_{adm}}{P_{applied}} - 1 \tag{7.62}$$

Where P_{adm} is the minimum value of the load at which local skin buckling occurs, the load at which local stiffeners buckling occurs or the load at which column buckling occurs.

The load at which pocket folding occurs (smallest local buckling of either skin pocket) is the pocket folding load. The percentage of pocket folding at limit load is as follows:

$$PF_{LL} = 1.5 \frac{P_{pocket}}{P_{applied}} 100\% \tag{7.63}$$

The applied load is the Ultimate load (UL), and the Limit load (LL) is by definition $^{UL}/_{1.5}$, where 1.5 is the safety factor j. For the Airbus A380 program the pocket folding load must exceed 80% of the Limit load. This is rather high, in general this value would be 60%. In this case $MS > 60\%$ for $t < 3.0$ mm and $MS > 80\%$ for $t > 3.0$ mm is used.

7.6.1.18 Effect of panel curvature

Initial buckling of slightly curved plates under combined longitudinal and circumferential direct stress with all edges simply supported (ESDU 02.01.50 [28]) will be defined. Curvature of the plate is defined by: $^{b^2}/_{Rt}$. The ratio of the buckling stresses of both the curves and flat plates is:

$$\frac{f_x}{f_0} = \frac{3(1-v^2)}{(\pi^4} \left(\frac{ab}{Rt}\right)^2 \frac{m^2}{\left(\frac{a^2}{b^2} + m^2\right)} + \frac{b^2 \frac{a^2}{b^2} + m^2}{4m^2a^2} \tag{7.64}$$

The fuselage geometry of Airbus A320 is $R = 2000$ mm. The curvature is approximately 5 for the Airbus A320. A plat panel has an infinite radius. Otherwise HSB 45400-01 [17] can be used for curvature smaller than $^{100t}/_{R} = 1$. This is true for the fuselage shells, which are thin walled. The equation becomes:

$$\sigma_b = \sigma_{bflat} + 0.2E\frac{t}{R} \tag{7.65}$$

7.6.2 Shear of stiffened panel

7.6.2.1 Elastic buckling strength of flat sheet in shear

General elastic buckling strength of flat sheet in compression and shear is given by (Bruhn C5.1 [27]):

$$\sigma_{cr} = \frac{\pi^2 k_c E}{12(1-v_e^2)} \left(\frac{t}{b}\right)^2 \tag{7.66}$$

Where k_c is the buckling coefficient which depends on the edge boundary conditions and sheet aspect ratio $(^a/_b)$ and loading situation. For shear:

$$k_s = 5.35 + 3.80 \left(\frac{b}{L}\right)^2 \tag{7.67}$$

The shear buckling load may be reduced to:

$$\tau_{cr} = K_s E \left(\frac{t}{b}\right)^2 \tag{7.68}$$

Where K_s is the shear buckling coefficient according to Rothwell (with $v = 0.3$ and simply supported):

$$K_s = 4.83 + 3.61 \left(\frac{b}{L}\right)^2 \tag{7.69}$$

For $b < L$, or in words the stiffener pitch is smaller than the frame pitch. Otherwise $L = b$ and $b = L$ for the described above.

7.6.2.2 Inelastic buckling strength of flat sheet in shear

Plasticity correction is required when:

$$\tau_{cr}\sqrt{3} > 0.5\sigma_{0.2} \tag{7.70}$$

The inelastic buckling strength is then reduced to:

$$\tau_{cr} = \frac{\eta\pi^2 k_s E}{12(1-v^2)}\left(\frac{t}{b}\right)^2 \tag{7.71}$$

Or:

$$\tau_{cr} = \eta\tau_{cr_e} \tag{7.72}$$

Where the plasticity reduction factor, η, depends on the problem type. In this case shear, thus η_6 in table 7.2:

$$\eta_6 = \frac{G_s}{G} \tag{7.73}$$

In addition plasticity is corrected for the value of $\tau_{cr}\sqrt{3}$, and divided by $\sqrt{3}$ after plasticity correction.

7.6.2.3 Diagonal tension factor

Net panel shear load is Q. The nominal shear stress is $\tau = {}^{Q}/_{bt}$. The shear load carried in diagonal tension is:

$$Q_{DT} = k_{DT}Q = k_{DT}\tau \cdot bt \tag{7.74}$$

Where for a flat web:

$$k_{DT} = \tanh\left(\frac{1}{2}\log_{10}\frac{\tau}{\tau_b}\right) \tag{7.75}$$

And according to goniometry:

$$\tanh(x) = \frac{\sinh(x)}{\cosh(x)} = \frac{e^x - e^{-x}}{e^x + e^{-x}} \tag{7.76}$$

The diagonal tension factor is defined for ${}^{\tau}/_{\tau_b} > 1.0$. If it is smaller the diagonal tension factor is zero.
Equilibrium is found following relations:

$$\sigma_{DT} \cdot t \cdot \frac{b}{2}\cos\alpha \cdot 2 \cdot \sin\alpha = Q_{DT} \tag{7.77}$$

$$-\sigma_{DT} \cdot t \cdot \frac{b}{2}\cos\alpha \cdot 2 \cdot \cos\alpha = P_{ST} \tag{7.78}$$

$$-\sigma_{DT} \cdot t \cdot L\sin\alpha \cdot \sin\alpha = P_{FR} \tag{7.79}$$

Which gives:

$$\sigma_{DT} = \frac{k_{DT}\tau}{\cos\alpha\sin\alpha} = \frac{2k_{DT}\tau}{\sin 2\alpha} \tag{7.80}$$

$$P_{ST} = -Q_{DT}\frac{\cos\alpha}{\sin\alpha} = -\frac{k_{DT}\tau \cdot bt}{\tan\alpha} \tag{7.81}$$

$$P_{FR} = -Q_{DT}\frac{b}{L}\tan\alpha = -k_{DT}\tau \cdot Lt\tan\alpha \tag{7.82}$$

The frame and stiffener loads are defined for super stiffener (index ST) and super frame (index FR). For the super-frame the thickness is the average of the 6 surrounding pockets. For the stiffener the average is from two surrounding pockets. The loads give super frame and super stiffener stresses and strains bases on the cross-sectional areas and Young's modulus of elasticity of the built-up super structure.

$$\varepsilon_{FR} = \frac{P_{FR}}{S_{FR}E_{FR}} \tag{7.83}$$

Same can be done for the stiffener. The strain in the skin is a function of both the diagonal tension in the skin (kQ) and the (residual) shear stress in the skin ($(1-k)Q$). The strain is determined in the direction of the diagonal tension:

$$\varepsilon_{\theta} = \frac{1}{E}(\sigma_{\theta} - v\sigma_{\theta+90^{\circ}}) \tag{7.84}$$

$$\varepsilon_{DT} = \frac{1}{E}(\sigma_{DT} + \sigma_t - v\sigma_c) \tag{7.85}$$

With the diagonal tension stress defined above and the tensile and compressive stress as a function of the residual shear stress $(1-k)\tau$ and angle of rotation θ. The angle θ is in direction of the diagonal tension.

$$\sigma_t(\theta) = (1-k)\tau \sin 2\theta \tag{7.86}$$

$$\sigma_c(\theta) = (1-k)\tau \sin 2\theta \tag{7.87}$$

$$\varepsilon_{DT} = \frac{\tau}{E}\left(\frac{sk}{\sin 2\theta} + (1-k)\sin 2\theta + v(1-k)\sin 2\theta\right) \tag{7.88}$$

The angle θ is found by minimum strain energy of web, flanges and stiffeners. This comes down to:

$$\cot \alpha^2 = \frac{\varepsilon_{DT} - \varepsilon_{FR} + \frac{1}{24}\left(\frac{b}{R}\right)^2}{\varepsilon_{DT} - \varepsilon_{ST}} \tag{7.89}$$

This is an iterative process, which starts at $\alpha = 45^{\circ}$ and $\cot = {}^{1}/_{\tan}$.

7.6.2.4 Stress distribution over stiffener and frame

The stress varies from a maximum at the neutral line of the beam to a minimum at the ends (gusset effect). The equation is derived from Bruhn figure C11.21 [27]. For the stiffener:

$$\frac{\sigma_{ST_{min}}}{\sigma_{ST}} = (1-k)\left(1.78 - 0.64\frac{b}{L}\right) + k \tag{7.90}$$

If this is equal to or larger than 1. For the frame:

$$\frac{\sigma_{FR_{min}}}{\sigma_{FR}} = (1-k)\left(1.78 - 0.64\frac{b}{L}\right) + k \tag{7.91}$$

7.6.2.5 Bending moments due to shell curvature

Stringers are subject to radial loads due to the root effect, which follows from skin bays flattening.

Bending moment in the super stiffener

Bending moment in the super stiffener half way from frames is given by:

$$M_{(L/2)^{DT}} = k\frac{bL^2}{24R}\tau \cdot t\tan\alpha \tag{7.92}$$

The moment compresses the skin and the stringer skin side flange. Bending moment in the super stiffener at frames is given by:

$$M_{(L)^{DT}} = -k\frac{bL^2}{24R}\tau \cdot t\tan\alpha \tag{7.93}$$

For frames fastened to the skin.

$$M_{(L)^{DT}} = -k\frac{bL^2}{12R}\tau \cdot t\tan\alpha \tag{7.94}$$

For floating frames. The moment compresses the stringer inner flange.

Bending moment in the frame

Bending moment in the frame mid-way from stiffeners:

$$M_{(b/2)^{DT}} = -k\frac{bL^2}{24R}\tau \cdot t\tan\alpha \tag{7.95}$$

This moment compresses the frame inner flange.

$$M_{(b)^{DT}} = k\frac{bL^2}{12R}\tau \cdot t\tan\alpha \tag{7.96}$$

This moment compresses the skin.

7.6.2.6 Skin stresses

The following stresses are based on the theoretical shear stress and the bending of the super-stiffener frames due curvature.

Compressive stress along the stiffener mid-way from frames

Skin stress for fastened stiffener mid-way from frames:

$$\sigma_{sk}^{DT} = \frac{E_{sk}}{E_{ST}^{DT}}\left(\sigma_{ST_{min}}^{DT} - \frac{M_{L/2}^{DT}}{I^{DT}}(d^{DT} + t_?)\right) \tag{7.97}$$

Depending on the definition of d^{DT}, $t_?$ should be omitted.

Pocket shear stress

The pcoket shear stress is derived from Bruhn figure C11.23 and C11.24 [27].

$$\frac{\tau_{max}}{\tau} = \sqrt{1 + \left(\frac{k_{DT}}{\tan 2\alpha}\right)^2} \tag{7.98}$$

Pad shear stress

The pad shear stress is given by

$$\frac{\tau_{max}}{\tau} = 1.3\frac{t}{t_p}\sqrt{1 + \left(\frac{k_{DT}}{1 + k_{DT}}\right)^2} \tag{7.99}$$

The shear stress is reduced due to the thickness increase from skin thickness to pad thickness. The factor 1.3 is likely from stiffness increase load attraction.

7.6.2.7 Stiffener and frame stresses

From super stiffener to stiffener and frame stresses. The stiffener mean stress in compression is given by:

$$\sigma_{st} = \frac{E_{st}}{E_{ST}}\sigma_{ST}^{DT} \tag{7.100}$$

Midway between frames, the maximum stress in compression, is given by:

$$\sigma_{st_{min}} = \frac{E_{st}}{E_{ST}}\sigma_{ST_{min}}^{DT} \tag{7.101}$$

Skin side flange half way between frames:

$$\sigma_{stsk}^{DT} = \frac{E_{st}}{E_{ST}^{DT}}\left(\sigma_{ST_{min}}^{DT} - \frac{M_{L/2}^{DT}}{I^{DT}}(d^{DT} - t_p)\right) \tag{7.102}$$

Skin side flange at frames:

$$\sigma_{stsk}^{DT} = \frac{E_{st}}{E_{ST}^{DT}}\left(\sigma_{ST}^{DT} - \frac{M_{L}^{DT}}{I^{DT}}(d^{DT} - t_p)\right) \tag{7.103}$$

Inner flange (cap) half way between frames:

$$\sigma_{sti}^{DT} = \frac{E_{st}}{E_{ST}^{DT}}\left(\sigma_{ST_{min}}^{DT} + \frac{M_{L/2}^{DT}}{I^{DT}}(h_{st} - d^{DT} + t_p)\right) \tag{7.104}$$

Inner flange (cap) at frames:

$$\sigma_{sti}^{DT} = \frac{E_{st}}{E_{ST}^{DT}}\left(\sigma_{ST_{min}}^{DT} + \frac{M_{L}^{DT}}{I^{DT}}(h_{st} - d^{DT} + t_p)\right) \tag{7.105}$$

Stress in the frame:

$$\sigma_{fr_{min}} = \frac{E_{fr}}{E_{FR}}\sigma_{FR_{min}}^{DT} \tag{7.106}$$

7.6.2.8 Forced crippling

Forced crippling is based on an empirical formula, Bruhn C11.22 [27]. Included is plasticity correction and upright thickness (h' or t_u).

$$\sigma = C1 \cdot k^{2/3} \cdot \left(\frac{t_u}{t}\right)^{1/3}, \quad \frac{t_u}{t} > 0.6 \tag{7.107}$$

Forced crippling occurs when the maximum compression is the stiffener reaches a value from the empirical formula. Material plasticity is taken into account. The actual crippling would take place in the skin side flange of the stiffener. Therefore σ_{crip} should equal the largest value of $|\sigma_{stsk}|$ (stress in the skin side flange of the stiffener). The empirical formula for crippling stress is:

$$\sigma_{crip} = -0.051 \frac{\sigma_{0.2st}}{\sqrt{\frac{\sigma_{0.2st}}{E_{st}} + 0.002}} k^{2/3} \left(\frac{h' E_{st}}{t E_{sk}} \right)^{1/3} \tag{7.108}$$

Where the upright thickness is defined by:

$$h' = \sqrt{t_{st}^2 + \frac{E_{sk}}{E_{st}} (t_p - t)^2} \tag{7.109}$$

If $t_p > 1.5t$ then $t_p = 1.5t$ in the calculation.

The shear stress at this point is the crippling shear stress, τ_{crip}. The maximum crippling stress is clipped at the material yield stress. Also the shear stress is clipped at the material yield stress. The same can be done for forced crippling of the frame.

7.6.2.9 Column buckling

Column buckling is covered by two equations: Johnson equation and Euler equation. the Johnson equation is valid for wave lengths smaller than the limit value λ_0' and Euler for larger wavelengths. The diagonal tension opposes buckling of the column, which is similar to an elastic foundation for the column. This support is expressed by the 'end fixity coefficient':

$$K_{DT} = \sqrt{\frac{1}{1 + k^2 \left(3 - 4\frac{b}{L}\right)}} \tag{7.110}$$

$$L_{DT} = K_{DT} L \tag{7.111}$$

Where L is replaced by $L/2$ as the buckling length. The column wavelength is then:

$$\lambda_{DT} = L_{DT} \sqrt{\frac{S_{ST}}{I_{ST}}} \tag{7.112}$$

Now the Euler buckling strength can be calculated:

$$\sigma_{crit} = \frac{\pi^2 E_{ST}}{\lambda^2} \tag{7.113}$$

The Johnson formula for low slenderness ratio is:

$$\sigma_{crit} = \sigma_{L0} - \frac{\lambda^2}{4\pi^2 E_{ST}} \sigma_{L0}^2 \tag{7.114}$$

Where σ_{L0} is the zero slenderness stress of the super stiffener, which is given by equation 7.54 The limit wave length between both the Johnson curve and the Euler curve can be calculated by having equal load and equal tangent. The limit wave length is:

$$\lambda_0' = \pi \left(\frac{2E_{ST}}{\sigma_{L0}} \right)^{0.5} \tag{7.115}$$

When the occurring wave length is smaller the Johnson curve is used when larger the Euler curve is valid. Now super stiffener column buckling occurs when either:

- the column buckling stress equals the mean super stiffener stress.
- or when the column buckling stress for the half column wave length equals the maximum super stiffener stress.

The smallest value of the two gives the column buckling stress, which gives the shear stress, τ_{column} at which column buckling occurs.

7.6.2.10 Skin material failure stress

The ultimate (allowable) shear stress is based on the tensile strength:

$$\tau_{all} = \frac{\sigma_{ult}}{2} \tag{7.116}$$

For a curved panel the following is defined:

$$\tau_{all} \frac{\sigma_{ult}}{2}(0.65 + \Delta) \tag{7.117}$$

$$\Delta = 0.3 \tanh\left(\frac{S_{fr}}{Lt}\right) + 0.1 \tanh\left(\frac{S_{st}}{bt}\right) \tag{7.118}$$

Included to the frame cross-section and the stiffener cross-section is the skin pad area (both for longitudinal and transverse directions). For now no skin pad is defined in frame direction.

7.6.2.11 Static margins

Forces crippling in stiffener:

$$MS_{crip} = \frac{\tau_{crip}}{\tau} - 1 \tag{7.119}$$

Forced crippling in frame:

$$MS_{crip} = \frac{\tau_{crip}}{\tau} - 1 \tag{7.120}$$

Skin failure:

$$MS_{ult} = \frac{\tau_{all}}{\tau} - 1 \tag{7.121}$$

Global buckling of super stiffener:

$$MS_{column} = \frac{\tau_{column}}{\tau} - 1 \tag{7.122}$$

Margins should be larger than 0.

7.6.2.12 Effect of panel curvature

Buckling coefficient

ESDU 02.03.18 [28] shows the buckling stress coefficient for curved plates in shear. However no formula is given for these curves. A first estimate of these curves is:

$$K_s = \left(4.83 + B\left(\frac{b}{L}\right)^2\right)\left(1 + C_1\frac{b}{\sqrt{Rt}} + C_2\frac{b^2}{Rt}\right) \tag{7.123}$$

Where $B = 3.61$ (ESDU) and C_1 and C_2 are derived from the ESDU figure 1 [28]. The constants are estimated at $C_1 = 0$ and $C_2 = 0.028$.

HSB 45400-01 [17] is valid for curvature smaller than $^{100t}/_{R}$. This is true for the fuselage shells, which are thin walled.

$$\tau_b = \tau_{bflat} + 0.1E\frac{t}{R} \tag{7.124}$$

Diagonal tension factor for curved panels

Unfortunately no mathematical formula is offered for this factor. In ESDU 77018 [28], the diagonal tension factor is a function of the ratio $10^3 \cdot {}^{t}/{}_{R}$ and grows rapidly. Typically the range of $10^3 \cdot {}^{t}/{}_{R}$ is 0.5 to 1.0 for fuselage shells. The increase of the diagonal tension factor is then roughly between 40 and 80%. The following relation was found from ESDU 77018 figure 1 [28]:

$$k_{DT} = \tanh\left(C \log_{10} \frac{\tau}{\tau_b}\right) \tag{7.125}$$

Where C is a linear function of ${}^{t}/{}_{R}$:

$$C = 0.5 + 0.60\left(\frac{t}{R}1000\right) \tag{7.126}$$

For ${}^{t}/{}_{R}$ smaller and equal to 3.0 and ${}^{\tau}/{}_{\tau_b}$ smaller and equal to 10.0.

7.6.3 Combined compression and shear of stiffened panel

The combined loading is based on the applied compressive load (P) and applied shear stress (τ). Two interaction curves are formulated. One for the failure load, which gives the Reserve Factor or Margin of Safety, and one for the pocket folding load, which gives the percentage of pocket folding at limit load.

7.6.3.1 Combine failure load

Additional input variables for the allowable compression and allowable shear stress at failure are:

P_{crit_0} The critical load compressive load (either column buckling or local skin or stiffener buckling).

τ_{crit_0} The critical shear stress, which gives stiffener crippling or column buckling.

These two values constitute the intersections with both interaction axes (compressive load and shear load). The compression and shear interaction formula is:

$$\frac{P_{crit}}{P_{crit_0}} + \left(\frac{\tau_{crit}}{\tau_{crit_0}}\right)^{1.5} = 1 \tag{7.127}$$

Furthermore the condition that the ratio of the compressive load and the shear load is equal to the applied ratio:

$$\frac{P_{crit}}{\tau_{crit}} = \frac{P}{\tau} \tag{7.128}$$

Combining both equations results in the critical compressive load and critical shear load.

7.6.3.2 Combined pocket folding load

Additional input variables for the pocket folding load and shear stress at pocket folding are:

P_{pocket} The compressive load at pocket folding

k_{dt_0} The average diagonal tension factor for pocket shear folding. This gives the average pocket folding shear stress, which is different from the linear average of the pocket folding shear stresses.

The average pocket folding shear stress is determined as follows:

$$\tau_{bp_0} = \frac{\tau_{applied}}{\left(\frac{1+k_{dt_0}}{1-k_{dt_0}}\right)^{\frac{1}{\log_{10}(e)}}} \tag{7.129}$$

In case of $\tau/\tau_b < 1.0$ the k_{dt_0} value is zero and then the τ_{bp_0} is taken as the linear average of τ_{bp_1} and τ_{bp_2}, which differs only a bit with using the linear average of the k_{dt_1} and k_{dt_2}. Otherwise it is possible to continue to work with negative values of k_{dt}.

The pocket folding load and the average folding shear stress constitute again the intersection with the interaction axes. The compression and shear interaction formula for pocket folding is:

$$\frac{P_p}{P_{pocket}} + \left(\frac{\tau_b}{\tau_{bp_0}}\right)^2 = 1 \tag{7.130}$$

Furthermore the condition that the ratio of the compressive load and the shear load is equal to the applied ratio:

$$\frac{P_p}{\tau_b} = \frac{P}{\tau} \tag{7.131}$$

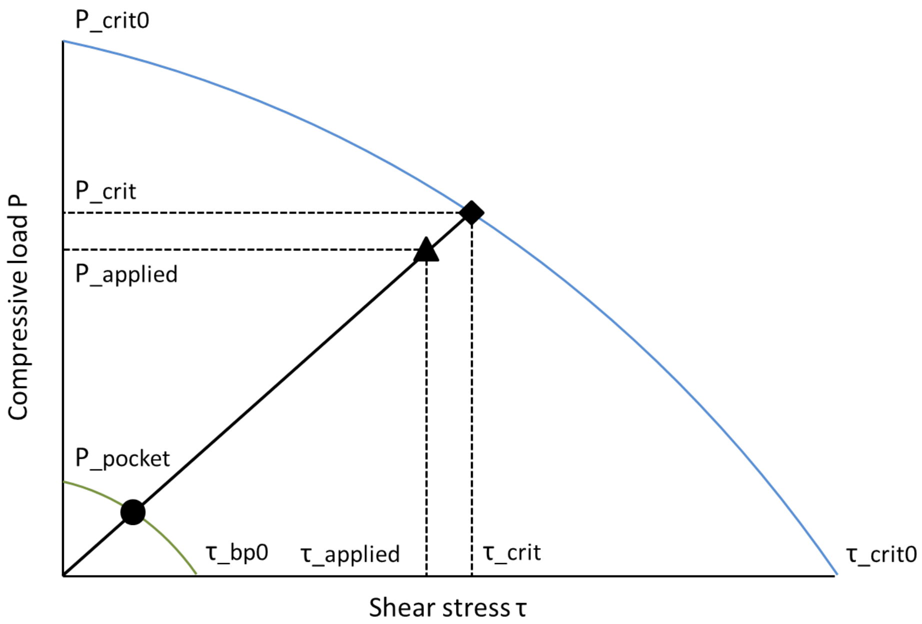

Figure 7.5: Interaction curves for combined loading

7.6.3.3 Margins

The Reserve Factor is:

$$RF = \frac{P_{crit}}{P} = \frac{\tau_{crit}}{\tau} \tag{7.132}$$

and the Margin of Safety:

$$MS = RF - 1 \tag{7.133}$$

The percentage of pocket folding at limit load is:

$$MS_{LL} = 1.5\frac{P_p}{P} \cdot 100\% \tag{7.134}$$

Chapter 8

Optimization

In order to optimize the structural concept to the objective of getting the required structural dimensions with minimized weight, an optimization program is developed. The optimization tool evaluated the optimum structural dimensions for the different structural and material configurations, according to the before mentioned design requirements and limit loads. The applied method to find the optimum design, which is a minimum weight design, is discussed in this chapter.

8.1 Implemented method 5-point

For metal buckling an optimization method is programmed, which consist of optimization two panels thicknesses for the criteria mentioned in section 7.6. The calculated running loads are valid for a combination of two half panels and a stringer. The area of the stringer is fixed and should not be optimized. The thickness of a panel should change in order to carry the loads on the panels. All the loads on the fuselage are calculated using an initial thickness. This thickness is the start criteria for both panels. Step by step the thickness of two panels is changed per time in order to meet the load requirements.

The optimization is done by going through the stringers and changing the thickness of the neighboring half skin panel. The thickness of left panel t_1 and thickness of right panel t_2 is assumed to be 1 mm. For these thicknesses the buckling stresses are calculated and the Reserve Factor and Margin of Safety are found. If these thicknesses are satisfies the criteria. The model will decide in which direction it will optimize the model, thus in this case decrease the skin thickness in order to find the minimum required thickness. The thickness will be changed by steps of $\Delta t = -0.1$. As shown in figure 8.1, alongside the basic combination five other combination of panel thicknesses are defined.

In the next step the model will look which of the five combinations satisfies the criteria. The combination with the lowest skin area which satisfy the criteria $(t_1 \cdot b_1 + t_2 \cdot b_2)$ is saved and set as basic. Hereafter again five combinations are defined till the basic combination remains as the only combination which satisfies the criteria and is saved as the panel thickness.

On the other hand if initial thicknesses do not satisfy the criteria. The model will choose to increase the thickness of the panels. The thickness will be changed by steps of $\Delta t = 0.1$. Again five combinations are defined and analyzed till one combination satisfies the criteria. If one or more combinations satisfy the criteria then the one with the smallest area is chosen and saved as thicknesses for the panel.

Further it is possible to optimize it for several load cases simultaneously. After a thickness combination is found for one load case, these thicknesses are saved as minimum thicknesses. For a new load case the panels are analyzed again, but this time the thickness can only increase, since it should satisfy all the load cases. Hereafter, the final thickness is saved.

After completion, the model will look to the next stringer with two neighboring panels. The thickness of the left panel of the second stringer was analyzed as the right panel of the first stringer. Therefore the thickness of the right panel of the first stringer is set as minimum thickness for the left panel of the second stringer. Therefore this panel can only be made thicker during the next analysis; the right panel of the second stringer is free to change in both ways. This procedure is repeated for each stringer and each bay.

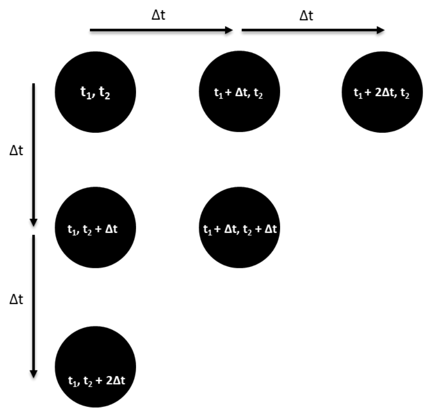

Figure 8.1: Optimization for two panels

8.2 Implemented method 1-point

For other evaluation criteria, like crack analysis and composite buckling analysis a simpler method is used. In these methods the panels are optimized separately. As shown in figure 8.2, alongside the basic combination one other panel thickness is defined.

Again an initial thickness is chosen for the panel. The calculation of method is done and the safety margin is found. If the initial thickness fails the criteria the thickness will be changed by steps of Δ till basic thickness and the extra defined thickness satisfy the criteria, whereas the remaining basic thickness is chosen and saved, since it has the lowest skin area. If the initial thickness satisfy the criteria the thickness will be changed by $-\Delta$ till the basic thickness remains as the only satisfying thickness. For crack analysis of metal an initial thickness and steps of $t_0 = 1$ mm and $\Delta = 0.1$ mm is used. For composite an initial thickness and steps of $t_0 = 1$ mm and $\Delta = 0.1$ mm is used.

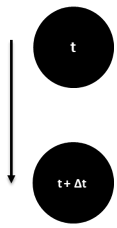

Figure 8.2: Optimization for one panel

Chapter 9

Model procedure

The general procedure of the model is given by figure 9.1. The model is created in Visual Basic Application and all the calculations are done in this environment. The output files are exported to and analyzed in Microsoft Office Excel. The model procedure can be divided in several steps and each step has its own output which is needed for the calculations in the upcoming step. The first step is the input, where the input parameters are entered and several options for the model are selected. The second step is the geometry, where the geometry is defined. During the third step, the weights and loads acting on the fuselage are calculated for various load cases. During the fourth step, the running loads, shear flows and stress distribution on the fuselage calculated. These loads are evaluated using design criteria in next step. The final step is the optimization of the fuselage panel thickness for the running loads and shear flows. Each step will be briefly explained in the upcoming sections.

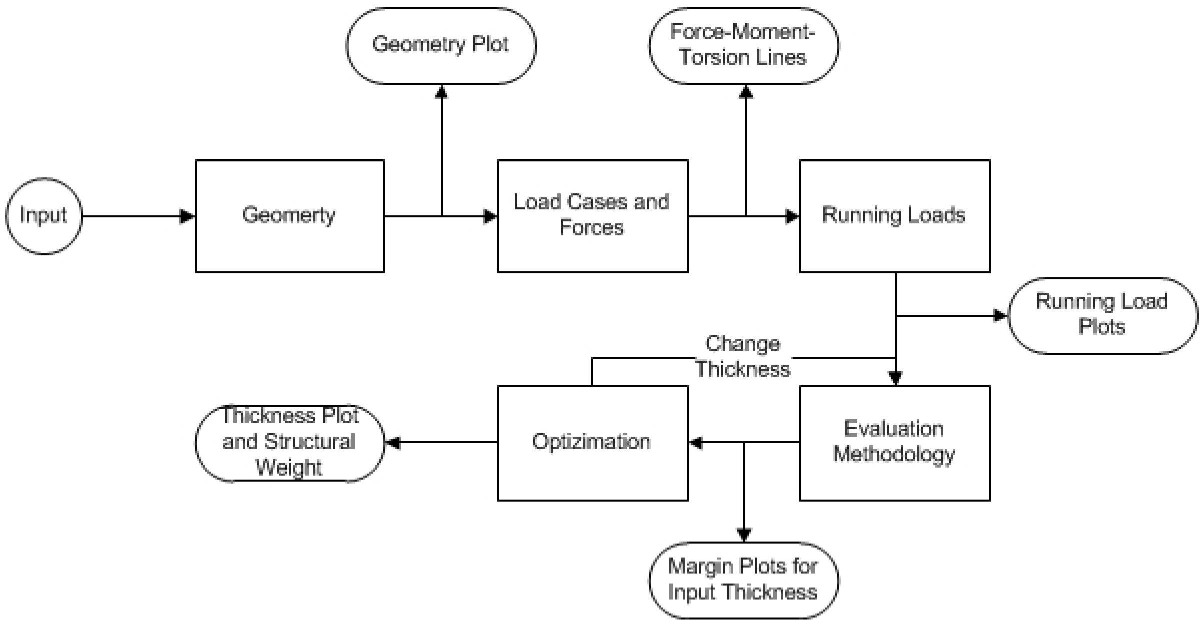

Figure 9.1: General process steps of the model

9.1 Dashboard

The model is programmed in Visual Basic Application environment and a dashboard is created in Microsoft Office Excel to run this model in an easy way. The dashboard has a simple function;

running the model. There are several buttons created in the dashboard. The first button is to plot the geometry of the aircraft fuselage. The results of the geometry creation i.e. the coordinates of the frames and stringers are calculated and written to an output sheet. The second button is to create the Force-Moment-Torsion lines, which are the loads acting on the fuselage structure. The force, moment and torsion loads are plot in diagram for each load case. The third button is to create and plot the running loads and shear flows distribution over the fuselage. The fourth button is used for the calculation of the structural weight of the fuselage for an input panel thickness. The fifth button is to evaluate the input panel thickness for the design criteria. The last and most important button of the model is the optimization button. This button will let the model run and search for the best possible thickness distribution of the fuselage by optimizing for the design criteria built in this model. The dashboard is shown in figure 9.2.

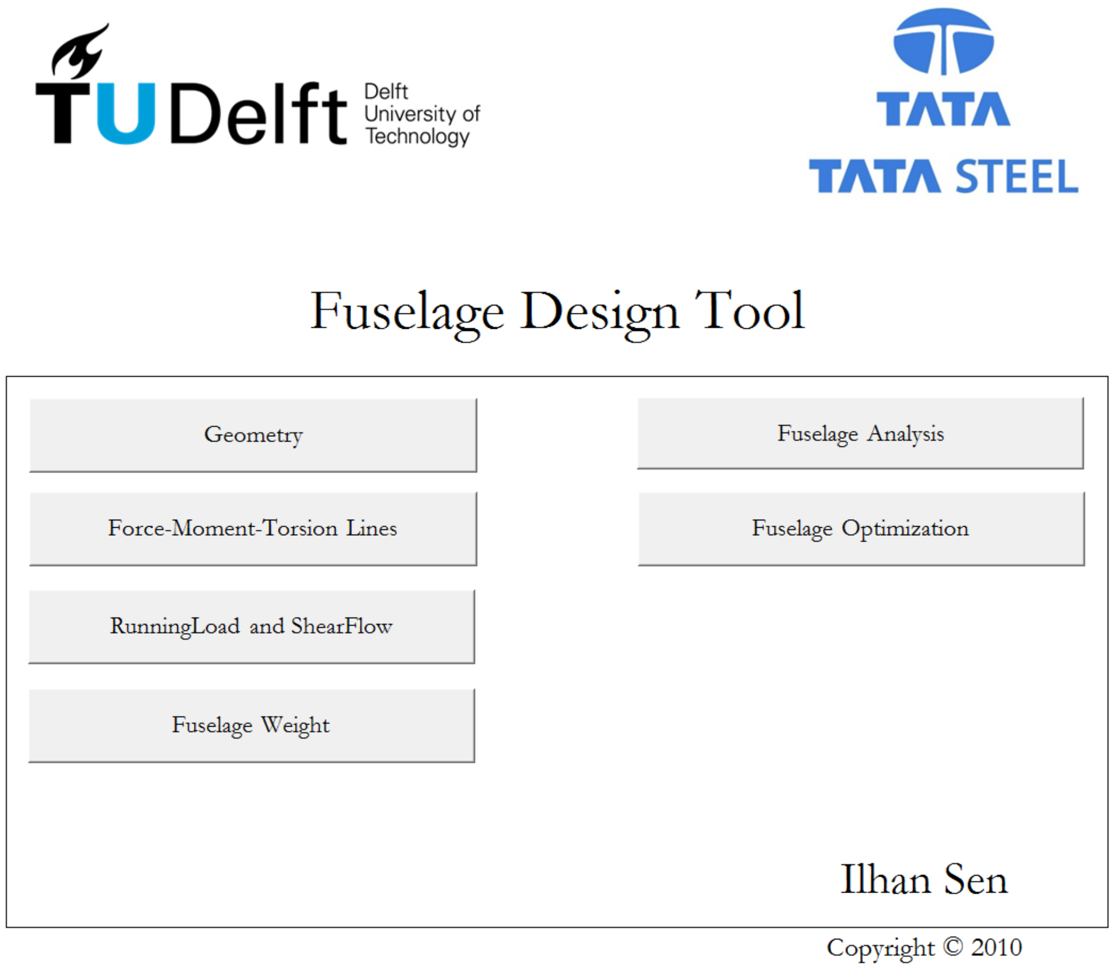

Figure 9.2: Dashboard of model

9.2 Input for model

In the input file, the input parameters for the model are defined and entered; further some choices are made before running the model. The input file consist of the aircraft parameters, like the number of frames and stringers, the size and dimensions of the aircraft, the weights related to the aircraft, the flight speed and range and other geometrical parameters. Further the flight parameters are also defined in the input file, for example the load factor and atmospheric parameters.

The material parameters with material limits are also specified in the input file. Next to this the elements, like stringers, paddings and rivets are specified and an option is available to select the type of element needed for the specific model run. The complete input file is given in appendix C.

9.3 Geometry process

After all the input parameters are loaded, the geometry creation will start. First the frames and bays are created. The fixed frames are defined according to the fixed locations. Hereafter the remaining frames are distributed by ratio between the fixed frame distances and placed evenly between the fixed frames. The position of each frame is calculated, while the bays are defined, since the space between two frames is a bay.

Next step is defining the initial shape and size of the cross-section of the fuselage. The fuselage has a cone shape at the nose and tail section, therefore the cross-section is smaller at the frames located in this section. Therefore the cross-section is sized by ratio, with at the nose and tail 20% the size of the initial cross-section. The number of stringers is also calculated by ratio for this cross-section. Otherwise there will be a large amount stringers placed on these cross-sections with a very small stringer spacing.

Once the number of stringers and cross-sections are defined, the stringer locations and the location of the midpoint of the skin, which is placed between the stringers, are calculated on each cross-section. Further the initial thickness of the skin and the area of stringer is defined. Now the geometry is defined and each frame, skin and stringer element has its initial size and X, Y, Z position. The space between two frames is called a bay, the space between two stringers is called a skin and the skin part along the bay length is called a panel.

Hence the neutral point and moment of inertia for each cross-section is calculated. The geometry creation part is ready and the result is visible in plot.

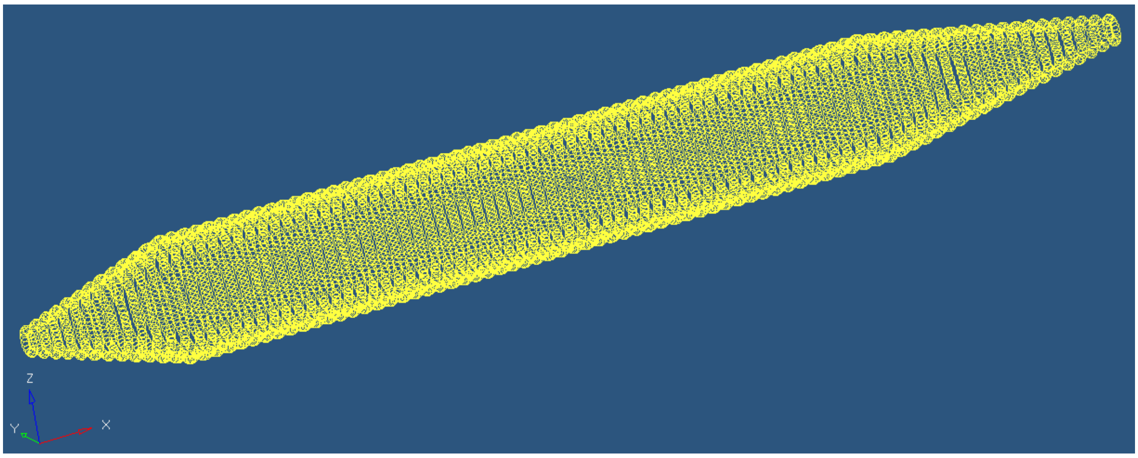

Figure 9.3: Fuselage lay-out generated in Hypermesh

9.4 Load cases and forces process

Once the geometry is created, the load distribution and the forces are calculated. There are several load cases defined. The free body diagram of the fuselage is applicable to all load cases; however each load case has its own set of values for the forces and distributions.

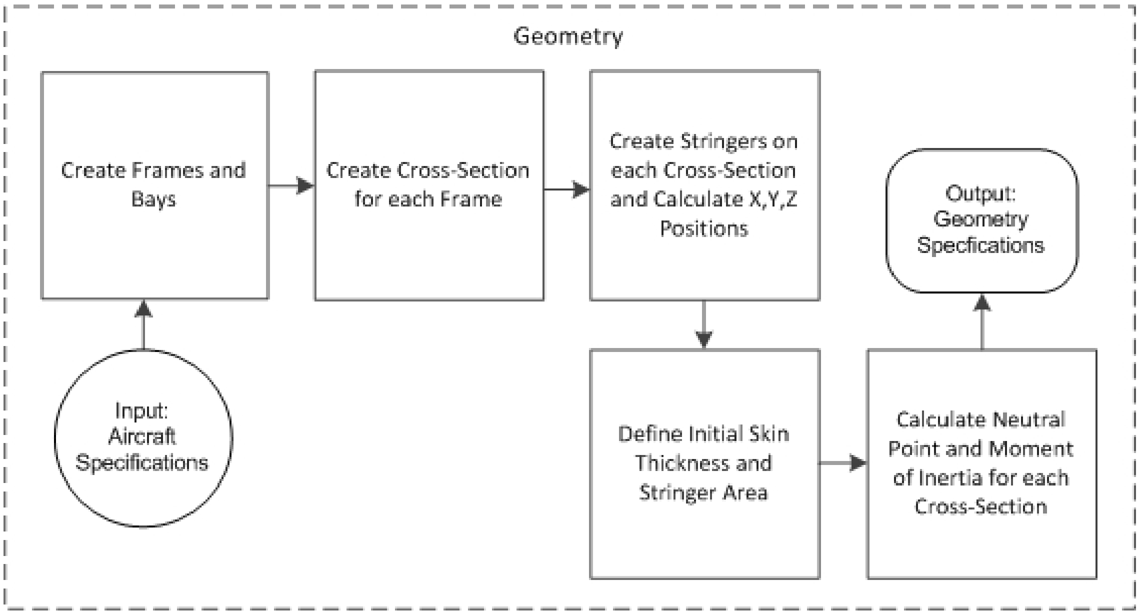

Figure 9.4: Geometry flow chart

First the initial weights and weights distributions are calculated using the aircraft parameters. Hereafter the specific aerodynamic forces are calculated. Further if applicable the ground forces are calculated for the load cases. The fuselage is assumed to be clamped at the wing section, thus the resulting spar forces are calculated using horizontal and moment equilibrium. Now all the forces and weight distributions are known, the Free Body Diagram of the fuselage and consequently the Force-Moment-Torsion lines are created for each load case.

9.5 Running loads process

The next part is the calculation of the running loads when the forces are applied to the fuselage. Since the moment of inertia of each cross-section and the location of the stringers are known, the stress due to the bending moment can be calculated on selected locations on the cross-section. The calculated stress applies for a stringer with two half plates on each side. Since this stress does not give the specific stress in each skin and stringer. This bending stress is converted to the force which applies on this section and is distributed all over the cross-section.

Hence the shear flow on each skin is calculated. Also the hoop stress is calculated in both longitudinal and circumferential direction. For this calculation no stringers are included, since this is the most conservative way.

Once the forces and the shear flow is known, the bending and shear stress is calculated on each stringer and skin location. After this these bending and shear stresses, which are on a frame, are interpolated to get an overall bending and shear stress for each panel on a bay. The result is given as output for each load case separate. The running loads are determined using the initial panel thicknesses and are not updated during the optimization procedure. The change of the running loads due to the thickness variation is assumed to be small.

9.6 Evaluation methodology process

The most important part of the model is the evaluation of material with use of methodology. This part is split into four sections and can be run separately by selecting the preferable methodology

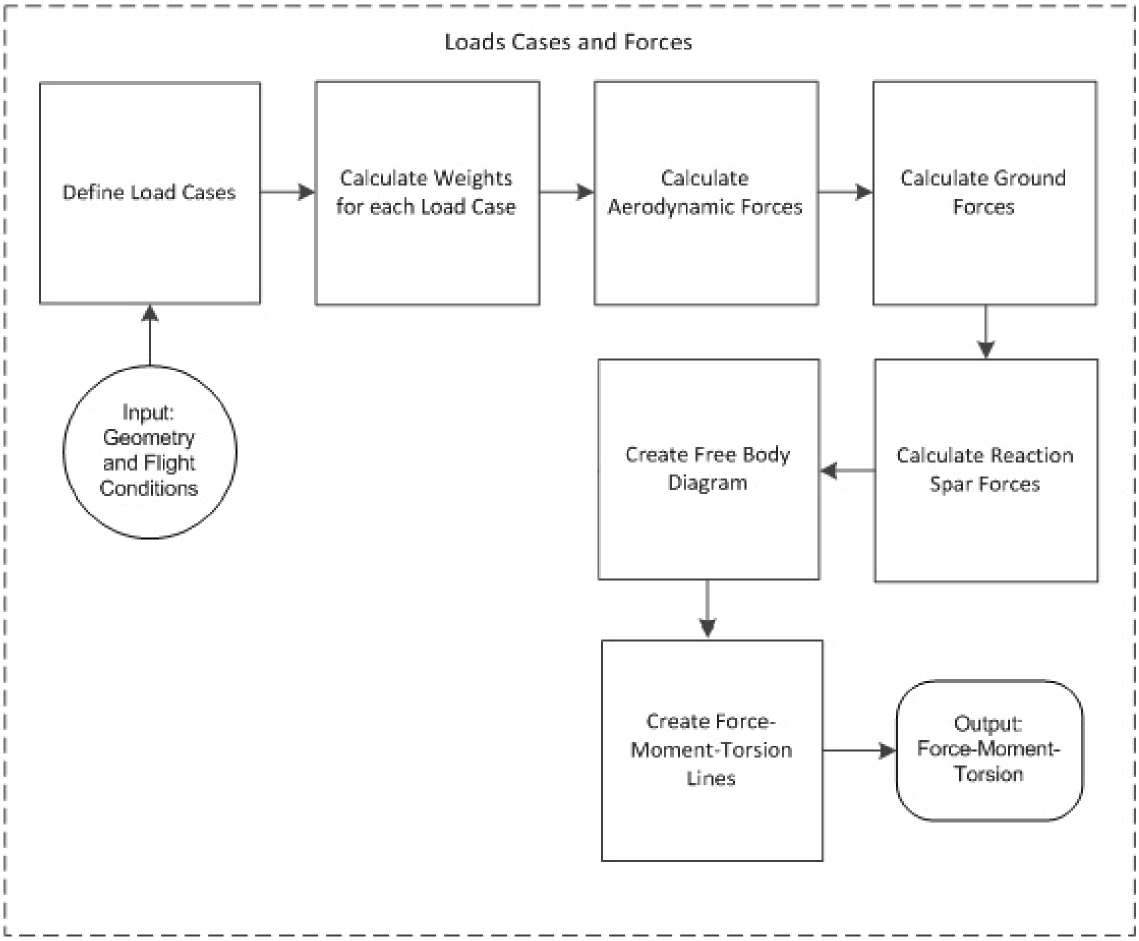

Figure 9.5: Load cases and forces flow chart

in the input file. The output is a margin of safety plot of the fuselage for each load case separate.

The first evaluation methodology is calculating the inspection threshold, which is a criteria defined by the design fatigue stress. Further the inspection period is calculated, which is defined according to the two-bay-crack criteria and the last is calculating the critical crack length, which is known as the fracture toughness of the structure. These criteria are calculated for an input thickness, by defining the limits for these criteria the margin of safety for each panel can be calculated for each criteria.

The second evaluation methodology depends on the strength of the material. The actual stress on the panel is compared with the yield and ultimate strength. This is separately done for tension, compression and shear stress. As a result a margin of safety for each panel is given.

The last two evaluation methodology depends on the type of material used. There are different methods used for metals and composite. The third methodology is specific for metals. In this method an extensive metal buckling analysis is performed. The method is split in three parts, compression of stiffened panel, shear of stiffened panel and combined compression and shear of stiffened panel. These methods include column buckling, local buckling, inter-rivet buckling, stiffener crippling, etc.

The fourth evaluation methodology is specific for composite materials. The material failure is evaluated with the Tsai-Hill criterion. After this the stability of the skin panel is evaluated by

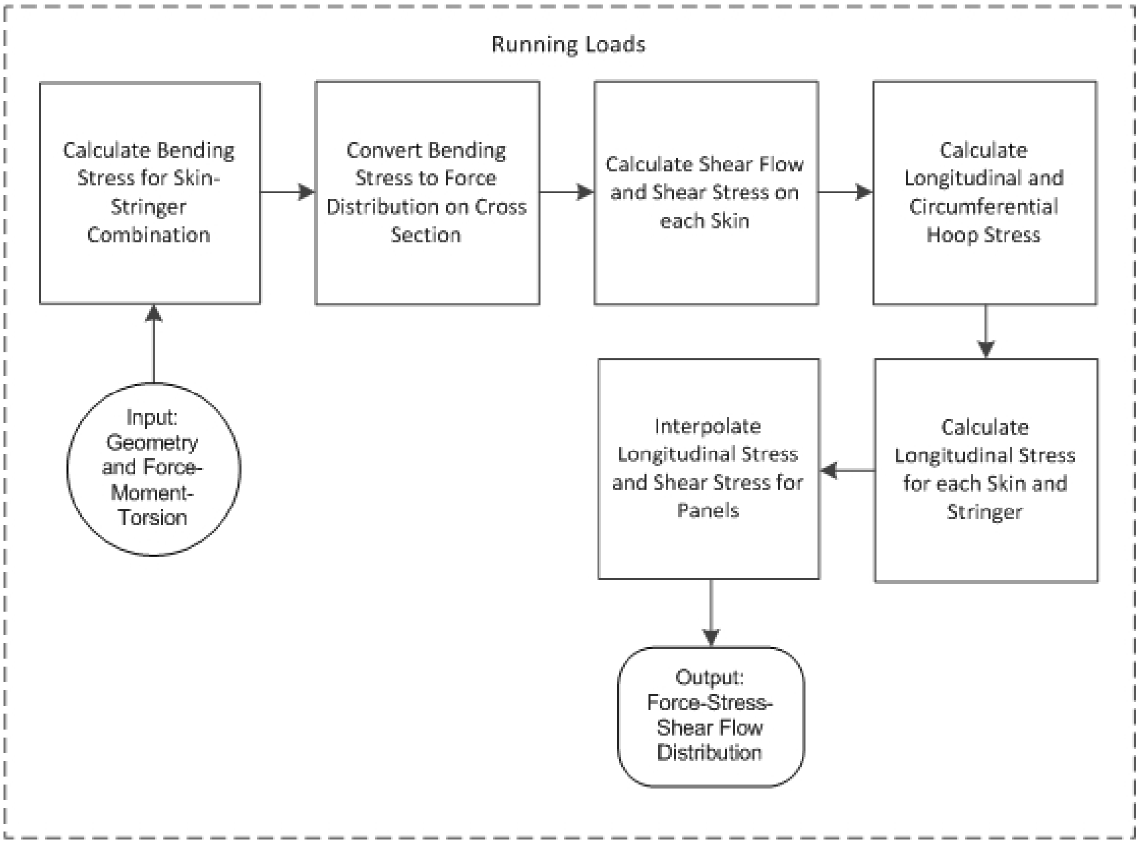

Figure 9.6: Running loads flow chart

calculating the critical buckling loads. The next step is the calculation of the critical load against wrinkling. Next to this the same is done for panel (global) buckling and torsion buckling. For each panel a margin of safety is determined for the input thickness according to these criteria.

9.7 Optimization process

The goal of the optimization process is to find the minimum required thickness for fuselage structure in order to withstand the forces exerted on the fuselage. There are two optimization methods used depending on the parameters, which are optimized. In the first optimization procedure, a first reference thickness is given for the skin panel. For this thickness the absolute safety margin MS is calculated for several evaluation method. The most critical or most undesirable safety margin is taken, which should lie between 0 and 1 in order to pass the criterion. If the criterion fails the optimization will go further by increasing the thickness. If the criterion passes the optimization will go further by decreasing the thickness. The most optimal thickness is found using this way and the relevant safety margin is given as output.

The second optimization method is only applied for the extensive metal buckling analysis. In this case two skin panels are simultaneously evaluated and each skin panel is evaluated twice, whereas the found maximum thickness will be the minimum required thickness for the panel.

9.8 Output for model

Some of the output of the model is given in chapter 10 and consists of the sub result as well as the final results of the model. The first output results consist of the Force-Moment-Torsion

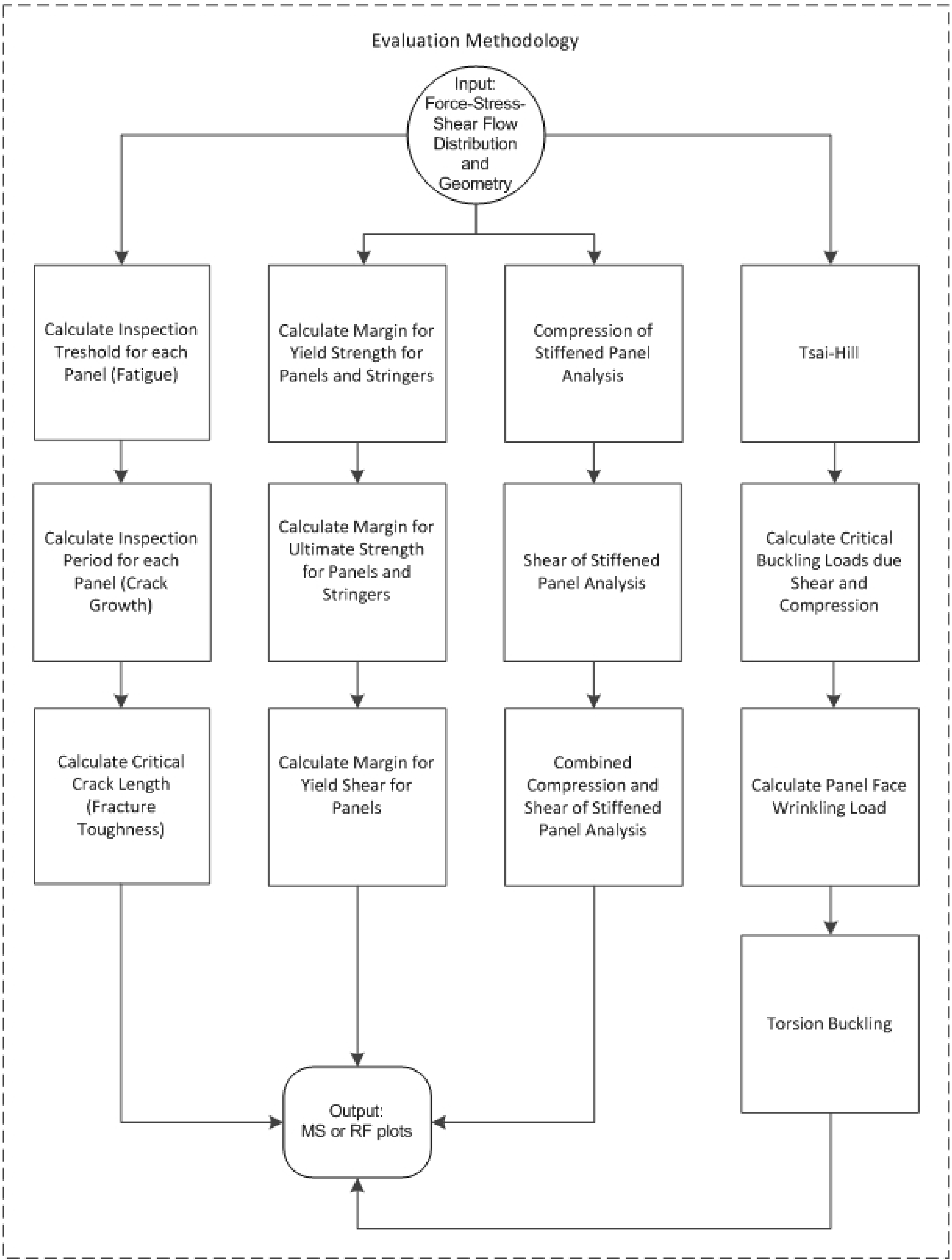

Figure 9.7: Evaluation methodology flow chart

lines, which are plotted for each load case. The second output is the running load and shear flow distribution along the fuselage panels for each load case. The third (optional) output is a safety margin plot for each evaluation method for a given thickness. The last and final output is the required minimum thickness for the fuselage structure with the corresponding safety margin

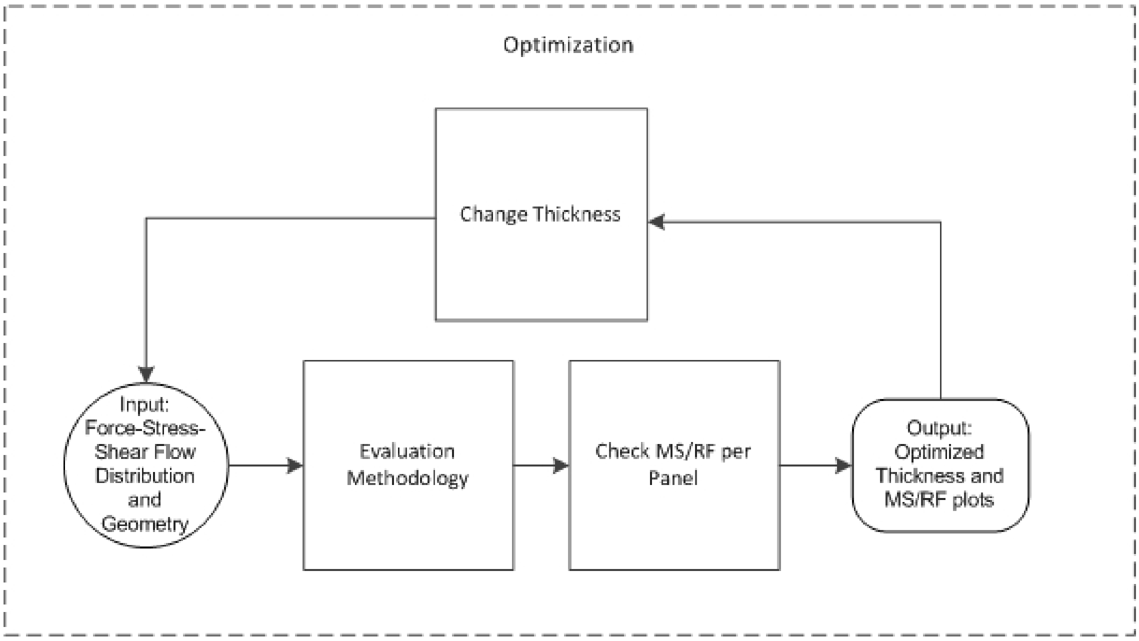

Figure 9.8: Optimization flow chart

plots for each evaluation method to check whether the thickness results satisfies the evaluation methods. The output results are presented in Microsoft Office Excel.

9.9 Validation and reliability

The model is validated by comparing the results of each individual output with the data of the reference aircraft. In this case the running loads and skin thicknesses of the Airbus A320 are compared to that of the model. The model is validated using these data and it is assumable that the used load cases are approaching the real load cases and gives a reliable set of load distributions for applying it on the fuselage model. Further the optimized thickness proved to be valid.

The reliability of the evaluation optimization depends on various factors. The evaluation methods are mostly simplified and applicable for single panels. In order to apply this to the whole construction, a safety factor above the loads is needed.

It is even known that for fatigue depending on the location on the fuselage a safety factor of 3 to 5 is used, since the fatigue behavior is much unexpected on several locations on the fuselage.

The metal buckling method is a more advanced method compared to the composite analysis method, therefore the output metals i.e. aluminum will be more reliable.

The tool consists of simplified expressions compared to full analysis tool used by the aircraft manufacturers. Each inaccuracy or an error margin will consist for each evaluated material or construction, therefore a comparison of materials and construction are not influenced by these inaccuracies, since this is applicable for each output. Thus the results are valid and will give reliable output for material evaluation and comparison.

Chapter 10

Validation results

In this chapter, the model is validated using a reference aircraft (Airbus A320) and the output results are given and discussed for this aircraft.

10.1 Material and configuration

Several material configurations are adopted for the model. These configurations are an aluminum stiffened shell and a CFRP stiffened shell configuration. For the aluminum concept, Aluminum 2024 is chosen for both skin and stringer material. In case of composite concept, quasi-isotropic composite lay-ups are adopted for skin and facings. Since fuselage structure is loaded in all directions, a quasi-isotropic choice of material is justified in this stage. The material of the stiffeners is assumed to be a quasi-isotropic carbon lay-up, in order to simply the load distribution between skin and stiffener. The assumed material properties and allowables are given for the materials in table 10.1, which are derived from material data available at Ces Edupack [29].

Property		**Aluminium 2024**	**Composite Quasi-isotropic**
Density	ρ [kg/m^3]	2800	1560
E-modulus	E [MPa]	70000	50000
Shear modulus	G [MPa]		18000
Poisson's ratio	ν [-]	0.3	0.318
Tensile yield strength	$R_{p02_{tens}}$ [MPa]	250	180
Compressive yield strength	$R_{p02_{comp}}$ [MPa]	250	140
Shear yield strength	$R_{p02_{shear}}$ [MPa]	150	140
Tensile ultimate strength	$R_{m_{tens}}$ [MPa]	375	
Compressive ultimate strength	$R_{m_{comp}}$ [MPa]	375	

Table 10.1: Material properties and allowables

10.2 Force and moment distribution

The first results of the model are the force and moment distributions of the fuselage for the assumed unit load cases, which are given in table 5.1 in chapter 5.

The weight distribution is given in figure 10.1, which shows that the most weight of the aircraft is distributed between the front bulkhead and rear bulkhead, since the entire payload is located here. The results of the force and moment distributions are given in figure 10.2 to 10.5. As seen in the plots the bending moment is the largest in the midsection of the fuselage for 1G, -1G, 2.5G abrupt ground breaking and landing. These load cases are strongly dependent on the weight and therefore have effect on the whole fuselage structure. For the abrupt ground breaking load case it is clearly visible that the breaking of the main landing gear lowers the bending moment in the front section due to the upward bending which is caused by breaking and which cancels the downward bending of the weight of the fuselage.

Further it is visible that the horizontal elevation deflection, lateral gust and side slipping flight load cases have large effect on the mid and rear section of the fuselage. These load cases are all in balanced in the center of gravity or the wing spar forces, therefore they have no effect on the front section of the fuselage.

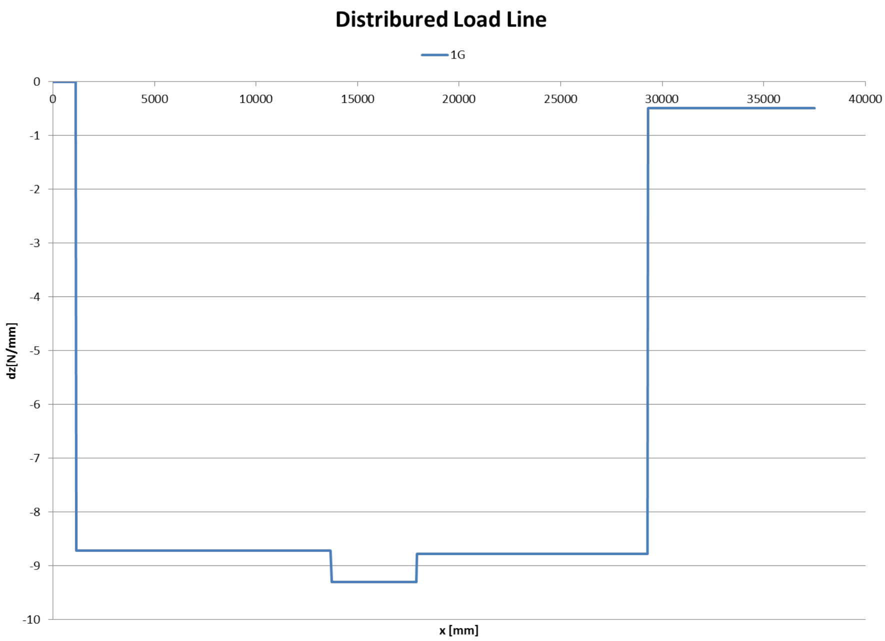

Figure 10.1: Weight distribution of fuselage

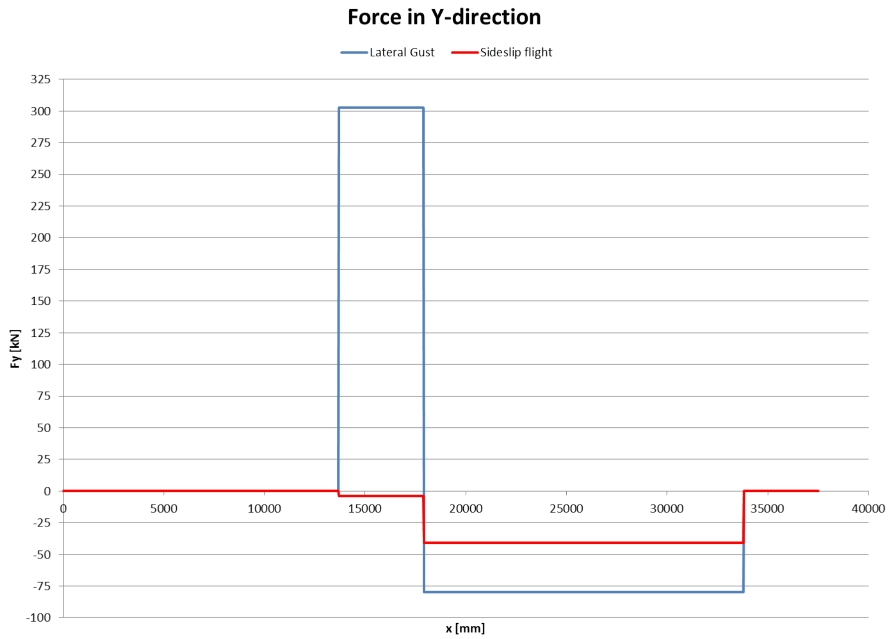

Figure 10.2: Force distribution in y-direction for load cases

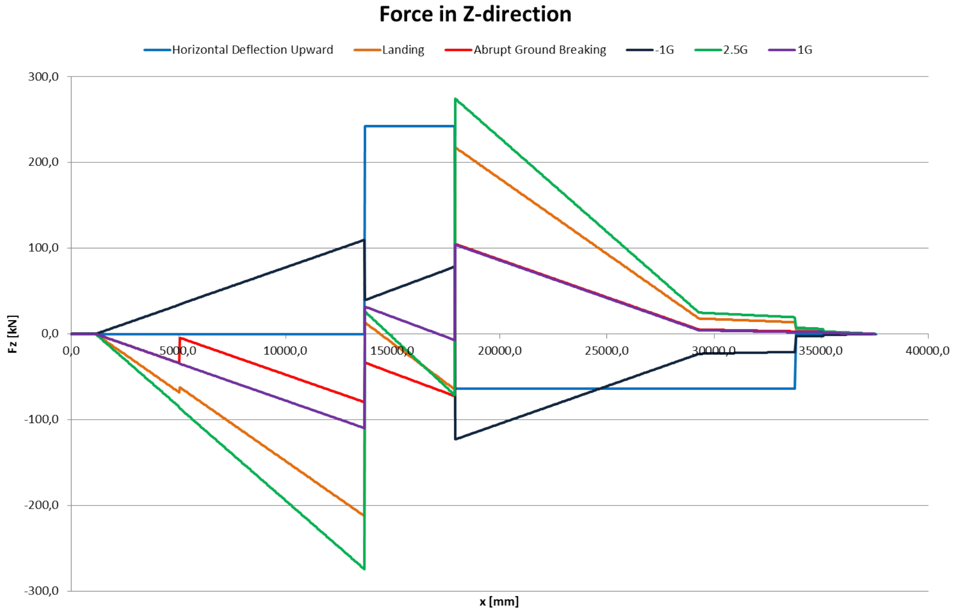

Figure 10.3: Force distribution in z-direction for load cases

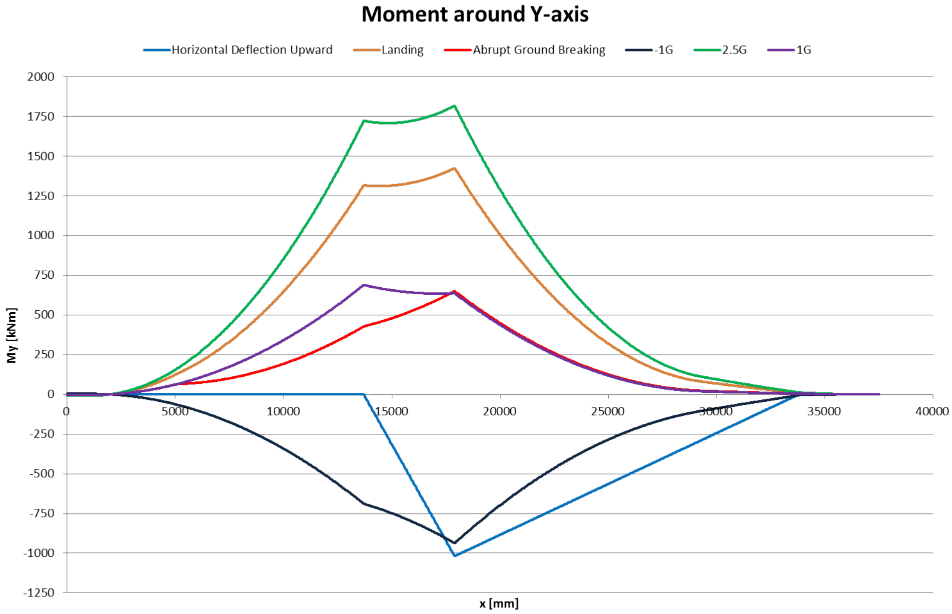

Figure 10.4: Moment distribution around y-axis for load cases

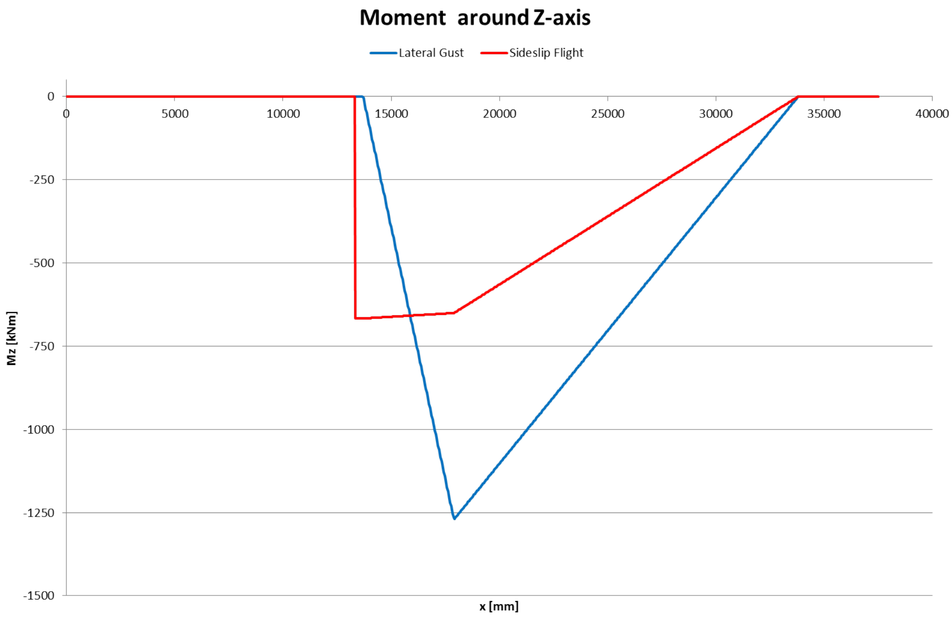

Figure 10.5: Moment distribution around z-axis for load cases

10.3 Maximum Loads

The maximum loads per load cases are plotted and given appendix D. Using the maximum load plots for each load cases the critical load cases or combination of load cases are find, the combined load cases are only load cases which will happen in real life. The cabin pressurization load case can always be combined with flight cases. The 1G load cases represent a steady flight and the original weight of the aircraft is assumed. Additional load cases such as lateral and horizontal gust are considered without weight. The 1G load case is added to these load cases if weight is considered.

The maximum hoop stress caused by pressurization is given figure 10.6. The longitudinal, circumferential and critical 1.33 times circumferential stress is plotted. The hoop stress depends on the radius of the fuselage cross-section. The hoop stress before front and after rear bulkhead is zero, however in this situation this is not considered and the hoop stress varies depending on the radius, which is linearly changing in the front and rear section.

The 2.5G flight load case has the largest effect on the mid-section as well as the 1G flight with horizontal deflection downward, which has even larger effect on the rear section. This creates tension on the top part, compression on the bottom part and shear at the side part of the fuselage. The lateral gust is the most critical load cases from the sides, which causes tension and compression on the side parts and shear on the top and bottom parts of the fuselage. There is no load case which creates critical load for the front section of fuselage.

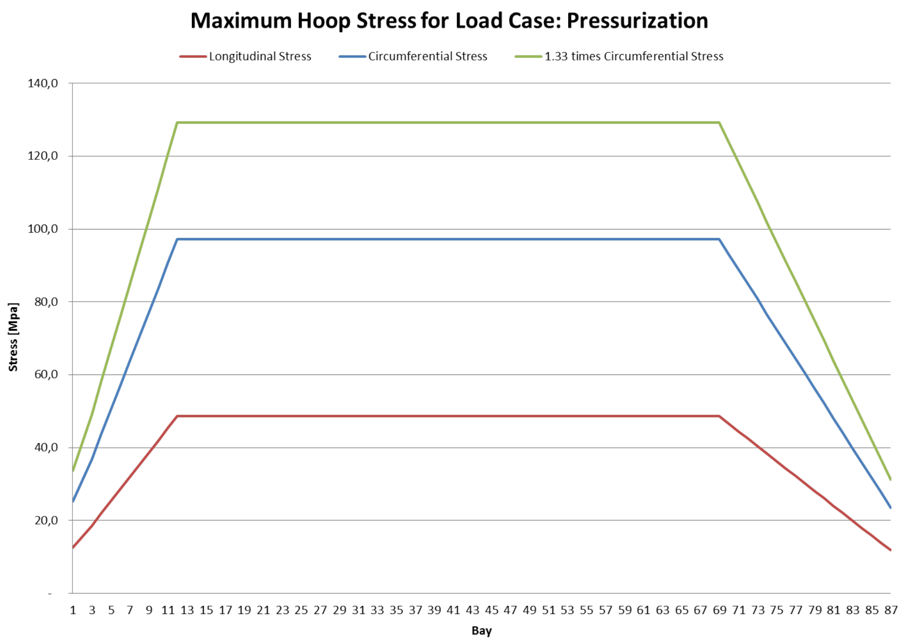

Figure 10.6: Stress caused by pressurization

10.4 Load case identification and selection

Using the maximum load plots for each load case a table is created which identifies the critical load cases for specific sections and parts for the type of load applicable on the fuselage. In table 10.2 these load cases are given. The combinations are realistic load cases and give the most critical load for a specific region. Using this table combination load cases are selected and listed in table 5.2. These load cases will be used for optimization of the skin panels. The unit load cases are given in table 5.1 in chapter 5. The stress distributions for these load cases is given in appendix E. These plots shows clearly the applied stresses on the fuselage per section.

	Top	Side	Bottom
Front	**Tension:** 2.5G + Cabin Pressurization **Compression:** -1G or Horizontal Deflection Upward **Shear:** Lateral Gust	**Tension:** Cabin Pressurization **Compression:** None **Shear:** 2.5G	**Tension:** -1G + Cabin Pressurization **Compression:** 2.5G **Shear:** None
Mid	**Tension:** 2.5G + Cabin Pressurization or 1G + Cabin Pressurization + Horizontal Deflection Downward **Compression:** -1G or Horizontal Deflection Upward **Shear:** Lateral Gust	**Tension:** Lateral Gust + Cabin Pressurization **Compression:** Lateral Gust **Shear:** 2.5G	**Tension:** -1G + Cabin Pressurization or Horizontal Deflection Upward **Compression:** 2.5G or 1G + Horizontal Deflection Downward **Shear:** Lateral Gust
Rear	**Tension:** 1G + Cabin Pressurization + Horizontal Deflection Downward **Compression:** Horizontal Deflection Upward **Shear:** Lateral Gust	**Tension:** Lateral Gust + Cabin Pressurization **Compression:** Lateral Gust **Shear:** 2.5G or 1G + Horizontal Deflection Upward	**Tension:** -1G + Cabin Pressurization or Horizontal Deflection Upward **Compression:** 2.5G or 1G + Horizontal Deflection Downward **Shear:** Lateral Gust

Table 10.2: Critical load case identification

10.5 Validation of running loads

Before optimizing the fuselage, the validation of the tool should be done by comparing the results of the running load plots and thickness plot with the reference data of Airbus A320 [30]. The reference data consist of stress distribution and thickness plots for the bays 27 to 63 for several load cases. The data is only available for the side and top part of the fuselage. In order to make a good comparison the normalized data is compared with the output of the tool, which means the stress is multiplied by the thickness in order to find the stress flow in a single panel. The compared load cases are pressurization, 1G flight and a combination of these two. Besides there is a maximum limit stress plot available, which gives the maximum stress distribution on the fuselage section.

The data of the top part of fuselage is chosen to validate the running loads, since the top part of the reference data is the most undisturbed data. The side parts are influenced by doors and windows and there is no data available for the bottom part. The circumferential and longitudinal stress due to cabin pressurization for both the reference and model are given in figure 10.7 and 10.8. It is clearly visible that the model data gives a good representation of reference data. There are some variations in the circumferential stress in the reference data, which is probably caused

	Combined Load Cases (CLC)	**ULC**
CLC8	-1G Maneuver	-ULC2
CLC9	-1G Maneuver + Cabin Pressurization	-ULC2 + ULC1
CLC10	2.5G Maneuver	2.5·ULC2
CLC11	2.5G Maneuver + Cabin Pressurization	2.5 · ULC2 + ULC1
CLC12	Lateral Gust + Cabin Pressurization	ULC3 + ULC1
CLC13	-Lateral Gust + Cabin Pressurization	-ULC3 + ULC1
CLC14	Horizontal Deflection Upward + Cabin Pressurization	ULC4 + ULC1
CLC15	1G Maneuver + Horizontal Deflection Upward	ULC2 + ULC4
CLC16	1G Maneuver + Horizontal Deflection Downward	ULC2 - ULC4
CLC17	1G Maneuver + Cabin Pressurization + Horizontal Deflection Downward	ULC1 + ULC2 - ULC4
CLC18	1.33 times Cabin Pressurization ($1.33 \cdot \Delta p$)	1.33 · ULC1
CLC19	5G Maneuvre	5·ULC2
CLC20	5G Maneuver + Cabin Pressurization	5 · ULC2 + ULC1

Table 10.3: Combined load cases (updated)

by small differences in the cross section radius or panel curvature or caused by the large doors which are placed at the back. The same holds for the longitudinal stress. In general the deviation is very limited and the model output gives a reliable set of running loads for cabin pressurization.

The normalized 1G flight and combined 1G and cabin pressurization stress distribution is given in figure 10.9 and 10.10. The result of the model for 1G flight is in the same range and gives a good representation of the 1G flight. The only difference is slow decreasing in the rear section of the reference data and the fast decreasing of the model results, this is caused by the weight of the rear section. The weight estimation of appendix B gives a lower estimated weight at the rear section. The combined load case has comparable results, since it is the sum of the load cases. The deviation of stress is limited and therefore the model result is a reliable set of running loads.

The deviation in the stresses are plotted given in figure 10.11. It is clearly visible that the stresses are in the range of the original stresses, the only large deviation is in the rear part with maximum of 27 MPa, which is the sum of the deviation of the two load cases a probably caused by the error in the weight estimation and panel curvature.

In addition the maximum limit stress data for the Airbus A320 data was available. These limits were quite higher than the maximum defined load cases, such as the 2.5G and cabin pressurization, see figure 10.12 These maximum limit stresses are estimated by using a safety factor above the 1G and cabin pressurization flight. A safety factor of 5 was needed to have the stresses in the same range. This extra load case will be used to check the maximum thicknesses, since the thickness of the panel is probably defined by these maximum stresses. This load case is also added to table 10.3

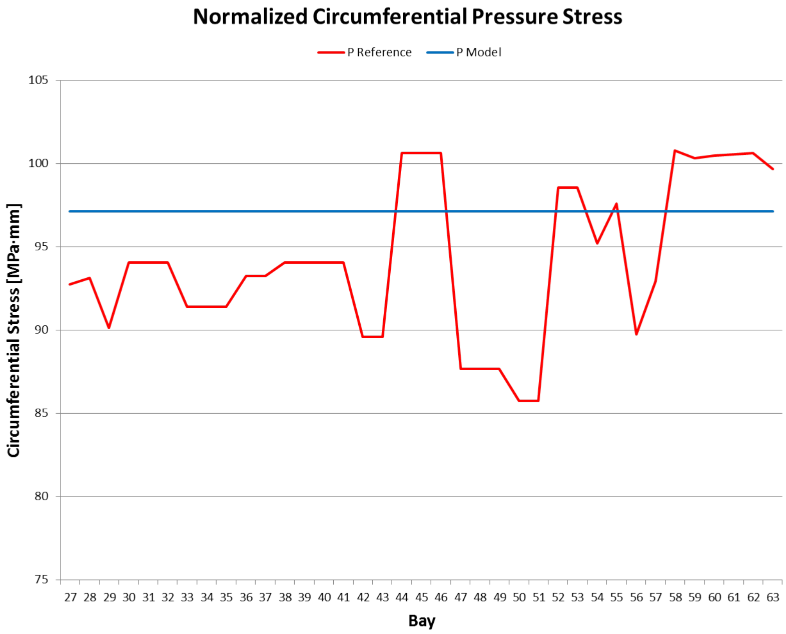

Figure 10.7: Normalized circumferential pressure stress for reference and model

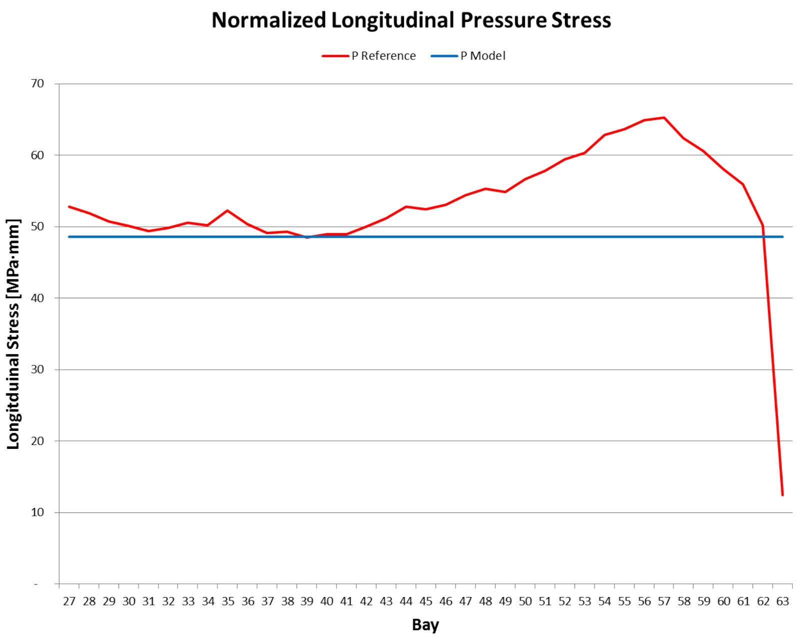

Figure 10.8: Normalized longitudinal pressure stress for reference and model

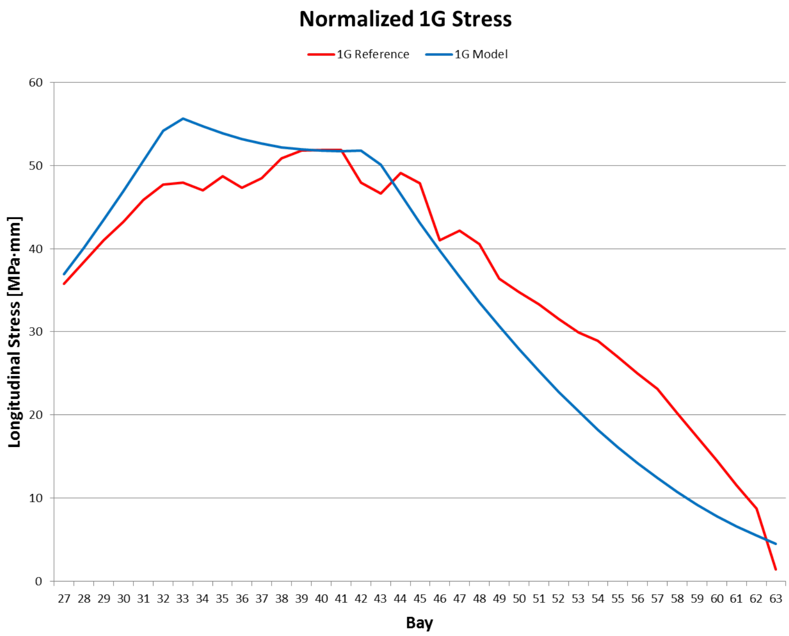

Figure 10.9: Normalized 1G stress for reference and model

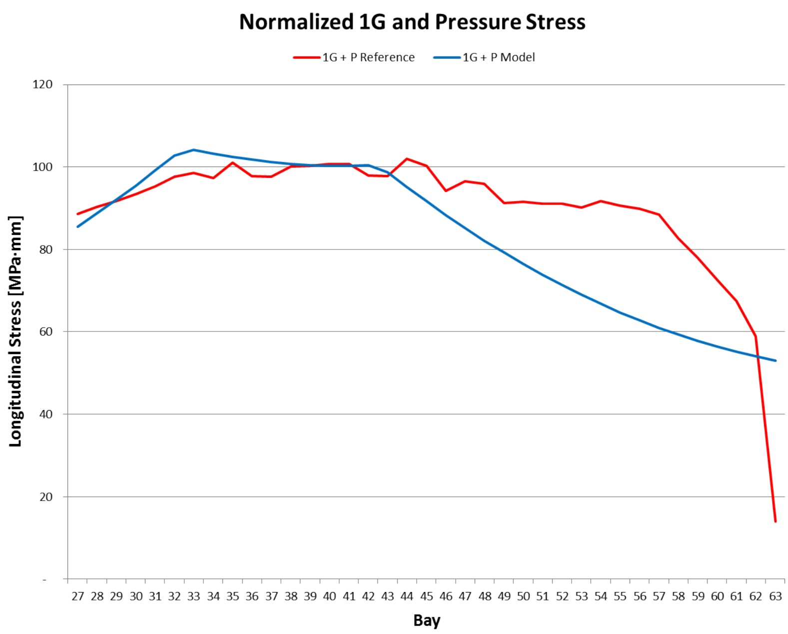

Figure 10.10: Normalized 1G and pressure stress for reference and model

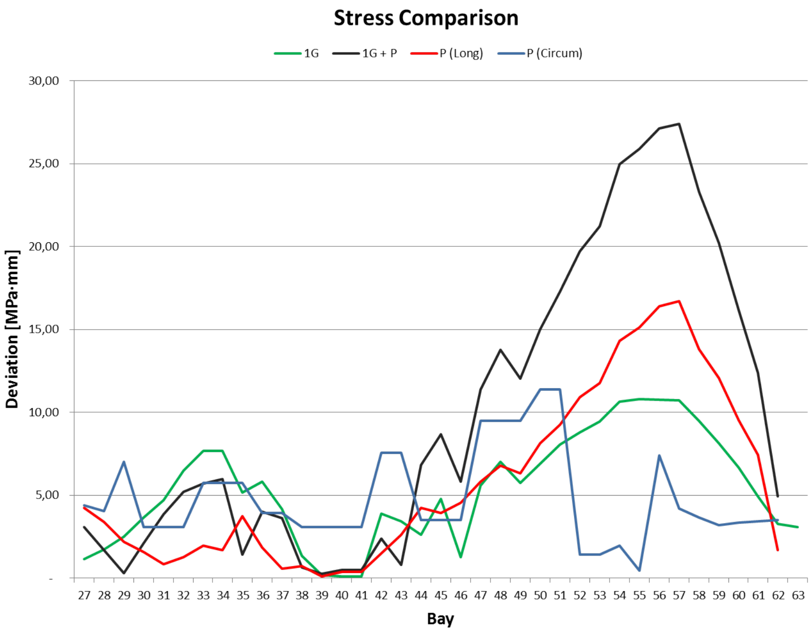

Figure 10.11: Absolute deviation of stresses for reference and model

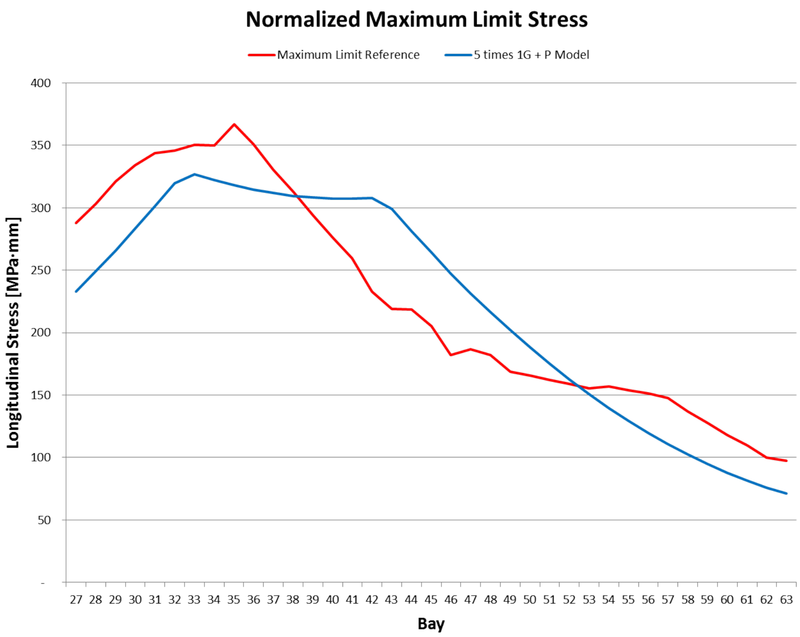

Figure 10.12: Maximum reference stress and assumed maximum model stress

10.6 Optimization of skin thickness

Since the running loads are validated the optimization for the skin panels can be done. The optimization of the skin panel for aluminum is done for two criteria, the metal buckling analysis and crack analysis. The criteria for yield and ultimate stress are integrated in the buckling analysis, so separate run is not needed.

10.6.1 Buckling analysis criteria

For the optimization it is chosen to optimize only two section of the fuselage, namely bays 14 to 29 and 43 to 58. The reason for choosing this section is due to the time needed to run the model and of course no reference data is available for other sections to compare the results. These sections are selected, because it is located just before and after the wing box. In the model there is no wing box assumed, therefore between these two section result in this region will not be realistic since other unknown load distributions dominates in this region due to the wing box. The optimization for buckling is done for a package of load cases. In total five times the model is ran for the buckling analysis for the load cases in package 1 to 5 and one time the model is ran for the crack analysis for the load cases in package 6, which are given in table 10.4.

Package	Load Cases
1.	CLC8 and CLC9
2.	CLC10 and CLC11
3.	ULC3, -ULC3, CLC12 and CLC13
4.	ULC4, CLC14, CLC15, CLC16 and CLC17
5.	CLC19 and CLC20
6.	CLC18

Table 10.4: Load case package

The optimization results are given in appendix F for each run. A thickness of 0.7 mm is set as minimum thickness in order to limit it for manufacturing and reparability requirement. In figure F.1 the result for package 1 is given. Here is clearly seen the top part are optimized for compression due to the -1G flight. In figure F.2 the result for package 2 is given. Due to this load case the whole bottom and side parts are optimized for compression and shear forces. In figure F.3 the result of package 3 is given. In this load cases the side panels are optimized for compression, therefore this package defines the panel thickness of the side part. In figure F.4 the result for package 4 is given. The horizontal elevator deflection is a critical load cases and defines mostly the panel thickness after the wing section.

However, an extra analysis is done for 5 times 1G and cabin pressurization to satisfy the maximum limit loads of the reference data. The result of package 5 is given in figure F.5. Finding the maximum thickness generated by package 1 to 5 gives us the minimal required thickness for buckling, which is given in figure F.6. The minimal required thickness is 0.9 mm, which is in the outer sections and top part of the fuselage. The minimal thickness in this region is generally defined by tension. The maximum required thickness is 1.5 mm at the bottom part of the mid-section. This thickness is defined by compression force. The thickness of the side panels is also critical for compression due to the lateral gust load case.

10.6.2 Crack analysis criteria

Now the optimization is done for the crack analysis criteria. For this criterion the circumferential stresses are used, therefore package 6 is used in this case to optimize the thickness. The results for this load case will give the limitation thickness for fatigue, crack growth and fracture toughness. The thickness distribution is equal all over the section, since the circumferential stress due to cabin pressurization is equal in these sections. The result of package 6 is given in figure F.7.

Combining the results of buckling and crack analysis shows that the crack analysis is the dominant criteria in the outer sections and in the top part of the fuselage section. The buckling analysis is the most critical on the bottom and side parts of the inner sections; however the crack analysis is also dominant in this region. Assuming the buckling load case occurs much more at the bottom and side panels, which makes buckling analysis the dominant criteria in this region. The minimum required thickness is 1.3 mm and maximum required thickness is 1.5 mm for buckling and crack analysis. Further the domination of the crack analysis complies with the fact that the Airbus A320 is designed for fatigue. For the optimized thickness the stress plot is given in figure F.9.

10.7 Thickness and stress validation

The available reference panel thickness and stress of the Airbus A320 for the corresponding bays is given in figure 10.13 and 10.14. In this thickness plot the influence of the center wing box, windows, (cargo)doors are clearly visible (yellow). The panel thickness is much larger in this area in order to compensate for cut-outs or abnormal shapes. The thicknesses and stresses of model and reference for the same sections are shown in figure 10.15 and 10.16. The grey parts in de model data comply with the cut-outs in the reference aircraft, which are not considered.

Comparing the thickness of the undisturbed area the minimum thickness is 1.2 mm and the maximum thickness is 1.6 mm, which is in the same range of 1.3 mm and 1.5 mm as optimized thickness for the model. With some change in evaluation criteria it is even possible to get the same thicknesses. However the panels influenced by the cut-outs should be determined with other methodology.

The stress distribution gives is also comparable results. The load case which defines the maximum stress of the reference data is not known, therefore especially in the mid-section the loads of reference model are difficult to determine. The model stresses at the top side are higher compared to reference data, but this is due to the lower (optimized) thickness in that section. Other load cases are probably defines the minimum thickness in this region.

The model results proof to be valid and give a reliable estimation of panel thicknesses and stresses for an aircraft fuselage.

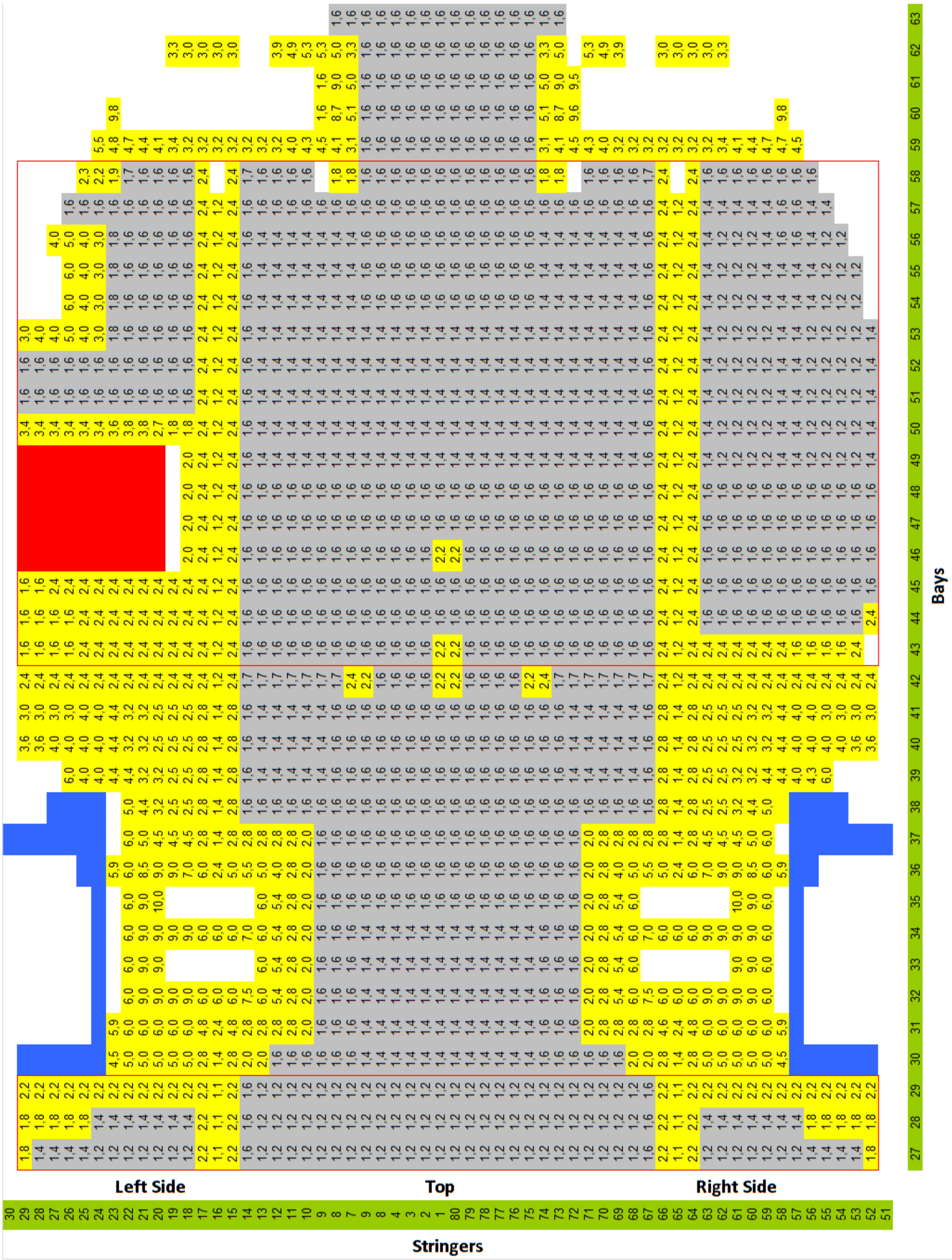

Figure 10.13: Reference thickness data for Airbus A320 in mm

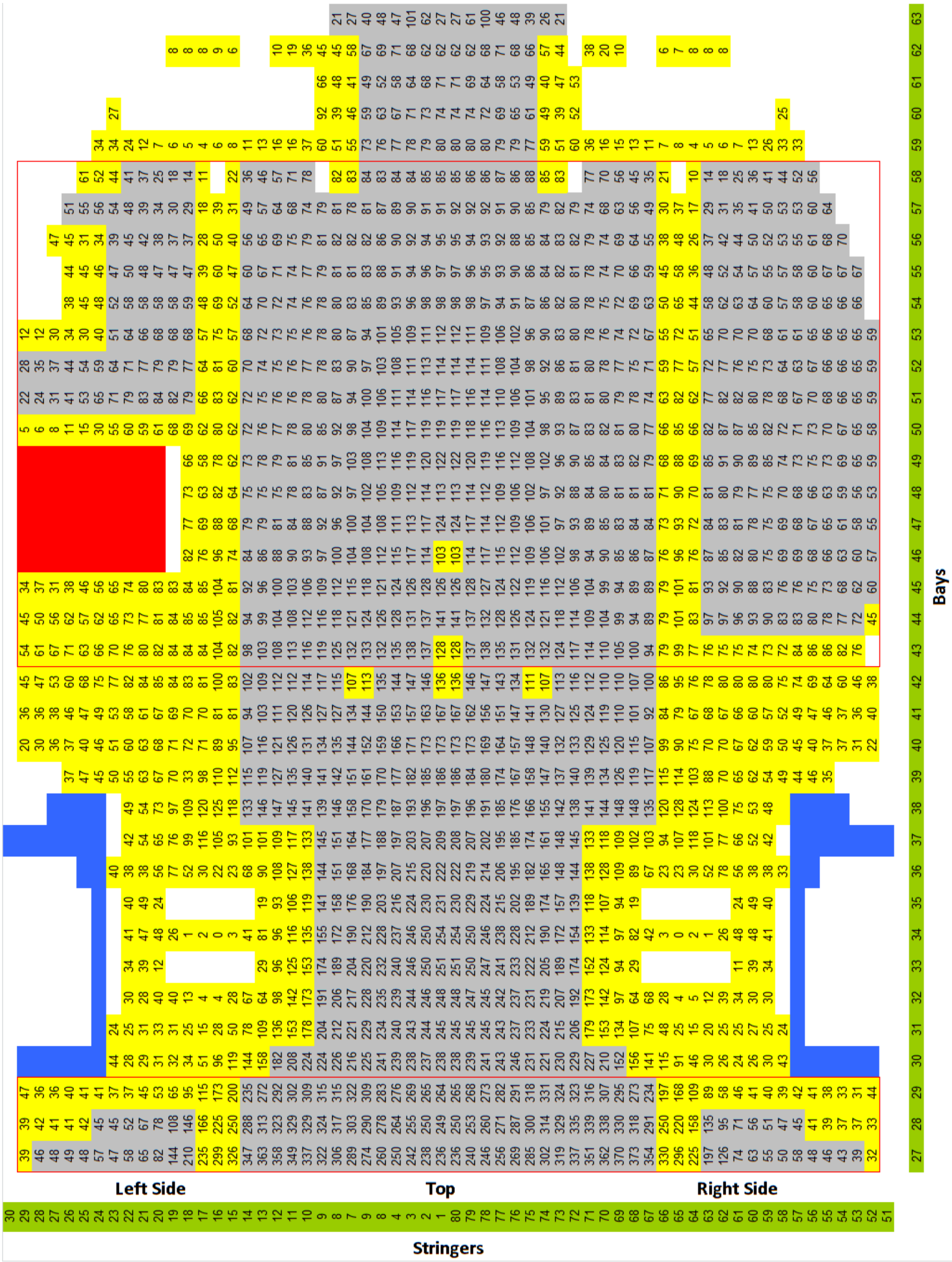

Figure 10.14: Reference maximum stress data for Airbus A320 in MPa

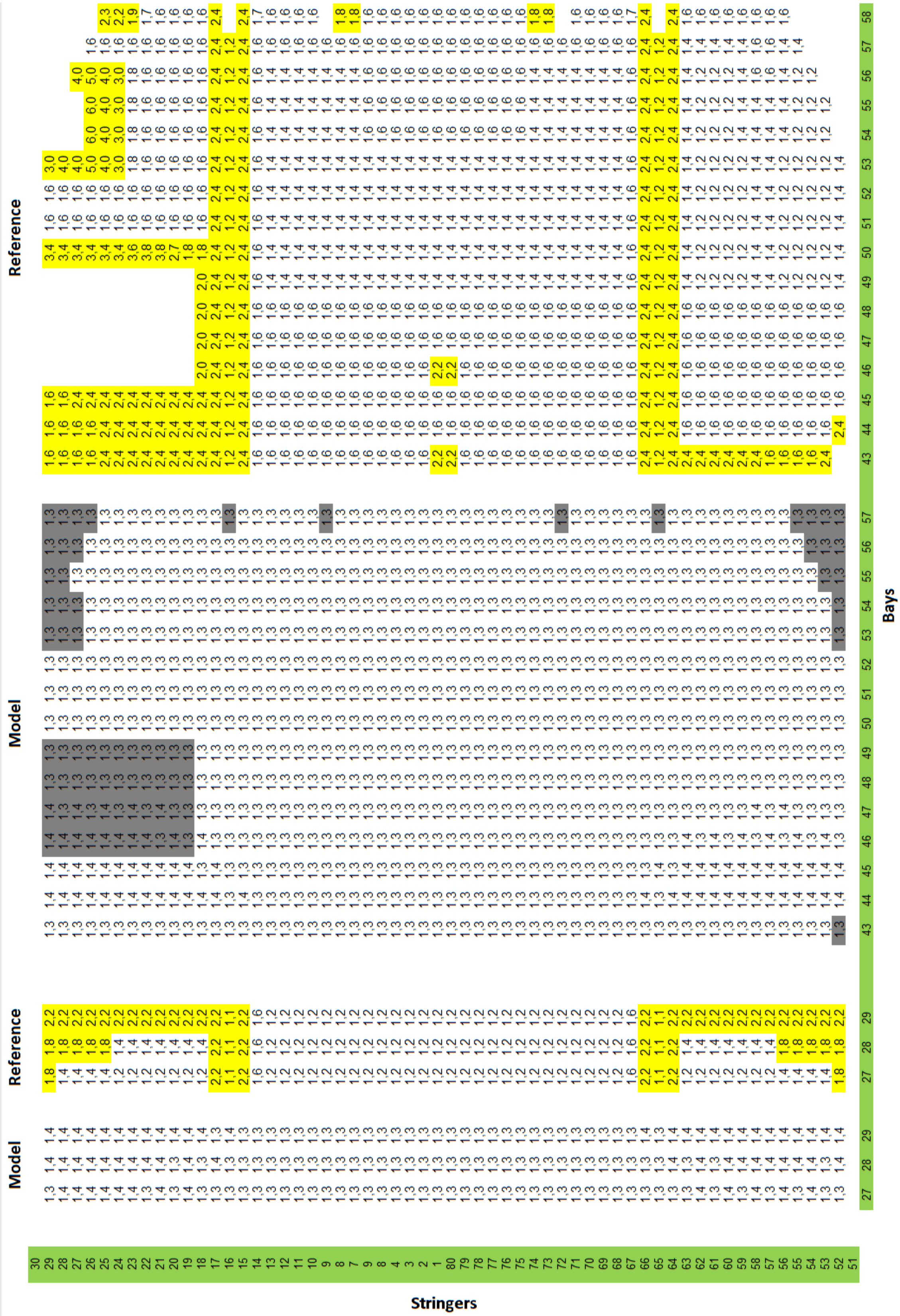

Figure 10.15: Model thickness versus reference thickness data for Airbus A320 in mm

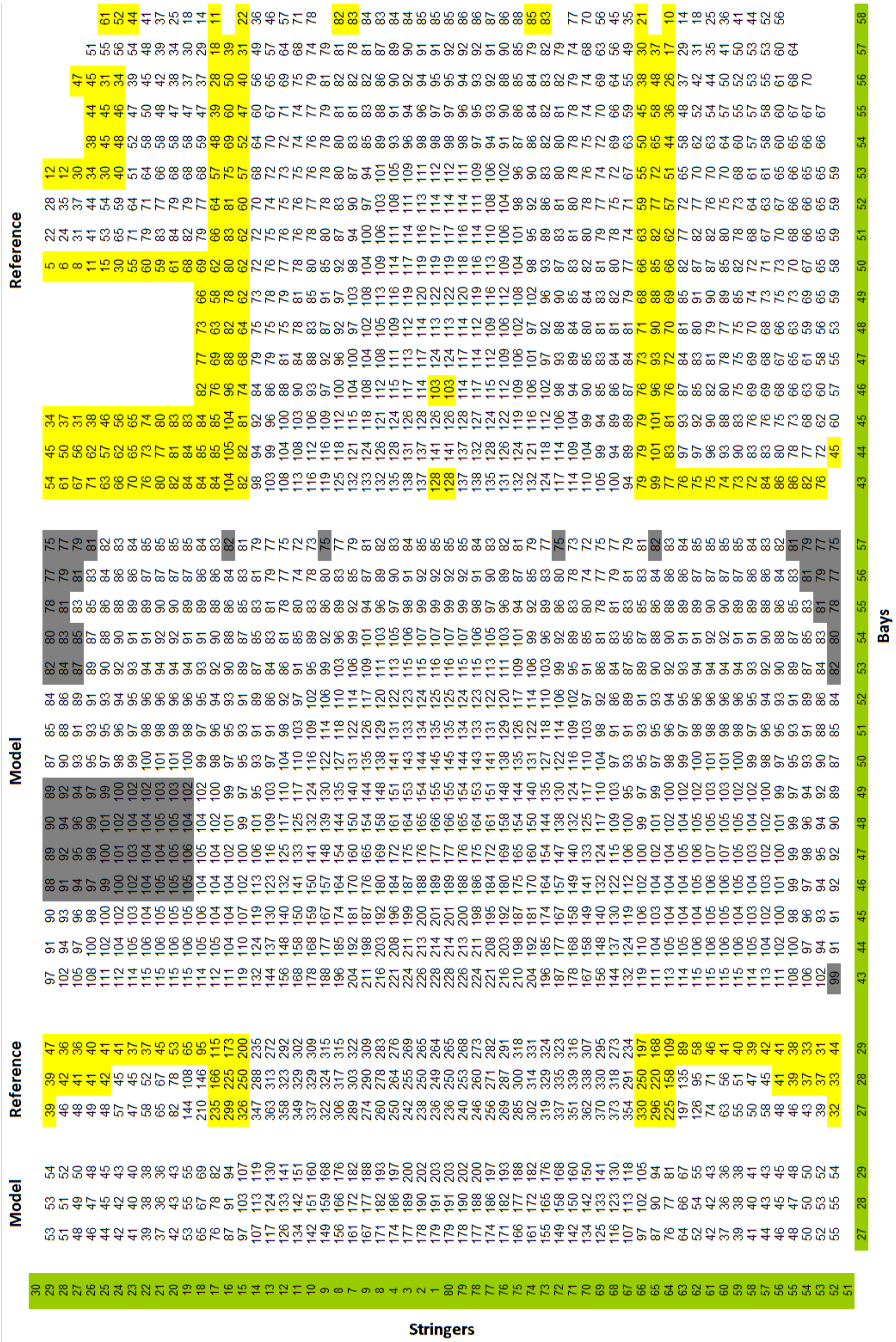

Figure 10.16: Model maximum stress versus reference stress data for Airbus A320 in MPa

Chapter 11

Discussion of composite

In this chapter the evaluation and optimization of composite is done and compared to the results of aluminum in order to predict the performance of composite fuselage structure.

11.1 Results for composite

The optimization for composite is also done for the bays 14 to 29 and 43 to 58. The optimization is done in a single run with all the considered load cases for aluminum in one package. The results for buckling analysis is given in figure F.10 and the result for strength analysis is given in figure F.11. The maximum required thickness per panel is selected and given in figure F.12. It is clearly visible that for composite a larger thickness is required compared to aluminum. The possible explanation for this is that the evaluation methods for composite do not consider stringers, it can be assumed as smeared thickness, and therefore all the forces are carried by the skin panels. This will give a larger thickness compared to skin-stringer combination. Further the design criteria for composite are simpler compared to the aluminum design criteria. Therefore the results are probable too conservative or too progressive, since many aspects of composites are still unknown. For the optimized thickness the stress plot is given in figure F.13.

11.2 Weight comparison

The weights for composite and aluminum configuration is calculated and given in table 11.1. The result shows that the composite structure is 18% lighter compared to aluminum. The weight of stringers is as expected, since the density of the composite is somewhat the half of aluminum. However for composite the methodologies does not check the stringers for buckling and for aluminum it does. Therefore it is possible the composite stringers will fail. It is expected the area of the composite stringer should be increased in order to pass stringer buckling, since the skin area is also increased compared to aluminum. Therefore the total weight saving of composite will be lower than the now calculated 18%. The skin weight of composite is larger than aluminum due to larger panel thicknesses.

In general composite fuselage structure will be lighter and will save operations cost due to the weight gain. However the used methodologies should be extended with more criteria to comply with other critical design aspects, which are now not included, for example crack analysis and laminate criteria since composite consist of layers. Further a cost analysis is required for composite and more investigation in de production techniques of composite. The production is still labor-intensive. Besides, many in-flight behavior of composite is unknown, therefore at this stage of composite design a large safety factor is used, which will undo the weight savings of composite. Composite materials can have the future, but more investigation is needed and many design problems should be solved.

	Aluminium 2024	**Composite Quasi-isotropic**	Difference in %
Skin [kg]	521	749	+44%
Stringer [kg]	1235	688	-44%
Total [kg]	1756	1437	-18%

Table 11.1: Weight of bays 14 to 28 and 43 to 57

Chapter 12

Conclusion

In this thesis work, a parametrical model design, analysis and evaluation tool for both metal and composite fuselage configurations is developed in order to gain insight into the structural performance of these material designs and obtain the required panel thickness for both aluminum and composite fuselages.

The developed method provides a well-organized approach for the fuselage analysis, covering the sequential steps for initial fuselage design. The results of the developed method are as expected and led to the following conclusions. The conclusions have been split up into elementary parts of the thesis project; the fuselage geometry creation, the fuselage load analysis and the evaluation of materials. Lastly, the performance of the complete model with composite is discussed.

Fuselage geometry

The geometry is created with assumptions and it gives a simplified version of fuselage geometry. The simplified geometry gives a good representation of the real fuselage, some specific regions such as wing section and cut-outs should get special attention, the loads acting in these regions are different, since now only undisturbed fuselage is considered. However the assumptions of no cut-outs and wing box has relatively small impact on the tool, since a fuselage has more undisturbed area and for material evaluation the deviation in running loads in these regions are considered for both materials. All in all the geometry is adequate to be used as model of a fuselage.

Forces and load cases

A simplified initial configuration is used to generate a first estimation of the load distribution, independent from applied materials and structural concepts. The dominating load cases are defined and the model give a suitable set of load distribution. The load analysis method proved to have reliable load results.

Running loads

The objective of this stage was to obtain the running loads in the fuselage structure. With the theoretical analysis method for the load estimation, it is possible to generate reliable load estimations using a limited amount of aircraft specific data. Using this analysis method, the load distribution can be calculated for several limit load cases; flight and ground load cases and cabin pressurization.

The running loads calculated are comparable with the available reference running loads. The running loads give a good overview about the stresses in the fuselage skin and stringer. The running loads for 1G flight and cabin pressurization are validated. The other load cases are also giving results as expected.

Evaluation of materials

A structural evaluation tool for complete fuselage structure has been created; this evaluation tool is applied on the Airbus A320 fuselage structure. For this aircraft, the evaluation of two different configurations is performed based on the output running loads. The implemented criteria are straight forward and could be easily changed or complemented with additional criteria. The criteria cover strength, buckling and crack analysis in this stage.

The used optimization method proofed to be reliable and suitable for structural optimization problems. The output format is very transparent en gives a clear overview of the design drivers in the different fuselage panels. However the method is very time consuming, since it recalculates the methods many times in order to find the optimal thickness.

The thicknesses at the side and bottom panels are set by the buckling analysis. The thicknesses at the top panels are set by the crack analysis. The crack and buckling analysis give good and reliable results. In the first instance the panel thicknesses for buckling analyses were lower than expected, however the used maximum limit load by Airbus is approximately 5 times larger than the 1G load. Using this assumed load case a better result for thickness is found for an undisturbed fuselage geometry.

Nevertheless, the resulting optimized panel thicknesses and stresses give a first estimation and can be used for several purposes, such as comparison of structural configurations, material performance and manufacturing design.

Performance of composite

The results for composite are given. The panels are thicker compared to aluminum, but in the evaluation methods no stringers are checked. The composite structure is 18% lighter than aluminum. It is expected the weight saving will be lower, if the stringers were checked. The optimized thickness and weight are only first estimations and further investigation is needed to enhance the design criteria for composite. The weights of the fuselage (bay 14 to 29 and bay 43-58) are summarized in table 11.1 for each concept considered. As mentioned before, the results for composite should be seen as a first estimation, due to the limited list of criteria.

Overall performance of model

The created model is able to perform as an analysis and design tool for aircraft fuselage. Further development and improvements on the tool are needed to cover more materials and configurations options.

Chapter 13

Recommendation

Several recommendations are made for improvements and further analysis on the design and analysis tool.

Geometry

- In order to improve the geometry it is possible to add windows, (cargo)doors or other cuts in fuselage. The influence of the cuts on the running loads should be taken into account as well as the evaluation method should be changed for this exception.
- The center wing box can be added into geometry. The effects of the center wing box should be analyzed in order to give a better load distribution around the center wing section.
- More geometry options should be added to the model, such as options to attach engines to the fuselage or changing the nose gear position in front of the front bulkhead and changing the position of the aerodynamic center of tail after the tail center of gravity.
- The fuselage shape in the front and rear section is changing linearly, this can be made parabolic in order to give better results.

Loads

- The method for estimation of the aircraft weight should be extended/changed in order to give a better initial weight for the tail section.
- The cabin pressure before front bulkhead and after rear bulkhead should be zero, this can be changed in the model to give better results.
- The effect of the hoop stress for non-circular shapes can be analyzed and implemented as well as the influences of the stringers.
- More load cases generating bending moment could be incorporated into the program. Especially load cases with large effect on the front and rear section, where now the thicknesses for buckling under the minimum required thickness.
- Apart from the evaluation of skin loads; also the frame and floor loads could be evaluated and used for structural dimensioning.

Evaluation

- The metal buckling analysis could be extended for the tension/shear effect on buckling. Now only compression/shear buckling effect is taken into account.
- The composite evaluation methods should be checked and extended, such as crack analysis of composite.

- Laminate criteria could be added to the composite methods. This allows the evaluation of other laminate lay-ups than quasi-isotropic in order to further optimize CFRP configuration.
- The selected material is applied to the whole fuselage structure, therefore a homogenous fuselage is created. There is a possibility to create heterogeneous fuselage with different materials per section.
- More configurations possibilities can be added to the model, such as skin only or sandwich configurations. Hereby the effects of the new configurations on the load distribution should be analyzed and the optimization or evaluation methods should be extended.
- The model could be extended to evaluate other upcoming materials, like fiber metal laminates.
- A method to evaluate the weight of joints, frames and cut-outs could be added in order to improve the estimation of the fuselage shell weight.
- A raw material analysis and material cost analysis for metal could be added to the tool in order to give an first impression about the needed amount of material and its cost.

Optimization

- A better and faster optimization method should be implemented in the model to give faster results.
- The optimization could be done for more criteria, such as stringer spacing and stringer area.

Validation

- The running loads for other load cases should be validated. Further the loads on the front and rear section, but also the loads on side and bottom panels should be validated.
- The shear flow should be validated for all load cases using existing data for reference aircraft.
- The validation of the running loads of model could be done by a FEM model, in order to proof the analytical model.

Tool

- An input file can be created for the parameters and option selections. This makes it much easier to change aircraft specifications and load cases.
- The creation of charts can be automated by implementing the creation of chart in the tool code, which will safe time afterwards by analyzing the results.
- The tool can be integrated into another program that analysis a full aircraft.

Other

- A composite cost study should be performed. This study must identify difference in cost between composite fuselage and an aluminum fuselage. A break-even point, a minimum amount of saved weight, can then be established beyond which it is cheaper to produce a composite fuselage.

Bibliography

[1] Airbus, "Ac a320 airplane characteristics," September 1, 2010.

[2] F. van Rijn van Alkemade, "A preliminary prediction method for the effect of new fuselage materials on transport aircraft weight," Master's thesis, Faculty of Aerospace Engineering, Delft University of Technology, 2007.

[3] A. Rothwell, *Structural design and optimisation, Part II*. Delft: Delft University of Technology, 2001.

[4] D. Roylance, "Pressure vessels," *Department of Materials Science and Engineering, Massachusetts Institute of Technology*, August 23, 2001.

[5] T. H. G. Megson, *Aircraft Structures for engineering students*. Burlington, MA: Butterworth-Heinemann, Elsevier Ltd, 4th ed., 1988.

[6] G. J. J. Ruijgrok, *Elements of airplane performance*. Delft University Press, 1994.

[7] E. Torenbeek, *Synthesis of subsonic airplane design*. Delft: Delft University Press, 1982.

[8] M. C. Y. Niu, *Airframe Structural Design*. Hong Kong: Hong Kong Conmilit Press LTD, 2nd ed., 1988.

[9] S. Timoshenko and D. Young, *Engineering Mechanics*. Mc-Graw-Hill Book Company, 4th ed., 1956.

[10] J. A. Authorities, *Joint Aviation Requirements 25*. Large Aeroplanes (Change 14), 1994.

[11] T. L. Lomax, *Structural Loads Analysis for Commercial Transport Aircraft: Theory and Practice*. AIAA Education Series, 1996.

[12] P. Astori, J. Hupperets, and M. J. L. van Tooren, "Load development for two aircraft fuselage using far criteria and paramtrised fe-models," *Delft University of Technology*, 2003.

[13] D. Howe, *Aircraft Conceptual Design Synthesis*. Professional Engineering Publishing Ltd, 2000.

[14] E. C. of Federal Regulations, "title 14." `http://ecfr.gpoaccess.gov`.

[15] J. de Jonge, D. Schütz, D. Lowak, and J. Schijve, "A standardized loadsequence for flight simulation test on transport aircraft wing structures," *NLR*, 1973.

[16] T. Swift, "Fail-safe design requirements and features, regulatory requirements," *AIAA*, vol. 2003-2783, 2003.

[17] HSB, *Handbuck Struktur Berechnung*. EADS Deutschland GmbH, 2002.

[18] P. Paris and F. Erdogan, "A critical analysis of crack propagation laws," *Journal of Basic Engineering, Transactions of the American Society of Mechanical Engineers*, pp. 528–534, December 1963.

[19] S. Suresh, *Fatigue of Materials*. Cambridge University Press, 2nd ed., 1998.

[20] F. van Keulen, *Collegedictaat Stijfheid en Sterkte III WB1309*. Delft: Delft University of Technology, 2000.

[21] E. J. Schut and M. J. L. van Tooren, "Design feasilization using knowledge-based engineering and optimization techniques," *Journal of Aircraft*, vol. 44-6, pp. 1776–1786, November-December 2007.

[22] H. A. Baluch, M. J. L. van Tooren, and E. J. Schut, "Design tradeoffs for fiber composite fuselages under dynamic loads using structural optimization," *AIAA*, 2008.

[23] L. P. Kollar and G. S. Springer, *Mechanic of Composite Structures*. Cambridge University Press, 2003.

[24] M. J. L. van Tooren, *Sandwich Fuselage Design*. PhD thesis, Delft University of Technology, 1998.

[25] R. T. Sullins, G. W. Smith, and E. E. Spier, "Manual for structural stability analysis of sandwich plates and shells," *Contractor Report CR-1457*, 1969.

[26] J. de Kanter, "Calculation methodology stiffened panel," December 2, 2008. Internal Report, Rederence Source no: 121340, Project number: 6303.

[27] E. Bruhn, *Analysis & Design of Flight Vehicle Structures*. Jacobs Publishing Inc., 1973.

[28] ESDU, *ESDU Data Sheets*. Engineering Sciences Data Unit, 2010.

[29] G. Design, "Ces edupack 2010 information resources," 2010.

[30] H. Van De Nieuwendijk, "Fat.stress max/min stress thickness, /stress/a30x/a31821," 2006. Type A320-200.

[31] H. Z. Jishi, "Design methods for large cut-outs in composite fuselage structures," Master's thesis, Cranfield University, 2007.

[32] J. J. M. Hupperets, "Top-down fuselage sizing," Master's thesis, Faculty of Aerospace Engineering, Delft University of Technology, 2003.

[33] M. J. L. van Tooren, "Response 1 airbus composite aircraft fuselages - next or never," *Around Glare*, vol. Part 3, pp. 145–157, 2004.

[34] W. Ramberg and W. Osgood, "Description of stress-strain curves by three parameters," *Technical Note No. 902*, 1943.

Appendix A

Reference aircraft

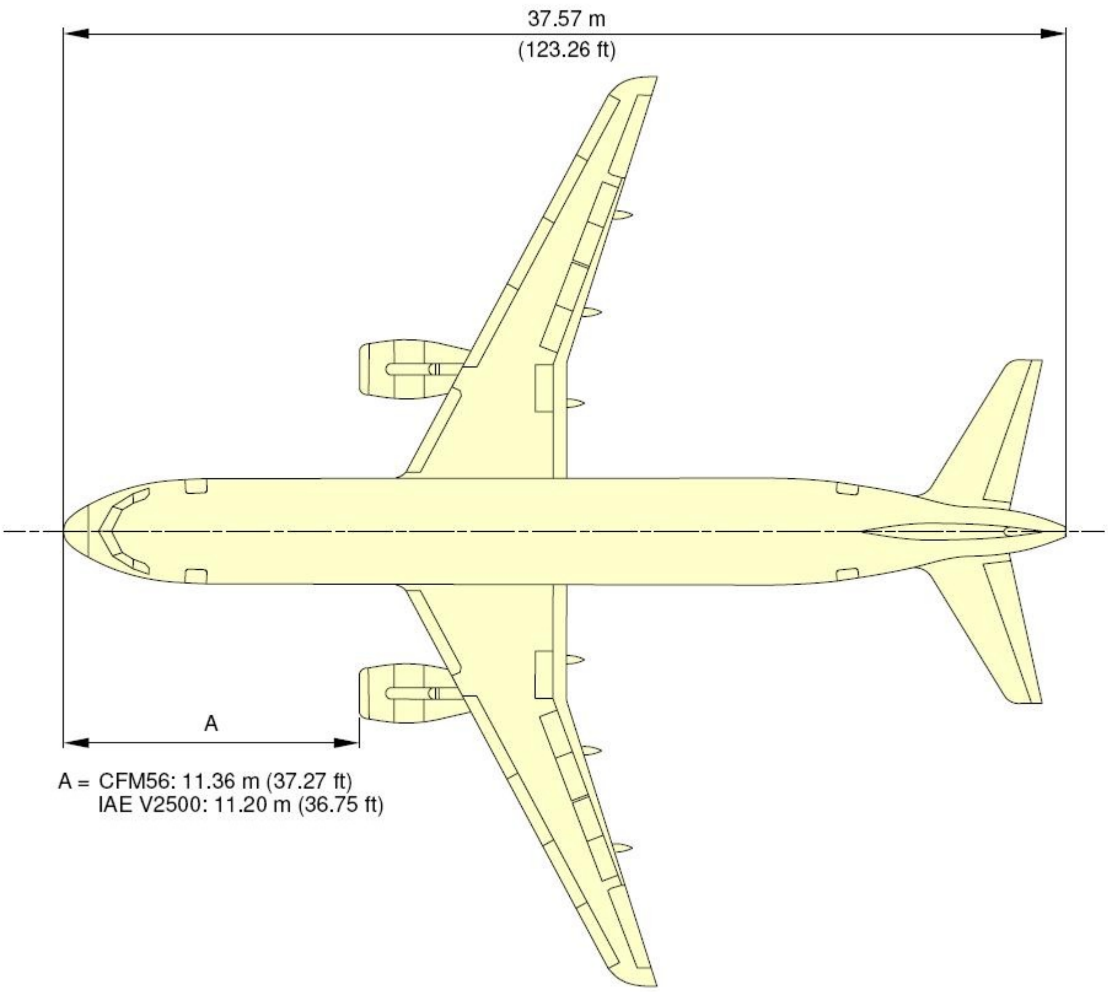

Figure A.1: Airplane dimensions top view

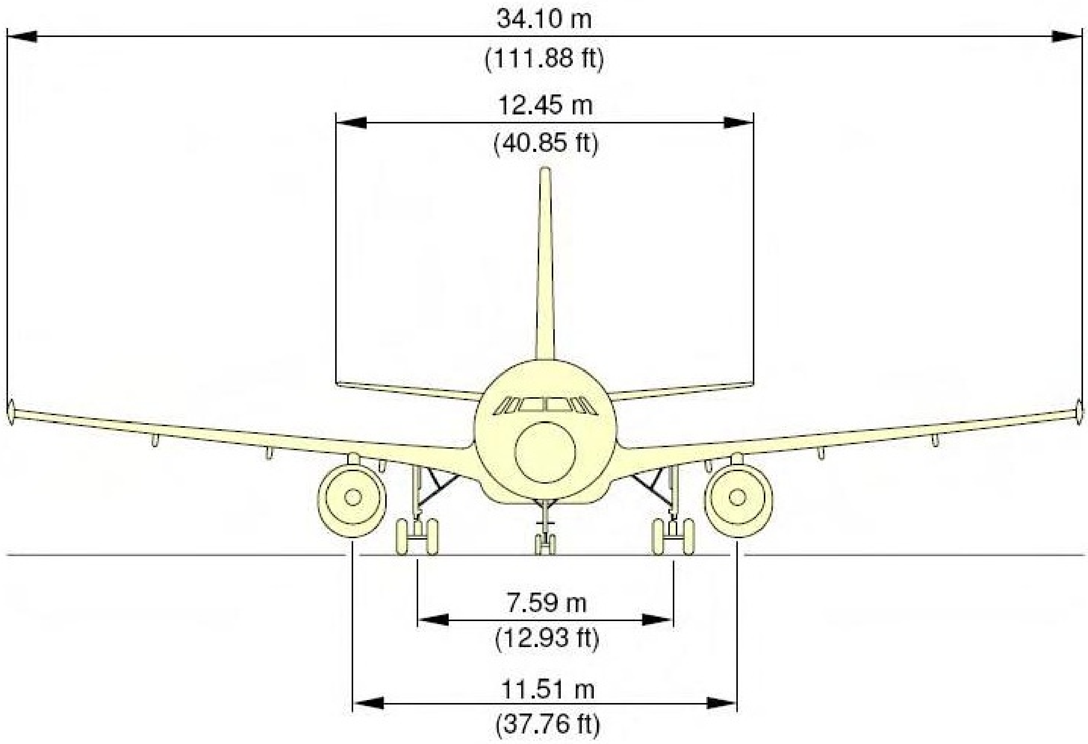

Figure A.2: Airplane dimensions front view

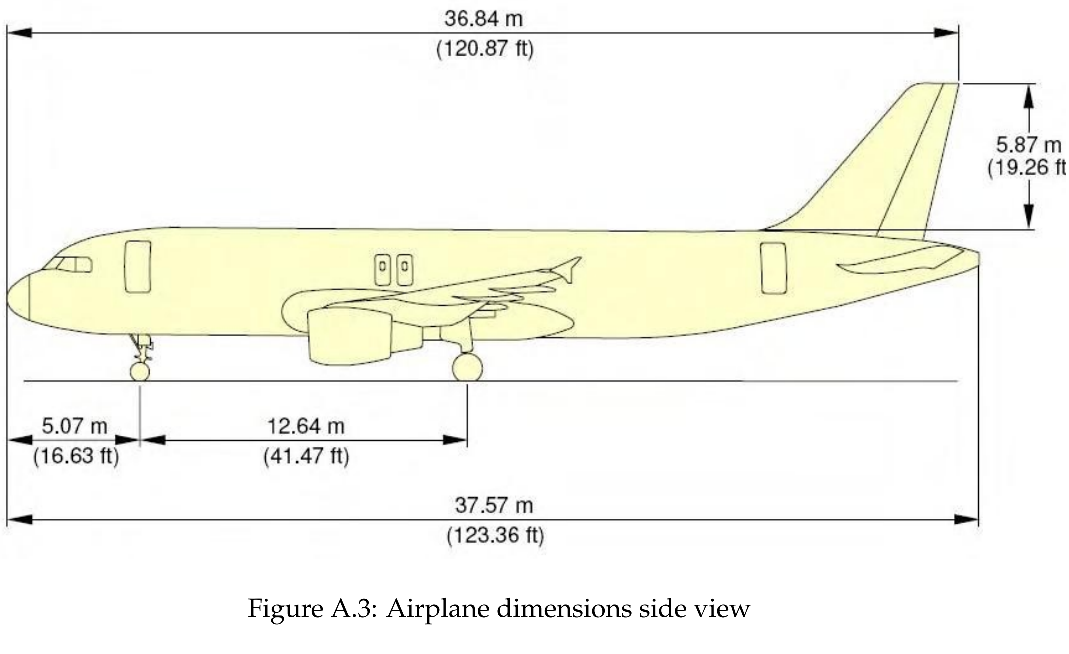

Figure A.3: Airplane dimensions side view

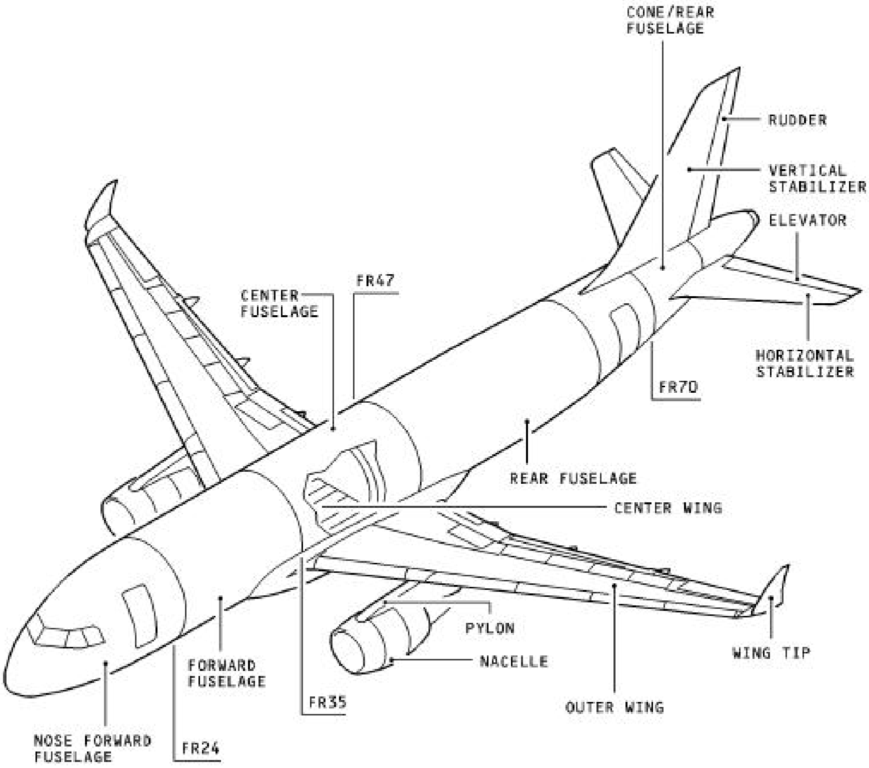

Figure A.4: Structural description

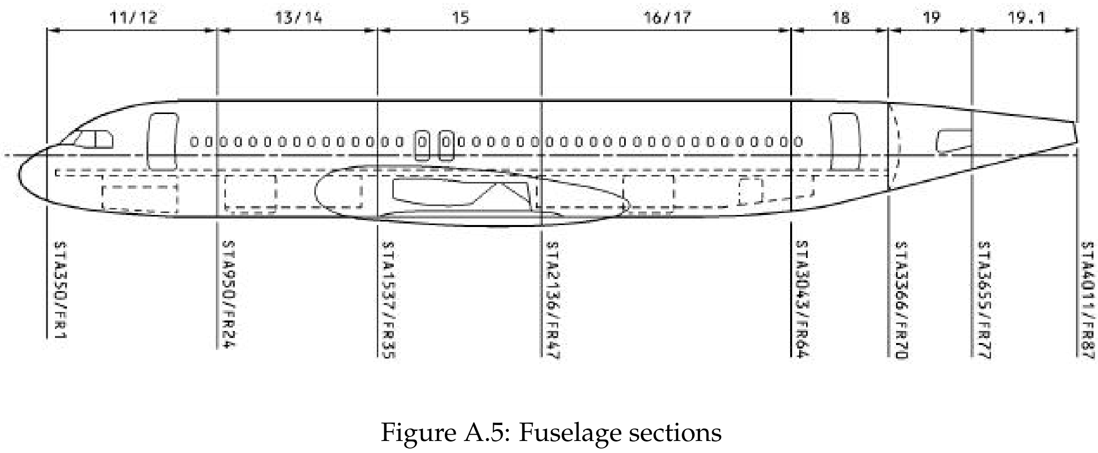

Figure A.5: Fuselage sections

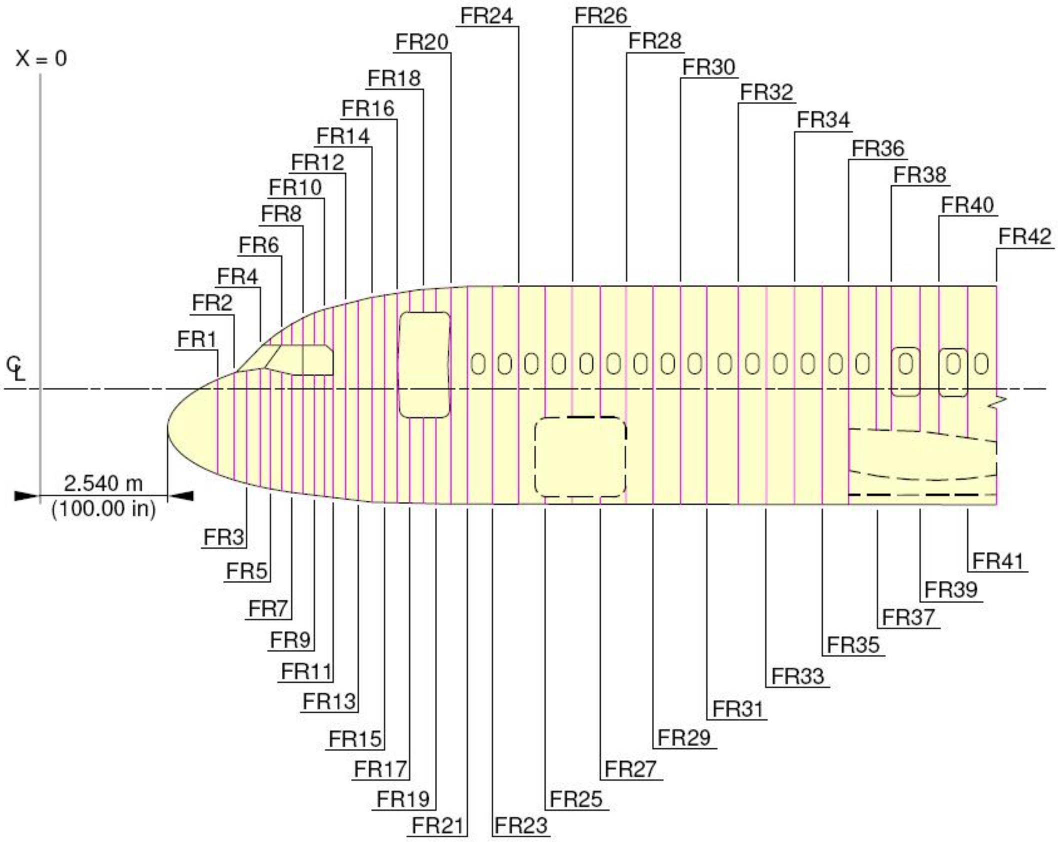

FR	H–ARM m (in)	FR	H–ARM m (in)	FR	H–ARM m (in)	FR	H–ARM m (in)
NOSE	2.540 (100.00)	11	5.794 (228.11)	23	8.966 (352.99)	34	14.834 (584.02)
1	3.500 (137.80)	12	6.052 (238.27)	24	9.500 (374.02)	35	15.367 (605.00)
2	3.850 (151.57)	13	6.311 (248.46)	25	10.033 (395.00)	36	15.900 (625.98)
3	4.090 (161.02)	14	6.570 (258.66)	26	10.566 (415.98)	37	16.408 (645.98)
4	4.330 (170.47)	15	6.828 (268.82)	27	11.100 (437.01)	38	16.688 (657.01)
5	4.546 (178.98)	16	7.087 (279.02)	28	11.633 (457.99)	39	17.255 (679.33)
6	4.762 (187.48)	17	7.318 (288.11)	29	12.167 (479.02)	40	17.534 (690.31)
7	4.967 (195.55)	18	7.599 (299.17)	30	12.700 (500.00)	41	18.101 (712.64)
8	5.194 (204.49)	19	7.830 (308.27)	31	13.233 (520.98)	42	18.694 (735.98)
9	5.394 (212.36)	20	8.077 (317.99)	32	13.767 (542.01)		
10	5.594 (220.24)	21	8.433 (332.01)	33	14.300 (562.99)		

Figure A.6: Frame Station 1 to 42

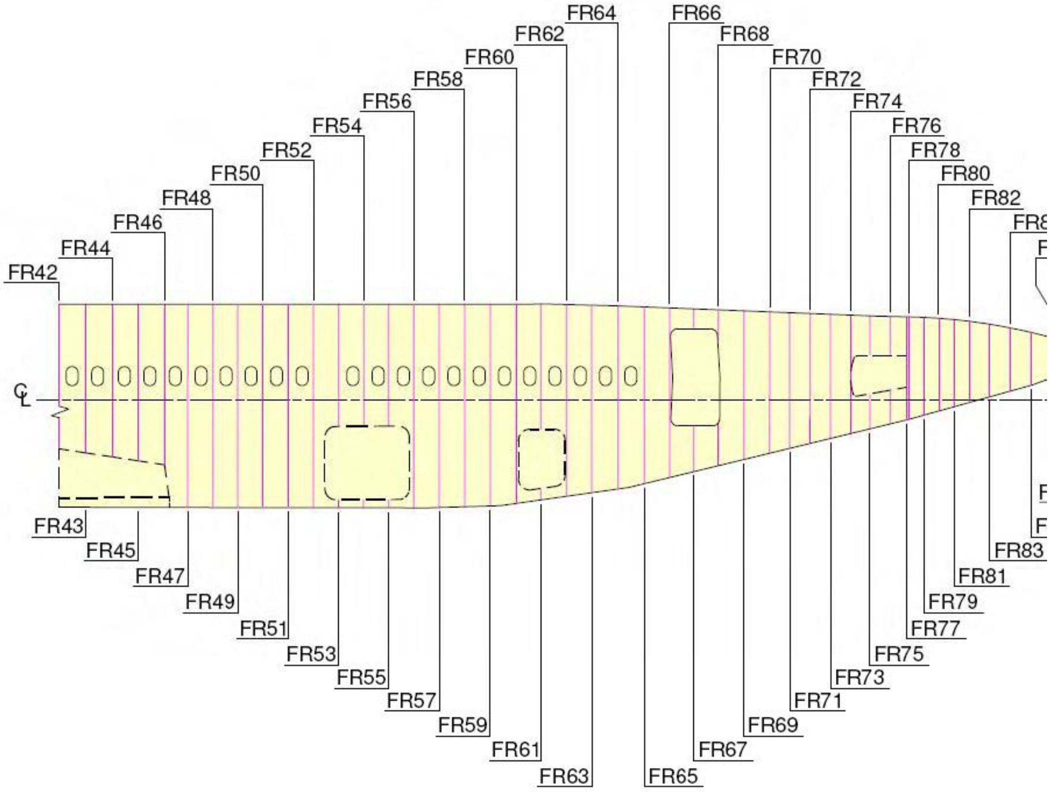

FR	H–ARM m (in)	FR	H–ARM m (in)	FR	H–ARM m (in)	FR	H–ARM m (in)
42	18.694 (735.98)	54	25.095 (987.99)	66	31.577 (1243.19)	78	36.657 (1443.19)
43	19.228 (757.01)	55	25.629 (1009.02)	67	32.074 (1262.76)	79	36.976 (1455.75)
44	19.761 (777.99)	56	26.162 (1030.00)	68	32.571 (1282.32)	80	37.295 (1468.31)
45	20.295 (799.02)	57	26.695 (1050.98)	69	33.096 (1302.99)	81	37.665 (1482.87)
46	20.828 (820.00)	58	27.229 (1072.01)	70	33.655 (1325.00)	82	38.035 (1497.44)
47	21.361 (840.98)	59	27.762 (1092.99)	71	34.055 (1340.75)	83	38.490 (1515.35)
48	21.895 (862.01)	60	28.296 (1114.02)	72	34.506 (1358.50)	84	38.945 (1533.27)
49	22.426 (882.99)	61	28.829 (1135.00)	73	34.906 (1374.25)	85	39.400 (1551.18)
50	22.962 (904.02)	62	29.362 (1155.98)	74	35.306 (1390.00)	86	39.855 (1569.09)
51	23.495 (925.00)	63	29.896 (1177.01)	75	35.719 (1406.26)	87	40.113 (1579.25)
52	24.028 (945.98)	64	30.429 (1197.99)	76	36.132 (1422.52)		
53	24.562 (967.01)	65	31.013 (1220.98)	77	36.545 (1438.78)		

N_AR_091006_1_0010302_0

Figure A.7: Frame Station 42 to 87

Appendix B

Aircraft weight distribution

According to Torenbeek [7] the aircraft operational empty weight can be divided into weight of the airframe structure, the propulsion group and the airframe equipment and services. The methods that calculate these group weights will be presented here. All weights are in Newton.

B.1 Airframe structure

The airframe structural weight is subdivided into weight of the fuselage, wing, tail, landing gear and surface controls.

B.1.1 Fuselage

The fuselage structural weight calculated here is only calculated to have an initial weight as of course calculating fuselage weight is the objective of this study after optimization.

$$W_{fus} = 0.23 g k_f \left(V_D \frac{l_f}{b_f + h_f} \right)^{0.5} S_G^{1.2} \tag{B.1}$$

In this equation k_f is 1.08 for pressurized fuselage. The fuselage gross weight S_G is calculated with:

$$S_G = \pi b_f l_f \left(1 - \frac{2}{l_f / b_f} \right)^{\frac{2}{3}} \left(1 + \frac{1}{(l_f / b_f)^2} \right) \tag{B.2}$$

For a double bubble fuselage and a triple bubble fuselage:

$$S_G = \pi b_f l_f \left(0.5 + 0.135 \frac{l_n}{l_f} \right)^{\frac{2}{3}} \left(1.015 + \frac{0.3}{(l_f / b_f)^{1.5}} \right) \tag{B.3}$$

B.1.2 Floor

The total floor weight is given by:

$$W_{fl} = 0.3074 \cdot \sqrt{150} \cdot S_{fl}^{1.045} \tag{B.4}$$

Where the passenger floor loading assumed to be 150 kg/m^2. The weight of the floor grid and seatrail is given by:

$$W_{fl_{grid}} = 0.66 \cdot b_f^{1.35} \cdot S_{fl} \tag{B.5}$$

$$W_{seatrail} = 1.8 \cdot S_{fl} \tag{B.6}$$

The total front and rear cargo floor weight is given by:

$$W_{flcg_f} = 0.3074 \cdot \sqrt(200) \cdot S_{cg_f}^{1.045} \tag{B.7}$$

$$W_{flcg_r} = 0.3074 \cdot \sqrt(200) \cdot S_{cg_r}^{1.045} \tag{B.8}$$

Where the cargo floor loading assumed to be 200 kg/m^2. The weight of the cargo floor grid is given by:

$$W_{fl_{gridcg}} = 0.66 \cdot (0.75 \cdot b_f)^{1.35} \cdot (S_{cg_f} + S_{cg_r}) \tag{B.9}$$

B.1.3 Bulkhead

The weight of front bulkhead and rear bulkhead is given by:

$$W_{fbh} = 9.1 + 7.225 \cdot \left(\frac{\Delta p}{g}\right)^{0.8} \cdot \left(\left(\pi \frac{D_{fbh_d}}{2}\right)^2\right)^{1.2} \tag{B.10}$$

$$W_{rbh} = 9.1 + 7.225 \cdot \left(\frac{\Delta p}{g}\right)^{0.8} \cdot \left(\left(\pi \frac{D_{rbh_d}}{2}\right)^2\right)^{1.2} \tag{B.11}$$

B.1.4 Wing

The wing weight for an aircraft with engines attached to the wing is:

$$W_{wing} = K_{wing} \cdot \mathrm{MZFW}(\frac{b_{wing}}{\cos\Delta})^{0.75}(1 + (1.905\frac{\cos\Delta}{b_{wing}}^{0.5})n^{0.55}\left(\frac{b_{wing}S_{wing}}{t_{root}\left(\frac{\mathrm{MZFW}}{g}\right)\cos\Delta}\right)^{0.3} \tag{B.12}$$

The wing proportionality factor K_{wing} is $6.33 \cdot 10^{-3}$ for two engines attached to the wing and for four engines it is $6.00 \cdot 10^{-3}$. The wing structure penalty is given by:

$$W_{wing_{str}} = 20.4 + 0.000907 \cdot 3.75 \cdot \mathrm{MTOW} \tag{B.13}$$

Where $3.75 = 1.5 \cdot 2.5$ is the safety factor times the maximum load factor.

B.1.5 Tail

The tail weight is divided in the weight of the horizontal and vertical tail.

$$W_{tail} = W_v + W_h \tag{B.14}$$

The horizontal tail can be calculated using:

$$W_h = S_h f_{yh} g \tag{B.15}$$

The factor f_{yh} is found by:

$$f_{yh} = -640.4f_{xh}^6 + 2844.4f_{xh}^5 - 4120f_{xh}^4 + 2612.8f_{xh}^3 - 816.11f_{xh}^2 + 186.21f_{xh} - 10.277 \tag{B.16}$$

in which f_{xh} is defined as:

$$f_{xh} = S_h^{0.2}\frac{1.25 \cdot 1000V_e}{\sqrt{\cos\Delta}} \tag{B.17}$$

The vertical tail weight is calculated in a very similar way:

$$W_v = k_v S_v f_{yh} g \tag{B.18}$$

The factor k_v is $1 + 0.15\frac{S_h h_h}{S_v b_v}$. The factor f_{yh} does not change, but in the f_{yh}-equation S_v should be entered instead of S_h. The tail structure penalty is given by:

$$W_{tail_{str}} = 0.1 \cdot W_{tail} \tag{B.19}$$

B.1.6 Landing gear

The landing gear consists of a main landing gear and a nose landing gear. The nose landing gear weight is calculated using:

$$W_{nlg} = 0.1 + 0.082 \cdot \text{MTOW}^{0.75} + 2.97 \cdot 10{-}6 \cdot \text{MTOW}^{1.5} \tag{B.20}$$

and the main landing gear weight is calculated using:

$$W_{mlg} = 18.1 + 0.131 \cdot \text{MTOW}^{0.75} + 0.019 \cdot \text{MTOW} + 2.23 \cdot 10^{-5} \cdot \text{MTOW}^{1.5} \tag{B.21}$$

B.1.7 Surface controls group

The surface controls group is correlated to the MTOW:

$$W_{sc} = 0.768 \cdot 0.64 \cdot \text{MTOW}^{\frac{2}{3}} \cdot 1.2 \cdot 1.15 \tag{B.22}$$

B.2 Propulsion group

The propulsion group consist of the engines, items associated with engine installation and operation, the fuel system and thrust reversing provisions. The propulsion group weight is calculated as follows. The total thrust is the thrust per engine times the number of engines.
The engine dry weight is then calculated using:

$$W_{eng} = 0.0169 \cdot g \cdot N_{eng} \cdot T_{eng} \tag{B.23}$$

The power plant weight can then be calculated:

$$W_{pwr} = 1.357 \cdot W_{eng} \tag{B.24}$$

This calculation is valid for podded jet engines equipped with thrust reversers. To arive at the toal propulsion group weight the nacelle weight is added:

$$W_n = 0.065 \cdot T_{tot} \tag{B.25}$$

$$W_{prop} = W_n + W_{pwr} \tag{B.26}$$

B.3 Airframe equipment and services

The airframe equipment and services group includes the APU, instruments, hydraulic, electric and electronic systems, furnishing and equipment, air conditioning, anti-icing equipment and other miscellaneous equipment.

B.3.1 Instruments, navigational and electronic equipment

$$W_{ieg} = 0.347 \cdot \text{OEW}_{est}^{\frac{5}{9}} \cdot \text{Range}^{\frac{1}{4}} \tag{B.27}$$

B.3.2 Hydraulic and pneumatic system

The weight of the hydraulic and pneumatic systems is dependent on the number of times the systems is duplicated. For a duplicated control system the weight is calculated with:

$$W_{hypn} = 0.011 \cdot \text{OEW}_{est} + 181 \tag{B.28}$$

and for a triplex system the weight is:

$$W_{hypn} = 0.015 \cdot \text{OEW}_{est} + 272 \tag{B.29}$$

B.3.3 Electrical system

The electrical system weight is dependent on the total electric generator power which in turn is dependent on the fuselage volume. The fuselage volume for a cylindrical or double bubble fuselage is calculated with:

$$vol_{fus} = 0.25 \cdot \pi \cdot b_f^2 \cdot l_f \left(1 - 2 \cdot \frac{b_f}{l_f}\right) \tag{B.30}$$

A tripple bubble fuselage has a volume of:

$$vol_{fus} = 0.25 \cdot \pi \cdot b_f^2 \cdot l_f \left(0.5 + 0.135 \cdot \frac{l_n}{l_f}\right) \tag{B.31}$$

Using the fusleage volume the total electric generator power is:

$$P_{el} = 3.64 \cdot vol_{fus}0.7 \tag{B.32}$$

Now the weight of the electrical system can be calculated:

$$W_{el} = 16.3 \cdot g \cdot P_{el} \left(1 - 0.033\sqrt{P_{el}}\right) \tag{B.33}$$

B.3.4 Furnishing and equipment

The weight of the furnishing and equipment is related to the MZFW:

$$W_{fur} = 0.196 \cdot \text{MZFW}^{0.91} \tag{B.34}$$

B.3.5 Air-conditioning system

The weight of the air-conditioning system is dependent on the total cabin length:

$$W_{ac} = 14.0 \cdot g \cdot l_c^{1.28} \tag{B.35}$$

B.3.6 APU group

The weight of the APU group is the weight of the APU and its systems. The APU weight is dependent on the bleed air flow and the fuselage volume:

$$W_{APU} = 0.65 \cdot g \cdot (0.4 \cdot vol_{fus})^{0.6} \cdot 11.7 \tag{B.36}$$

The APU group weight W_{APUG} is in general two time the APU weight.

B.3.7 Cabin and flight crew

The number of cabin crew members is dependent on the number of passengers. In general 1 crew member is needed for every 35 passengers. The number of cockpit crew members is dependent on the aircraft type and therefore an input for the program.

$$W_{crew} = N_{cabcrew} \cdot 68 \cdot g + N_{flightcrew} \cdot 93 \cdot g \tag{B.37}$$

B.3.8 Baggage and cargo containers

The weight of the baggage and cargo containers is dependent on the bulk volume. A density of 21.5 kg/m^3 is used, taken from the Boeing 747.

$$W_{bcc} = 21.5 \cdot g \cdot vol_{bulk} \tag{B.38}$$

B.3.9 Paint

Paint is related to the MTOW:

$$W_{pt} = 0.006 \cdot \text{MTOW} \tag{B.39}$$

B.3.10 Passenger's comfort

The weight for items related to passenger comfort is dependent on a factor for passenger cabin supplies (K_{pcs}), a factor for portable water and closets (K_{pwt}) and a factor for safety equipment (K_{se}):

$$W_{pc} = N_{pax} \cdot g \cdot (K_{pcs} + K_{pwt} + K_{se}) \tag{B.40}$$

The factors are dependent on the aircraft range:

- $\text{Range} < 1500 \cdot 1.852 : K_{pcs} = 6.35$, $K_{pwt} = 0.68$, $K_{se} = 0.907$
- $\text{Range} < 3000 \cdot 1.852 : K_{pcs} = 6.35$, $K_{pwt} = 1.36$, $K_{se} = 2.95$
- $\text{Range} > 3000 \cdot 1.852 : K_{pcs} = 8.62$, $K_{pwt} = 2.95$, $K_{se} = 3.4$

B.3.11 Residual fuel

$$W_{resf} = 0.151 \cdot \left(W_{fuel} \cdot \frac{1.17}{0.78}\right)^{\frac{2}{3}} \tag{B.41}$$

B.3.12 Miscellaneous equipment

The weight of the miscellaneous equipment W_{mis} is 2% of all OEW parts.

B.3.13 Airframe equipment and services

The total weight of all airframe equipment and services items is the summation of all previously calculated items:

$$W_{eq} = W_{ieg}+W_{hypn}+W_{el}+W_{ac}+W_{APUG}+W_{fur}+W_{crew}+W_{bc}+W_{pt}+W_{pc}+W_{resf}+W_{mis} \tag{B.42}$$

B.4 Weight distribution

The weight along the complete fuselage is given by:

$$W_1 = W_{fus} + W_{fl} + W_{ac} + W_{el} + W_{fur} + W_{hypn} + W_{ieg} + W_{mis} \tag{B.43}$$

$$W_2 = W_{flcg_f} \tag{B.44}$$

$$W_3 = W_{flcg_r} \tag{B.45}$$

$$W_4 = W_{fuel_{mid}} + W_{wing_{str}} \tag{B.46}$$

$$W_5 = W_{APUG} + W_{tail_{str}} \tag{B.47}$$

$$W_6 = 0 \tag{B.48}$$

The weight distribution q_x is then calculated by dividing the weight W_x by the corresponding length l_x.

Appendix C

Model input

C.1 Parameters

C.1.1 Load factor

$n_{steady} = 1$	Load factor during steady flight [-]
$n_{man_{max}} = 2.5$	Maximum load factor for maneuver [-]
$n_{man_{min}} = -1$	Minimum load factor for maneuver [-]
$n_{gust_{max}} = 3$	Maximum load factor for gust [-]
$n_{gust_{min}} = -1.5$	Minimum load factor for gust [-]
$n_{land} = 2$	Load factor for landing [-]
$j_{safety} = 1.5$	Safety factor above loads [-]

C.1.2 Cross-section and lay-out of fuselage

$N_{str} = 80$	Number of stringers [-]
$N_{frm} = 88$	Number of frames [-]
$t_{sk_0} = 1$	Initial thickness for skin panels [mm]
$A_{str_0} = 180$	Initial area for stringers [mm^2]
$R_1 = 1975$	Radius 1 for cross-section [mm]
$R_2 = 1975$	Radius 2 for cross-section [mm]
$R_2 = 1975$	Radius 2 for cross-section [mm]
$B_{f_1} = 3950$	Fuselage width 1 for cross-section [mm]
$B_{f_2} = 3950$	Fuselage width 2 for cross-section [mm]
$d_1 = 0$	Height 1 for cross-section [mm]
$d_2 = 0$	Height 2 for cross-section [mm]

C.1.3 Atmospheric data

$g = 9.80665$	Gravity constant [m/s²]
$\rho_0 = 1.225$	Density at zero height [kg/m³]
$p_0 = 101325$	Pressure at zero height [N/m²]
$T_0 = 288.15$	Temperature at zero height [K]
$a = -0.0065$	Temperature gradient [K/m]
$R = 287.05$	Gas constant [J/kg · K]
$\gamma = 1.4$	Specific heat [-]
$T = 215.1$	Temperature at cruise height [K]
$z_{cab} = 2400$	Cabin pressure height [m]
$z_{op} = 11278$	Operating altitude [m]
$U_{gust_e} = 15.24$	Equivalent gust speed [m/s]

C.1.4 Location

$L_f = 37570$	Fuselage length [mm]
$L_c = 27500$	Cabin length [mm]
$X_{cg} = 17500$	Distance to center of gravity of aircraft [mm]
$X_{cg_h} = 35100$	Distance to center of gravity of horizontal tail [mm]
$X_{ac} = 15700$	Distance to aerodynamic center of aircraft [mm]
$X_{ac_h} = 33800$	Distance to aerodynamic center of horizontal tail [mm]
$X_{fbh} = 1140$	Distance to front bulkhead [mm]
$X_{rbh} = 29300$	Distance to rear bulkhead [mm]
$X_{nlg} = 1140$	Distance to nose landing gear [mm]
$X_{mlg} = 17710$	Distance to main landing gear [mm]
$X_{fs} = 13700$	Distance to front spar [mm]
$X_{rs} = 17900$	Distance to rear spar [mm]
$H_{cg} = 1800$	Height of center of gravity of aircraft [mm]
$G_{cg_h} = 6500$	Height of center of gravity of tail [mm]
$R_n = 500$	Wheel radius nose landing gear [mm]
$R_m = 500$	Wheel radius main landing gear [mm]
$X_{eng} = 13300$	Location of the engine [mm]
$Y_{eng} = 5800$	Location of the engine [mm]
$\phi = 6$	Roll angle [deg]
$\psi = 6$	Yaw angle [deg]
$\delta_e = 8$	Elevator pitch angle [deg]

C.1.5 Coefficients

$C_L = 1.1$	Lift coefficient [-]
$C_{M_{ac}} = -0.025$	Moment coefficient at aerodynamic center [-]
$\eta_h = 0.85$	Tail configuration coefficient [-]
$k_r = 0.9$	Aircraft response factor for abrupt elevation maneuvres [-]
$I_z = 0.3 \cdot 10^12$	Moment of inertia fuselage (assumption) [mm^4]

C.1.6 Weights

$\mathrm{MTOW} = 73500$	Maximum take-off weight [kg]
$\mathrm{OEW} = 42100$	Operating empty weight [kg]
$\mathrm{WPAY} = 15445$	Payload weight [kg]
$T = 115000$	Thrust per engine [N]

C.1.7 Other aircraft related data

$\mathrm{Range} = 4800$	Range of aircraft [km]
$M = 0.82$	Mach speed at cruise [-]
$N_{pax} = 179$	Number of passengers [-]
$V_{ff} = 37.5$	Volume bulk loading [m^3]
$N_{eng} = 2$	Number of engines [-]
$S_{fl} = 108$	Floor surface area [m^2]
$S_{crgf} = 12.75$	Cargo floor area front [m^2]
$S_{crgb} = 25.75$	Cargo floor area rear [m^2]
$D_{fbhd} = 1.76$	Diameter of front bulkhead [m]
$D_{rbhd} = 2.94$	Diameter of rear bulkhead [m]
$t_{croot} = 0.135$	Thickness chord ratio at wing root [-]
$c_{rootcord} = 6.1$	Wing root cord [m]
$b_{wing} = 34.09$	Wing span [m]
$\lambda_w = 28$	Sweep back angle of wing [deg]
$\lambda_v = 40$	Sweep back angle vertical tail [deg]
$\lambda_h = 32$	Sweep back angle of horizontal tail [deg]
$S_w = 122.4$	Wing area [m^2]
$S_h = 31$	Horizontal tail area [m^2]
$S_v = 21.5$	Vertical tail area [m^2]
$S_e = 1$	Elevator surface area [m^2]
$A_w = 9.5$	Wing aspect ratio [-]

$A_h = 5$	Horizontal tail aspect ratio [-]
$A_v = 4$	Vertical tail aspect ratio [-]
$\mathrm{MAC_w} = 3.81$	Mean aerodynamic chord of wing [m]
$\mathrm{MAC_v} = 1$	Mean aerodynamic chord of vertical tail [m]

C.1.8 Material specification

C.1.8.1 Metal

$\mathrm{Name} = \text{"Aluminum"}$	Name of material
$\mathrm{Type} = \text{"Metal"}$	Type of material
$E = 70000$	E-modulus [MPa]
$\nu = 0.3$	Poisson's ratio [-]
$\rho = 2800$	Density of material [$^{\mathrm{kg}}/_{\mathrm{m}^3}$]
$n = 16$	Ramberg Osgood coefficient [-]
$R_{p02_{tens}} = 250$	Yield strength for tension [MPa]
$R_{p02_{comp}} = 250$	Yield strength for compression [MPa]
$R_{p02_{shear}} = 200$	Yield strength for shear [MPa]
$R_{m_{tens}} = 375$	Ultimate strength for tension [MPa]
$R_{m_{comp}} = 375$	Ultimate strength for compression [MPa]
$C_1 = 53$	Constant 1 for S-N curve [$^{\mathrm{N}}/_{\mathrm{mm}^2}$]
$C_2 = 235$	Constant 2 for S-N curve [$^{\mathrm{N}}/_{\mathrm{mm}^2}$]
$C_3 = 4.32$	Constant 3 for S-N curve [-]
$C_4 = 3.86$	Constant 4 for S-N curve [-]
$\beta = 1$	Geometry related constant [-]
$K_{I_c} = 40$	Fracture toughness value [$^{\mathrm{MPA}}/_{\sqrt{\mathrm{m}}}$]
$m = 3$	Paris's exponent/coefficient of model influence [-]
$C = 2.5389 \cdot 10^{-11}$	Paris's coefficient/empirical crack-growth constant [-]

C.1.8.2 Composite

$\mathrm{Name} = \text{"Quasi} - \text{IsotropicCFRP"}$	Name of material
$\mathrm{Type} = \text{"Composite"}$	Type of material
$E = 50000$	E-modulus [MPa]
$G = 18000$	Shear modulus [MPa]
$\nu = 0.318$	Poisson's ratio [-]
$\rho = 1560$	Density of material [$^{\mathrm{kg}}/_{\mathrm{m}^3}$]
$R_{p02_{tens}} = 180$	Yield strength for tension [MPa]

$R_{p02_{comp}} = 180$ Yield strength for compression [MPa]

$R_{p02_{shear}} = 140$ Yield strength for shear [MPa]

$R_m = 180$ Ultimate strength [MPa]

$E_c = 160$ E-modulus of core material [MPa]

$G_c = 50$ Shear modulus [MPa]

$\rho_c = 110$ Density of material [$^{kg}/_{m^3}$]

$\nu_c = 0.318$ Poisson's ratio of core material

C.1.9 Limits

$a_0 = 1$ Initial crack length for fracture toughness [mm]

$a_f = 75$ Critical crack length for fracture toughness [mm]

$a_{frac} = 600$ Crack length for crack growth [mm]

$N_{crack} = 4 \cdot 7000$ Critical inspection interval for crack growth [cycle]

$N_{fatigue} = 4 \cdot 20000$ Critical inspection threshold for crack initiation [cycle]

C.1.10 Element properties

C.1.10.1 Stringer

See figure C.1.

$\text{Name} = \text{"H} - \text{stringer"}$ Name of stringer

$s_1 = 0$ Stringer shape definition 1 [mm]

$s_2 = 8$ Stringer shape definition 2 [mm]

$s_3 = 0$ Stringer shape definition 3 [mm]

$s_4 = 3$ Stringer shape definition 4 [mm]

$s_5 = 30$ Stringer shape definition 5 [mm]

$s_6 = 3$ Stringer shape definition 6 [mm]

$s_7 = 22$ Stringer shape definition 7 [mm]

$s_8 = 3$ Stringer shape definition 8 [mm]

$s9 = 3$ Stringer shape definition 9 [mm]

$s10 = 0$ Stringer shape definition 10 [mm]

$R_{cap} = 0$ Stringer shape definition radius cap [mm]

$R_{mid} = 0$ Stringer shape definition radius mid [mm]

$t_{cap} = 0$ Stringer shape definition thickness cap [mm]

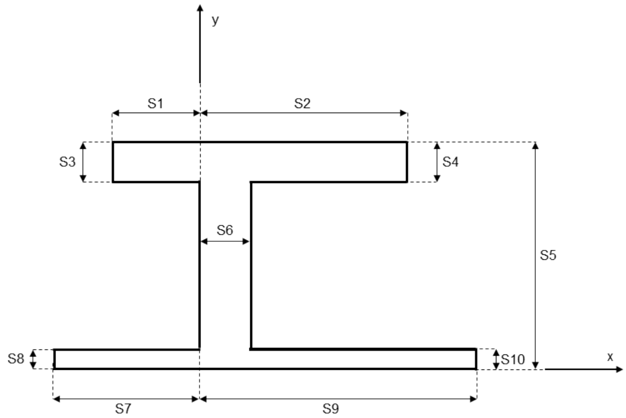

Figure C.1: Stringer and frame properties

C.1.10.2 Frame

See figure C.1.

$\text{Name} = \text{"V} - \text{stringer"}$	Name of frame
$s_1 = 0$	Frame shape definition 1 [mm]
$s_2 = 8$	Frame shape definition 2 [mm]
$s_3 = 0$	Frame shape definition 3 [mm]
$s_4 = 3$	Frame shape definition 4 [mm]
$s_5 = 30$	Frame shape definition 5 [mm]
$s_6 = 3$	Frame shape definition 6 [mm]
$s_7 = 22$	Frame shape definition 7 [mm]
$s_8 = 3$	Frame shape definition 8 [mm]
$s9 = 3$	Frame shape definition 9 [mm]
$s10 = 0$	Frame shape definition 10 [mm]
$R_{cap} = 0$	Frame shape definition radius cap [mm]
$R_{mid} = 0$	Frame shape definition radius mid [mm]
$t_{cap} = 0$	Frame shape definition thickness cap [mm]

C.1.10.3 Padding

$\text{Name} = \text{"Integrated"}$	Name of padding
$t_p = 4$	Padding thickness [mm]
$w = 33$	Padding width [mm]

C.1.10.4 Rivet

$\text{Name} = \text{"Rivet} - \text{Countersunk"}$	Name of rivet
$k_{ir} = 0.66$	Inter-rivet buckling coefficient [-]
$b_{pitch} = 24$	Rivet pitch length [mm]

C.2 Option selection

- Skin material selection
- Stringer material selection
- Stringer type selection
- Frame type selection
- Padding type selection
- Rivet type selection

Appendix D

Maximum loads result

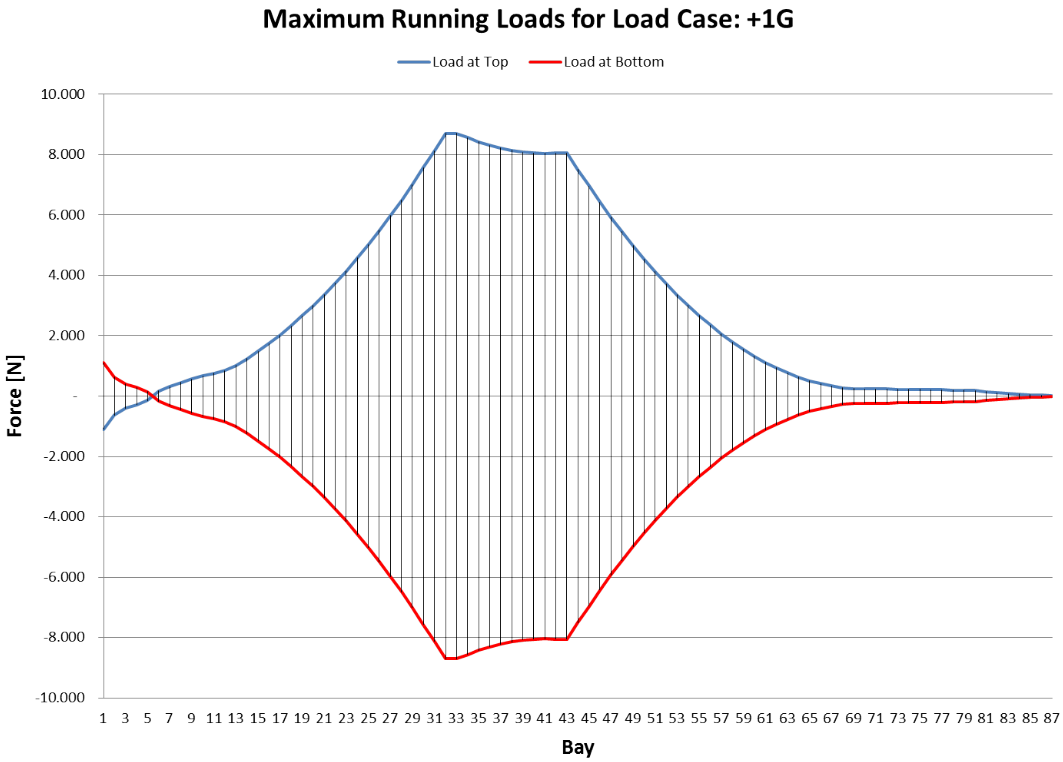

Figure D.1: Running load for 1G flight (ULC2)

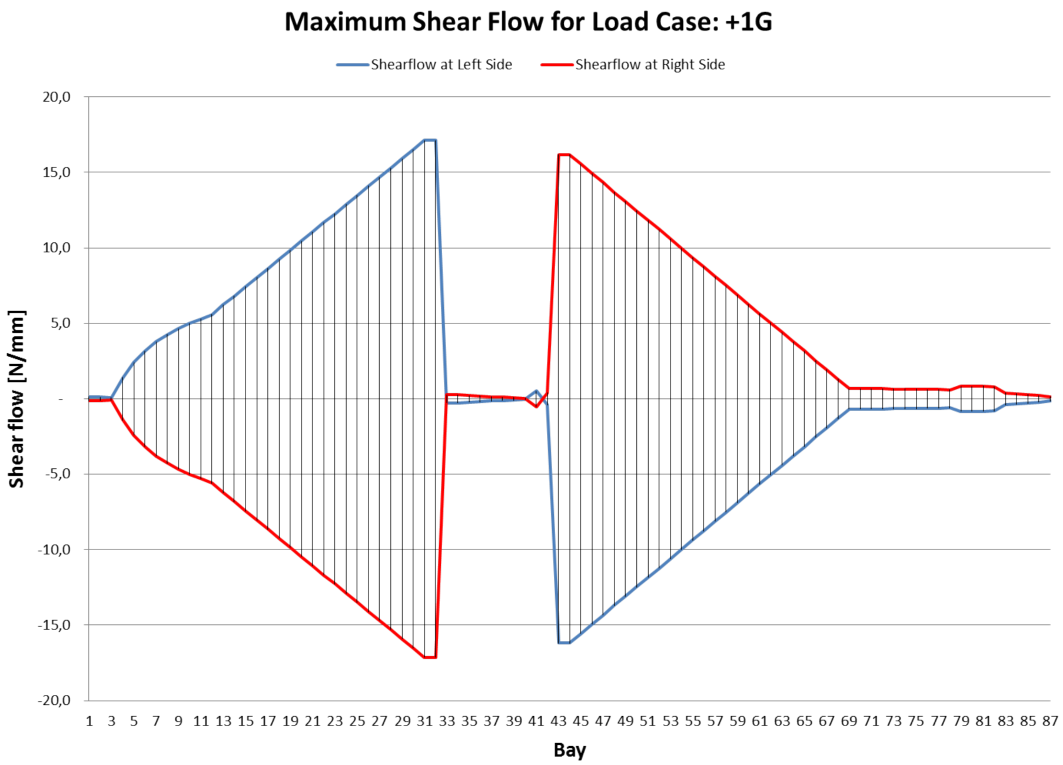

Figure D.2: Shear flow for 1G flight (ULC2)

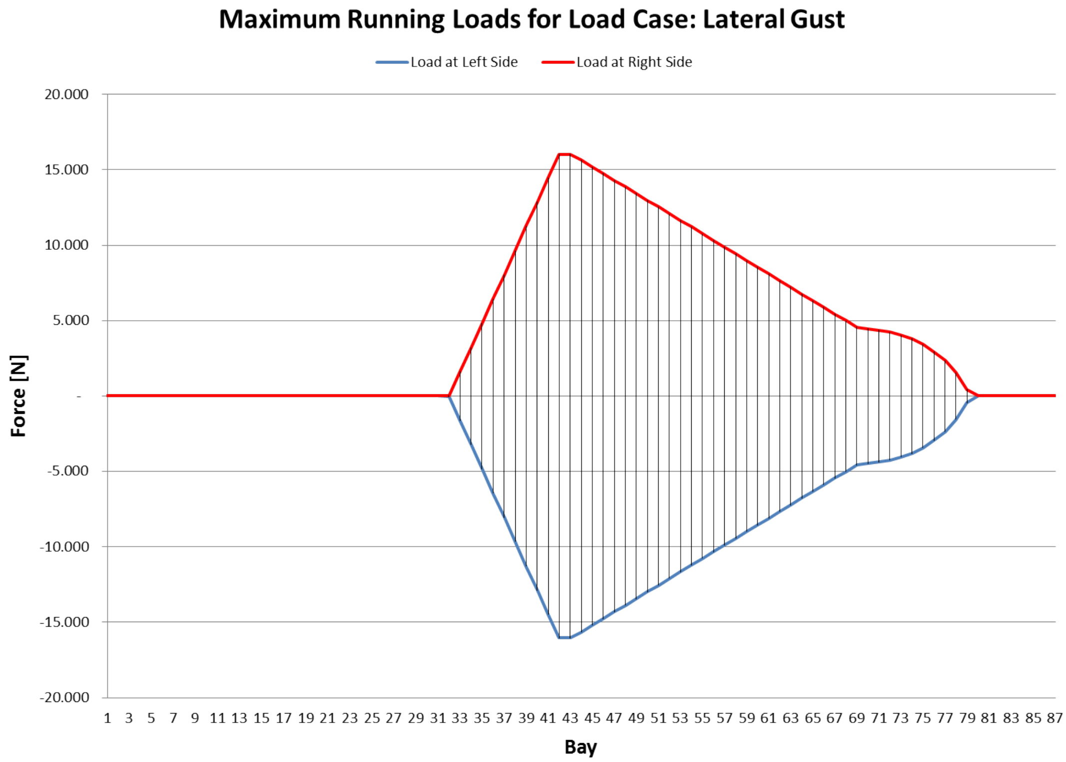

Figure D.3: Running load for lateral gust (ULC3)

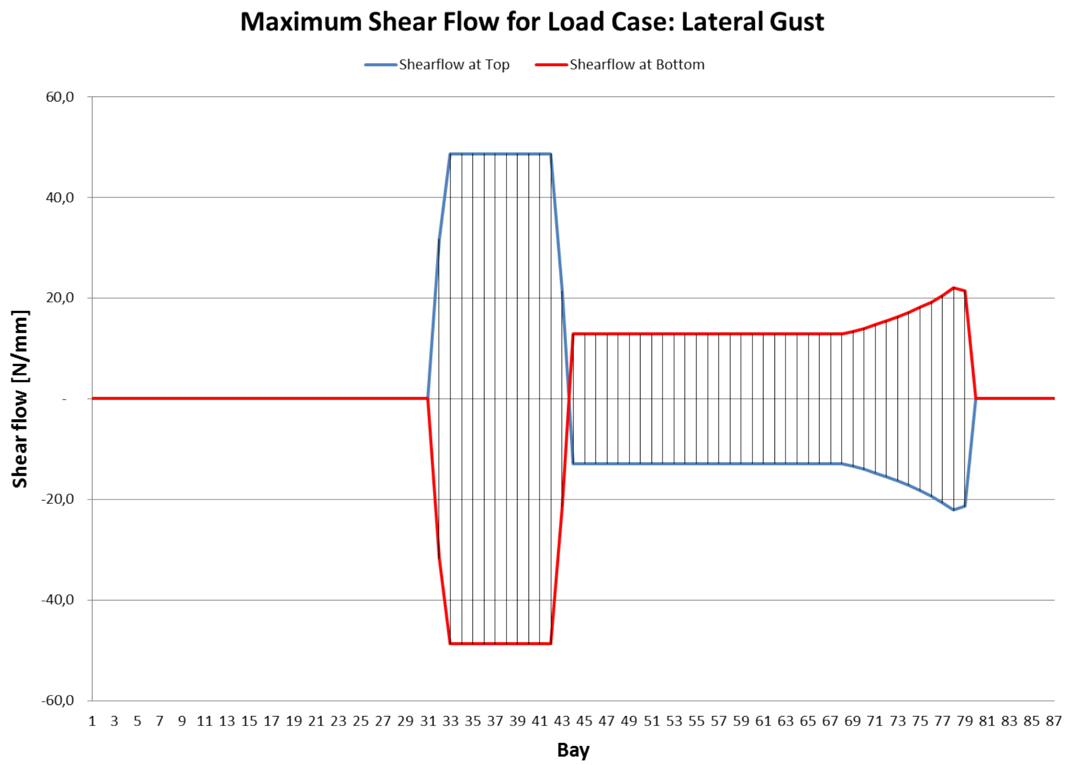

Figure D.4: Shear flow for lateral gust (ULC3)

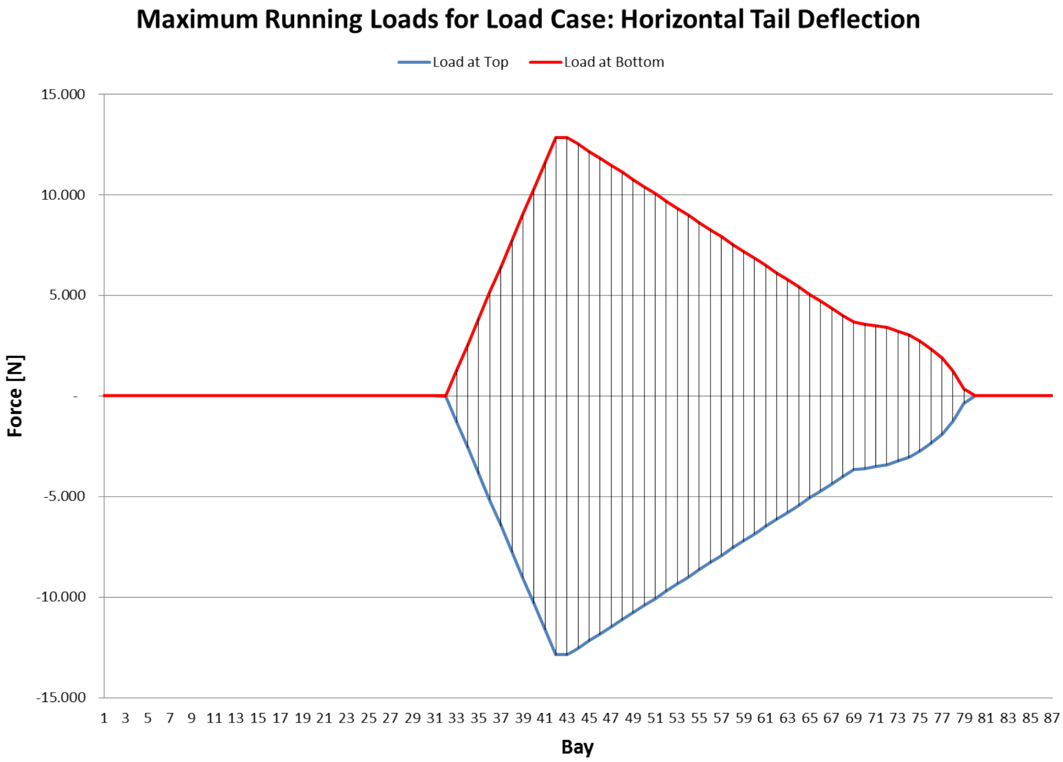

Figure D.5: Running load for horizontal deflection upward (ULC4)

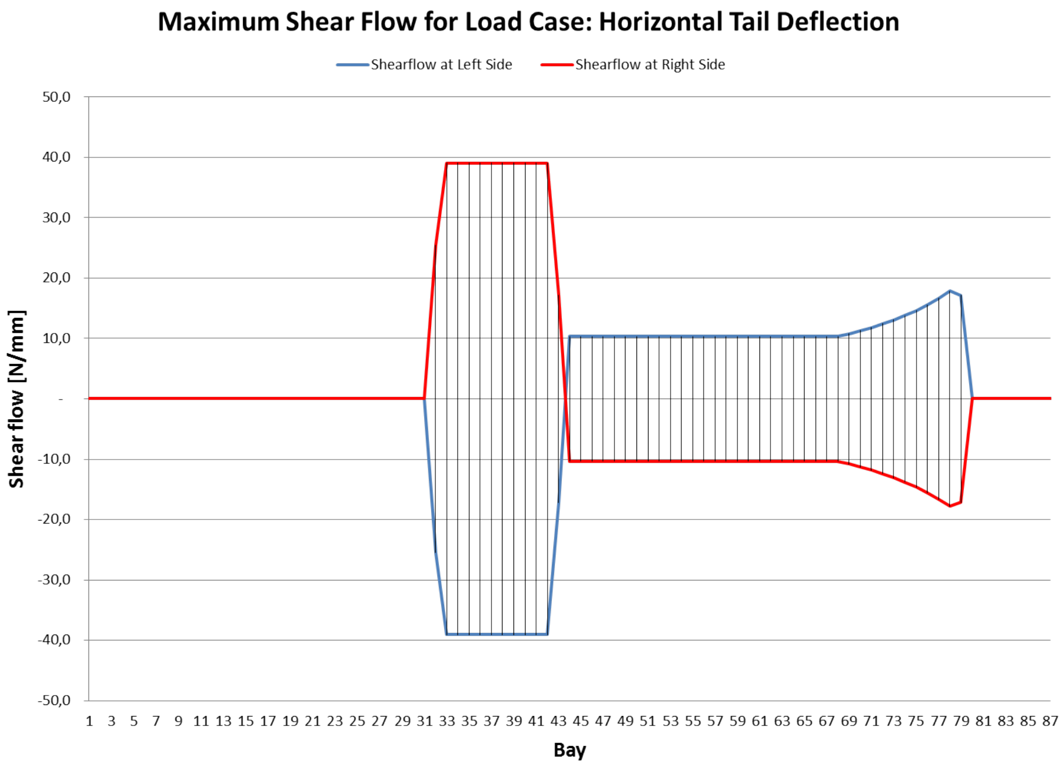

Figure D.6: Shear flow for horizontal deflection upward (ULC4)

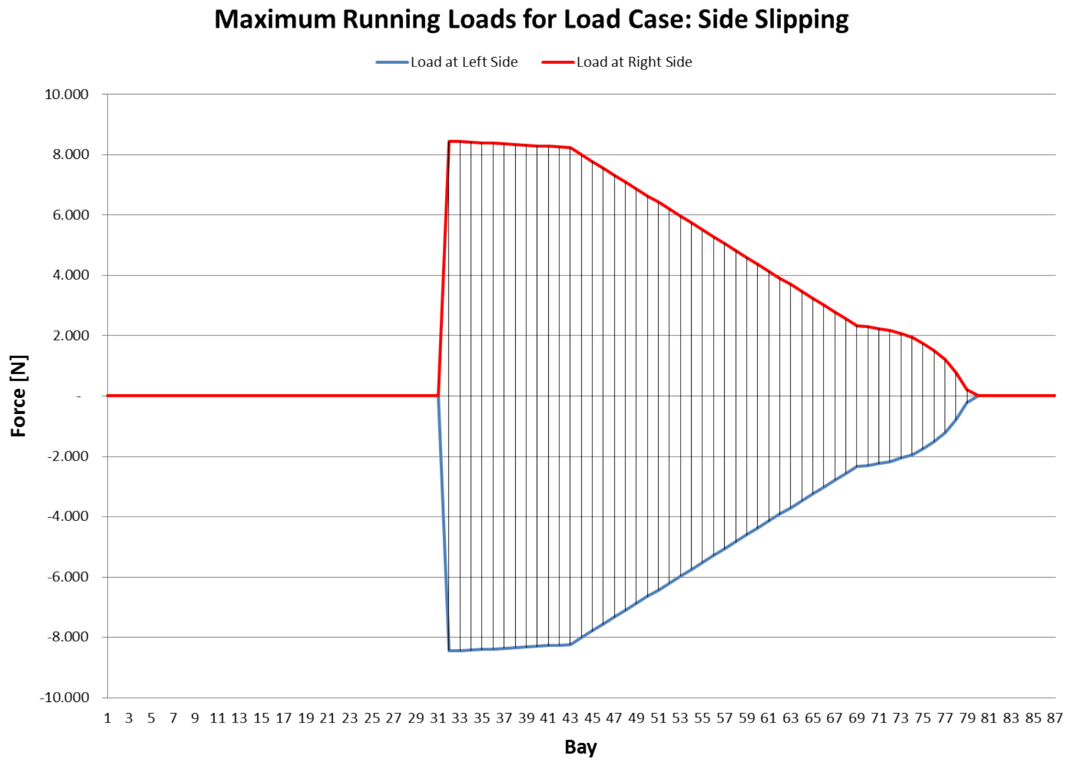

Figure D.7: Running load for sideslip flight (ULC5)

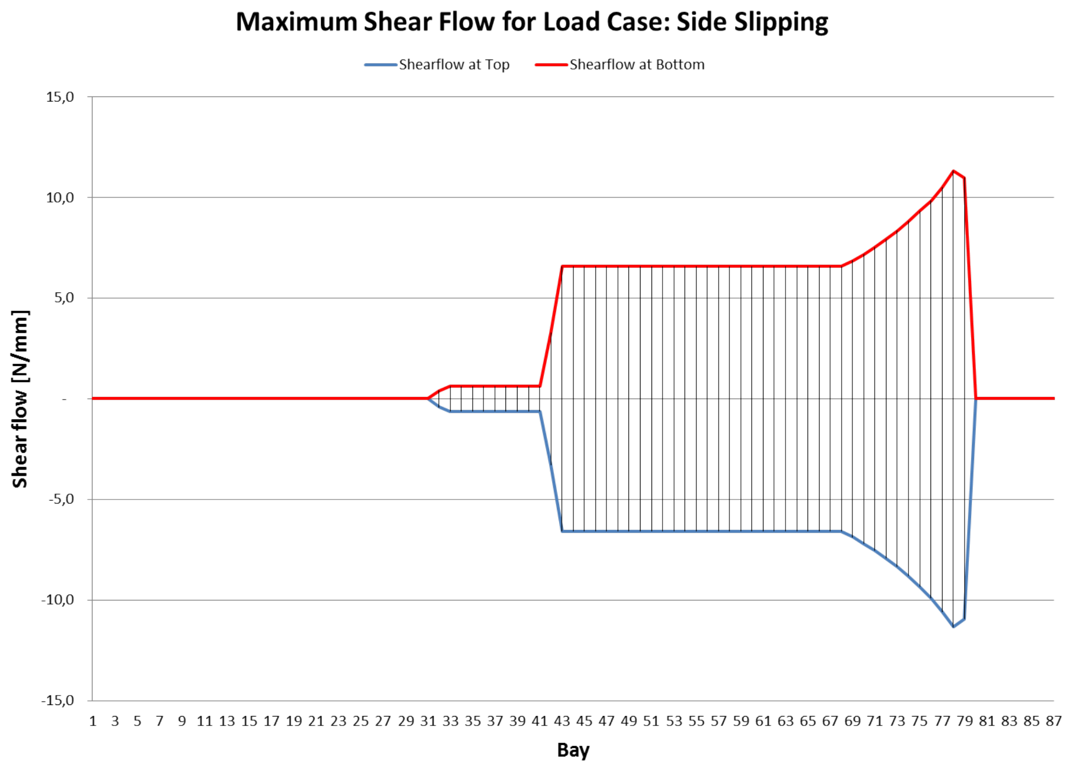

Figure D.8: Shear flow for sideslip flight (ULC5)

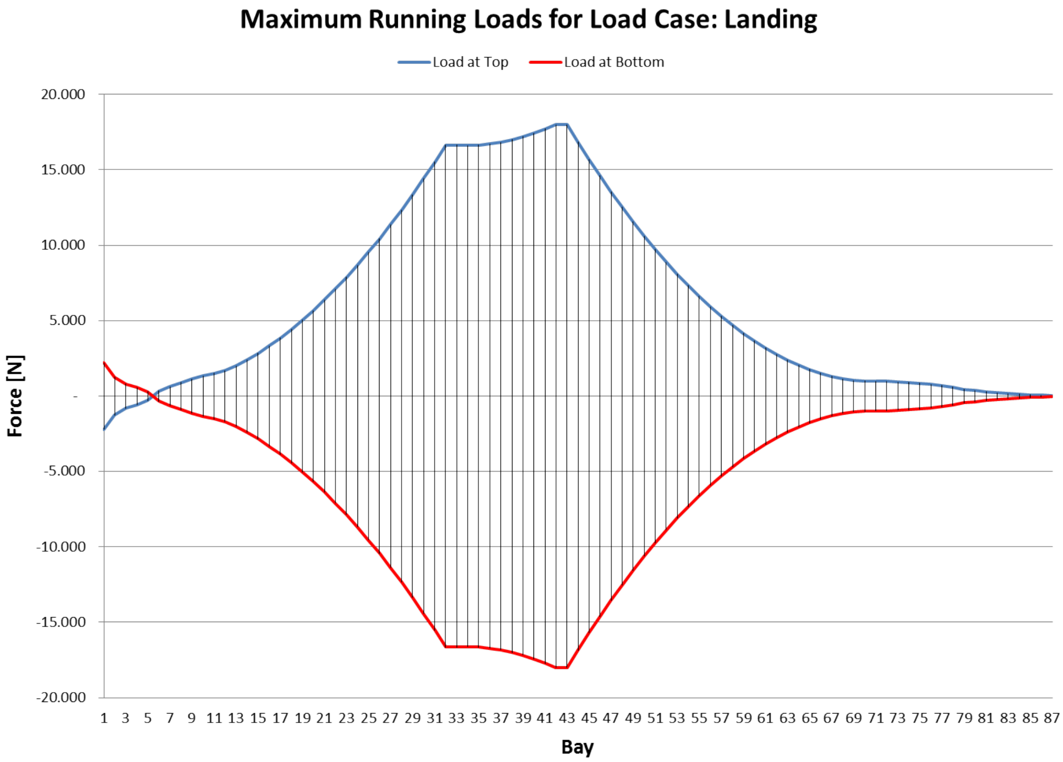

Figure D.9: Running load for landing (ULC6)

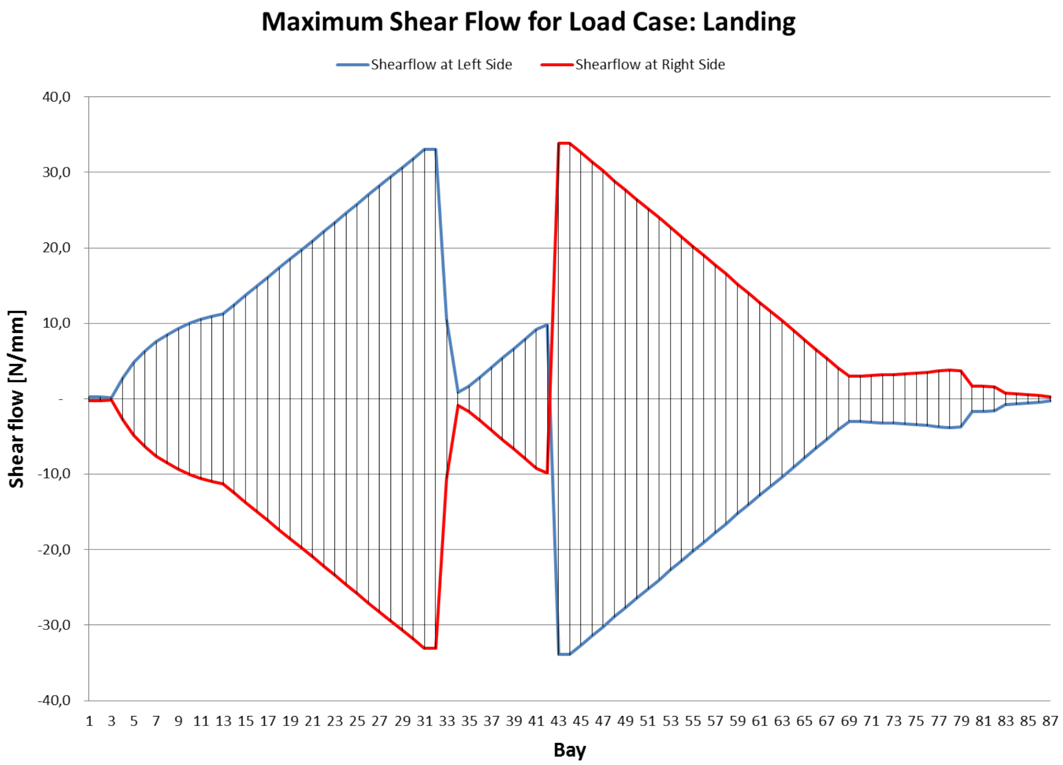

Figure D.10: Shear flow for landing (ULC6)

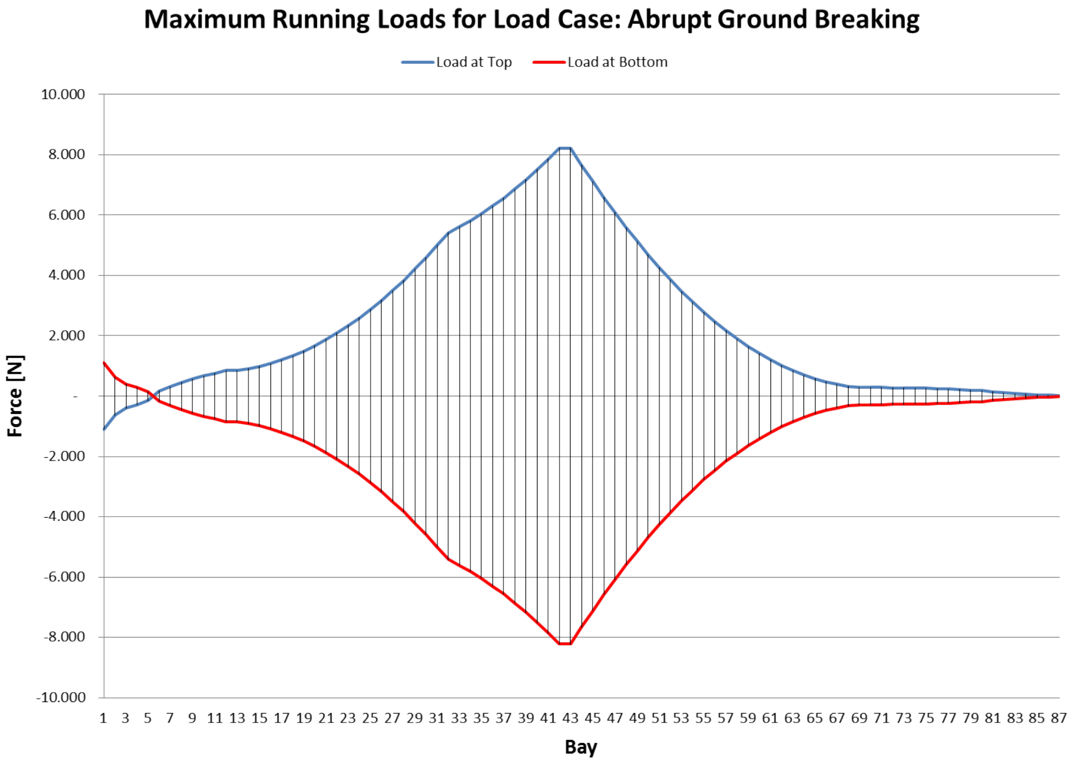

Figure D.11: Running load for abrupt ground breaking (ULC7)

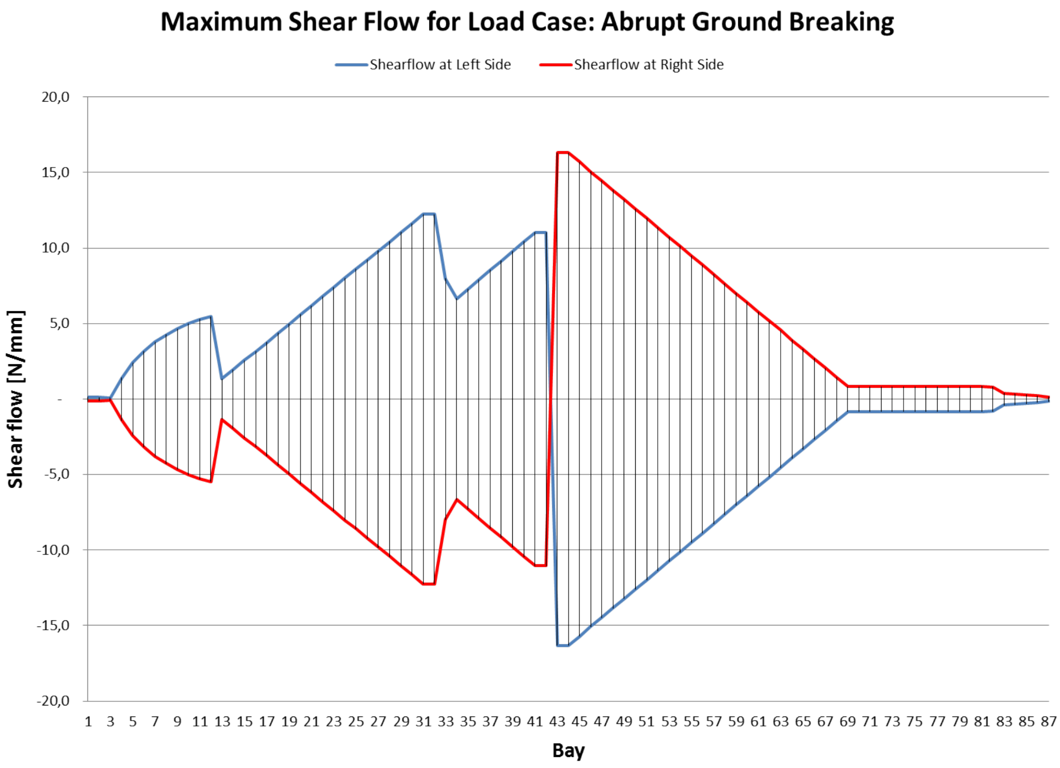

Figure D.12: Shear flow for abrupt ground breaking (ULC7)

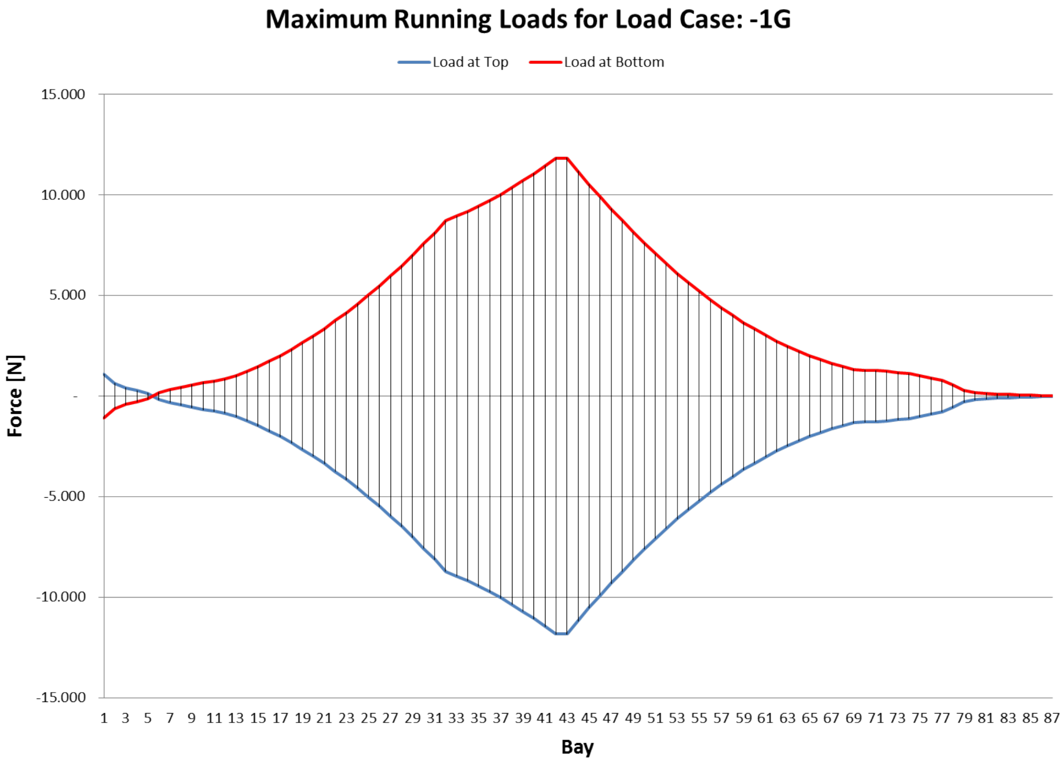

Figure D.13: Running load for -1G flight (CLC8)

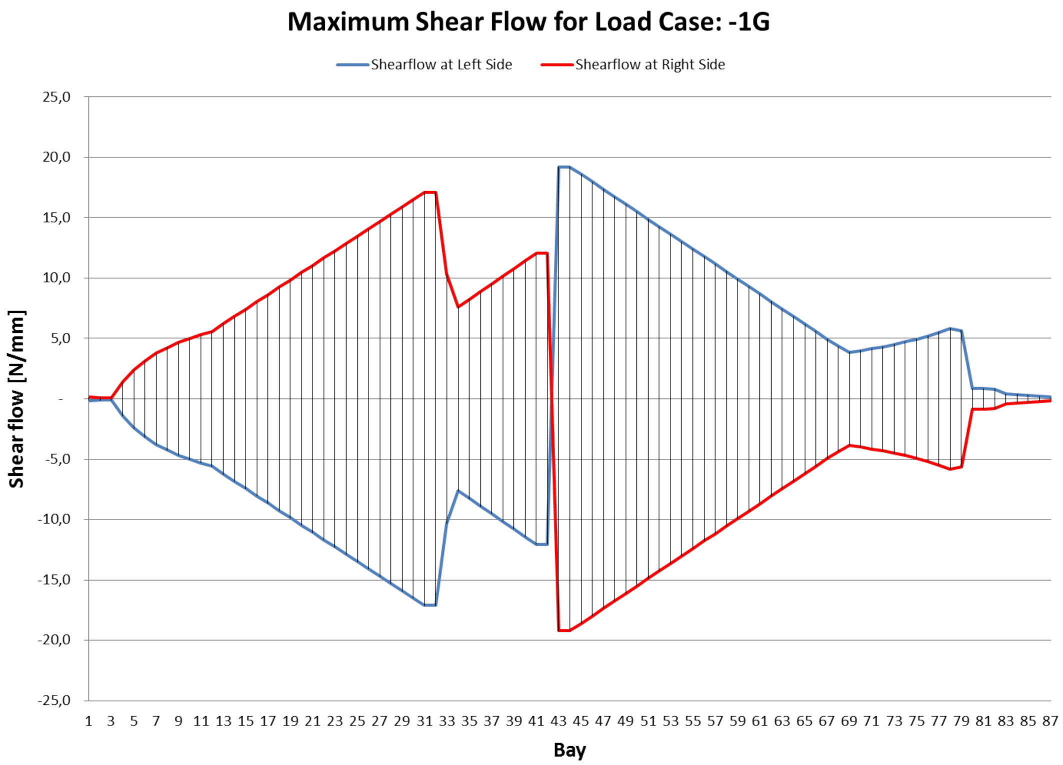

Figure D.14: Shear flow for -1G flight (CLC8)

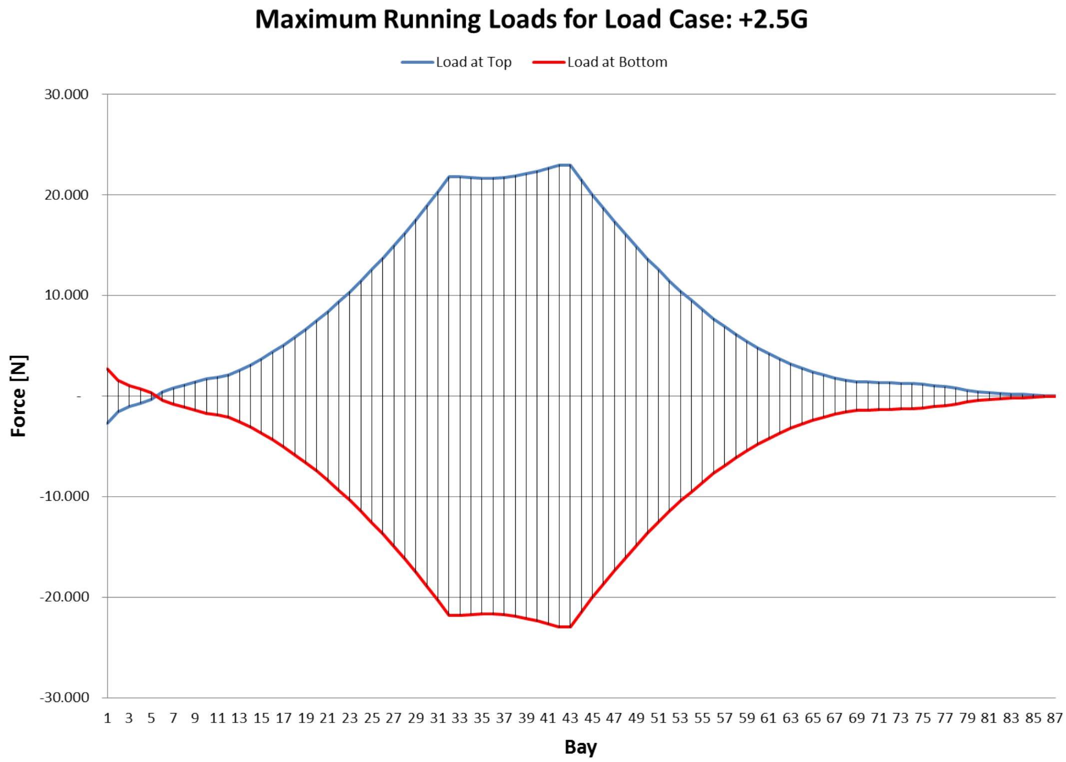

Figure D.15: Running load for 2.5G flight (CLC10)

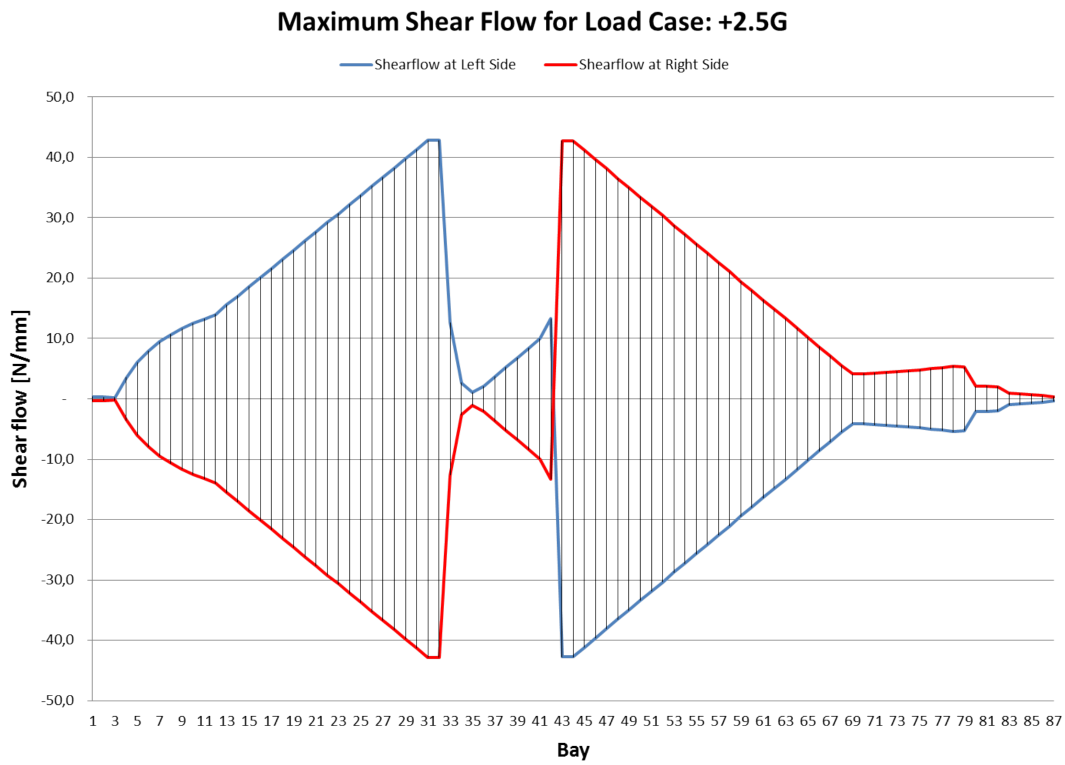

Figure D.16: Shear flow for 2.5G flight (CLC10)

Appendix E

Stress distribution

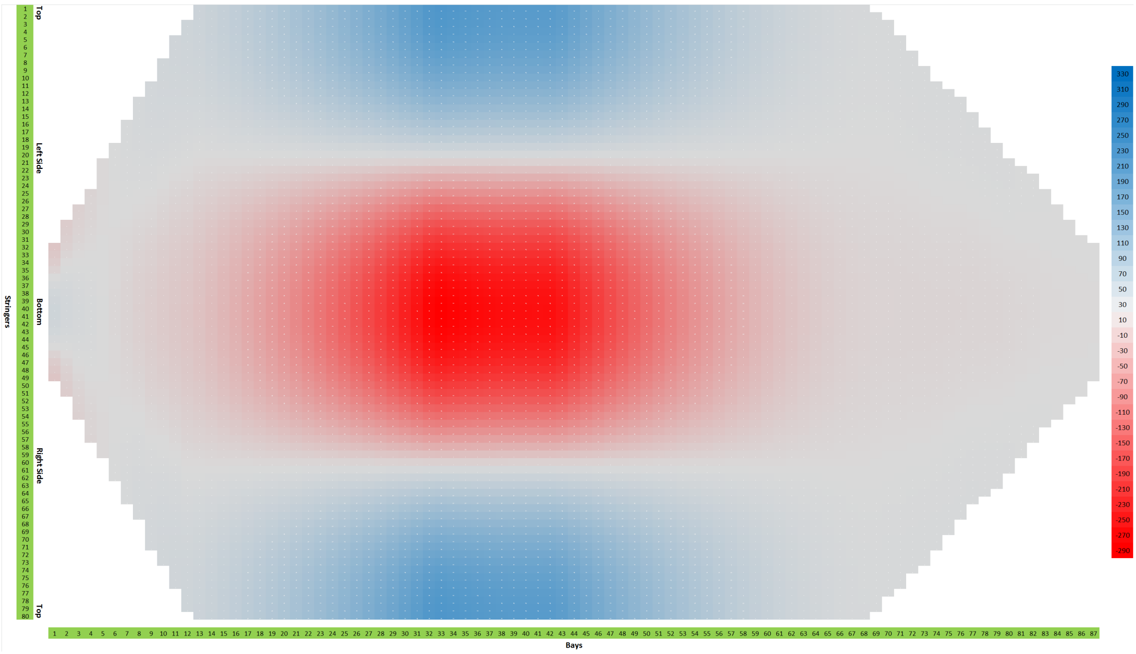

Figure E.1: Normalized longitudinal stress for 1G (ULC2) in MPa

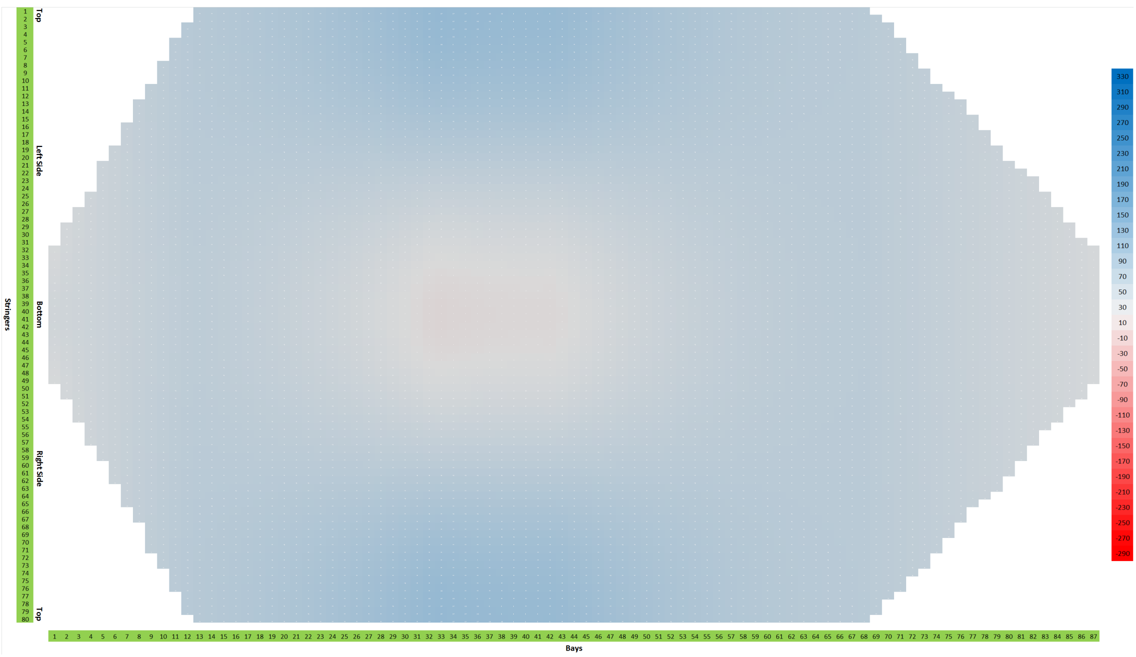

Figure E.2: Normalized longitudinal stress for 1G and Δp (ULC2 + ULC1) in MPa

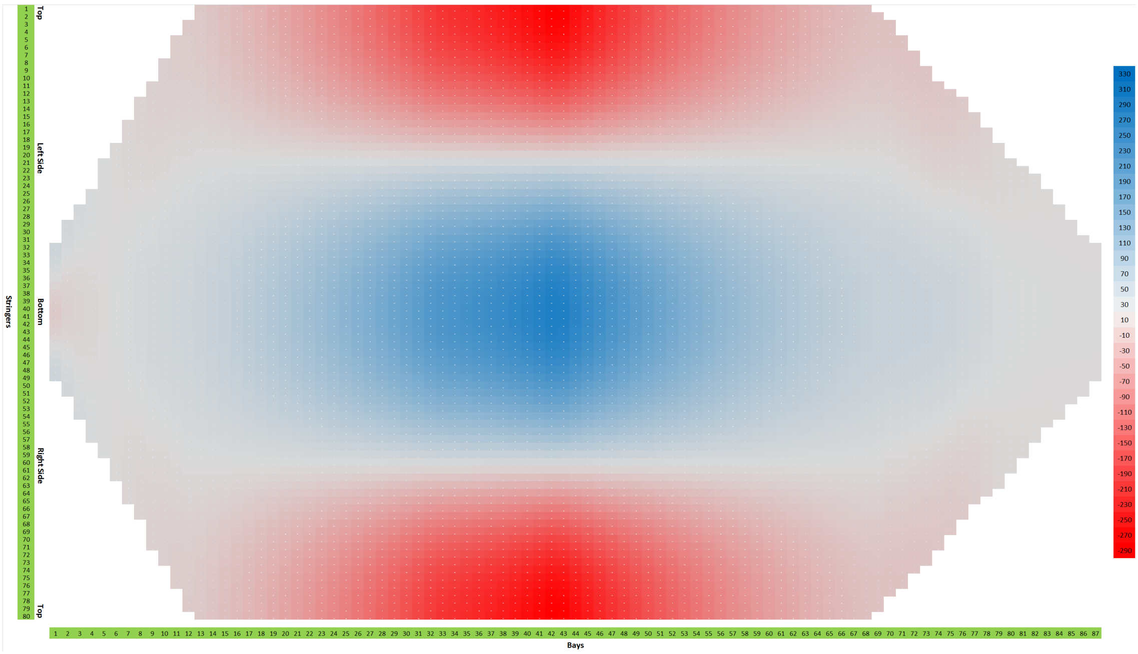

Figure E.3: Normalized longitudinal stress for -1G (CLC8) in MPa

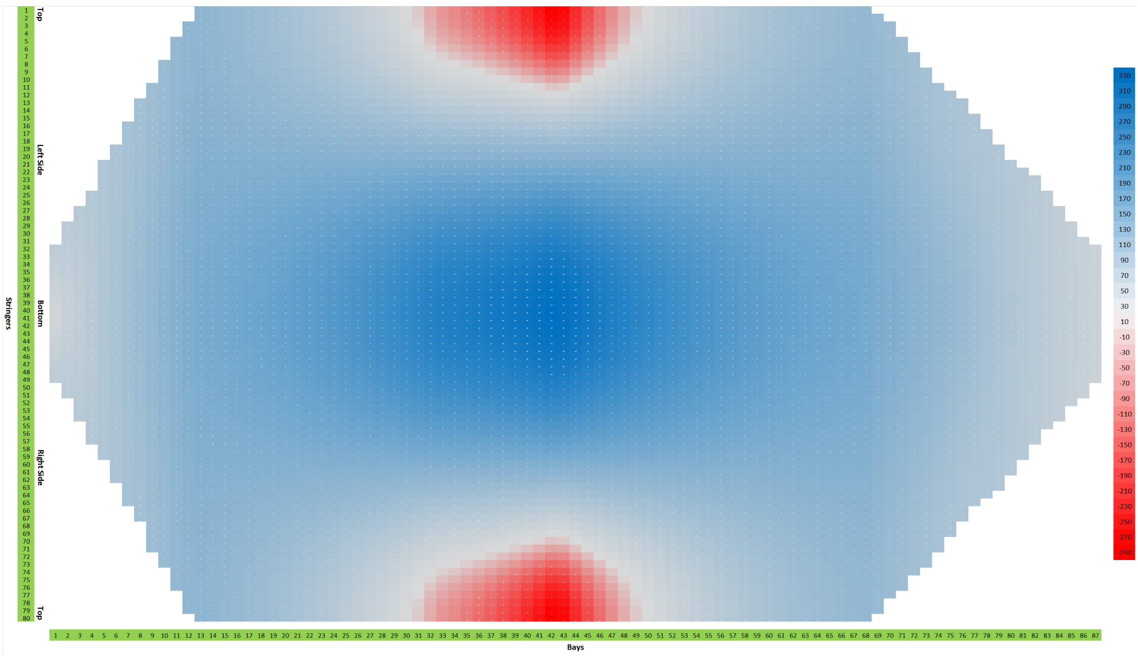

Figure E.4: Normalized longitudinal stress for -1G and Δp (CLC9) in MPa

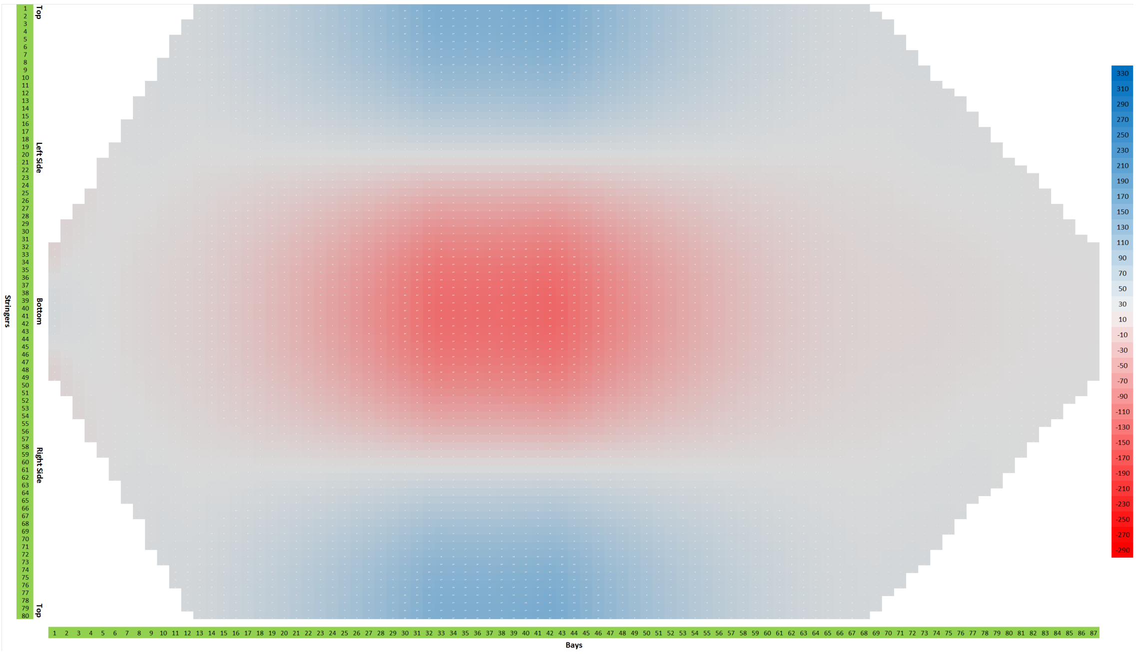

Figure E.5: Normalized longitudinal stress for 2.5G (CLC10) in MPa

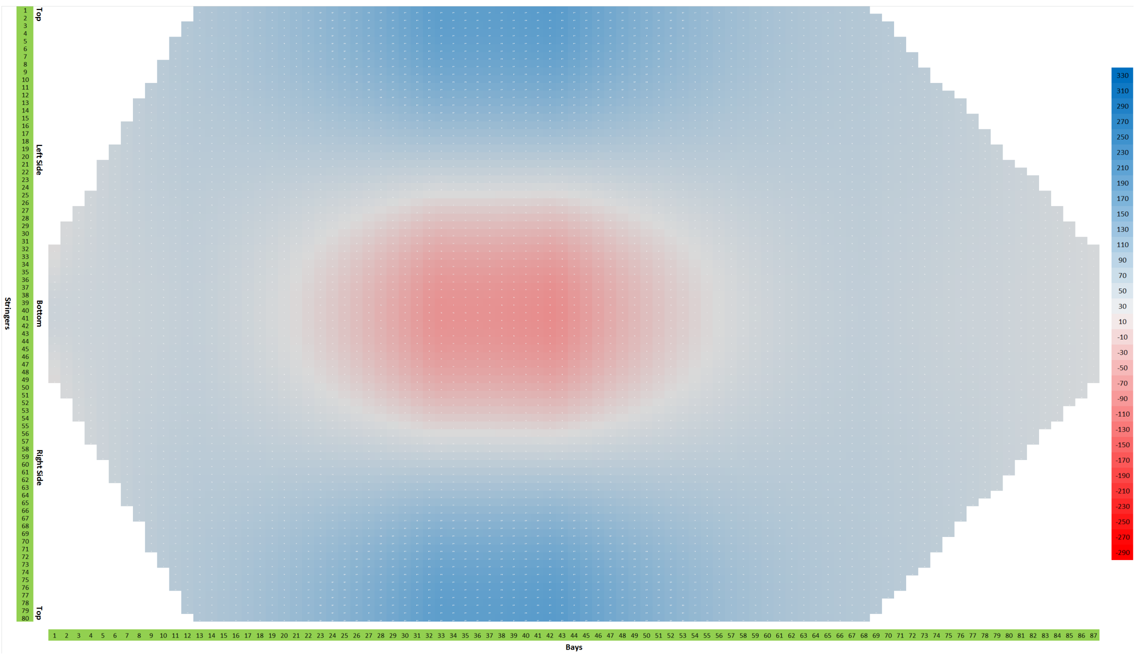

Figure E.6: Normalized longitudinal stress for 2.5G and Δp (CLC11) in MPa

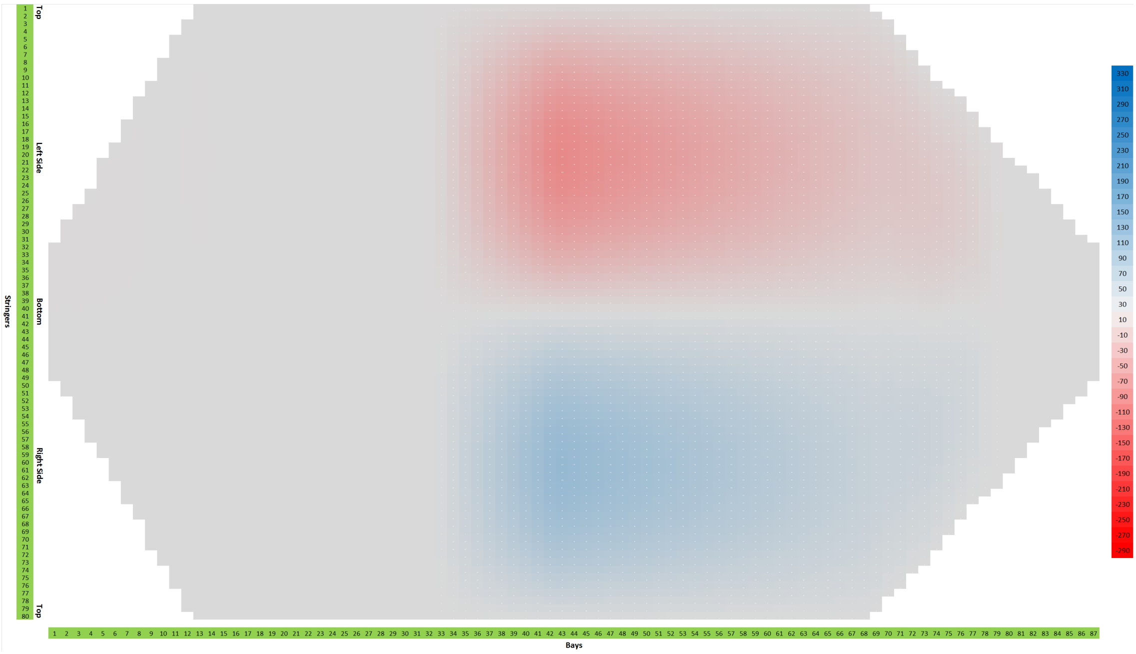

Figure E.7: Normalized longitudinal stress for lateral gust (+) (ULC3) in MPa

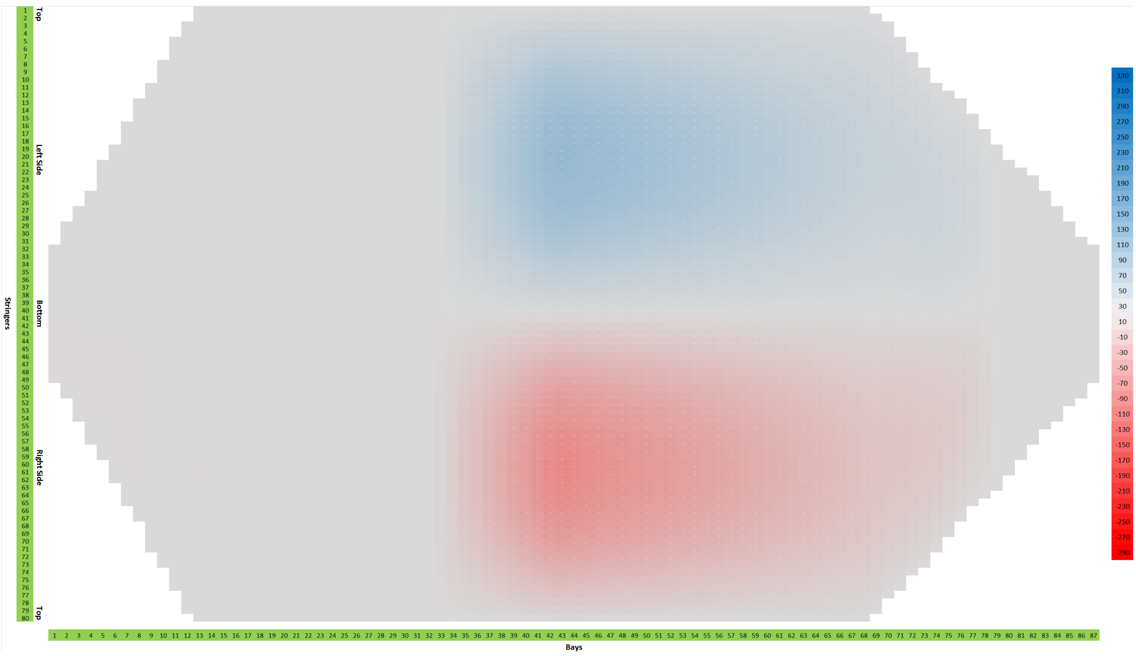

Figure E.8: Normalized longitudinal stress for lateral gust (-) (ULC3) in MPa

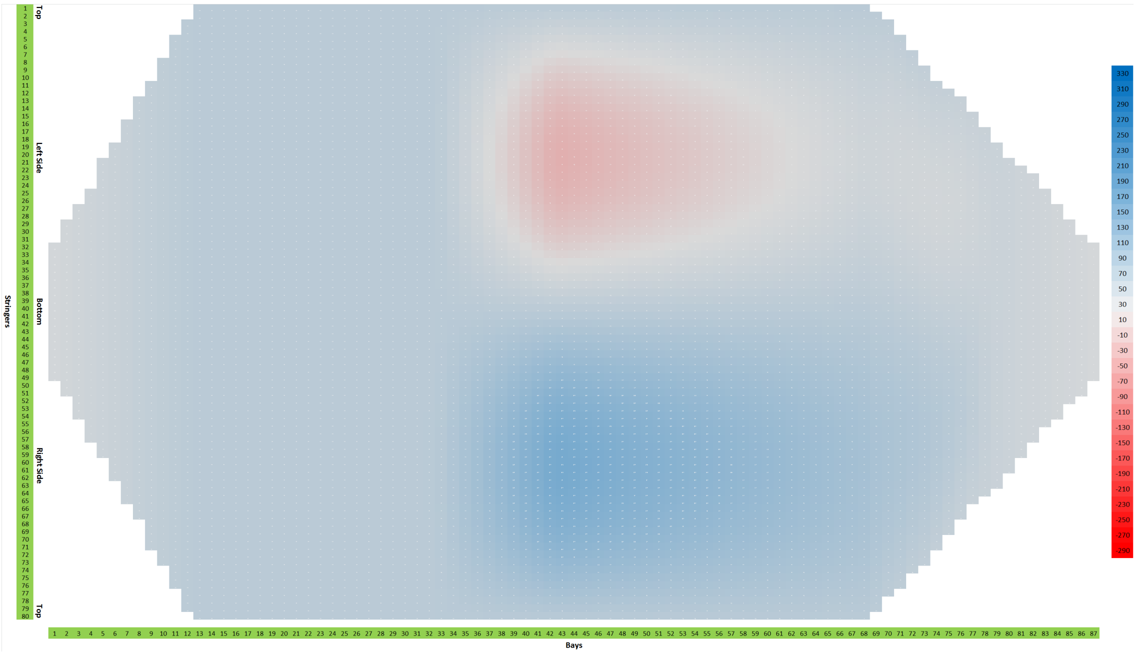

Figure E.9: Normalized longitudinal stress for lateral gust (+) and Δp (CLC12) in MPa

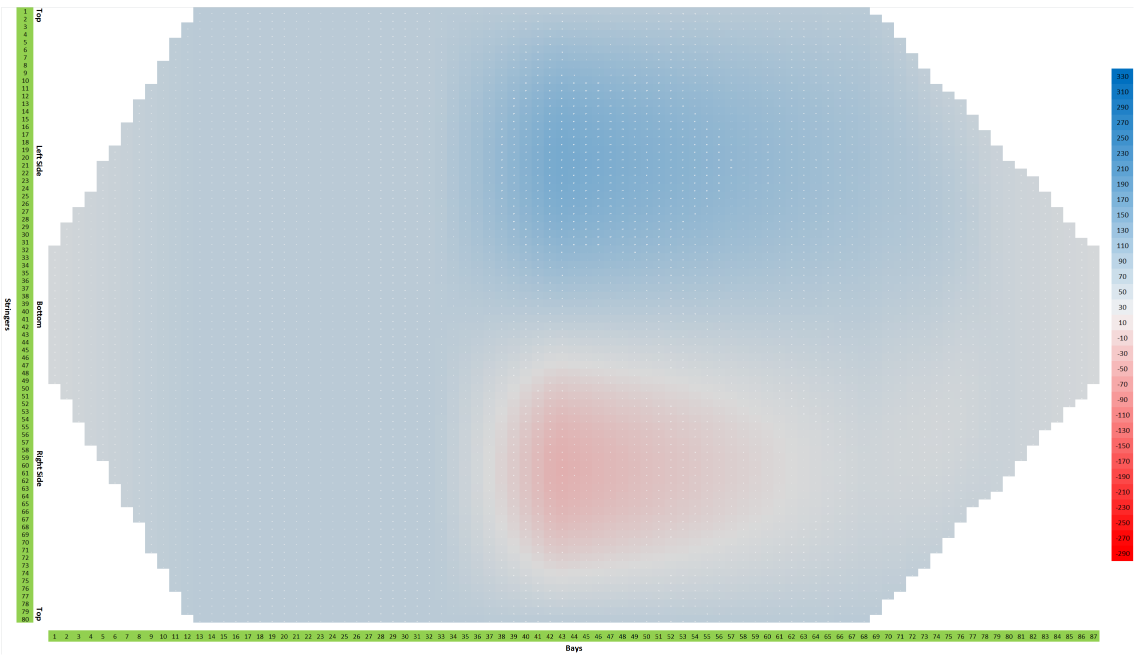

Figure E.10: Normalized longitudinal stress for lateral gust (-) and Δp(CLC13) in MPa

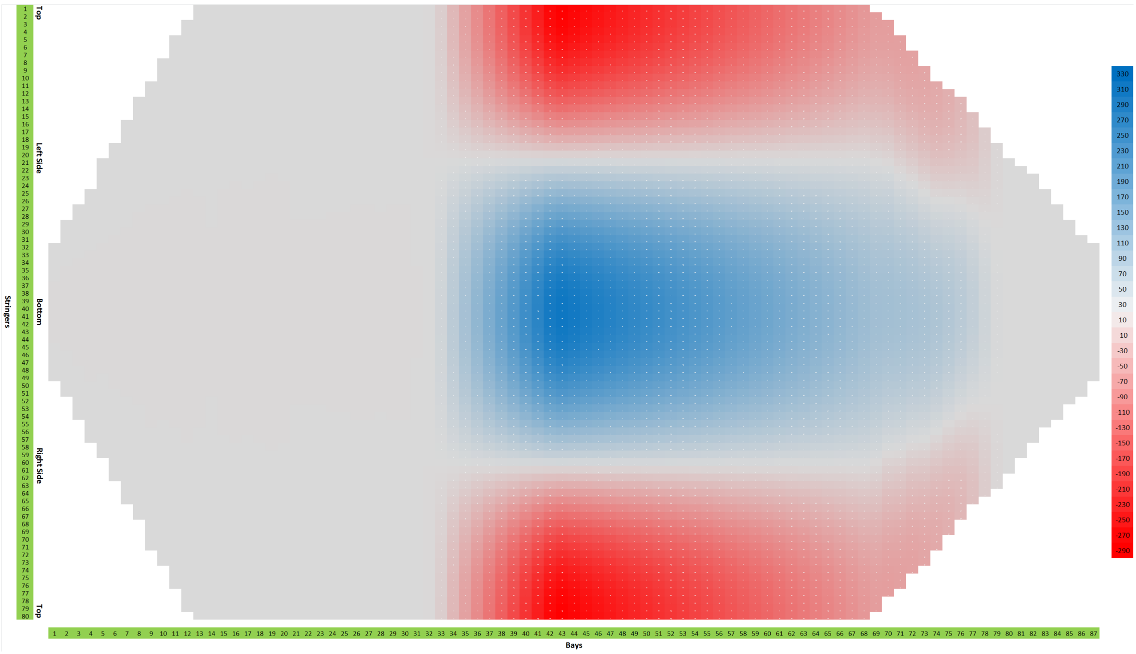

Figure E.11: Normalized longitudinal stress for horizontal deflection upward (ULC4) in MPa

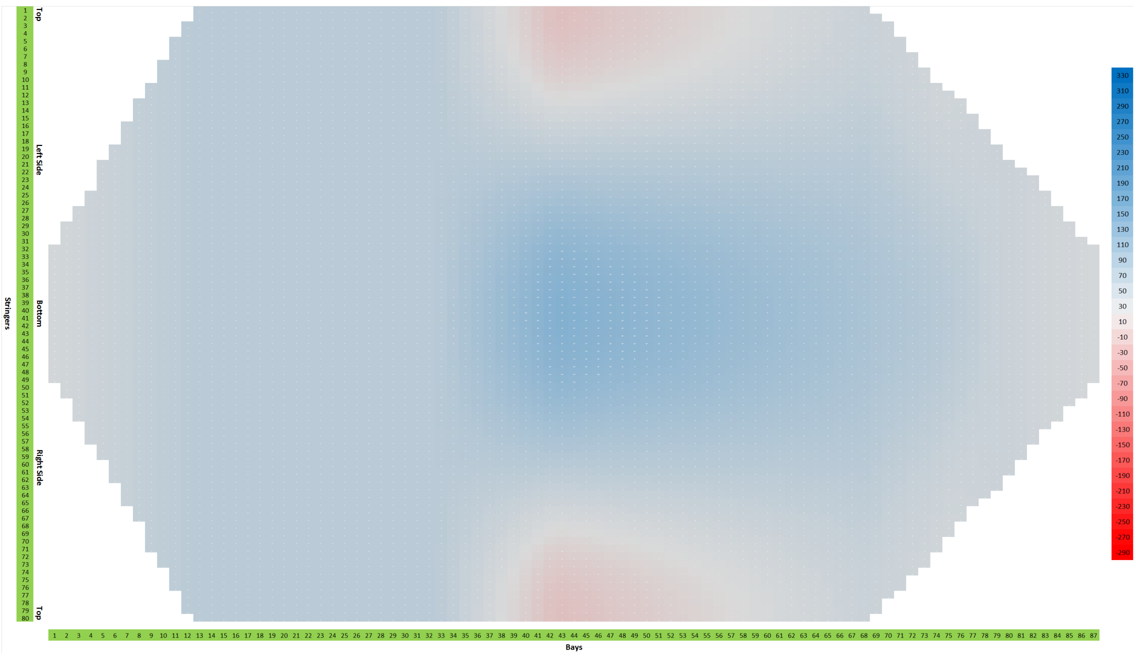

Figure E.12: Normalized longitudinal stress for horizontal deflection upward and Δp(CLC14) in MPa

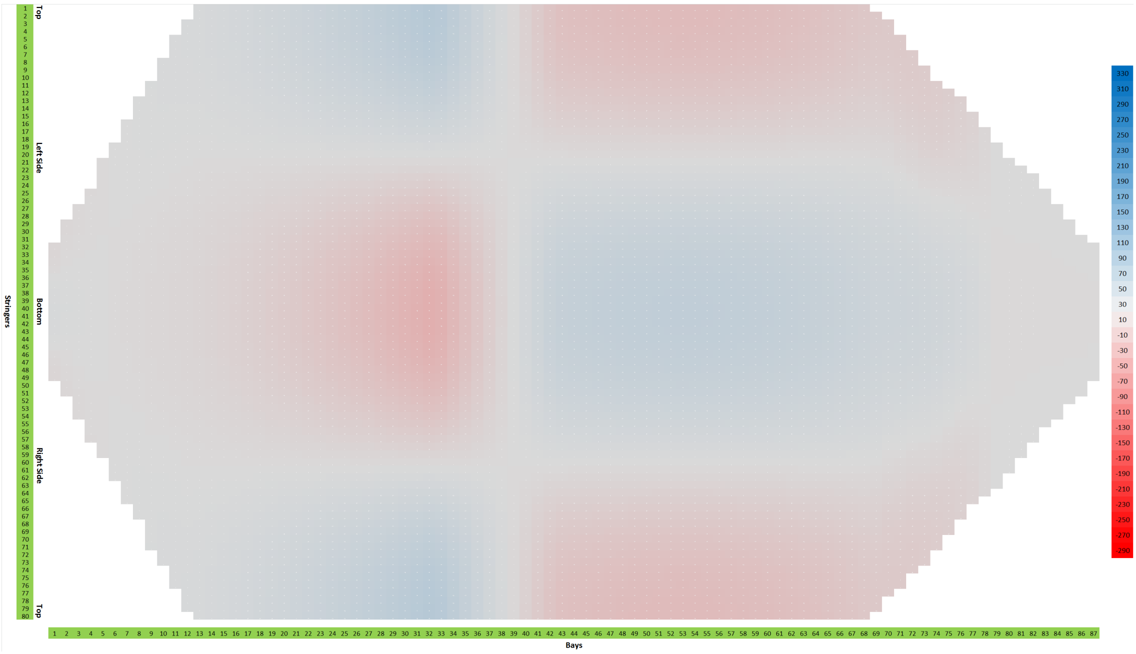

Figure E.13: Normalized longitudinal stress for 1G and horizontal deflection upward (CLC15) in MPa

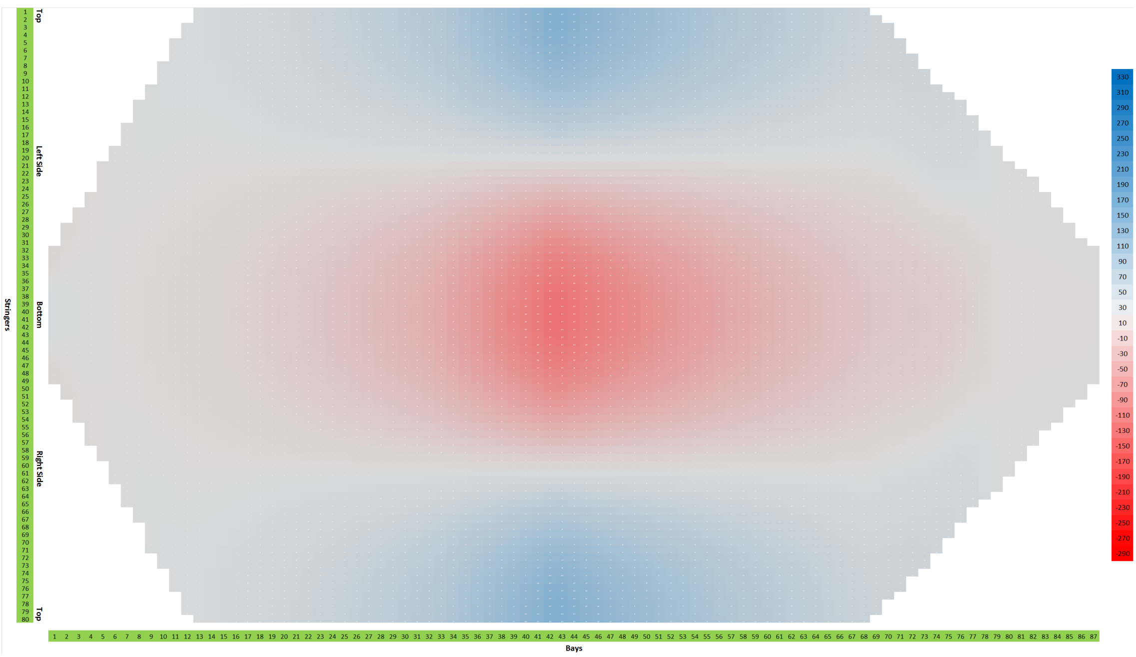

Figure E.14: Normalized longitudinal stress for 1G and horizontal deflection downward (CLC16) in MPa

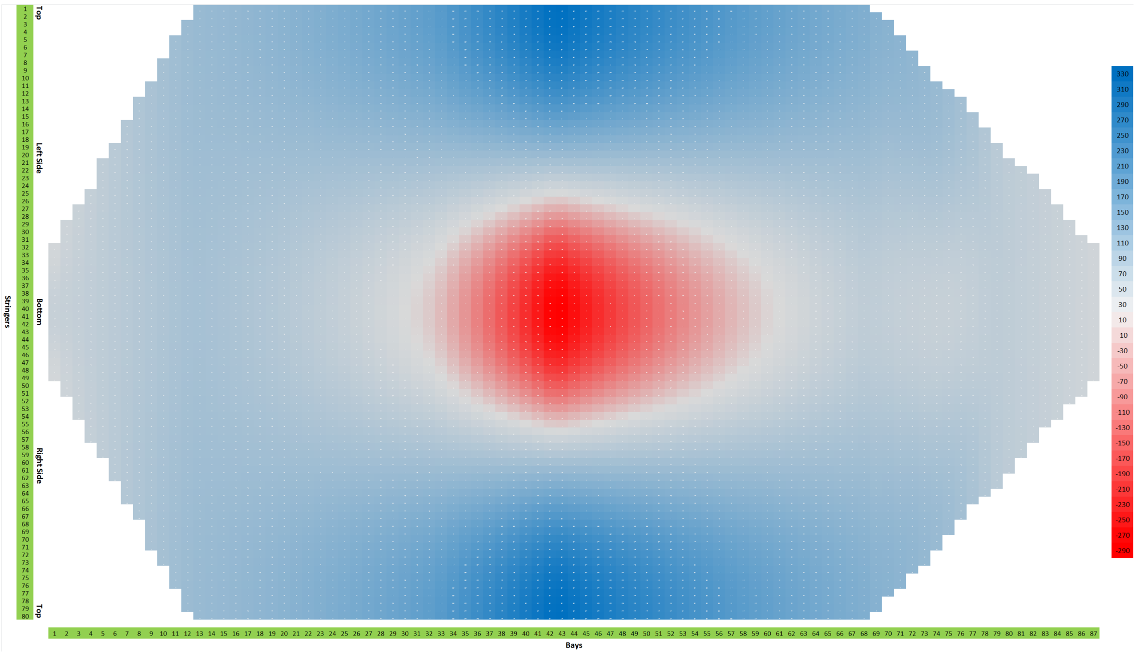

Figure E.15: Normalized longitudinal stress for 1G, Δp and horizontal deflection downward (CLC17) in MPa

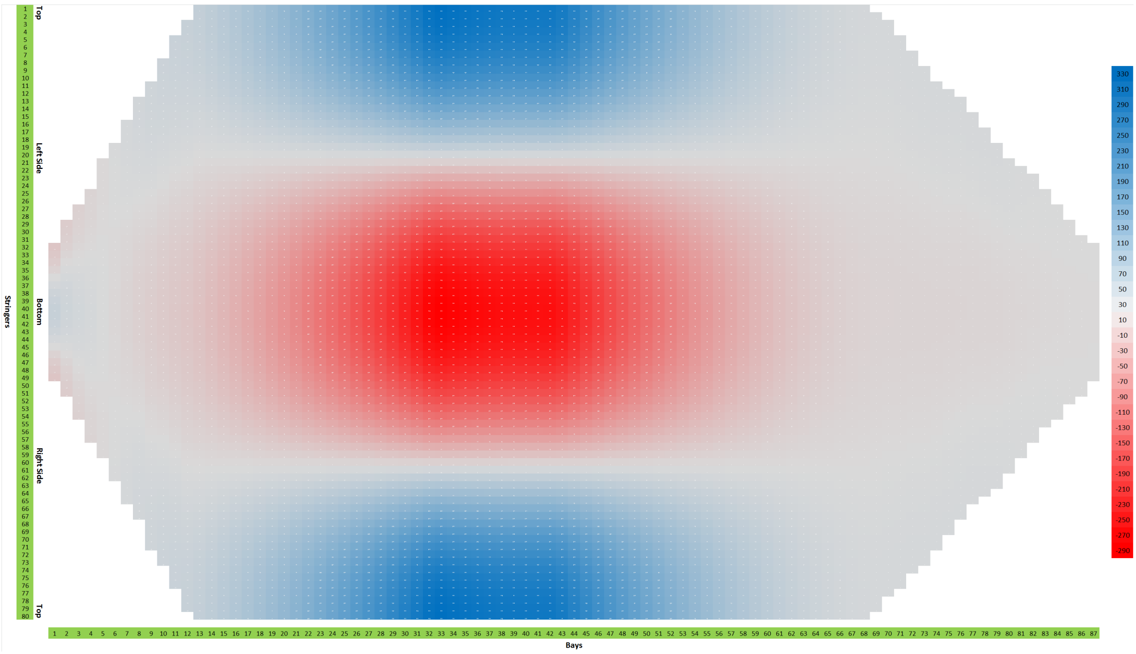

Figure E.16: Normalized longitudinal stress for 5G (CLC19) in MPa

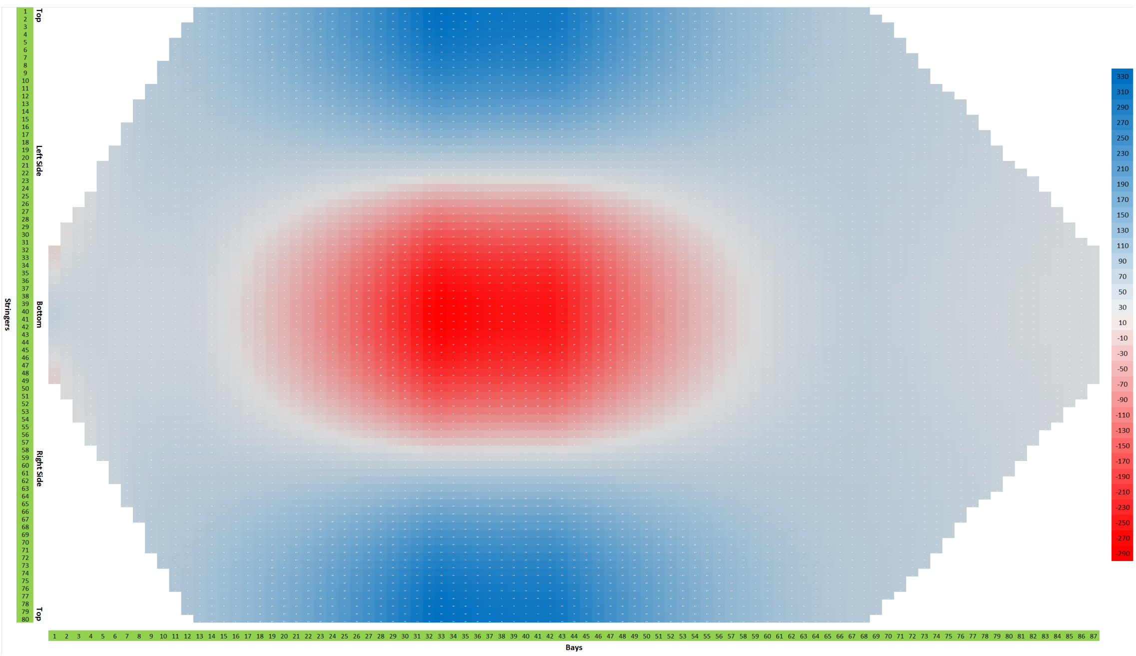

Figure E.17: Normalized longitudinal stress for 5G and Δp (CLC20) in MPa

Appendix F

Optimization result

F.1 Aluminum

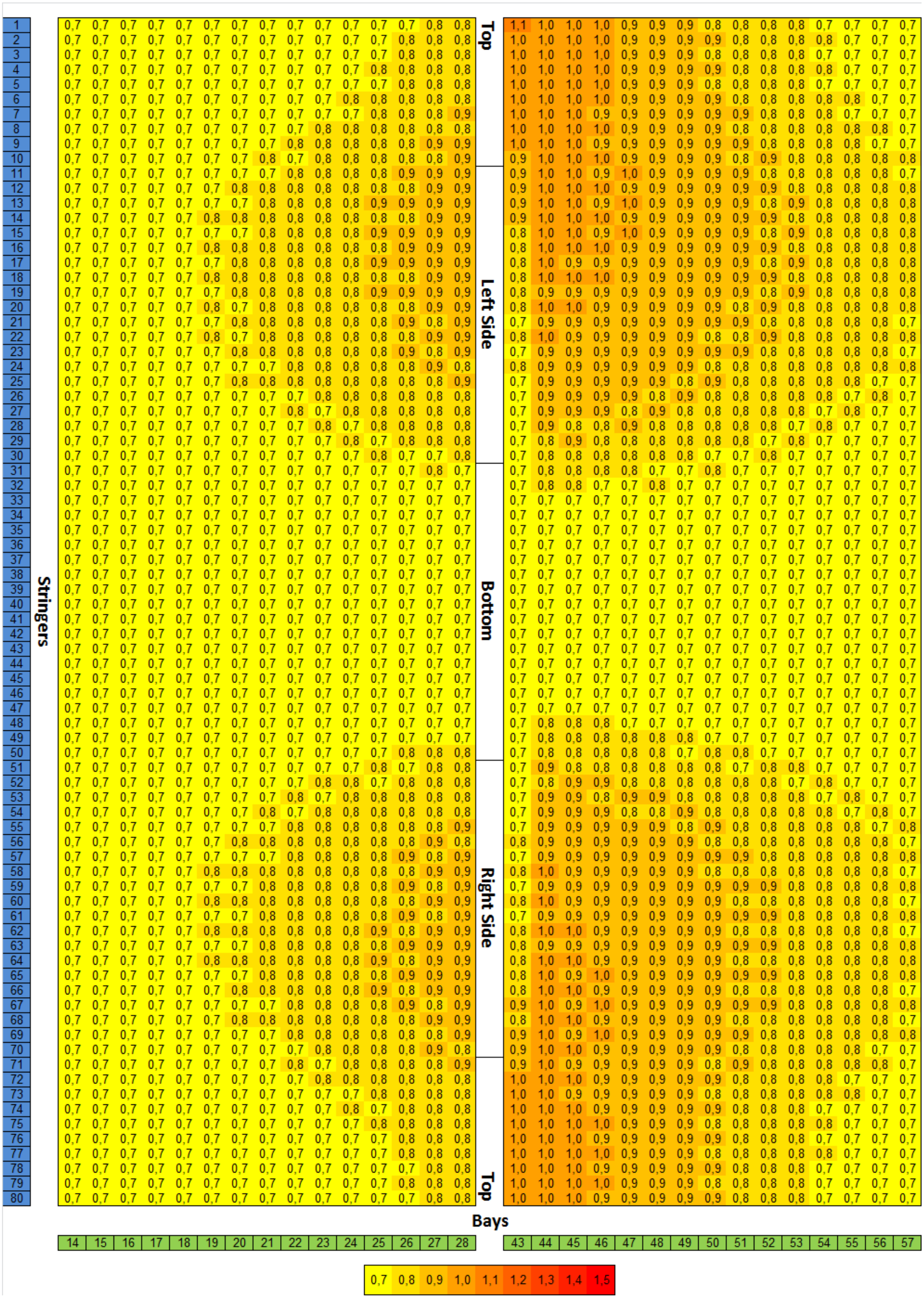

Figure F.1: Optimized thickness for package 1 in mm

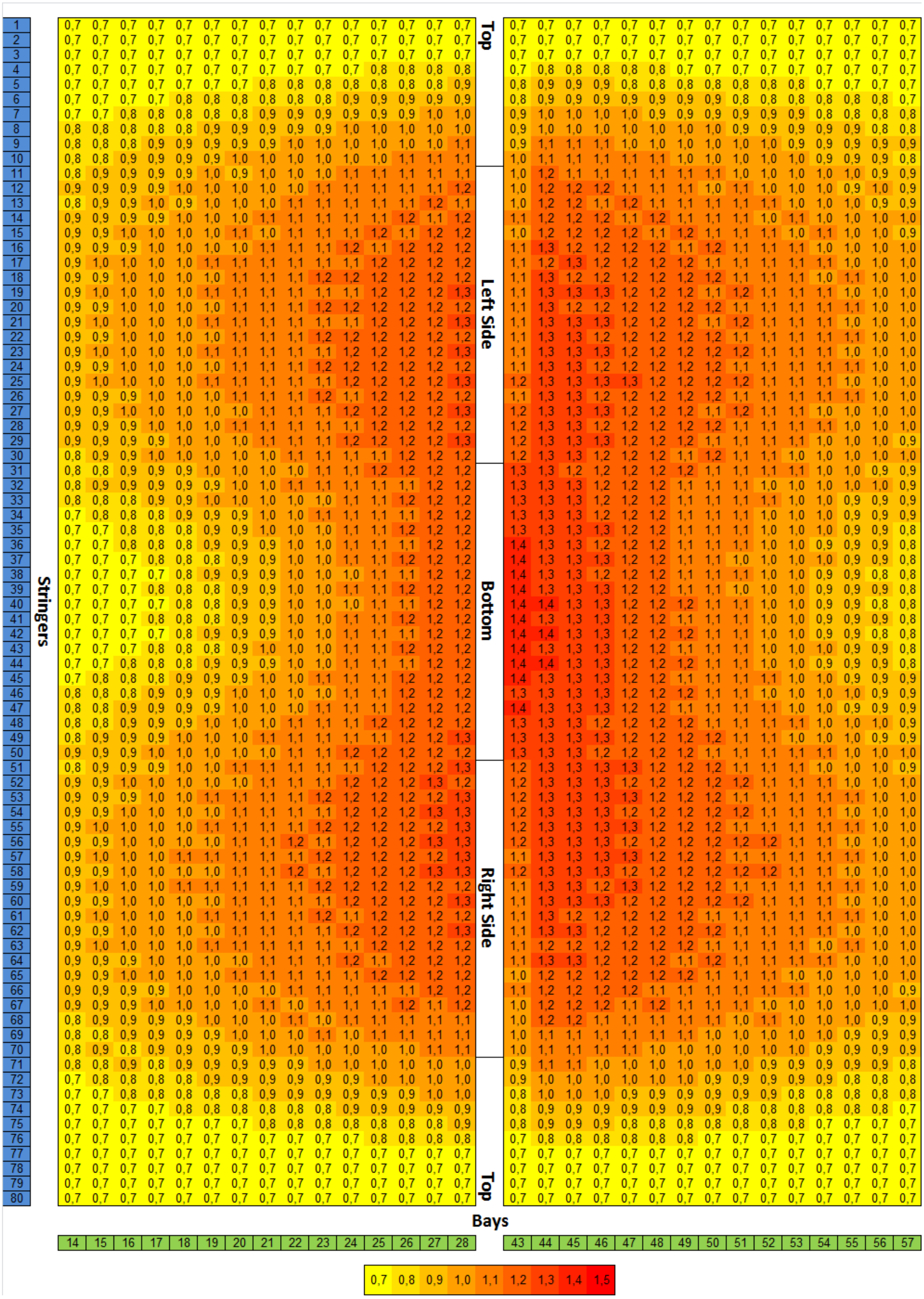

Figure F.2: Optimized thickness for package 2 in mm

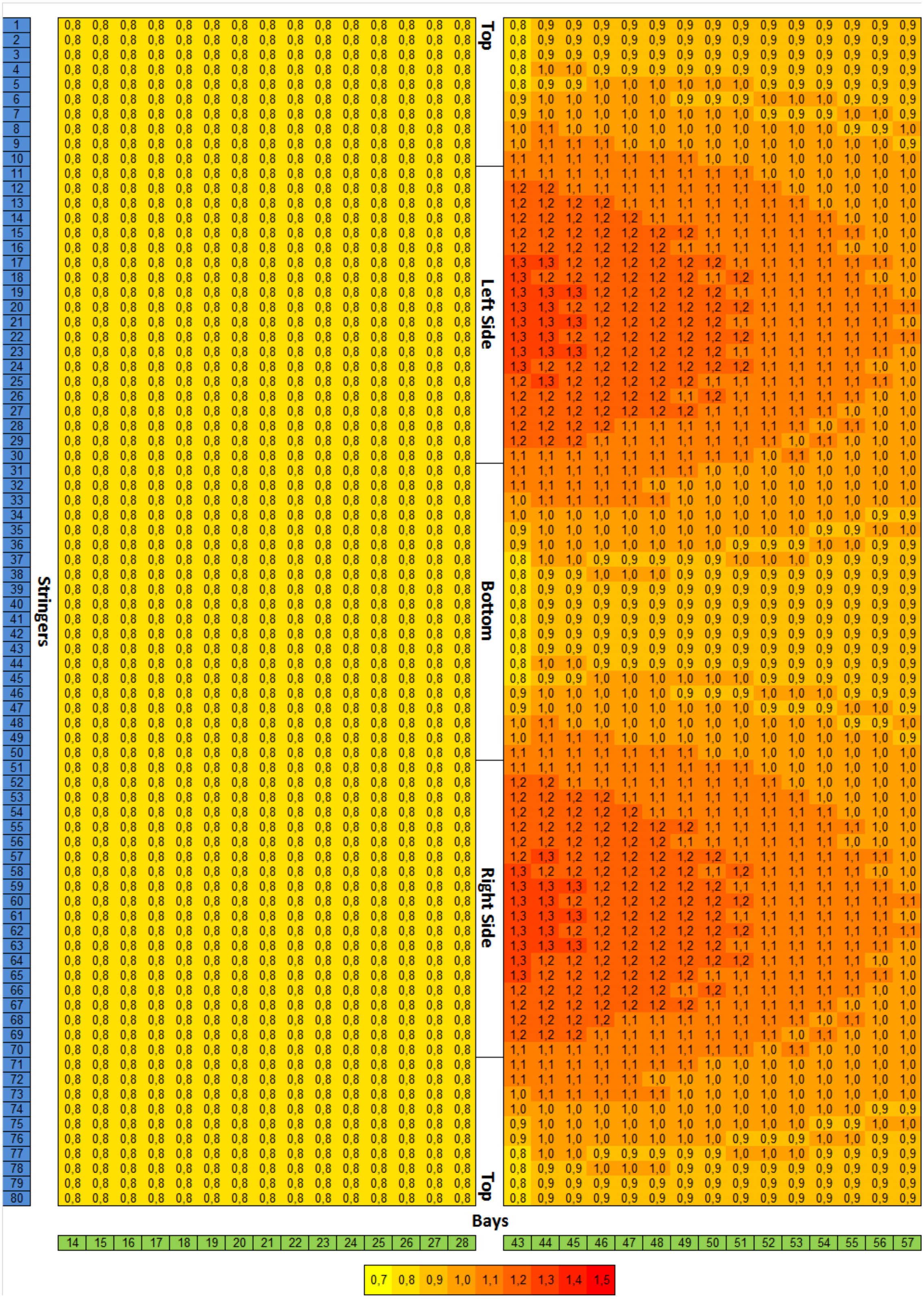

Figure F.3: Optimized thickness for package 3 in mm

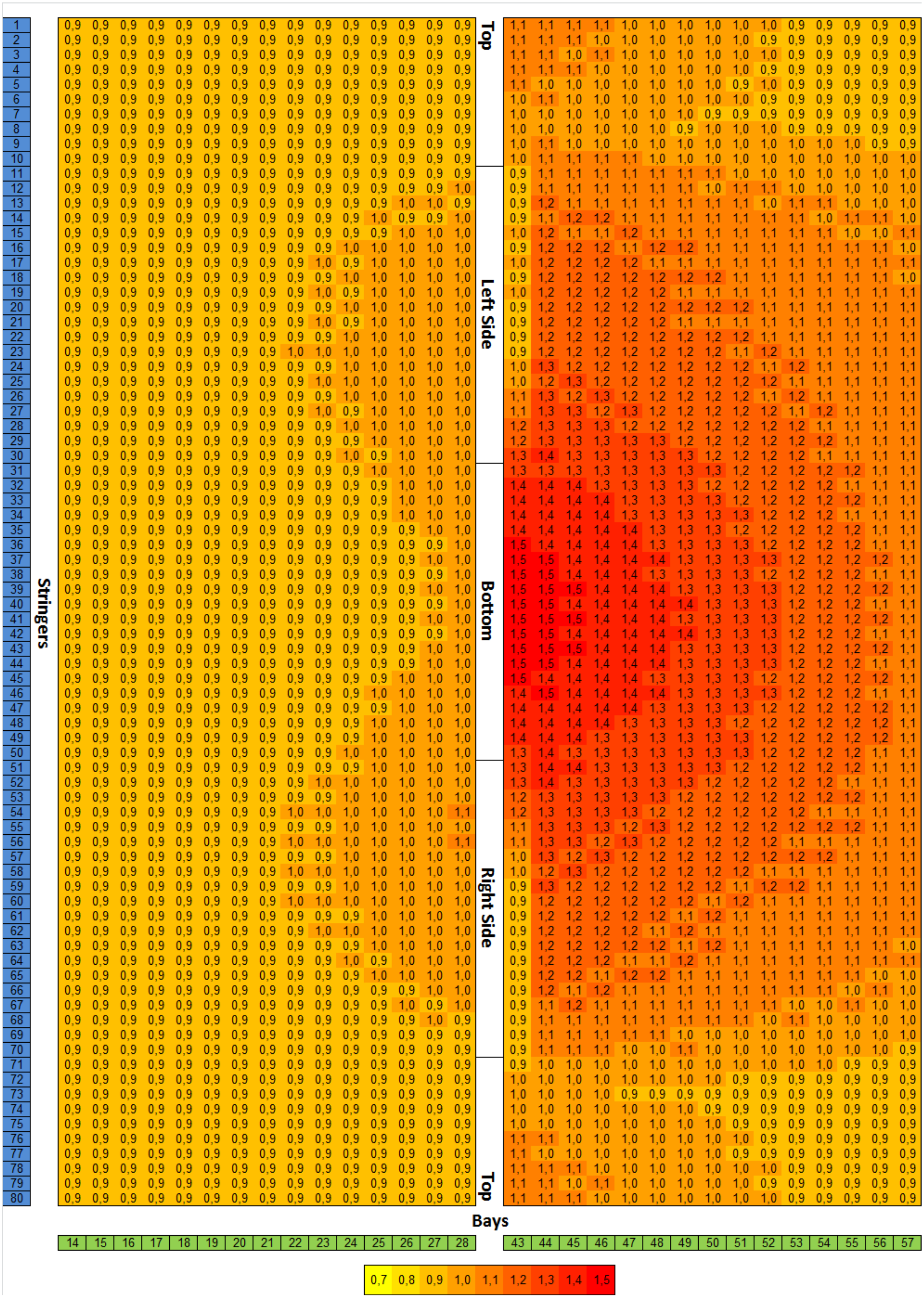

Figure F.4: Optimized thickness for package 4 in mm

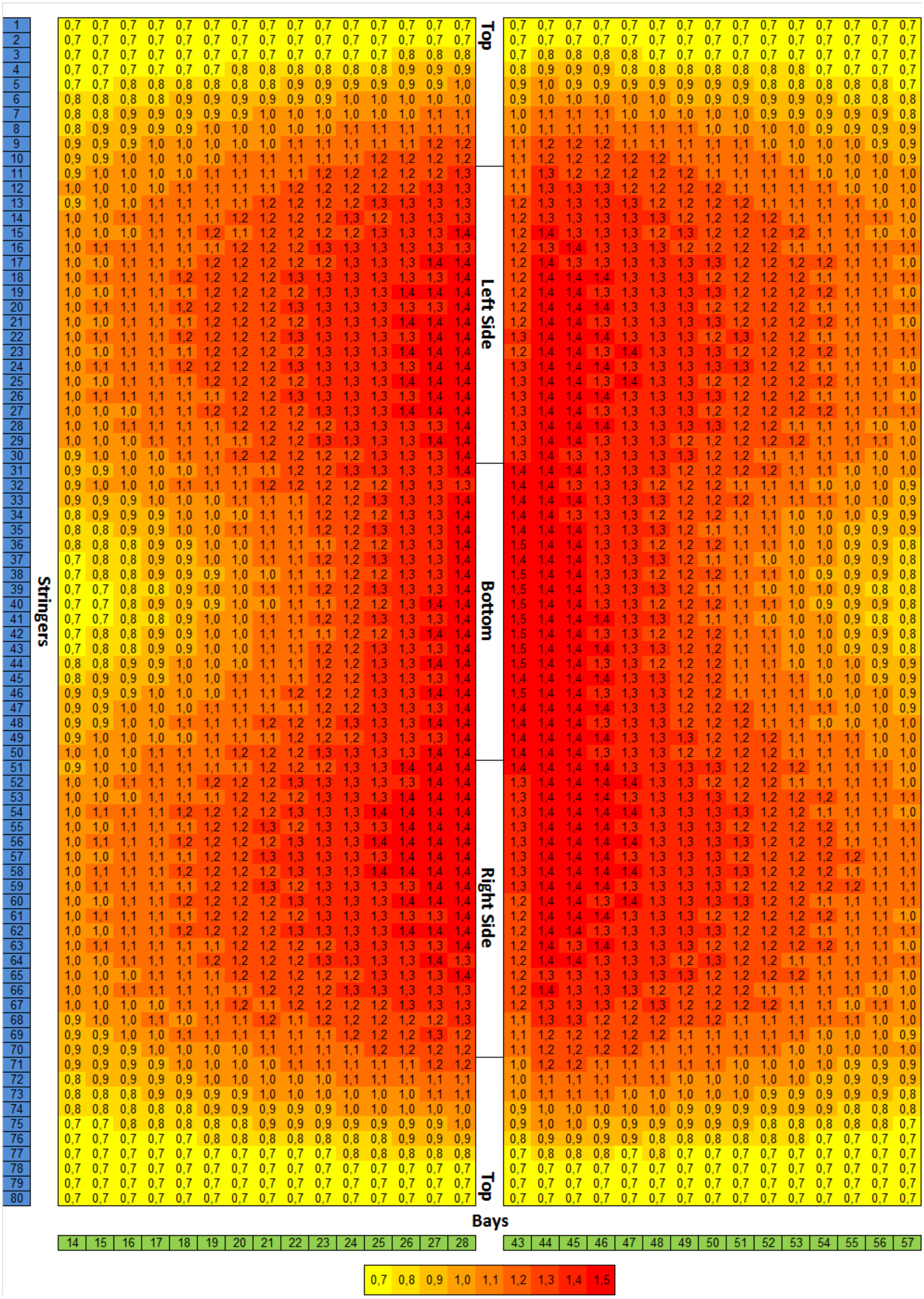

Figure F.5: Optimized thickness for package 5 in mm

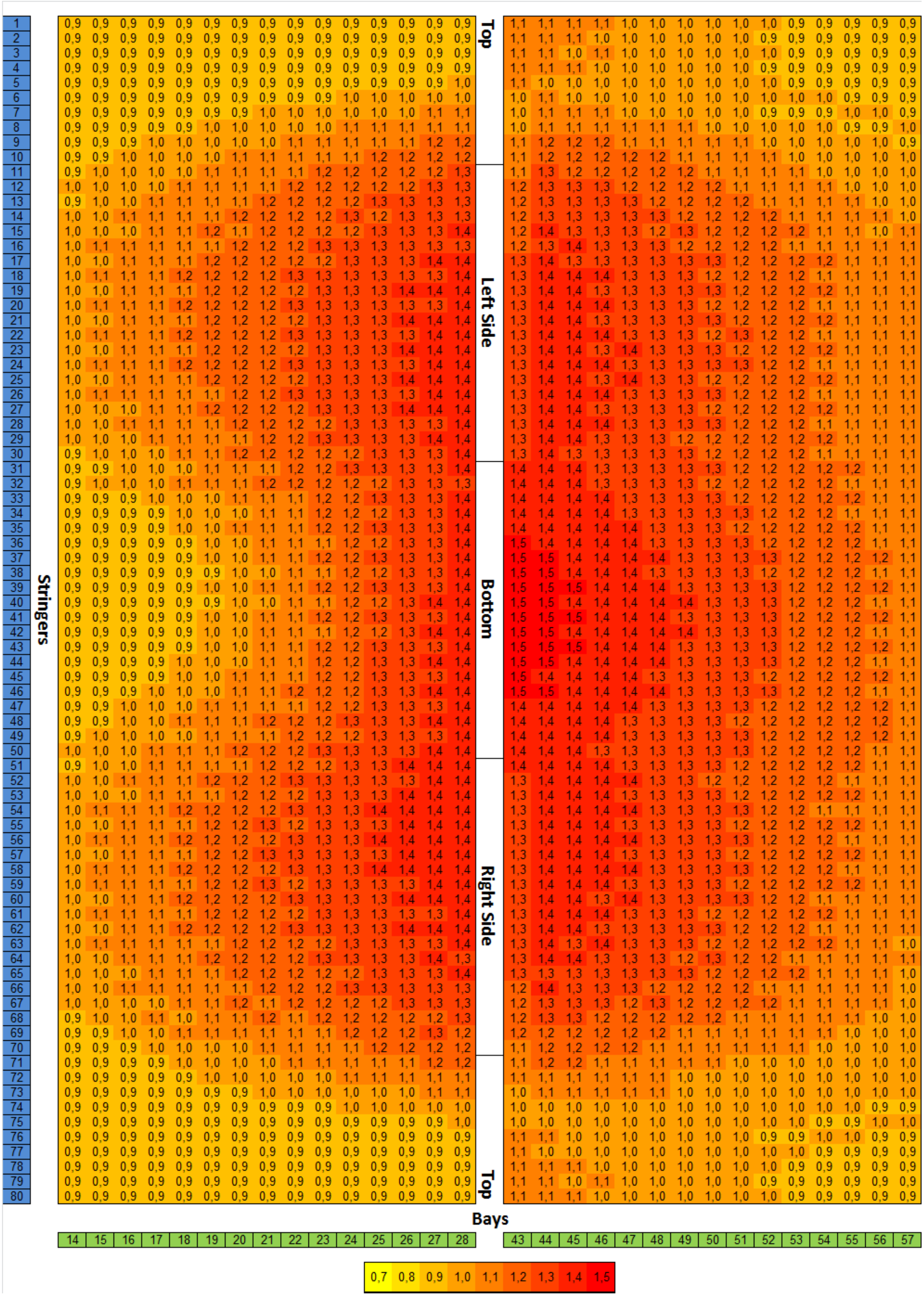

Figure F.6: Maximum optimized thickness for buckling (package 1 to 5) in mm

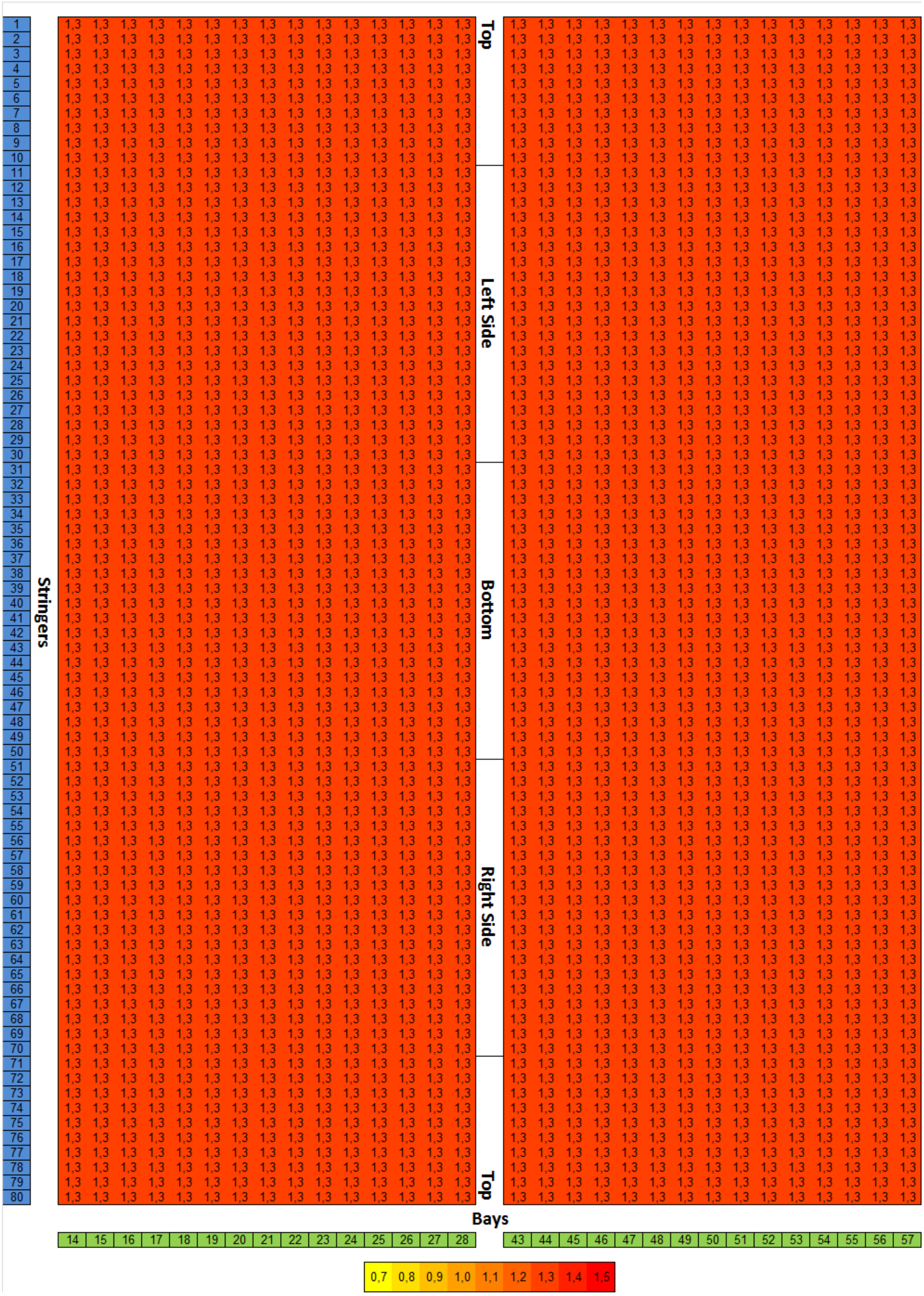

Figure F.7: Optimized thickness for package 6 in mm

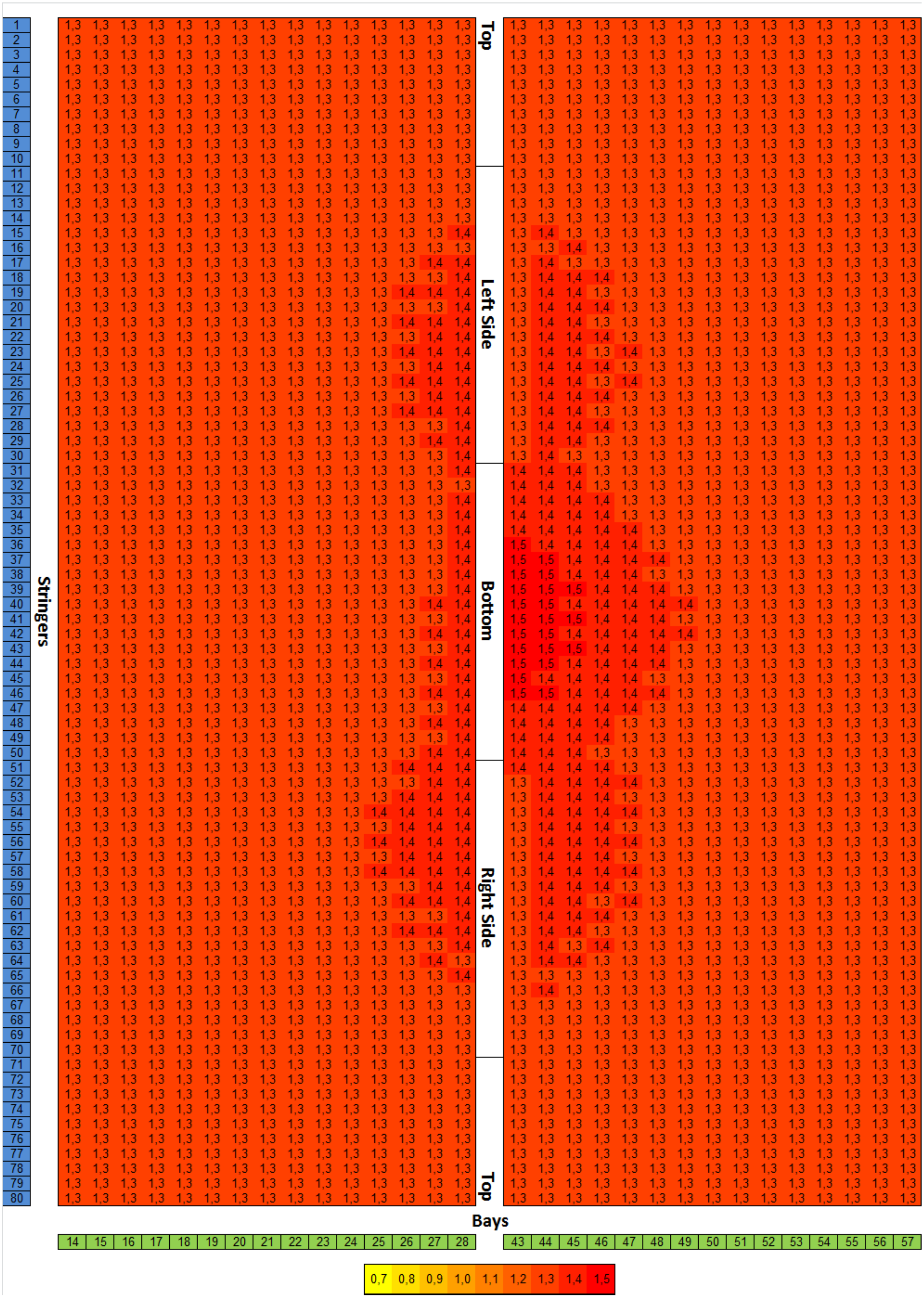

Figure F.8: Maximum optimized thickness for buckling and crack analysis in mm

Stringers	14	15	16	17	18	19	20	21	22	23	24	25	26	27	28		43	44	45	46	47	48	49	50	51	52	53	54	55	56	57
1	71	77	84	91	99	107	116	125	135	145	156	168	179	191	203	Top	228	214	201	189	177	166	155	145	135	125	116	107	99	92	85
2	71	77	84	91	99	107	116	125	134	145	155	167	178	190	202		226	213	200	188	176	165	154	144	134	124	115	107	99	92	85
3	70	77	83	90	98	106	115	124	133	143	154	165	177	188	200		224	211	198	186	175	164	153	143	133	123	115	106	98	91	84
4	70	76	82	89	97	105	113	122	131	141	152	163	174	186	197		221	208	195	184	172	161	151	141	131	122	113	105	97	90	83
5	69	75	81	88	95	103	111	120	129	139	149	160	171	182	193		216	203	192	180	169	158	148	138	129	120	111	103	96	89	82
6	68	74	80	86	93	101	109	117	126	136	145	156	166	177	188		210	198	187	175	165	154	144	135	126	117	109	101	94	87	81
7	67	72	78	84	91	98	106	114	123	132	141	151	161	172	182		204	192	181	170	160	150	140	131	122	114	106	99	92	85	79
8	65	71	76	82	89	96	103	111	119	127	136	146	155	165	176		196	185	174	164	154	144	135	127	118	110	103	96	89	83	77
9	64	69	74	80	86	92	99	106	114	122	131	140	149	158	168		187	177	167	157	147	138	130	122	114	106	99	92	86	80	75
10	62	67	72	77	83	89	95	102	109	117	125	133	142	150	160		178	168	158	149	140	132	124	116	109	102	95	89	83	78	73
11	60	64	69	74	79	85	91	97	104	111	118	126	134	142	150	Left Side	167	158	149	141	133	125	117	110	103	97	91	85	80	74	72
12	58	62	66	71	76	81	86	92	98	104	111	118	125	133	141		156	148	140	132	124	117	110	104	98	92	86	81	78	77	75
13	56	60	63	67	72	76	81	86	92	97	103	110	116	123	130		144	137	130	122	115	109	103	97	91	86	84	83	81	79	77
14	54	57	60	64	67	72	76	80	85	90	95	101	107	113	118		132	124	119	112	106	100	95	93	91	89	87	85	83	81	79
15	51	54	57	60	63	67	70	74	78	83	87	92	97	102	105		119	110	106	102	100	99	97	95	93	91	89	87	85	83	81
16	49	51	54	56	59	62	65	68	71	75	79	82	87	90	94		111	104	103	104	102	101	99	97	95	93	90	88	86	84	82
17	47	48	50	52	54	56	59	61	64	67	70	73	76	77	81		113	105	104	104	104	102	100	98	96	94	92	90	88	86	83
18	44	45	46	48	49	51	53	55	56	58	61	63	64	66	67		114	105	104	104	105	104	102	99	97	95	93	91	89	86	84
19	41	42	43	44	45	46	47	48	49	50	51	53	52	54	55		115	106	104	105	106	105	102	100	98	96	94	91	89	87	85
20	39	39	39	39	40	40	40	41	41	42	42	42	42	42	43		115	106	105	106	107	105	103	101	98	96	94	92	90	87	85
21	38	38	38	38	38	38	38	38	38	38	38	38	37	36	36		115	106	105	106	107	105	103	101	98	96	94	92	90	87	85
22	38	38	38	39	39	39	39	39	40	40	40	40	39	38	38		115	106	104	105	105	105	102	100	98	96	94	91	89	87	85
23	39	39	39	39	40	40	40	41	41	42	42	42	41	40	41		114	105	103	104	103	104	102	99	97	95	93	91	89	86	84
24	39	40	40	40	41	41	42	42	43	43	44	44	44	43	43		113	104	102	103	102	102	100	98	96	94	92	90	88	86	83
25	40	40	41	41	42	42	43	43	44	45	46	46	46	45	45		111	102	100	101	100	101	99	97	95	93	90	88	86	84	82
26	40	41	41	42	43	43	44	45	46	46	47	48	48	47	48		108	100	98	99	99	99	97	95	93	91	89	87	85	83	81
27	41	41	42	43	43	44	45	46	47	48	49	50	50	50	50		106	97	96	97	98	96	94	93	91	89	87	85	83	81	79
28	41	42	43	43	44	45	46	47	48	49	51	52	52	53	52		102	94	93	94	95	94	92	90	88	86	84	83	81	79	77
29	42	42	43	44	45	46	47	48	49	51	52	53	55	55	54		99	91	91	92	92	90	89	87	85	84	82	80	78	77	75
30	42	43	44	45	46	47	48	49	51	52	54	55	57	57	56		94	87	88	90	88	87	85	84	82	81	79	77	76	74	72
31	42	43	44	45	46	48	49	50	52	53	55	56	58	60	58	Bottom	87	83	83	86	85	83	82	80	79	77	76	74	73	71	70
32	43	44	45	46	47	48	50	51	53	54	56	58	60	61	61		82	79	78	80	80	79	78	77	76	74	73	72	70	69	67
33	43	44	45	46	48	49	50	52	54	55	57	59	61	63	62		83	82	81	81	83	82	81	80	78	77	75	74	72	71	69
34	43	44	46	47	48	50	51	53	54	56	58	60	62	64	62		85	84	83	82	84	84	83	82	80	79	77	75	74	72	71
35	43	45	46	47	49	50	52	53	55	57	59	61	63	65	63		87	86	85	84	84	86	85	83	82	80	79	77	75	74	72
36	44	45	46	47	49	50	52	54	56	58	60	62	64	66	64		86	87	87	86	84	86	86	85	83	82	80	78	77	75	73
37	44	45	46	48	49	51	53	54	56	58	60	62	65	67	65		87	86	88	87	86	87	88	86	84	83	81	79	78	76	74
38	44	45	47	48	49	51	53	55	57	59	61	63	65	67	65		88	86	88	88	87	88	89	87	85	84	82	80	78	77	75
39	44	45	47	48	50	51	53	55	57	59	61	63	65	67	66		89	87	88	89	87	87	88	88	86	84	82	81	79	77	75
40	44	45	47	48	50	51	53	55	57	59	61	63	66	66	66		89	87	88	89	88	86	87	88	86	84	83	81	79	77	76
41	44	45	47	48	50	51	53	55	57	59	61	63	66	66	66		89	87	88	89	88	86	87	88	86	84	83	81	79	77	76
42	44	45	47	48	50	51	53	55	57	59	61	63	65	66	66		89	87	88	89	87	86	87	88	86	84	82	81	79	77	75
43	44	45	47	48	49	51	53	55	57	59	61	63	65	65	65		88	86	87	88	87	86	88	87	85	84	82	80	78	77	75
44	44	45	46	48	49	51	53	54	56	58	60	62	65	65	65		87	86	87	87	86	86	88	86	84	83	81	79	78	76	74
45	44	45	46	47	49	50	52	54	56	58	60	62	64	64	64		85	86	87	86	84	85	86	85	83	82	80	78	77	75	73
46	43	45	46	47	49	50	52	53	55	57	59	61	63	63	63		85	84	85	84	83	84	85	83	82	80	79	77	75	74	72
47	43	44	46	47	48	50	51	53	54	56	58	60	62	62	62		84	83	83	82	82	83	83	82	80	79	77	75	74	72	71
48	43	44	45	46	48	49	50	52	54	55	57	59	61	61	61		83	82	81	80	82	82	81	80	78	77	75	74	72	71	69
49	43	44	45	46	47	48	50	51	53	54	56	58	60	59	59		81	79	78	78	80	79	78	77	76	74	73	72	70	69	67
50	42	43	44	45	46	48	49	50	52	53	55	56	57	57	58		86	83	82	83	84	83	82	80	79	77	76	74	73	71	70
51	42	43	44	45	46	47	48	49	51	52	54	55	55	55	56	Right Side	91	87	86	86	87	87	85	84	82	81	79	77	76	74	72
52	42	42	43	44	45	46	47	48	49	51	52	53	53	53	54		97	91	90	88	89	90	89	87	85	84	82	80	78	77	75
53	41	42	43	43	44	45	46	47	48	49	51	51	51	51	52		102	94	93	91	92	94	92	90	88	86	84	83	81	79	77
54	41	41	42	43	43	44	45	46	47	48	49	48	48	49	50		105	97	96	94	95	96	94	93	91	89	87	85	83	81	79
55	40	41	41	42	43	43	44	45	46	46	47	47	46	47	48		108	100	98	97	98	99	97	95	93	91	89	87	85	83	81
56	40	40	41	41	42	42	43	43	44	45	46	45	44	45	45		111	102	100	99	100	101	99	97	95	93	90	88	86	84	82
57	39	40	40	40	41	41	42	42	43	43	44	43	42	42	43		112	104	102	100	101	102	100	98	96	94	92	90	88	86	83
58	39	39	39	39	40	40	40	41	41	42	42	41	41	40	40		114	105	103	102	103	104	102	99	97	95	93	91	89	86	84
59	38	38	38	39	39	39	39	39	40	40	40	40	39	38	38		115	106	104	104	104	104	102	100	98	96	94	91	89	87	85
60	38	38	38	38	38	38	38	38	38	38	38	38	37	36	36		115	106	105	105	104	105	103	101	98	96	94	92	90	87	85
61	39	39	39	39	40	40	40	41	41	42	42	43	42	43	43		115	106	105	105	105	105	103	101	98	96	94	92	90	87	85
62	41	42	43	44	45	46	47	48	49	50	51	53	53	55	55		115	106	105	105	106	104	102	100	98	96	94	91	89	87	85
63	44	45	46	48	49	51	53	55	56	58	61	63	65	67	69		114	105	106	104	105	104	102	99	97	95	93	91	89	86	84
64	47	48	50	52	54	56	59	61	64	67	70	73	76	78	82		112	105	104	104	104	102	100	98	96	94	92	90	88	86	83
65	49	51	54	56	59	62	65	68	71	75	79	83	87	91	94		111	104	104	104	102	101	99	97	95	93	90	88	86	84	82
66	51	54	57	60	63	67	70	74	78	83	87	92	97	103	107		119	110	107	102	100	99	97	95	93	91	89	87	85	83	81
67	54	57	60	64	67	72	76	80	85	90	95	101	107	113	119		132	124	119	113	106	101	95	93	91	89	87	85	83	81	79
68	56	60	63	67	72	76	81	86	92	97	103	110	117	124	130		144	137	130	123	116	109	103	97	91	86	84	83	81	79	77
69	58	62	66	71	76	81	86	92	98	104	111	118	126	133	141		156	148	140	132	125	117	110	104	98	92	86	81	78	77	75
70	60	64	69	74	79	85	91	97	104	111	118	126	134	142	151		168	158	150	141	133	125	117	110	103	97	91	85	80	74	72
71	62	67	72	77	83	89	95	102	109	117	125	133	142	151	160	Top	178	168	159	150	141	132	124	116	109	102	95	89	83	78	73
72	64	69	74	80	86	92	99	106	114	122	131	140	149	159	168		188	177	167	157	148	139	130	122	114	106	99	92	86	80	75
73	65	71	76	82	89	96	103	111	119	127	136	146	156	166	176		196	185	174	164	154	144	135	127	118	110	103	96	89	83	77
74	67	72	78	84	91	98	106	114	123	132	141	151	161	172	182		204	192	181	170	160	150	140	131	122	114	106	99	92	85	79
75	68	74	80	86	93	101	109	117	126	136	145	156	167	177	188		211	198	187	176	165	154	144	135	126	117	109	101	94	87	81
76	69	75	81	88	95	103	111	120	129	139	149	160	171	182	193		216	203	192	180	169	158	148	138	129	120	111	103	96	89	82
77	70	76	82	89	97	105	113	122	131	141	152	163	174	186	197		221	208	196	184	172	161	151	141	131	122	113	105	97	90	83
78	70	77	83	90	98	106	115	124	133	143	154	165	177	189	200		224	211	199	187	175	164	153	143	133	123	115	106	98	91	84
79	71	77	84	91	99	107	116	125	134	145	155	167	178	190	202		226	213	200	188	176	165	154	144	134	124	115	107	99	92	85
80	71	77	84	91	99	107	116	125	135	145	156	168	179	191	203		228	214	201	189	177	166	155	145	135	125	116	107	99	92	85

Bays

40	70	100	130	160	190	220	250

Figure F.9: Maximum stress on aluminum panel in MPa

F.2 Composite

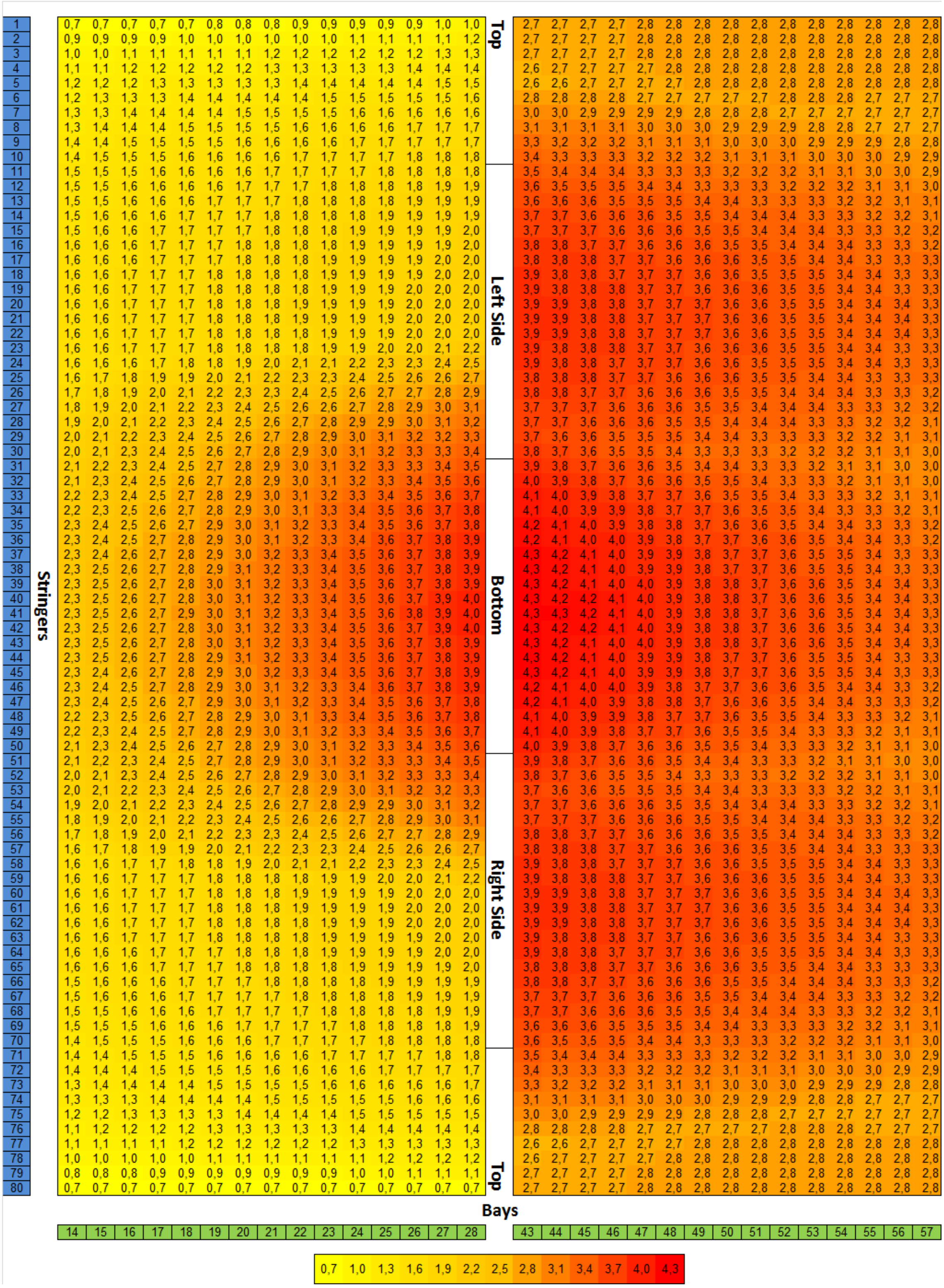

Figure F.10: Optimized thickness for buckling analysis in mm

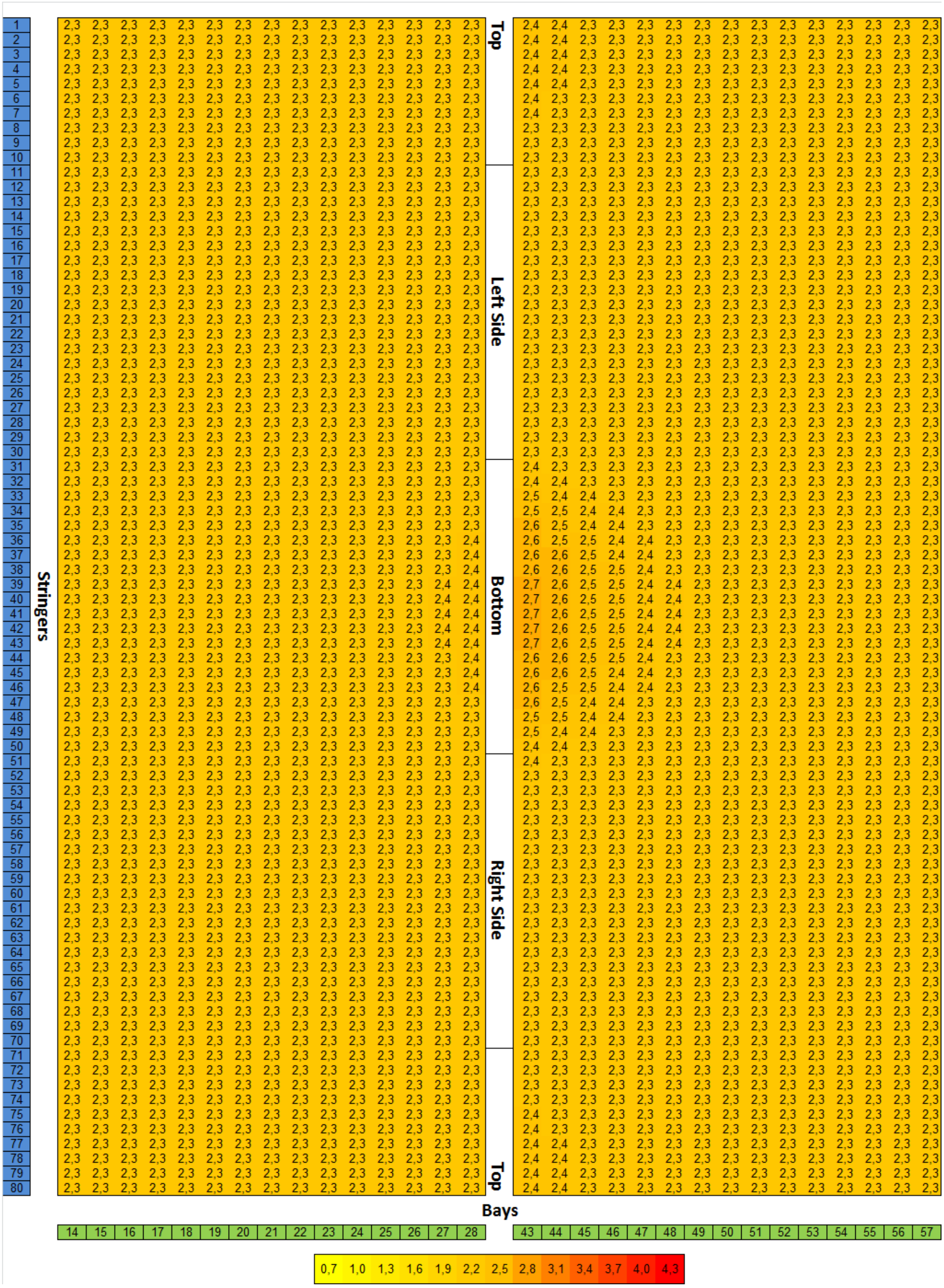

Figure F.11: Optimized thickness for strength analysis in mm

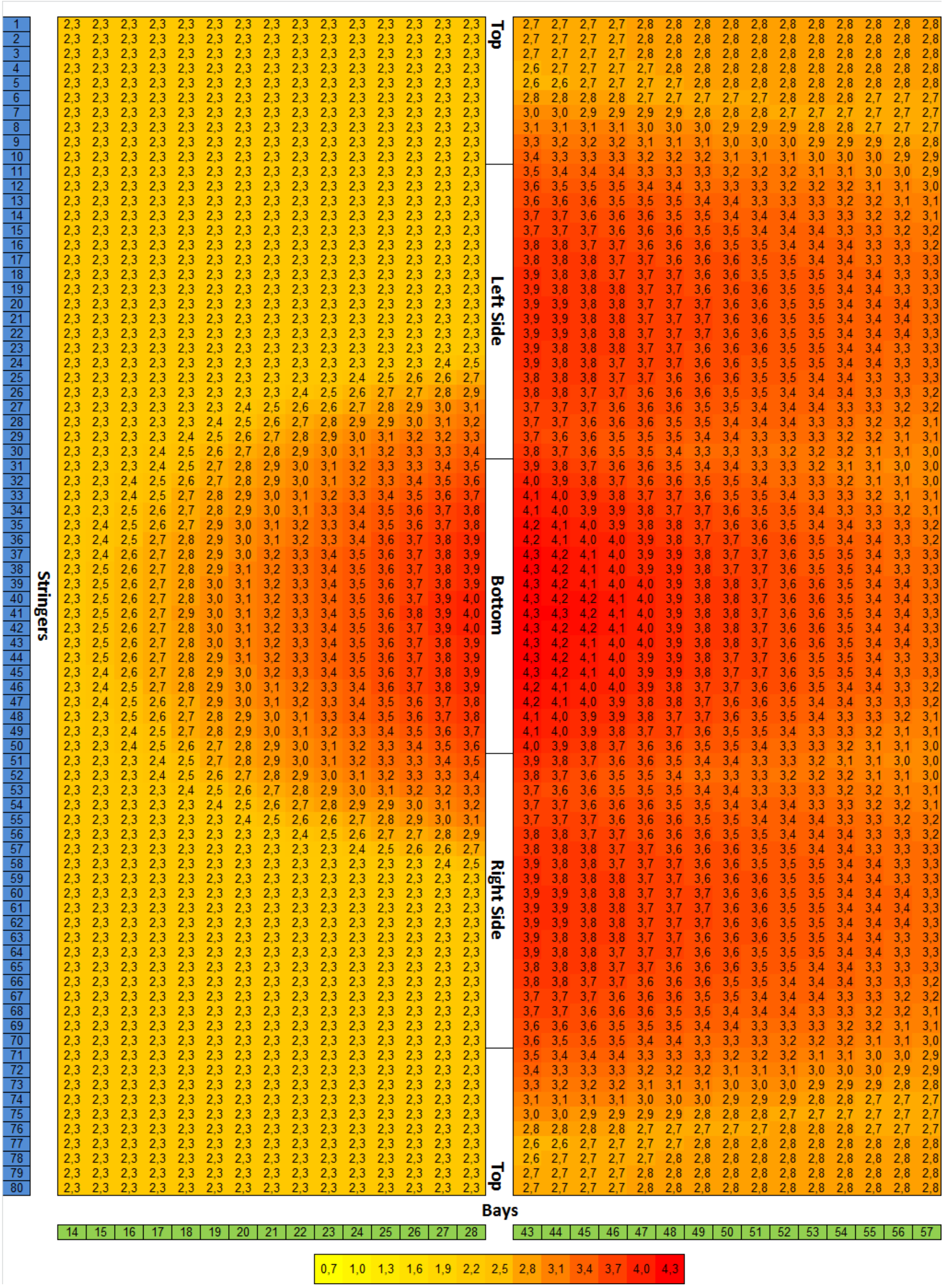

Figure F.12: Maximum optimized thickness for buckling and strength analysis in mm

Stringers	Region	14	15	16	17	18	19	20	21	22	23	24	25	26	27	28
1	Top	40	44	47	51	55	59	64	69	74	79	85	91	97	103	110
2	Top	40	43	47	51	55	59	64	69	74	79	85	90	96	103	109
3	Top	40	43	47	50	55	59	63	68	73	78	84	90	96	102	108
4	Top	39	43	46	50	54	58	63	67	72	77	83	88	94	101	107
5	Top	39	42	46	49	53	57	62	66	71	76	81	87	93	99	105
6	Top	38	41	45	48	52	56	60	65	70	74	80	85	91	97	103
7	Top	38	41	44	47	51	55	59	63	68	73	78	83	88	94	100
8	Top	37	40	43	46	50	53	57	61	66	70	75	80	86	91	97
9	Top	36	39	42	45	48	52	55	59	63	68	73	77	82	88	93
10	Top	35	38	40	43	46	50	53	57	61	65	70	74	79	84	89
11	Left Side	34	36	39	42	45	48	51	54	58	62	66	71	75	80	85
12	Left Side	33	35	37	40	43	45	49	52	55	59	63	67	71	76	80
13	Left Side	32	34	36	38	40	43	46	49	52	56	59	63	67	71	75
14	Left Side	30	32	34	36	38	41	43	46	49	52	55	59	62	66	70
15	Left Side	29	31	32	34	36	38	40	43	45	48	51	54	57	61	64
16	Left Side	28	29	30	32	34	35	37	39	42	44	47	50	52	55	59
17	Left Side	26	27	28	30	31	33	34	36	38	40	42	45	47	50	53
18	Left Side	25	26	26	27	29	30	31	33	34	36	38	40	42	44	47
19	Left Side	23	24	24	25	26	27	28	29	30	32	33	35	37	39	41
20	Left Side	22	22	22	23	23	24	25	26	27	28	29	30	31	33	34
21	Left Side	21	21	21	21	21	21	22	22	23	23	24	25	26	27	28
22	Left Side	22	22	22	22	22	22	22	22	22	22	21	21	21	21	22
23	Left Side	22	22	22	22	22	22	22	22	22	22	22	22	22	22	22
24	Left Side	22	22	22	23	23	23	23	23	23	23	23	23	23	22	22
25	Left Side	22	23	23	23	23	23	24	24	24	24	23	23	22	22	21
26	Left Side	23	23	23	23	24	24	24	24	23	23	23	22	22	22	21
27	Left Side	23	23	24	24	24	24	24	23	23	23	22	22	22	21	21
28	Left Side	23	24	24	24	24	24	23	23	23	22	22	22	22	22	21
29	Left Side	23	24	24	24	24	24	23	23	23	22	22	22	22	22	22
30	Left Side	24	24	25	24	24	23	23	23	22	22	22	22	22	22	22
31	Bottom	24	24	25	24	24	23	23	23	22	22	22	22	22	23	23
32	Bottom	24	25	24	24	23	23	23	23	23	23	23	23	23	23	23
33	Bottom	24	25	24	24	23	23	23	23	23	23	23	23	23	23	23
34	Bottom	24	25	24	24	23	23	23	23	23	23	23	23	23	23	23
35	Bottom	25	24	24	23	23	23	23	23	23	23	23	23	23	23	24
36	Bottom	25	24	24	23	23	23	23	23	23	23	23	23	23	24	24
37	Bottom	25	24	24	23	23	23	23	23	23	23	23	23	24	24	24
38	Bottom	25	24	23	23	23	23	23	23	23	23	23	24	24	24	25
39	Bottom	25	24	24	23	23	23	23	23	23	23	23	24	24	24	25
40	Bottom	25	24	24	23	23	23	23	23	23	23	24	24	24	24	25
41	Bottom	25	24	24	23	23	23	23	23	23	23	24	24	24	24	24
42	Bottom	25	24	24	23	23	23	23	23	23	23	23	24	24	24	24
43	Bottom	25	24	23	23	23	23	23	23	23	23	23	24	24	24	25
44	Bottom	25	24	23	23	23	23	23	23	23	23	23	23	24	24	24
45	Bottom	25	24	23	23	23	23	23	23	23	23	23	23	23	24	24
46	Bottom	25	24	24	23	23	23	23	23	23	23	23	23	23	23	24
47	Bottom	24	24	24	23	23	23	23	23	23	23	23	23	23	23	23
48	Bottom	24	25	24	23	23	23	23	23	23	22	22	23	23	23	23
49	Bottom	24	25	24	24	23	23	23	22	22	22	22	22	22	23	23
50	Bottom	24	24	24	24	23	23	22	22	22	22	22	22	22	22	23
51	Right Side	24	24	24	24	23	23	22	22	22	22	22	22	22	22	22
52	Right Side	23	24	24	24	23	23	22	22	22	22	22	21	22	22	22
53	Right Side	23	24	24	24	24	23	23	22	22	22	21	21	21	22	21
54	Right Side	23	23	24	24	24	24	23	22	22	22	22	22	21	21	21
55	Right Side	23	23	23	23	24	24	23	23	22	22	22	21	21	21	21
56	Right Side	22	23	23	23	23	23	23	23	23	23	22	21	21	21	21
57	Right Side	22	22	22	23	23	23	23	23	23	23	22	22	22	21	21
58	Right Side	22	22	22	22	22	22	22	22	22	23	22	22	22	22	21
59	Right Side	22	22	22	22	22	22	22	22	22	22	22	22	22	21	21
60	Right Side	21	21	21	21	21	21	21	22	22	23	23	23	24	24	25
61	Right Side	22	22	23	23	23	24	25	25	26	27	28	28	29	30	31
62	Right Side	23	24	25	25	26	27	28	29	30	31	32	33	35	36	38
63	Right Side	25	26	27	27	29	30	31	32	34	35	37	38	40	42	44
64	Right Side	26	27	28	30	31	33	34	36	38	39	41	43	45	48	50
65	Right Side	28	29	30	32	34	35	37	39	41	43	46	48	51	53	56
66	Right Side	29	31	32	34	36	38	40	42	45	47	50	53	56	59	62
67	Right Side	30	32	34	36	38	41	43	46	48	51	54	57	61	64	67
68	Right Side	32	34	36	38	40	43	46	49	52	55	58	62	65	69	73
69	Right Side	33	35	37	40	43	45	48	52	55	58	62	66	70	74	78
70	Right Side	34	36	39	42	45	48	51	54	58	62	66	70	74	78	83
71	Top	35	38	40	43	46	50	53	57	61	65	69	73	78	82	87
72	Top	36	39	42	45	48	52	55	59	63	67	72	76	81	86	91
73	Top	37	40	43	46	50	53	57	61	65	70	75	80	85	90	95
74	Top	38	41	44	47	51	55	59	63	68	72	77	82	87	93	99
75	Top	38	41	45	48	52	56	60	65	69	74	79	85	90	96	102
76	Top	39	42	46	49	53	57	61	66	71	76	81	86	92	98	104
77	Top	39	43	46	50	54	58	62	67	72	77	83	88	94	100	106
78	Top	40	43	47	50	55	59	63	68	73	78	84	89	95	101	108
79	Top	40	43	47	51	55	59	64	69	74	79	84	90	96	102	109
80	Top	40	44	47	51	55	59	64	69	74	79	85	91	97	103	109

Stringers	43	44	45	46	47	48	49	50	51	52	53	54	55	56	57
1	99	94	88	83	77	72	68	64	59	55	52	48	45	42	39
2	98	93	88	83	77	72	68	63	59	55	52	48	45	42	39
3	98	92	87	82	76	71	67	63	59	55	51	48	44	41	39
4	97	91	86	81	76	71	66	62	58	54	51	47	44	41	38
5	95	90	84	79	75	70	65	61	57	53	50	46	44	41	38
6	91	86	81	76	73	68	64	60	56	52	49	46	43	40	38
7	86	81	77	73	69	65	62	58	54	51	48	45	42	40	37
8	81	77	73	69	66	62	58	55	52	49	46	43	41	38	36
9	77	73	69	65	62	58	55	52	49	46	44	41	39	37	34
10	72	69	65	61	58	55	52	49	46	43	41	39	37	35	33
11	67	64	61	57	55	51	48	46	43	41	39	36	35	33	31
12	62	60	56	53	51	48	45	43	41	38	36	34	33	32	32
13	58	55	52	49	47	44	42	40	38	36	34	33	33	33	32
14	53	50	47	45	43	40	38	37	35	34	34	34	33	33	33
15	47	45	43	41	39	37	36	36	35	35	34	34	34	33	33
16	42	40	38	37	37	37	36	36	36	35	35	34	34	34	33
17	39	38	38	38	38	37	37	36	36	36	35	35	35	34	34
18	39	39	38	38	38	37	37	37	36	36	35	35	35	34	34
19	39	39	39	38	38	37	37	37	36	36	36	35	35	35	34
20	39	39	39	38	38	38	37	37	36	36	36	36	35	34	34
21	39	39	39	38	38	38	37	37	36	36	36	36	35	34	34
22	39	39	39	38	38	37	37	37	36	36	35	35	35	34	34
23	39	39	38	38	38	37	37	37	36	36	35	35	35	34	34
24	38	38	38	38	37	37	37	36	36	35	35	35	34	34	33
25	38	38	37	37	37	36	36	36	35	35	35	34	34	34	33
26	37	37	37	37	36	36	35	35	35	35	34	34	34	33	33
27	37	36	36	36	36	35	35	35	34	34	34	33	33	33	32
28	36	35	35	35	35	34	34	34	34	33	33	33	32	32	32
29	34	34	34	34	34	33	33	33	33	33	32	32	32	32	31
30	33	33	33	33	32	32	32	32	32	32	31	31	31	31	31
31	31	31	31	31	31	31	31	30	30	30	30	30	30	30	30
32	29	29	29	29	29	29	29	29	29	29	29	29	29	29	29
33	29	29	29	29	30	29	29	29	29	29	29	29	29	29	29
34	30	30	30	30	30	30	30	30	30	30	30	30	29	29	29
35	30	31	31	31	31	30	30	30	30	30	30	30	30	30	30
36	31	31	31	31	31	31	31	31	31	30	30	30	30	30	30
37	31	31	31	31	31	31	31	31	31	31	31	30	30	30	30
38	32	32	32	32	32	31	32	31	31	31	31	31	31	31	30
39	32	32	32	32	32	32	32	31	31	31	31	31	31	31	30
40	32	32	32	32	32	32	32	31	31	31	31	31	31	30	31
41	32	32	32	32	32	32	32	31	31	31	31	31	31	30	31
42	32	32	32	32	32	32	32	31	31	31	31	31	31	30	30
43	32	32	32	32	32	31	32	31	31	31	31	31	31	30	30
44	31	31	31	31	31	31	31	31	31	31	31	30	30	30	30
45	31	31	31	31	31	31	31	31	30	30	30	30	30	30	30
46	30	30	31	30	31	30	30	30	30	30	30	30	30	30	29
47	30	30	30	30	30	30	30	30	30	29	30	29	29	29	29
48	29	29	29	29	29	29	29	29	29	29	29	29	29	29	29
49	29	29	29	29	29	29	29	29	28	28	29	28	28	28	28
50	30	30	31	31	31	30	30	30	30	30	30	30	30	30	30
51	32	32	32	33	32	32	32	32	32	32	31	31	31	31	31
52	34	34	34	34	34	34	34	33	33	33	32	32	32	32	32
53	36	36	35	35	35	35	35	34	34	34	33	33	33	33	32
54	37	37	36	36	36	35	35	35	35	34	34	34	33	33	33
55	38	37	37	37	36	36	36	35	35	35	34	34	34	33	33
56	38	38	38	37	37	37	36	36	36	35	35	34	34	34	33
57	39	38	38	38	37	37	37	36	36	36	35	35	35	34	34
58	39	39	38	38	38	37	37	37	36	36	35	35	35	34	34
59	39	39	39	38	38	37	37	37	36	36	35	35	35	35	34
60	39	39	39	38	38	38	37	37	36	36	36	36	35	34	34
61	39	39	39	38	38	38	37	37	36	36	36	36	35	34	34
62	39	39	39	38	38	37	37	37	36	36	35	35	35	34	34
63	39	39	38	38	38	37	37	36	36	36	35	35	34	34	34
64	38	38	38	38	37	37	37	36	36	35	35	35	34	34	33
65	41	39	37	37	37	36	36	36	35	35	35	34	34	34	33
66	46	44	42	40	38	36	35	35	35	35	34	34	34	33	33
67	51	49	46	44	42	40	38	36	34	34	33	33	33	33	32
68	56	53	51	48	46	43	41	39	37	35	33	33	32	32	32
69	61	58	55	52	50	47	45	42	40	38	36	34	32	32	31
70	66	63	59	56	53	50	48	45	43	40	38	36	34	32	31
71	70	67	63	60	57	54	51	48	45	43	41	38	36	34	32
72	75	72	67	64	61	57	54	51	48	45	43	40	38	36	34
73	79	76	71	67	64	60	57	54	51	47	45	42	40	38	35
74	84	79	75	71	68	63	60	57	53	50	48	44	42	39	37
75	88	83	79	75	71	67	63	59	56	52	49	46	43	40	38
76	93	88	83	78	74	70	65	61	57	53	50	47	44	41	38
77	97	91	85	80	76	71	66	62	58	54	51	47	44	41	38
78	98	92	87	82	77	71	67	63	59	55	51	48	44	41	39
79	99	93	88	83	77	72	67	63	59	55	52	48	45	42	39
80	99	94	88	83	77	72	68	64	59	55	52	48	45	42	39

Bays

20	35	50	65	80	95	110

Figure F.13: Maximum stress on composite panel in MPa